# A RAPID INUNDATION FLOOD CELL MODEL FOR FLOOD RISK ANALYSIS

**Martin Krupka**

Submitted for the degree of Doctor of Philosophy

Heriot-Watt University

School of the Built Environment

April 2009

## ABSTRACT

Government flooding policy across Europe, and in the UK, has switched from flood defence to flood risk management. The approach requires the evaluation of the consequences of all possible asset failures over a range of flood probabilities. For a typical flood system this necessitates the simulation of thousands of inundation permutations. As a consequence, the speed of simulation is a significant factor in the practical implementation of this approach.

This thesis reports on the development and testing of a Rapid Flood Inundation Model (RFIM) designed to satisfy this requirement. The model consists of a precalculation part, and a subsequent rapid flood inundation prediction. Three variations of the rapid inundation routine are presented. The algorithms differ in the way in which the flood depth on the communication links between the cells is calculated. The latter version also permits a spatially limited estimation of flow velocities.

The RFIM was applied to the Greenwich and Thamesmead embayments on the River Thames in London. The main objectives of the RFIM testing were: to evaluate the predictive capabilities of the simple volume spreading method used. In order to undertake the task a Monte Carlo analysis was performed and the flood extent maps were compared to predictions produced by the two-dimensional hydrodynamic model, TUFLOW.

The overall performance of the model was found to be acceptable, although some inaccuracies in the predictions, as a result of the oversimplification of the hydraulics, were observed. These were discussed and recommendations were given to improve model behaviour. The computational speeds were found to be acceptable and within the required limits. It is therefore suggested that the proposed Rapid Flood Inundation Model can be used for flood predictions in urban areas for the purpose of flood risk management.

Dedicated to my beloved parents

For their continuous support and encouragement

## ACKNOWLEDGEMENT

I would like to express my sincere gratitude and appreciation to Professor Gareth Pender and Dr. Steve Wallis for their continuous support, supervision and enthusiasm during the course of this study.

I would like to specially thank to Dr. Sylvain Neélz for providing the TUFLOW inundation predictions against which the developed model has been compared.

I would also like to extend my thanks to my girlfriend and parents for their continued support and encouragement throughout the period of this study.

The research reported in this thesis was conducted as part of the Flood Risk Management Research Consortium. The FRMRC is supported by grant GR/S76304 from the Engineering and Physical Sciences Research Council, in partnership with the Natural Environment Research Council, the DEFRA/EA Joint Research Programme on Flood and Coastal Defence, UKWIR, the Scottish Executive and the Rivers Agency (Northern Ireland). This financial support is gratefully acknowledged. I am also grateful to Environment Agency for providing LiDAR DEM data.

# TABLE OF CONTENTS

## LIST OF FIGURES

# 1 Introduction

Humans have always built their settlements close to rivers, to ensure access to water supply, to exploit attractive rich soils, for ease of transport and for trading advantage. In many cases they built properties on floodplains, making them vulnerable to the danger of flooding. Up to today, urban flood events have contributed most to the overall flood risk exposure of communities and attempts to mitigate flooding in urban areas have been one of society's main accomplishments, ranging from gaining more control over the river or stream to the development of new settlements in the locations where no such risk exists. According to United Nations University (2004) floods presently impact an estimated 520+ million people per year worldwide, resulting in estimates of up to 25,000 annual deaths. Additionally the number of people worldwide vulnerable to devastating floods is expected to increase to 2 billion by 2050 due to climate change, deforestation, rising sea levels and population growth in flood-prone areas. Recent floods in Europe in 1997 and 2002 and in New Orleans in 2005 have highlighted the serious hazards posed by flooding.

In the UK, fatalities as a result of flooding are rare (over the last few decades the fatalities directly due to flooding have been about 1 per year) compared to developing countries; however, the social and economic consequences of flooding in the UK, although rather small, do impact local communities significantly. Nearly two million properties in floodplains along rivers, estuaries and coasts in the UK are potentially at risk of river or coastal flooding with potential average annual damage of £ 1.4 billion (Foresight, 2004). Devastating floods in 1998, 2000 and most recently in the summer of 2007 showed the importance of flood risk management and mitigation.

Since the early 1990s the occurrence of floods has increased worldwide and has resulted in increased attention being drawn to assessing flood risk and to directing resources into flood management projects in order to mitigate flood risk. The research of revised methods of flood risk assessment and management has been further motivated by climate change issues, which materialize in the predictions of future climate scenarios. In the UK, the consequences of climate change were presented in the Foresight study

(2004), which concluded that the number of people at risk from river and coastal flooding could more than double by the 2080s depending on future socio-economic policies. It was also shown that the implementation of a range of responses could eliminate the growth of flood risk significantly in the long term. The study also showed that investment in better modelling and prediction techniques is needed in order to ensure effectiveness in planning and management of flood risk mitigation measures. As a result, the UK Government initiated a Making Space for Water (2004) programme, which focused on improving flood risk assessment and management methods in order to reduce the threat to people and their property and to deliver the greatest environmental, social and economic benefit. The funding mechanisms were secured for adopting the *risk and systems based approach* to flood management. Furthermore, the Flood Risk Management Research Consortium (http://www.floodrisk.org.uk/) came into being, allowing the funding of multi-disciplinary research projects that provide research to support improvements in flood risk management.

These advances in flood management are also reflected by actions of the European Union, who provided legislation that promotes preliminary flood risk assessment, flood hazard maps, flood risk maps and flood risk management plans. All member states, including the UK, are obliged to produce the documents stated above in a given time scale. The period in which the documents should be reviewed is also specified (The European Parliament and the Council of the European Union, 2007).

In order to better understand the problem of flooding it can be analysed from the point of view of systems engineering science. The history of the systems engineering approach can be traced back to the 1940s. Since then it has become an important interdisciplinary field of engineering that focuses on the development and organization of complex systems. The formalized methods of analysing systems have been developed and are being applied to problems in diverse technical disciplines, flood risk analysis and management being one of them. The systems approach is also popular because it allows the problem to be analysed in holistic ways taking into account the complexity not only of the technical or engineering components, but also of the social and environmental interactions, which are especially important in flood management. The flood system can be divided into elements connected to each other by relationships.

Each element and relationship can then be modelled and analysed separately, while interactions can also be taken into account.

In the need to analyse the risks in the flood system the concept of source-pathway-receptor was developed. The sources are represented by meteorological factors such as rainfall, snow-melt, waves and storm surges or surcharging sewer systems in the case of urban floods. The water is then conveyed through pathways, which are represented by the catchment, the floodplain and the infrastructure including flood defences, storage reservoirs etc. Finally, the receptors of food risk are reached – such as people, property and the environment where the economic, social and environmental consequences of flooding occur.

The components of the flood system are affected by various aspects that change in time. The main drivers of change in the flood risk system are economic, social-demographic and climatic.

The scale of the economic impact is given by the value of properties that are at risk of flooding. Some of the Foresight future scenarios predicted growth in economy and investments, which would result in higher number of properties being at the risk of flooding in the future (Hall et al., 2007). In such a case effective flood management measures need to be introduced in the risk-prone areas in order to maintain current levels of the risk of flooding.

The demographics also affects consequences of flooding. The vulnerability to flooding and its impacts depend on socio-demographic properties of the communities living in flood risk areas. The elderly, children and people whose mobility is limited by ill-health or disability are more vulnerable to flooding and are subject to more severe consequences in the case of flooding disasters. The demographic issues on floodplains cannot be easily managed, but certain improvements can be achieved through focus on flood risk awareness and flood warning. The demographic properties of the communities at risk also change in time. Some Foresight scenarios predict increased future floodplain occupancy up to a doubling of the number of people at risk from flooding in 2080 (Green, Penning-Rowsell, 2007).

Socio-economic forces and factors are not drivers of flood risk, because they principally affect receptors, rather than sources. Climate change is on the opposite side of the system primarily affecting the sources of a flood risk system, which in general cannot be managed. According to the Intergovernmental Panel on Climate Change (2007) changes in precipitation and temperature will lead to changes in runoff. Runoff is projected with high confidence to increase by 10 to 40% by mid-century at higher latitudes while the precipitation variability will also increase resulting in seasonal runoff shifts. In the UK, the future changes in precipitation statistics are highly uncertain not only in magnitude, but also in the space and time distribution, which are factors that affect flood wave formation. Reynard (2007) notes that quantifying changes in flooding as a result of climate change remains a major scientific challenge due to an uncertainty cascade associated with the specific aspects of any climate change impact study.

With the increased pressure on flood risk management, the risk in a flood system needs to be assessed. Typically a flood system consists of an urban area defended from the river by an embankment. The source of flooding can be described by a return period, indicating the probability that a certain value (such as flow rate or water level in the river) will be exceeded. Additionally, the performance of flood defences (such as embankment) can be described by a structural reliability curve. Finally, these probability values can be combined and the probability that flood defences would breach can be calculated.

In the case of a flood defence breach water floods the floodplain. The flooding scenario can be modelled and flood characteristics can be calculated. When the probability of a flooding incident is combined with the flood extent information the probability of exceeding a certain water level in a certain location can be quantified. If a damage function relationship between water level and damage is available then the economic consequences of the flood can be estimated. Similar relationships can be derived for non-economic consequences too. At the end of this flood risk assessment procedure the probabilities are connected with consequences enabling flood risk to be quantified.

In a typical flood-defended urban area the flood defence can be divided into tens or hundreds of sections of different reliability properties. Each flood defence section is considered to have two system states – failed or not failed. Therefore, the number of

flood event simulations that need to be assessed is calculated as $2^n$, where $n$ is the number of flood defence sections. The number of necessary flood simulations is of the order of thousands. Currently no numerical modelling technique can deliver all the calculations within a reasonable time scale. The runtime of an inundation model is critical to the runtime of the whole flood risk model. As a result each flood inundation calculation needs to be carried out very quickly in a time of the order of seconds.

The problem of limited time being available for a large number of simulations can be solved by either increasing the computational resources available or by the introduction of new fast flood modelling techniques. Although the power of computers steadily increases over time, the resources required for the application of current two-dimensional numerical models will not be available in the near future. Similarly, advances in computer technology that enable the use of parallel processors in order to share the load on several computational units are of little benefit because the flood inundation process is of a sequential nature, which does not allow such techniques to be exploited efficiently.

This thesis considers the alternative option, i.e. the development and application of a rapid flood model, specifically one that simulates the spreading of a volume of water over a floodplain in order, primarily, to estimate the flood extent and depth of inundation resulting from a breach or overtopping of a flood defence structure in a complex urban area.

The objectives of this thesis are to review currently existing rapid flood modelling techniques, develop computationally efficient yet sufficiently robust volume-based flood spreading algorithm and test its application on artificial terrain as well as on selected floodplain test sites. Additionally, this thesis aims to provide guidance on model application and its suitability for flood risk assessment.

## 1.1 Thesis overview

Following this introduction chapter:

Chapter 2 gives a basic overview of flood modelling techniques ranging from one-dimensional methods to several two-dimensional approaches. The suitability of these models to flood risk assessment applications is discussed. Remotely sensed terrain data are studied next with respect to their usage in flood modelling. Finally, the definition of flood risk and flood hazard is explained as well as how they can be estimated.

Chapter 3 presents the development of the Rapid Flood Inundation Model (RFIM) based on the spreading of a volume of inundation. A flood cell building algorithm and three versions of a fast inundation algorithm are proposed, and the rules that control the flood spreading are demonstrated on an example terrain. The calculation of local velocities is also briefly explained. Lastly the coding structure of the model is presented and input and output files are described.

In Chapter 4, the performance of the model is discussed when applied to a simple artificial topography and to complex urban terrains. First, the ability of the algorithm to mimic two-dimensional spreading of a flood is tested and then different aspects of model behaviour are studied in detail with respect to the test sites, breach locations and magnitudes of flood. The RFIM results are also compared to TUFLOW model predictions obtained using the same boundary conditions. Different types of model irregularities are discussed in detail and solutions are proposed.

Chapter 5 presents the main conclusions drawn from the model tests, and contains suggested recommendations for model improvements.

# 2 Numerical modelling and flood risk assessment of floodplain flows

The prediction of flooding has been the subject of much research over the last few decades. Ever since one-dimensional computational modelling of unsteady flow in channels became an almost routine task by the 1970s and 1980s, there have been several attempts to develop models that also cater for floodplain hydraulics and for main channel – floodplain interaction. Until about 2000, many of these models belonged in one or two categories: quasi-two dimensional models (also known as storage cell models) or two-dimensional models. In the former, the floodplain is represented by a series of inter-connected cells to store water or which may also allow water to spread across the floodplain using standard resistance or weir equations to calculate the flow between cells (Cunge, 1975). With the increasing availability of floodplain digital terrain models over the last 10 years, the storage cell approach has been replaced by two-dimensional models. Two-dimensional models solve the two-dimensional shallow water equations and simulate both mass and momentum conservation (Liggett, 1975b) or alternatively solve simplified flow equations on a raster grid (Bates and De Roo, 2000). The advantages of the one-dimensional concept applied to main channels and the two-dimensional discretization of floodplains have been recently employed in coupled 1D-2D models (Syme, 1991, 2001; Lin et al., 2006). This chapter gives background information on all of these types of modelling techniques, and the use of digital elevation models for flood modelling. The uncertainty associated with numerical models is also discussed and calibration and validation issues of such models are explained.

## 2.1 One-dimensional models

The one-dimensional modelling approach treats the river channel as a set of cross sections perpendicular to the flow direction. The floodplain is treated as an extended river cross-section. The one-dimensional St Venant equations are applied, with conveyance estimated using a uniform flow law. The one-dimensional discretisation is

well suited to parameterisation using traditional surveying methods to obtain channel cross-sectional geometry. Models such as MIKE11 (DHI), ISIS (Halcrow & Wallingford Software, 1997) and HEC-RAS (US Army Corps of Engineers) are examples of commercial one-dimensional models widely used in practice.

The propagation of flood waves is controlled by a mass balance (Eq. 2.1) and by a balance of the various forces contributing to the equation of motion (momentum equation - Eq. 2.2). The basic shallow water theory assumption is that the pressure varies hydrostatically in the vertical. The independent variables are longitudinal distance $x$ and time $t$ and dependent variables are water depth $h$ and volumetric flow rate $Q$. These equations are often referred to as the St Venant equations.

$$\frac{\partial A}{\partial t} + \frac{\partial Q}{\partial x} = 0 \tag{2.1}$$

$$\frac{\partial Q}{\partial t} + \frac{\partial}{\partial x}(uQ) + gA\left(\frac{\partial h}{\partial x} - S_0 + S_f\right) = 0 \tag{2.2}$$

(1) (2) (3) (4) (5)

where $Q$ is the volumetric flow rate in the channel [$m^3/s$], $x$ is the distance along the channel [m], $A$ is the flow cross sectional area [$m^2$], $t$ is the time [s], $h$ is the water depth [m], $u$ is the flow velocity [m/s], $S_0$ is the slope of the channel bed [-], $S_f$ is the friction slope [-] and $g$ is the gravitational acceleration [$m/s^2$]. Derivation of these equations can be found in Cunge et al. (1980).

In the momentum equation (Eq. 2.2), (1) represents local inertia (or acceleration), (2) represent advective inertia, (3) represents the pressure differential, (4) and (5) account for the bed and friction slope respectively.

Term (5) can be represented by the Manning or Chezy equation. The Manning or Chezy friction coefficient in one-dimensional models represents not only river bed roughness, which is its physical meaning, but also higher dimensional phenomena of lateral and vertical flows and turbulence. Normally, the friction coefficient is used as a model calibration parameter, which means that the friction coefficient also accounts for imperfections of the numerical method. As a result, the calibration values of friction

parameters can differ from the physical values related to the material of the river bed (Wallis & Knight, 1984; Shiono & Knight, 1991).

The St Venant equations are hyperbolic partial differential equations and cannot be solved analytically. The primary difficulty in solving them arises because of their nonlinearity. However there are two fundamental numerical solution methods that can be used. Liggett and Cunge (1975a) give more information on the *method of characteristics* and *finite difference methods*. The finite difference methods can be divided into two groups – *explicit* schemes, in which the time step $\Delta t$ and space step $\Delta x$ are restricted by the Courant-Friedrichs-Lewy condition in order to maintain stability of the solution, while *implicit* difference schemes have the advantage of unrestricted $\Delta t$ and $\Delta x$ values. Implicit methods are unconditionally stable, but more complicated solution methods are needed in order to solve the equations at each time step.

To solve the St Venant equations numerically boundary and initial conditions are required to state the relationships between the model domain and its surroundings, and to set up the parameter values at the beginning of the computation, respectively. The initial condition for flow routing in open channels specifies flow depth and velocity or discharge at every computational point along the channel reach before the commencement of the unsteady flow calculation. In terms of discharge it can be expressed as

$$Q(x,0) \qquad \text{(Eq. 2.3)}$$

where the first argument refers to the distance coordinate and the second refers to the time coordinate. The boundary conditions are expressed at the upstream and downstream ends of the model domain. In the case of the full dynamic momentum equation or the diffusion approximation both upstream and downstream boundary conditions are needed. The upstream boundary condition can be expressed in terms of discharge or flow depth (Eq. 2.4).

$$Q(0,t) \quad \text{or} \quad h(0,t) \qquad \text{(Eq. 2.4)}$$

Similarly, the downstream boundary condition can be expressed as:

$$Q(L,t) \quad \text{or} \quad h(L,t) \quad \text{or} \quad Q(L,h) \qquad \text{(Eq. 2.5)}$$

where L is the length of the river reach and Q(L,h) is the relationship in which downstream flow rate is expressed as a function of water level. For supercritical flow the conditions need to be satisfied only at the upstream boundary.

The continuity and momentum equations are applied to the discretized channel forming a large set of non-linear equations. The number of equations depends on the size of the model – two equations describe relationships at each node (cross section) plus two equations are needed at each boundary. The model can consist of several thousands of nodes and at each time step the set of equations needs to be solved either by an explicit method (nodes treated sequentially) or by an implicit approach (nodes treated simultaneously) (Cunge et al., 1980). For the latter a diagonal matrix often ensues, which is easily solved using a standard method. Non-linearities in the equations are dealt with by iteration within time steps normally using the Newton-Raphson method (Cunge et al., 1980). In the case of branched or looped channel networks the matrix becomes more complicated (the matrix is largely empty, however), but powerful methods have been developed for its solution (Evans et al., 2007).

The St Venant equation system is of a hyperbolic nature, which arises from the presence of advective acceleration and local acceleration terms. Either in the search for analytical solutions (which are available only under very simplified conditions (Ponce & Simons, 1977)) or to simplify numerical solution, practitioners have sought to simplify the full St Venant equations and to use zero-inertia approaches whenever justified by the physical conditions (Cunge et al., 1980, Hunter et al., 2007).

### *2.1.1 Simplified channel flow equations*

The simplifications focus on neglecting one or more terms in the momentum equation (Eq. 2.2). The momentum equation expresses the balance of momentum sources and sinks for the computational element. The diffusion model assumes that the inertia terms (*1* and *2*) in Eq. 2.2 are negligible compared with the pressure (*3*), gravity (*4*) and friction (*5*) terms. The kinematic model assumes an even more simplified situation by neglecting also the pressure term (*3*) resulting only in a balance of gravity and friction

forces in the momentum equation. Although approximate, both the kinematic and diffusion models have been shown to be fairly good descriptions of the physical phenomenon in a variety of cases. Validity criteria for the kinematic and diffusive wave approximations were derived by Ponce et al. (1978).

The kinematic model, generally, cannot describe the subsidence of the flood wave and backwater effects, because of the missing pressure term (*3*), and fails when the neglect of the pressure term is not justified. Additionally, the kinematic model does not allow for physical attenuation, thus it will be valid only when no attenuation is present. The attenuation often observed in numerical solutions of the kinematic model is of an artificial nature (numerical damping).

The diffusion model applies to a wider range of slopes and flood wave periods than the kinematic model, with the added advantage that it allows for physical attenuation by neglecting only the inertia terms. As the diffusion approximation is able to represent backwater effects, it requires both upstream and downstream boundary conditions (Cunge et al., 1980).

Ponce & Simons (1977) and Ponce et al. (1978) state that for most applications the diffusive models are able to simulate the physical phenomena with sufficient accuracy. However, the bed slope and the flood wave period determine the range of their applicability.

### *2.1.2 Limitations of one-dimensional models*

Although one-dimensional models have been successfully used in practice, some complications are associated with their use on natural rivers. Cross-section locations have to be chosen with care in order to represent the terrain correctly (Samuels, 1990) and a skilled modeller is required for such a task. Each cross-section can be divided into panels in order to account for the variability of the velocity field and the roughness across the watercourse width (e.g. a panel representing the left floodplain, a panel representing the main channel and a panel representing the right floodplain). Each of the panels can be assigned a different roughness coefficient. The resistance equation is then

applied separately to each panel and the panel conveyance values are summed to obtain the cross-section value.

Although the St. Venant equations have been confirmed by *experimental work*, their use to simulate *natural rivers* is subject to several complications. In most cases the natural river flow is curvilinear, meandering within valley limits and the two- and three-dimensional nature of the flow processes may not be well represented by cross sections that are separated by hundreds of meters. Additionally, during floods water spills over bank and inundates floodplains, forming new flow paths that may not be well described by the lateral extension of the main channel cross section. Although the one-dimensional approximation to river hydraulics is limited by the assumptions and issues mentioned above, one-dimensional models are computationally efficient and have been proved to produce useful predictions in cases when these assumptions are met.

## 2.2 Two-dimensional models

Similarly to one-dimensional models, two-dimensional modelling methods are based on governing shallow water equations – a continuity equation (Eq. 2.6) and two momentum equations (Eq. 2.7 and Eq. 2.8) in x- and y-directions (direction of motion) (Liggett, 1975b). Equations 2.6 – 2.8 can be viewed as an extension of the one-dimensional equations (Eq. 2.1 – Eq. 2.2) into a second dimension:

$$\frac{\partial h}{\partial t}+\frac{\partial}{\partial x}(Uh)+\frac{\partial}{\partial y}(Vh)=0 \qquad \text{(Eq. 2.6)}$$

$$\frac{\partial U}{\partial t}+U\frac{\partial U}{\partial x}+V\frac{\partial U}{\partial y}+g\frac{\partial h}{\partial x}=g\left(S_x-S_{fx}\right) \qquad \text{(Eq. 2.7)}$$

$$\frac{\partial V}{\partial t}+U\frac{\partial V}{\partial x}+V\frac{\partial V}{\partial y}+g\frac{\partial h}{\partial x}=g\left(S_y-S_{fy}\right) \qquad \text{(Eq. 2.8)}$$

where U, V denote the Cartesian mean velocity in the x- and y-directions respectively [m/s], h is the water depth, $S_x$ and $S_y$ are the slopes of the bed in the x- and y-directions [-] and $S_{fy}$ and $S_{fx}$ are the friction slopes [-], usually represented by empirical friction formula. Models solving full shallow water equations are referred to as two-dimensional hydrodynamic models. Terms accounting for Coriolis force, wind stress, infiltration or

turbulence can also be added to the equations. In equations Eq. 2.6 – Eq. 2.8 the vertical dimension is suppressed as all quantities are depth-averaged.

Numerous classes of two-dimensional models have been developed. The majority of the numerical methods used to solve the shallow water equations fall into three categories as regards the space discretisation – finite difference, finite volume and finite element methods.

TUFLOW (Syme, 1991, 2001) and DIVAST (Falconer, 1986) models are examples of the most widely used finite difference approach. Both solve the full two-dimensional shallow-water equations using a form of alternating direction implicit (ADI) solver.

TELEMAC-2D (Hervouet and Petitjean, 1999), which was developed by Electricité de France, is an example of the application of the two-dimensional finite element method. It uses an unstructured mesh of triangular finite elements, on which the variables are defined.

The comparisons of two-dimensional modelling techniques have been published. Horritt and Bates (2001a) compared TELEMAC-2D with the raster-based model LISFLOOD-FP (presented in section 2.5) predictions and concluded that both models performed to a similar level of accuracy.

Another comparison was carried out by Wicks et al. (2004), who tested ISIS Flow (quasi-2D flood cell code), LISFLOOD-FP, TUFLOW and TELEMAC-2D models on the Greenwich embayment on the River Thames. It was concluded that surprisingly the ISIS Flow and TUFLOW predicted similar maximum flood extent maps, while LISFLOOD-FP and TELEMAC-2D showed slightly different predictions.

Up to date the most detailed benchmark testing of two-dimensional models is that published by Hunter et al. (2008), who tested six models – DIVAST, DIVAST-TVD, TUFLOW, JFLOW, TRENT and LISFLOOD-FP on an urban catchment in Glasgow. All models performed similarly with only minor differences. Some produced oscillatory water level behaviour, which did not affect the general flood propagation throughout the floodplain. It was concluded that the uncertainty over boundary conditions may be more

important than the process representation (hydraulic complexity) of the model. It was also found that the minor differences between models could easily be subsumed within parameter optimisation, particularly given uncertainties in terrain and boundary condition data.

Some of the two-dimensional finite difference modelling approaches are applied in a package with one-dimensional calculation of the flow in the river main channel. There are several ways in which these two submodels can be merged together and these are described in section 2.3.

Although two-dimensional models are being used in both research and practise, simplifications similar to those related to one-dimensional models (section 2.1.2) have been proposed and tested in order to use more economically the rather limited computational resources, enabling more runs to be done within a limited time. Two-dimensional models are usually simplified in terms of a decrease in complexity of the flow description or a decrease in the scale of the terrain representation.

Two-dimensional models require more detailed input data due to their two-dimensional space discretisation. Currently used remote sensing techniques are capable of providing modellers with the detailed floodplain topography description (section 2.9). The accuracy of the digital elevation model is crucial to the ability of two-dimensional models to correctly predict flow (Néelz and Pender, 2006). The remotely sensed data can also give information on the land use, from which the spatially distributed parameters, such as friction coefficient values can be derived. Wilson and Atkinson (2003) estimated friction coefficients from a Landsat TM image and tested the sensitivity of predictions to spatially distributed friction. They concluded that the effect of distributed friction on the flood wave is small when compared to uncertainties associated with underlying terrain elevation.

In practice the friction coefficient is used as calibration parameter, which means that the optimum value found by calibration may not be the same as the physical friction of floodplain (for example Hunter et al, 2005).

## 2.3 Coupled 1D-2D models

The idea of coupling one-dimensional and two-dimensional models aims to combine the advantages of both systems in order to increase the accuracy of the model. A one-dimensional representation of a river channel is computationally efficient and is capable of dealing with structures, while a two-dimensional approach is able to capture two-dimensional nature of floodplain flow. As a result, elements of a one-dimensional nature – pipes and channels - are modelled using a one-dimensional discretisation, while the overland flow on floodplains is calculated by two-dimensional methods. The one-dimensional and two-dimensional models can be integrated in two ways – with interfaces defined along vertical or horizontal planes.

Coupling along vertical planes fully separates the main channel modelled in one-dimension and the floodplains modelled in two-dimensions. In a model coupled along a horizontal plane, two-dimensional grid cells are placed above the one-dimensional main channel with the border being at the bank full level. In this schematization, the St Venant equations are applied only up to riverbank level and the flow above is calculated by the two-dimensional scheme. In cases when the main channel width is smaller than the grid size of the two-dimensional domain, the horizontal plane connection is preferred.

Another crucial point in 1D-2D models is the treatment of the border between the one-dimensional and two-dimensional domains. It has been recognized that the correct estimation of bankfull flow is very important for correct floodplain inundation predictions regardless of the type of model used. When the estimation of bankfull discharge is correct then the inundated area will also be approximately correct (Horritt and Bates, 2001b). The better the description of the flow field along the 1D-2D link (more complicated in terms of hydraulic processes that are taken into account), the better are the results obtained (Liang et al., 2007). Many coupled 1D-2D models take into account only a mass transfer interaction between the main channel and the floodplain, but Liang et al. (2007) showed that the predictions are more realistic when the momentum transfer was also included, although this can have an adverse impact on model stability.

There are two ways of coupled model development – either by programming an interface for already available one-dimensional and two-dimensional codes or by programming a software package that includes both. An example of the former is a linkage of ISIS and DIVAST models that take account of both mass and momentum transfer, described in Lin et al. (2006) and Liang et al. (2007); examples of the latter are TUFLOW (Syme, 1991, 2001) or Delft-1D2D (Frank et al., 2001).

TUFLOW (Syme, 1991, 2001) is a two-dimensional finite difference model that uses the alternating direction implicit (ADI) scheme solving the full two-dimensional shallow water equations. This is coupled with an explicit finite difference scheme solving the full one-dimensional flow equations. Such a combination is capable of capturing rapid wetting and drying of flooded areas, achieving effective modelling of hydraulic structures and treating levees and embankments. TUFLOW has been tested in urban area case studies and was shown to perform well compared to other numerical codes (e.g. Wicks et al, 2004; Hunter et al., 2008).

Coupled 1D-2D models have proved to be successfully applicable in many inundation prediction studies, however, their suitability for flood risk assessment application is limited by their relatively long run time requirements.

## 2.4 Storage cell models

Storage cell models are referred to as quasi two-dimensional models because they account for the two-dimensional nature of floodplain flow, but do not discretize the terrain as a two-dimensional computational grid, but instead treat floodplains as a system of flood storage cells. Each cell communicates with the neighbouring cells through local one-dimensional relationships (Cunge, 1975; Cunge, Holly, Verwey 1980). It was hypothesised that floodplain flows are primarily influenced by bed roughness rather than topographically induced velocity gradients, allowing the inertial terms to be dropped from the shallow water equations (Cunge, Holly, Verwey, 1980). The kinematic approximation is introduced to the model through relationships between flood cells.

In order to allow the model to predict the flooding pattern on the floodplain the flood cells need to be correctly recognized by the modeller who has to be familiar with flooding in the concerned area. Maps of spatial extent of recent floods can produce an invaluable insight to this problem by revealing the natural system of flood compartments as was demonstrated by Timbe & Willems (2004).

The area $A_i$ of each cell $i$ is defined by a water level $y_i$ in the cell and by natural borders, such as dykes, roads, banks, etc. It is assumed that the water level surface is horizontal within the cell and the discharge exchanges between adjacent cells are a function of these free surface elevations. The change in volume stored in a flood cell is described as a sum of inflows to and outflows from the cell:

$$A_{s_i}(y_i)\frac{dy_i}{dt} = \sum_k Q_{i,k} \qquad \text{(Eq. 2.9)}$$

where $A_s(y_i)$ is the free surface area in the flood cell $i$ and $\sum_k Q_{i,k}$ is the flow balance between flood cell $i$ and adjacent cells $k$. It is assumed that the change in free surface area over a time step $\left(\frac{\partial A_{s_i}}{\partial y_i}\Delta y_i\right)$ is small compared to the free surface area $A_{s_i}$.

The flow exchange relationship between adjacent cells are considered as being one-dimensional and can be of two types: (1) river links where there are no obstacles to flow and a mean roughness coefficient can be applied (head loss is uniform along the pathway), and (2) weir type losses, where a road or embankment forms the border and head loss is restricted to a short pathway length. In the case of river type links a uniform flow formula is used – Strickler's or Manning's equation with friction represented by the respective resistance coefficient. For weir type links, standard broad-crested weir relationships are used.

The quasi two-dimensional approach was first successfully applied in practice by Zanobetti et al. (1970), who built a flood model of the Mekong Delta in order to assess proposed flood mitigation measures. This large-scale mathematical model consisted of 300 flood cells covering an area of 50 000 km$^2$. The flood cells were arranged in the

form of mesh groups forming a parabolic system of finite difference equations that replaced the differential equations. An unconditionally stable implicit numerical scheme was used in order to avoid a small time step and to decrease the computational time. The extended form of a double sweep method was used to solve the system of equations, using newly emerging computers. The application of the model in the scale of the Mekong Delta project showed the feasibility of using the flood cell approach in practice.

Since the 1970s, the quasi-two dimensional approach has been applied in software packages used by practitioners. Mike 11 (DHI), ISIS (Halcrow and Wallingford Software) and HEC-RAS (US Army Corps of Engineers) are examples of software that use this approach. In all these models, a one-dimensional model ranging from kinematic to fully dynamic is applied in the main channel, and the floodplain is connected to the main channel by similar relationship to those between individual flood cells. Individual flow rates between main channel and floodplain cells therefore depend on difference in water levels.

The quasi-2D storage cell approach combines reasonable run time with accuracy as shown by Wicks (2004) on the Greenwich embayment study site. The benchmarking reported surprising similarity in predictions of flood extent calculated by the flood cell version of ISIS and the hydrodynamic two-dimensional model TUFLOW.

## 2.5 Raster-based models

The flood cell size used in raster-based models is defined by the Digital Elevation Model (DEM) resolution and each floodplain pixel in the grid is treated as an individual storage cell, with inter-cell fluxes, calculated by uniform flow formulae, similar to quasi-2D approach. The complexity of the hydraulic processes is sacrificed in favour of higher calculation speed. On the other hand, however, a higher topograpic resolution (larger number of ‘raster flood cells’) results in a longer run-time.

LISFLOOD-FP consists of a one-dimensional kinematic wave approximation to channel flow, solved by an explicit finite difference scheme, and a two-dimensional representation of floodplain flow (De Roo et al., 2000; Bates & De Roo, 2000; Horritt and Bates, 2001a) calculated using an analytical flow equation.

The response of LISFLOOD-FP to a change of the DEM resolution on the River Severn was studied by Horritt and Bates (2001b). Model resolution varied from 1000 m to 10 m and predictions were compared with satellite observations of the inundated area and with ground measurements of the flood wave travel time. The expected increase in the quality of the predictions was found only down to a resolution of 100 m, and the use of higher resolution data, surprisingly, did not lead to improved flood extent predictions.

Fewtrell (2007) tested the response of LISFLOOD-FP predictions to spatial grid coarsening, but in more complicated terrain in an urban area. It was reported that the performance of the model decreases with larger DEM grid sizes. Two methods of spatial coarsening were tested – one in which buildings and ground elevations are coarsened together as one layer compared to one when the ground layer is coarsened separately and added to an unchanged building layer. The latter method showed better predictions of flood extent by preserving the important details in the buildings layer. However, the comparison to a high-resolution simulation showed that some important detail in the ground layer was lost.

Horritt and Bates (2002) tested the sensitivity of LISFLOOD-FP, HEC-RAS and Telemac-2D to friction. Two values of the Manning coefficient were tested – one representing the main channel and one representing the floodplain. The model was more sensitive to main channel friction, as the main channel friction affects the amount of water that spills over to the floodplain. The optimum values of the friction parameter used in LISFLOOD-FP were found to be unrelated to the friction coefficient that represents the modelled surface.

In some LISFLOOD-FP applications, saw-tooth oscillations in the solution were encountered (Horritt and Bates, 2001a,b), resulting in the need to use small time steps, which significantly increased the run time. This problem originates from the mass exchange between the adjacent flood cells. If the water level difference in these cells is too small compared to the volume exchanges during one time step (especially in cells located on the border between channel and floodplain), the ratio of the water levels in these cells tends to oscillate and the solution becomes highly dependant on the ratio of grid size and time step. In the original LISFLOOD-FP the time step was selected by the user, and a process of trial and error was required in order to achieve a non-oscilatory

solution. In order to avoid oscillations, a flow limiter was introduced in areas of very deep water, by setting a maximum flow between cells to ensure that the change in depth is not high enough to cause a reverse of flow in the next time step. The application of the flow limiter led to increased sensitivity of floodplain flows to grid cell size and to time step.

Hunter et al. (2005) proposed an alternative approach by introducing an adaptive time step algorithm in order to better use computing resources while maintaining stability. The algorithm was analogous to the Courant-Friedrichs-Lewy condition for advective flows (Cunge, Holly, Verwey, 1980). A von Neumann stability analysis yielded a time step that is controlled by the grid spacing ($\Delta x$) and the depth available for the flow ($h_{flow}$). The calculated time step changed during the course of a simulation, but was fixed in space at each time step.

The performance of adaptive time stepping in LISFLOOD-FP was successfully tested and simulations compared favourably (Hunter et al., 2005) to analytical solutions and real world data. Solutions were also independent of grid size and choice of time step. The revised LISFLOOD-FP comes at a higher computational cost, however, especially when applied to high resolution DEMs. Its run time is much longer than that suitable for flood risk studies.

## 2.6 Rapid inundation methods

No precise definition of the term 'rapid inundation model' exists, but, generally, it denotes a method that can produce a flood inundation prediction in a timescale of the order of seconds. It was explained above that the speed of calculation of flood models can be increased by coarsening the spatial resolution and/or by increasing the time step. But even such measures do not lead to a performance fast enough to meet the time requirements for application in a flood risk analysis framework. Although computer technology advances in terms of the increase of processors' speed and the developments in applications of multiple computational units, however, such improvements do not suffice to allow full or simplified hydrodynamic models to be used in flood risk analysis.

The use of parallel processors in flood modelling using LISFLOOD was studied by Neil (2008). It was showed that this model represents floodplain inundation process in sequential steps, which does not allow parallel techniques to be exploited efficiently. According to Amdahl's law (Wikipedia, 2008) the maximum expected speed-up obtained by parallelisation is limited by the percentage of processes that can be parallelized and by the number of computational units. However, the number of computational units higher than a certain threshold would not further decrease the run-time. Neil (2008) reported a decrease of run-time of the LISFLOOD model when run on a multi-core processor concluding that 4 cores decrease the model run-time to a third. It was also found that larger computational domains, in terms of the number of pixels, give higher speed-up. Although these findings are relatively promising the run-time of hydrodynamic or raster-based models is still not sufficient for flood risk analysis, even if the parallel computational units are used. Faster and less complex modelling techniques are therefore required.

Currently available GIS software packages can be applied in a flood extent calculation for the purpose of flood risk analysis, but no development of realistic rapid flood spreading has been reported, owing to the fact that the GIS programming environment is not suitable for such task. A very simple flood extent estimation GIS technique was used by Horritt and Bates (2001a) in order to test whether a flooding at the test site was not of a trivial nature. The floodplain was treated as a single flood cell, the volume of water was allowed to fill all the depressions and the flood extent was derived as an intersection of the water level with the DEM. The main disadvantage of this approach was that the water level was considered horizontal throughout the whole floodplain and the local depressions, which were not hydraulically connected to the main inundation, were predicted as flooded.

A rapid GIS-geomorphological routing model was studied by Lhomme et al. (2004). The model was developed to simulate urban stormwater runoff as an alternative to physically based models. Rainfall was routed downstream along pathways by means of a lag and route model in order to estimate the hydrograph at the outlet of the catchment using information present in DTM. The rainfall at a given cell in the domain produced an elementary hydrograph at the outlet. The elementary hydrographs of all cells were

then added in time and space and produced complete hydrograph at the outlet. It was shown that this model can lead to accurate simulations while requiring shorter set-up time compared to physically based models. Although this model simulates stormwater runoff and cannot be applied to fluvial flooding it demonstrates the benefits of automated application of DTM analysis in order to route water over the terrain.

Although the volume-based approach to rapid flood inundation, which is considered in this research, has been used in the past (Beven, 2007), it has not been widely studied due to the lack of high-resolution spatially distributed topographic data and the fact that the flood risk assessment approach to flood risk management has only recently been adopted in the UK.

## 2.7 Model uncertainty

Numerical models are inevitably an incomplete representation of reality producing predictions that are always uncertain to some extent. The awareness and understanding of this uncertainty and its quantification can bring insight into the real predicting capabilities of the model.

*Uncertainty is a general concept that reflects the lack of sureness about something, ranging from just a sort of complete sureness to an almost complete lack of conviction about an outcome (Sayers et al., 2002c).*

From the general point of view the whole decision making process in the area of flood risk suffers with uncertainty. According to Samuels (2006) the uncertainties associated with estimation of flood risk can be divided into three categories - our lack of knowledge of the behaviour of the physical world (knowledge uncertainty), its inherent variability (natural variability) and the complexity of our social values and objectives (decision uncertainty).

- Uncertainty that arises from model approximation to physical processes, inaccuracies of input data, parameter estimation and inaccuracies of numerical methods is referred to as **knowledge uncertainty**. Further research and

development of more accurate mathematical and numerical methods can lead to reducing knowledge uncertainty.

- **Natural variability** of climate, weather and rainfall in particular, is responsible for uncertainty that cannot be reduced. Probability distributions are used to provide estimates of the likelihood of occurrences of events outside the range of gathered data. Magnitudes of flood events are usually referred to in return periods, which give us an idea about past probability of flood event occurrence, but can with no certainty predict its next occurrence.

- **Decision uncertainty** is a state of rational doubt as to what to do. There is always an uncertainty surrounding the selection of a particular course of action. Realizing that there is uncertainty in decision making can lead to selecting better options.

From the numerical model point of view three types of uncertainties can be defined (Willems, 2000; cited from Timbe & Willems, 2004; FloodRiskNet, 2007):

- **Input uncertainties** – are defined by measurement errors (if the model input is directly measured) or estimation errors (if the input is estimated). Floodplain geometry errors, initial and boundary conditions errors also contribute to input uncertainties.

- **Parameter uncertainties** – similarly to input uncertainties, these can consist of measurement or estimation errors. The effective values of parameters required by a model may be dependent on model implementation and boundary conditions. Parameters may also change with the resolution of the model.

- **Model structure uncertainties** – represent the modeller's limitations in describing physical reality perfectly. They depend on the modeller's choice between a number of different conceptual models of the processes involved (sections 2.1-2.6). Additional uncertainty is introduced by the numerical methods that approximate the partial differential equations. The model structure

uncertainties can be considered as the remaining uncertainties after the use of error-free input and after an optimal calibration.

Apart from the uncertainties mentioned above there are also errors involved in the calibration and validation process. The observed datasets used as a comparison are also subject to uncertainty. Calibrating a model to an erroneous dataset will certainly lead to errors, while the validation of the model against an erroneous dataset will not lead to correct assessment of the model performance.

The type of model should be chosen wisely with regard to minimizing the uncertainty. Selection of a more complex model will minimize the model structure uncertainties, but additional complexity will increase parameter requirements and the uncertainty associated with them. In such cases the output from a more complex model can become more uncertain than the result obtained from a simpler model.

The input and parameter uncertainties are affected by the spatial resolution of the model. The models are generally sensitive to the spatial resolution of input data, while the parameter uncertainty is very often affected by the fact that the parameters cannot be measured at the required resolution.

The model structure uncertainty may be affected by their nonlinearity to a great extent. The flood wave movement problem is nonlinear and the numerical models try to account for it with greater or lesser success. Beven (2001) refers to the research in the area of nonlinear dynamics, which suggests that where there is even a slight error in the behaviour of an approximate model of a (known) system, the model will not be able to reproduce correctly the extremes of the distribution of the output variables either for short time scales or for integrated outputs over long time scales. Such a categorical statement on the general behaviour of models raises awareness about whether they really can replicate the behaviour of a nonlinear system.

When carrying out the analysis and quantification of the uncertainty of the model output the individual input uncertainties need to be combined. It can be done by a calculation or, in the case of more complex model relationships, by simulation.

The general propagation of uncertainty of input variables can be calculated by:

$$R = R(x, y, z) \qquad \text{(Eq. 2.10)}$$

where $R$ equals the response of interest and $x$, $y$ and $z$ are the variables upon which $R$ depends. In case of normally distributed and uncorrelated variables the uncertainty of the response can be calculated by:

$$R_{unc} = \sqrt{\left[\left(\frac{\partial R}{\partial x}\right)x_{unc}\right]^2 + \left[\left(\frac{\partial R}{\partial y}\right)y_{unc}\right]^2 + \left[\left(\frac{\partial R}{\partial z}\right)z_{unc}\right]^2} \qquad \text{(Eq. 2.11)}$$

where the partial derivatives reflect the relative importance of each of the input variables on the response variable, whilst the $_{unc}$ terms reflect the relative uncertainties in the input variables.

In complex models, the application of Eq. 2.11 becomes difficult and the error propagation needs to be obtained by simulation. For the simulation approach the input uncertainties are represented as probability distributions, which are combined to provide an output probability distribution. Monte Carlo methodology is a typical example used for simulating error propagation through a model. The Monte Carlo approach investigates a model by randomly generating many combinations of input variables and observing the changes in the output. It can take account of any distribution and correlation between variables and can include all sources of uncertainty. The computational resources requirements pose the only disadvantage (FloodRiskNet, 2007).

## 2.8 Model calibration and validation

For the reason of uncertainty in model predictions and regardless of their internal complexity, spatially-distributed flood inundation models require verification and independent calibration-validation to assess and establish the quality of predictions and to estimate model parameters. In some cases there are ways of estimating the parameters derived from their physical meaning (e.g. floodplain friction may be estimated from

land cover data), but in most cases robust calibration becomes the only way of reducing uncertainty in model predictions.

The terms verification, calibration and validation have been defined by Refsgaard (2001) and Hunter et al. (2007). In general, they refer to:

- ***Verification***: Code verification involves comparison of the numerical solution generated by the code with one or more analytical solutions or with other numerical solutions. Verification ensures that the computer program accurately solves the equations that constitute the discretized system.

- ***Model calibration*** is defined as the procedure of adjusting the parameter values of a model to reproduce the response of a system under study within the range of accuracy specified in the performance criteria. In the calibration process the parameter sets that lead to the best representation of the measured data are identified. The aim of the model calibration is to assess and constrain model uncertainty.

- ***Model validation*** is defined as the process of demonstrating that a given site-specific model is capable of making accurate predictions, defined with respect to the application in mind, for events or periods outside a calibration scenario. A model is said to be validated if its accuracy and predictive capability in the validation phase have been proven to lie within acceptable limits of errors for a particular practical purpose.

A model can be calibrated in a traditional way by seeking a single value of any parameter that optimises the numerical value of an *objective function* that assesses the agreement between simulated and observed data. Such an approach does not account for the intercorrelation between parameters, for autocorrelation or for insensitive parameters (Beven and Binley, 1992). It also does not take account of equifinality when local minima, valleys and plateaux in the parameter response surface exist.

The equifinality, defined by Beven (1993, cited from Beven, 2001; Romanowicz et al, 1996), is the concept stating that the same or very similar quality of predictions

(measured by some objective function) can be obtained for different parameter sets. In other words equally acceptable parameter sets exist that might be found in very different parts of the parameter space, as was shown for example by Aronica et al. (1998). This may apply also to predictions obtained from a perfect numerical model with no model structure uncertainties.

To overcome this complication, sets of parameters rather than single parameter values should be assessed. Beven and Binley (1992) outlined the following premise:

*It is suggested that because all model structures must, to some extent, be in error and that all observations and measurements on which model calibration is based must also be subject to error, then there is no reason to expect that any one set of parameter values will represent a true parameter set (within some particular model structure) to be found by some calibration procedure. Rather, it is suggested that it is only possible to make an assessment of the likelihood or possibility of a particular parameter set being an acceptable simulator of the system.*

A concept of generalised likelihood uncertainty estimation methodology (GLUE) (Beven and Binley, 1992; Romanowicz et al., 1994; Romanowicz et al., 1996; Romanowicz and Beven, 2003) was developed in order to account for the above premise. GLUE transforms the problem into a search for parameter sets, which would give reliable simulations for a wide range of model inputs. There is no requirement to maximize (or minimize) any objective function, but, information about the performance of different parameter sets is derived from some index of goodness of fit (likelihood measure). GLUE allows for multiple high likelihood areas in the parameter space to be identified.

GLUE requirements (Beven and Binley, 1992) are:

- An appropriate definition of the initial range and distribution of parameter values.

- A formal definition of a likelihood measure.

- A procedure for using likelihood weights in uncertainty estimation.

- A procedure for updating likelihood weights recursively as new data become available.

Initially a sample of feasible models of the system defined by the range of the parameter space is generated. This requires that the modeller decides on the boundaries of the parameter space and also on the parameter distribution function within that range (prior distribution of the parameters). The chosen range should be wide enough to encompass the expected response of the model. In the case of little prior knowledge the uniform distribution function would be appropriate. The assumption of a uniform prior distribution is unlikely to prove critical, because as soon as the distribution of calculated (posterior) likelihood values is calculated this should dominate the uniform prior distribution.

Each model (parameter set) is then assigned a likelihood of being a simulator of the system. The likelihood of a model may be zero when it is considered that the set of parameter values gives a behaviour that is not characteristic of the system. The sum of all model likelihoods is 1. The evaluation (likelihood function) is based on a comparison between observed and predicted values. Any interaction between the parameters is not a problem in the GLUE procedure; it will be implicitly reflected in the likelihood values.

The choice of likelihood function is determined by the objectives of the modelling. There are many objective functions that could be used, including the sum of square errors or the sum of absolute errors between modelled and observed data at points where both data are available. More specific likelihood functions have been tested in flood modelling, such as a *measure of fit* between the spatial raster-defined extent of simulated and predicted flood (Horritt and Bates, 2001b; Bates et al., 2004). The selection of the likelihood function is subjective but should reflect the observations available as well as the purposes for which the model is used.

The simulations with the likelihood measure significantly greater than zero may be retained and the others rejected as nonbehavioral. The likelihood values are then

rescaled such that the sum of all the likelihood values equals one, which yields the distribution function for the parameter sets.

The likelihood value associated with the set of parameter values reflects the degree of belief of the modeller that a set of parameter values are a simulator of the system. That degree of belief may be carried over to the predicted variables – each predicted variable will be associated with the likelihood as a probabilistic weighting function. This allows assessment of the uncertainty associated with the predictions – the results of the individual simulations may be ranked in order of magnitude and, using the likelihood weights associated with each run, a distribution function of the predicted values may be calculated. Then the parameters of this distribution may be determined, such as the weighted mean and centroid values or selected quantiles.

## 2.9 Remotely sensed data to support flood inundation modelling

The quality of terrain description is fundamental to flood inundation modelling and the ability of the digital terrain model construction technique to capture all the key features of the terrain is crucial. Digital terrain models (DTM) usually take the form of a digital surface model of a real ground surface in the form of a matrix of square grid cells with the mean cell elevation stored in a two dimensional array (Smith et al., 2005).

Smith et al. (2005) also gives three concepts of terrain description:

*A Digital Surface Model (DSM) is a representation of any surface by using three-dimensional (3D) coordinates, normally X, Y, Z Cartesian coordinates. The surface might be part of a small object or it may be a very large object such as the earth. A Digital Elevation Model (DEM) specifically relates to the elevation and therefore height, and so will be defined as a DSM of the Earth's surface. It is used generically to define the ground surface, also called a Digital Terrain Model (DTM), plus the tops of features above the ground surface such as man-made structures and vegetation. The process of eliminating non-ground points from a DEM to obtain a DTM is often referred to as filtering or stripping.*

For the purpose of this study the term Digital Elevation Model (DEM) will be used as the urban test case datasets cover elevations of both the earth's surface and man-made objects.

### *2.9.1 Construction and further processing of remotely sensed data*

A Digital Elevation Model (DEM) is a raster map of the terrain, which is divided into small cell elements - pixels. Each pixel is described by a value of terrain elevation. Lidar (**Li**ght **D**etection **a**nd **R**anging) and SAR (**S**ynthetic **A**perture **R**adar) airborne scanning techniques have been successfully applied in flood inundation modelling to collect such data. Lidar is widely used to produce extensive datasets of digital terrain maps while SAR is used to generate accurate maps of inundation extent of past flood events. Aerial photography of flood events can also be used to validate models.

**Lidar** is an airborne scanning technique, which uses a laser to measure the distance between an aircraft and the ground. It can rapidly generate high-density, high-accuracy, geo-referenced digital elevation data. The accuracy of Lidar data depends on the elevation of the overflight, delivering higher accuracy data from lower altitude flights. Lidar data can typically be collected at ~ 0.25-3.0 m horizontal resolution with a vertical accuracy of $\pm$ 0.05-0.25 m (Smith et al., 2005).

Lidar is based on the combination of three different data collection tools: a laser scanner mounted on an aircraft: a Global Positioning System (GPS) providing the laser sensor position; and an Inertial Navigation System (INS) or Inertial Measurement Unit (IMU) providing the orientation of the aircraft (Neélz & Pender, 2006). The laser provides light pulses directed towards the ground. Each laser pulse is reflected by the ground or by objects above the ground. In some cases multiple returns from the same laser pulse can be recorded (for example several layers of vegetation and ground cover). Each laser return provides a measured distance, which is then combined with simultaneous INS and GPS measurements to provide georeferenced 'raw' Lidar data points.

The raw data collected by Lidar have to be processed to correct erroneous topographic features caused by false reflection of the signal. The most problematic areas are where

trees or hedges cover land surface and give more than one signal reflection. In such cases the last reflection is selected as being representative of the terrain surface.

Lidar is capable of producing high height accuracy models when compared to other airborne DEM techniques. It can generate a DEM of a surface with little or no texture. The errors in Lidar originate from inaccurate set-up of the measurement unit or atmospheric delay on laser pulse. Although Lidar works during both day and night it cannot work in certain weather conditions (strong winds, fog or clouds). Lidar also cannot penetrate a water surface and hence cannot collect the river channel elevation data.

**SAR** is a class of active radar systems used for flood extent mapping. SAR systems can be mounted on both satellite and airborne platforms. The latter have significant advantages in terms of resolution and accuracy. Radarsat sensors have repeat times of the order of 10-35 days and resolution of ~ 12.5 m. Airborne SAR systems are capable of much higher resolution (0.5-1 m pixel size), at sampling rates of up to ~500 $km^2$ per hour (Neélz et al., 2006).

SAR images can be taken through the clouds both day and night. The main limitation of SAR imagery is the inaccuracies of height data in water body regions and within the vicinity of bright targets (unlike Lidar). The accuracy can also be decreased by a presence of tree cover.

SAR images also need to be processed before they can be used for model validation. SAR technology is able to distinguish the type of terrain surface by assessing the nature of the returned signal. A map built of such a signal needs to be geo-corrected and then processed to yield flood outlines using a statistical active contour algorithm ('snake'), for example the one developed by Horritt (1999), capable of segmenting the radar image into wet and dry zones to an accuracy of ~ 1 pixel. The snake algorithm can have difficulties with recognizing the flooded shoreline in urban areas due to overly complex radar returns from buildings and other features, as was reported by Neélz et al. (2006).

### *2.9.2 Application of remotely sensed data*

Remotely sensed data started to be widely used with the increasing popularity of two-dimensional models. Finite difference two-dimensional models use regular grids that can be easily overlayed on the DEM raster grid. In cases, when the resolutions of the hydraulic model and the DEM do not conform, GIS tools are used to transform the DEM to the required resolution. Usually, the time needed to set up the model is relatively short. In fact, the use of two-dimensional remotely sensed data in a one-dimensional model takes more effort compared to using it in a two-dimensional model, requiring some modelling skill in recognizing appropriate cross-section locations to parameterise the main channel (Samuels, 1990).

Although the relative ease with which large datasets of remotely sensed data are obtained can hardly be compared to other mapping techniques, there are data errors that are subject to considerable variability, depending on scanning system characteristics, flight altitude, observation angle, surface material, slope of terrain, etc. (Ahokas et al., 2003). Marks & Bates (2000) compared flood predictions made on DEMs derived from contour data to those obtained from Lidar scanning and concluded that the bulk behaviour of a flood was replicated by both models, while the local behaviour was sensitive to small changes in surface elevation. Neélz & Pender (2006) also studied the sensitivity of flood model results to DEM data and tested the effect of errors in DEMs on flood predictions in an urban area by comparing the use of DEMs with various levels of errors. Some erroneous DEMs were constructed on the basis of a benchmark DEM by incorporating an error with the same statistical properties as typically found in LiDAR data. It was found that the distribution of the flow between the different flow routes was significantly affected by the DEM errors. The magnitude of the observed differences was such that cases, where this would result in large differences in terms of final or maximum inundation extent and water levels, are possible. Significant effects were also observed in terms of modelled water levels and flow velocities. Additional artificial roughness caused by errors in a DEM significantly slowed down the flow in the simulation, in a manner similar to that which is achieved by greatly increasing values of Manning's $n$. It was also concluded that the choice of an appropriate value of $n$ might be much less important than the understanding of the artificial roughness

introduced by the errors in the DEM. Wilson & Atkinson (2005a) studied the effect of terrain uncertainty on the prediction of flood inundation using contour data. One hundred different, but equally probable, elevation scenarios were generated and compared using the LISFLOOD-FP inundation model. It was shown that the inaccuracies in terrain description have significant effects on inundation predictions and the effect of such uncertainty increased both with distance downstream and throughout the time of the simulation.

Wilson & Atkinson (2005b) tested the quality of DEMs constructed from interferometric synthetic aperture radar (InSAR) and those obtained from Ordnance Survey contour data. Both data types were supplemented by differential global positioning system (DGPS) measurements. The results showed the usefulness of non-Lidar DEMs, which are easier to obtain in developing countries or areas where airborne terrain scanning is not feasible. DGPS measurements obtained on foot improved significantly the accuracy of InSAR data or contour data especially in flat areas where contour data lacked height information because small errors in local elevations can have a significant impact on predicted flood extent and model accuracy. The LISFLOOD-FP simulation of observed floods on the River Nene, Northamptonshire, England in 1998 showed great differences in predicted inundation between simulations based on InSAR data, contour elevation data and contour elevation data corrected by DGPS. It was shown that the selection of an elevation dataset has a large effect on the prediction of flood wave.

Generally, DEMs do not represent small size linear topographic features (walls, ditches or embankments) particularly well, yet these features may significantly affect the flow. DEMs need to be checked and corrected therefore, if possible, by application of other techniques in order to incorporate those small size elements. Improper representation of these features can lead to inaccurate flowpath predictions that may result in incorrect estimation of flood characteristics.

Airborne scanning techniques are also deficient in areas of steep slopes and dense vegetation, which are typically observed on river banks. Neélz et al. (2006) reported that large differences (up to ~ 1 m at several locations) were observed when comparing bank levels from cross sections obtained from ground-based survey techniques and from a

Lidar DEM. Correct riverbank elevations are crucial for predicting the capacity of the main channel and for estimation of flow onto floodplains.

Another complication originates from the fact that Lidar is not able to penetrate water with the signal bouncing from the water surface. Bathymetry measurements are therefore necessary to provide the modeller with the information on the channel depth. The unavailable bathymetry data problem may be avoided by using a form of main channel flow 'calculation' that doesn't require such data. JFLOW, for example, estimates the bankfull flow as a flood of 2 years return period (Bradbrook et al., 2004). In most two-dimensional models, however, bathymetry measurements are necessary to describe the profile of the main channel.

The importance of remotely sensed data increases in urban areas. Gathering a similar quality dataset by application of standard mapping techniques in urban areas would be impossible or too costly. Hunter et al. (2008) tested different two-dimensional codes on a small urban catchment and concluded that the terrain DEM data available from modern Lidar systems are sufficiently accurate and resolved for simulating urban flows, but such data need to be fused with digital map data containing buildings and land use to gain maximum benefit from the information contained therein.

## 2.10 Flood risk

Understanding the level of flood risk (Defra, 2004; ICE, 2001) is a key issue in the successful management of flooding. Resources available for the mitigation of flood consequences are always limited and therefore the main aim of assessing flood risk is to direct the resources available to those areas where they can be of most benefit. A risk-based approach identifies components of the flooding system as well as associated consequences, which enables valid comparison with other investment decisions to be made. Assessment of flood risk is therefore fundamental to the application of any optimisation or prioritisation measures. The UK government has developed a national-level flood risk methodology in a strategy programme called Making Space for Water (Defra, 2004). It addressed the messages from the Foresight Future Flooding report (Foresight, 2004; Thorne et al., 2007) and provided a methodology for the assessment and prioritisation of flood risk management, and coastal erosion risk management.

The overall national flood policy in the UK and in Europe recently changed its focus from relying on certainty of flood defences (ICE, 2001). Flood defences were designed to prevent flooding up to a specific level of severity. But for higher loads or unexpected situations they fail or are overtopped. Bearing this in mind, it was realised that to focus only on flood defences is not sufficient and a more holistic approach is required, comprising non-structural measures such as flood forecasting, warning and response systems (Tapsell & Ball, 2007), land-use planning, flood insurance and self-help strategies, that can deliver significant reduction in flood consequences.

It was also realised that a traditional design approach that focuses on designing for a particular flood event (typically the 1 in 100 year probability of flooding) does not take account of the impact of floods greater than the design event. Flood management based on risk methods is able to mitigate the consequences of events of unexpected severity.

European Commission (2000; cited in DEFRA, 2003) defines risk as:

*Risk – the probability and severity of an adverse effect/event occurring to man or the environment following exposure, under defined conditions, to a risk source(s).*

In terms of *flood risk* the exposure to the risk source can be characterized by the following expression (DEFRA, 2003):

$$E = f(F, L, P) \qquad \text{(Eq. 2.12)}$$

Where $E$ is the nature/extent of effects (on those exposed), $F$ represents flood characteristics (water depth, flow velocity), $L$ denotes location characteristics (density and nature of housing, etc) and $P$ is the population characteristics (age, health, etc.).

Risk generally has two components - the chance (probability) of an event occurring and the impact (consequence) associated with that event:

$$risk = f(probability, consequence) \qquad \text{(Eq. 2.13)}$$

Consequence refers to the undesirable outcome or harm that would arise if a risk were realised. The risk can be reduced both by addressing the probability (e.g. improved flood defences, change in land use in upper catchment resulting in decreased peak flow) or the consequence (e.g. change in urban planning, increasing awareness of floodplain residents, improvements in flood warning, crisis management, post event help, insurance) (Defra, 2004). Consequences used to comprise mainly damage caused to industry and properties, but recently more weight is being placed on risk to people and on the social impacts caused by flooding. The social consequence of flooding depends to some extent on how the flood risk is perceived and how prepared and risk tolerable the communities are (Ball & Green, 2007; Tapsell & Ball, 2007). ICE (2001) offers interesting insights on how a single flooding event can cause terrifying experience to flood victims and their families.

Intuitively it may be assumed that events with the same numerical value of risk have equal significance but this is often not the case. Samuels (2006) points out that it is also important to understand the nature of the risk, distinguishing between rare, catastrophic events and more frequent less severe events. Low probability/high consequence events should be treated differently to high probability/low consequence ones.

To assess the probability and consequence of each flooding scenario a flood system can be simplified into three elements (Figure 2-1):

**Sources of risk -** meteorological factors such as rainfall, snow melt, waves and storm surge.

**Pathways -** catchment and floodplain topography. Flood management measures can change the behaviour of pathways by capturing water upstream, increasing the channel capacity, or designing a channel bypass.

**Receptors of risk -** exposure and vulnerability of people, property and environmental features that may be harmed by flooding.

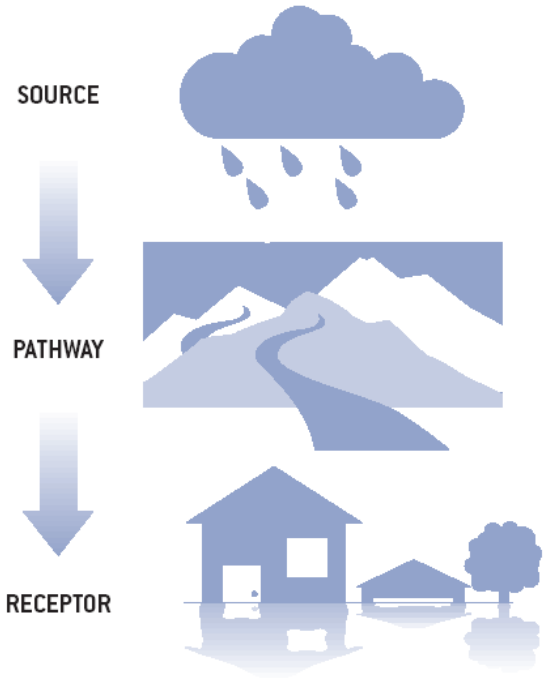


**Figure 2-1: Source-Pathways-Receptors concept (adapted from ICE, 2001)**

In relation to flooding, it can be seen that management of the risk is heavily biased to the receptor end of the scale. The source cannot be controlled (precipitation), while the pathway (land use and watercourses) can have scope for management. Ultimately however the receptor (people and property) can have the greatest control exerted on them (ICE, 2001).

According to Sayers et al. (2002a,b) and Gouldby et al. (2008) each element of flood risk can be quantified as shown on Figure 2-2. The source of flooding (load) can be described by the return period, indicating in statistical terms how frequently a particular load will be exceeded. Additionally, the performance of a flood defence is described by a structural reliability curve that depends on the structure, material, failure mechanisms and current condition of the asset (Figure 2-3). The flood characteristics of each flood incident scenario, such as flood extent, water depth or flow velocity, can be calculated by the flood model.

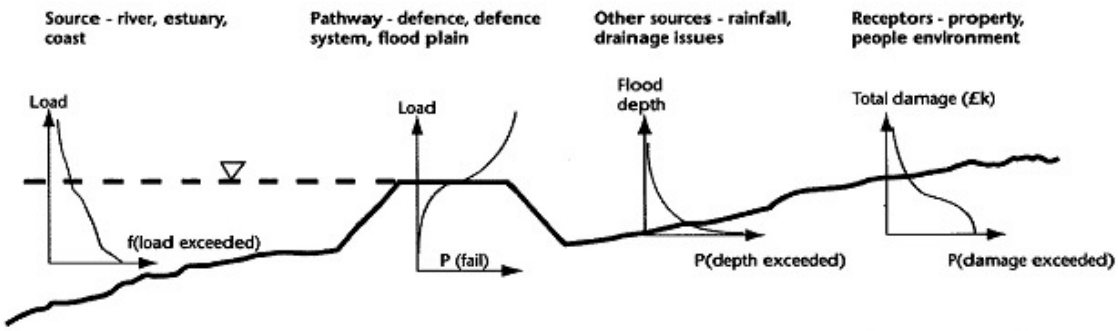


**Figure 2-2: Generic risk characteristic curves used in the first generation RASP methods (Sayers et al., 2002a)**

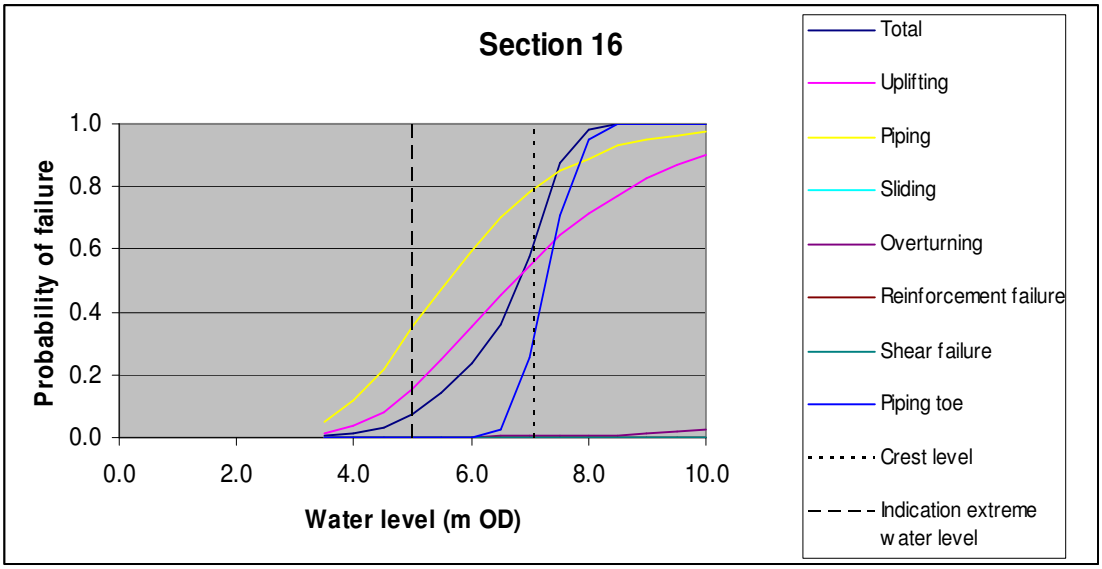


**Figure 2-3: Example of flood defence fragility curve. Lines in the graph represent different breach mechanisms (adapted from Bettess, 2007).**

Next, a map of the probability of flooding on the floodplain can be constructed (Figure 2-4). Similarly, the probabilities of exceeding a certain water depth or flow velocity in certain locations can then be quantified.

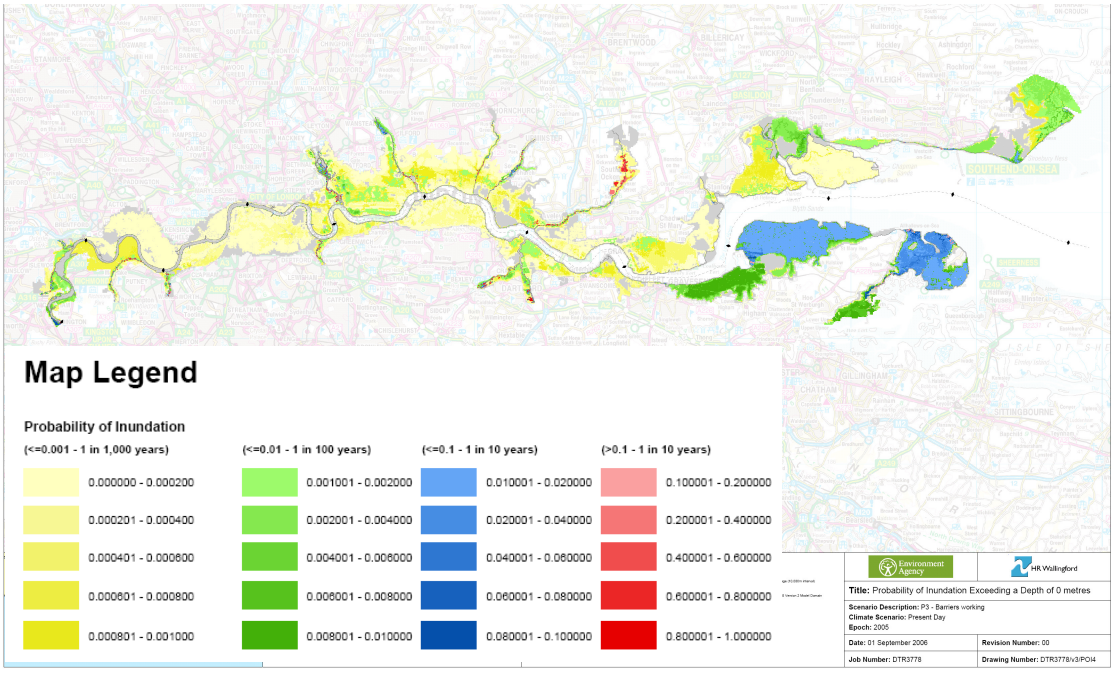


**Figure 2-4: Example of map of probability of flooding on The Thames (adapted from Bettess, 2007).**

Finally, to determine the map of expected consequences in monetary terms, the damage caused by flooding to the assets lying within the area of hazard has to be identified and the economic value of these assets has to be estimated. The non-economic flood consequences of flooding can also be included in a form of economic damage units. As a result, a map of expected annual damage can be constructed (Figure 2-5) and the damage curve, which is the relationship between the damage caused and the probability that such damage is exceeded can be estimated. More details on the step-by-step flood risk assessment analysis can be found in Samuels (2006).

Flood risk assessment helps to target flood mitigation resources. To determine the weak elements of the flooding system, whose improvement would deliver the highest benefit, the contribution of each of these elements to the overall flood risk needs to be assessed individually using the flood model. The number of resultant scenarios that needs to be modelled is dependent on two parameters – on the number of defences and on the number of loading conditions. Each flood defence is considered to have two system states - failed or not failed. This means that the theoretical number of possible system states is $2^n$, where $n$ is the number of defences within the defence system (HR Wallingford, 2006). Based on this, the number of flood event simulations that need to be carried out for a typical urban floodplain can be of order of thousands. The second

variable – the number of loading conditions - is dependent on the complexity of the flood defence scheme and the severity of the flood event, and can increase the number of required simulations still further.

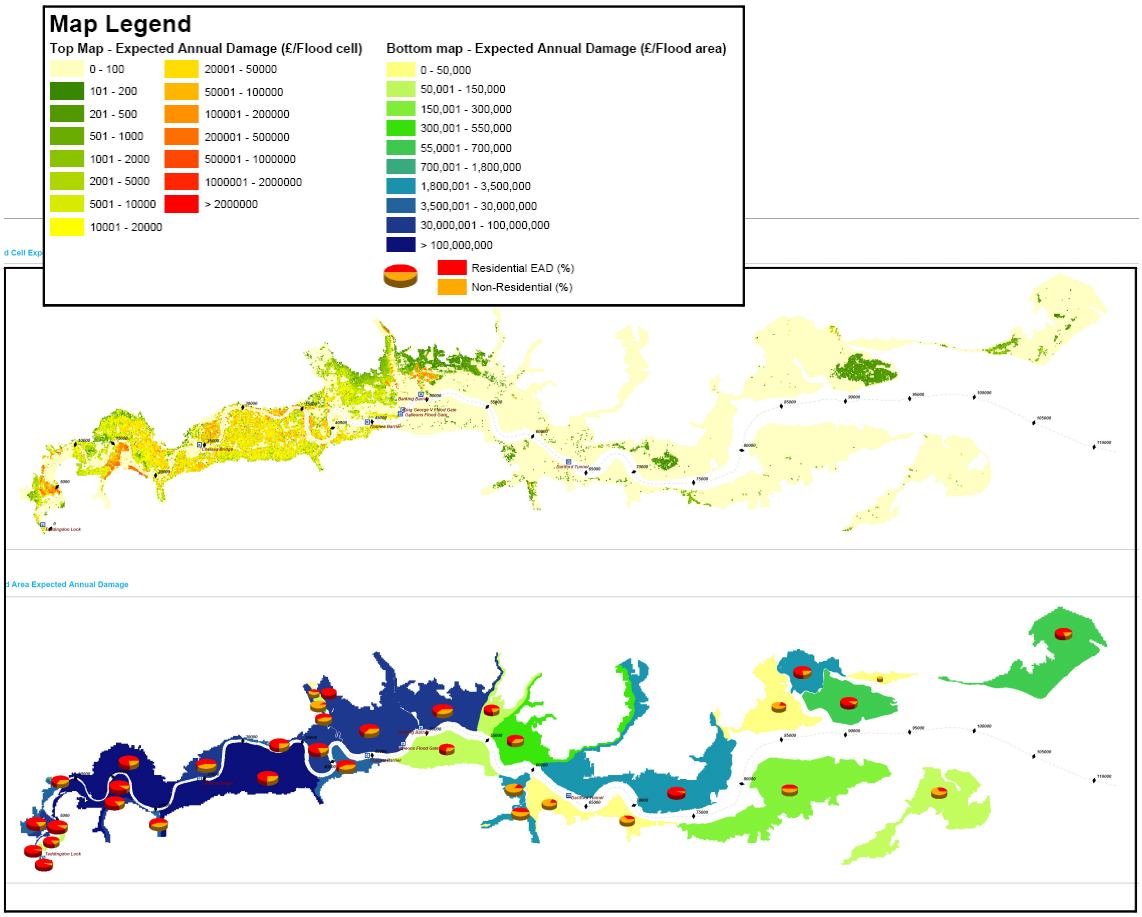


**Figure 2-5: Example of a map of expected annual damage (adapted from Bettess, 2007).**

The number of simulations can be reduced by taking account of defence fragility, ignoring failures with a very low probability of occurrence and assuming that situations where more than two defences fail during one event have a negligible contribution to flood risk.

Hall et al. (2003) and Gouldby et al. (2008) presented an application of the flood risk assessment methodology at a national-scale and regional-scale respectively.

### *2.10.1 Flood hazard*

Flood hazard is defined as:

*The potential of a risk source to cause an adverse effect(s)/event(s) - (European commission, 2000; cited from DEFRA, 2003).*

The risk to people includes not only death (usually drowning) or injury as an immediate consequence of a flooding event, but also death or injuries associated with the event, but occurring after it. Increased rates of some common mental disorders such as anxiety and depression following floods have also been observed.

The main factors of flood hazard are the properties of the flood itself and the presence of flood risk mitigation measures such as warning systems or evacuation plans. Social factors like vulnerability, behaviour or awareness should be also taken into account. Statistics published by the World Health Organization (2002) show that the number of flooding events has increased in Europe over last two decades of the 20$^{th}$ century, while the average number of casualties per flood event has decreased (Figure 2-6). This shows that although the danger of flooding in Europe is an increasingly important issue, the increased focus on flood hazard mitigation appears to have been successful.

DEFRA (2003) give the list of the main flood hazard factors and their combinations that lead to a risk of injury or death. High hazard areas are those where velocities are high, the water is deep or the flooding occurs suddenly. Also a lack of flood warning, especially in densely populated areas is a particularly dangerous feature.

From the issues mentioned above, the combination of *depth and velocity* is generally considered to be the fundamental cause of death or serious injury during floods. Extensive research has been carried out in this area and relationships that quantify flood hazard as a function of flooding parameters have been derived. The equations are based either on experimental research or on the theoretical stability of a man in flowing water (Abt et al., 1989; quoted in DEFRA, 2003) or refer also to the impact of flowing water on a building's stability resulting in fatalities (Vrouwenvelder and Steenhuis, 1997; RESCDAM, 2000; both quoted in DEFRA, 2006).

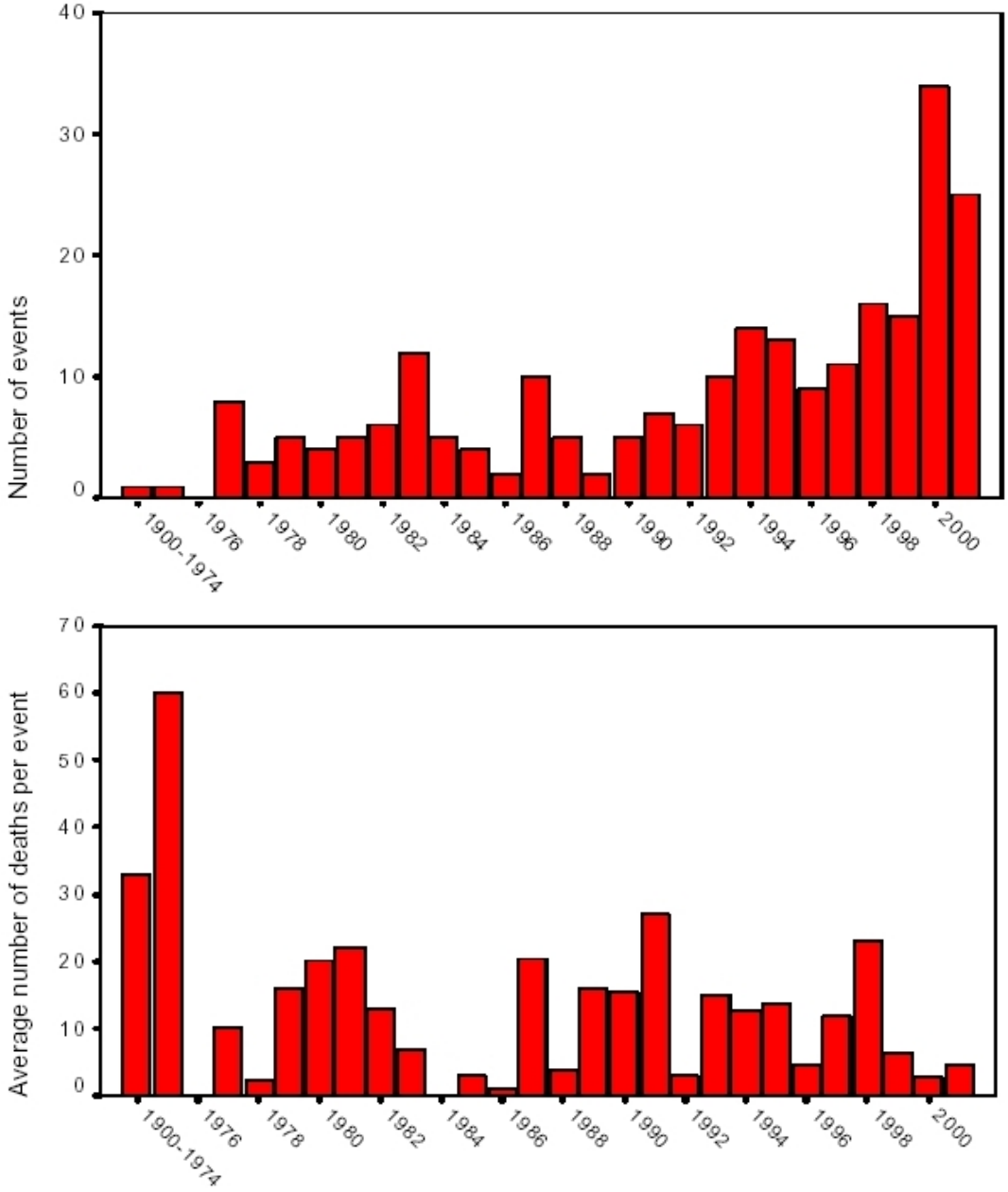


**Figure 2-6: Number of flooding events and average number of deaths per flood event in Europe (adapted from World Health Organization, 2002)**

Graham (1999; cited in DEFRA, 2003) modelled a loss of life due to a dam failure and considered also the effect of non-structural 'soft' flood mitigation measures. The calculated fatality rates were therefore based on flood severity as well as on the amount of warning and awareness and the understanding of the magnitude of the risk by the population.

DEFRA (2003, 2006) defined the methodology to estimate flood risk to people in a form of the likely annual number of deaths or injuries. It takes account of three elements affecting flood hazard: *flood characteristics* (for example depth, velocity, etc.), *location characteristics* (for example whether most of the people are inside/outside at the moment of flooding, the nature of housing) and *population characteristics* (for example age, health, etc.). Detailed guidelines on quantifying these factors were derived. The methodology was based on defining zones of different flood hazard and estimating the total number of people and the likelihood that they would be injured or killed during a flood for each zone. Further details on the step-by-step flood hazard calculation can be found in DEFRA (2006).

In the second phase of the Flood Risk to People research DEFRA (2006) also gave an overview of depth and velocity functions that could be used to quantify local flood hazard. The following expression was found to be reliable for determining the threshold for the loss of a person's stability when subject to flood flow:

$$HR = d \cdot (v + 0.5) \qquad \text{(Eq. 2.14)}$$

where $HR$ represents flood hazard [$m^2/s$], $d$ is the depth of flooding [m] and $v$ denotes the velocity of floodwater [m/s]. Figure 2-7 presents Eq. 2.14 in context to experimental work, including an indication of typical height times mass for different ages, and shows thresholds indicating the hazard associated with different depth-velocity combinations.

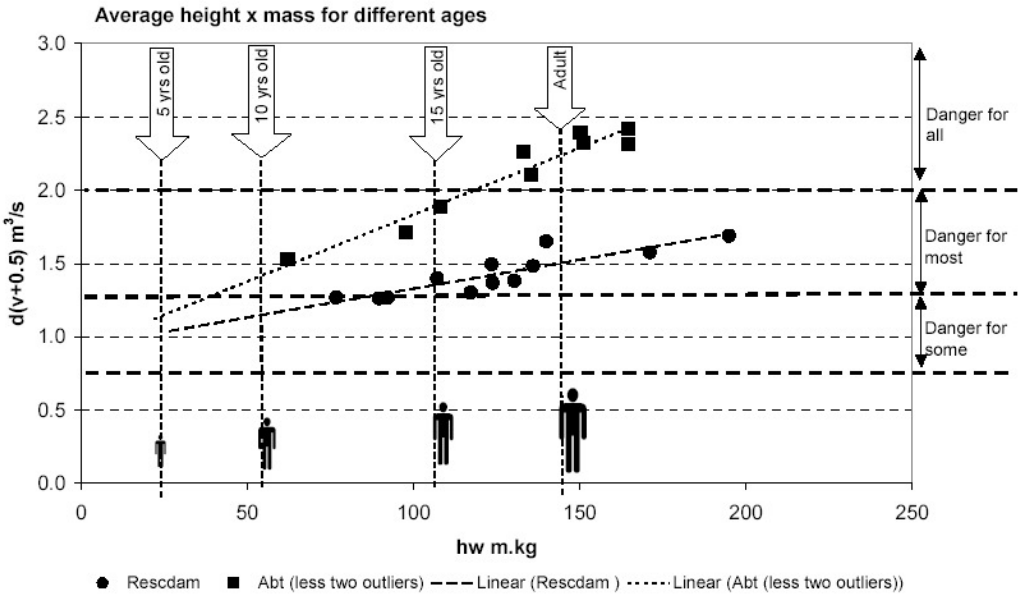


**Figure 2-7: The interpretation of experimental data to derive flood hazard thresholds (adapted from DEFRA, 2006)**

In context with the DEFRA methodology the model described in this thesis (RFIM) can be used to deliver the required *flood characteristics* assessment. To this end, the RFIM is able to predict water depth and local flow velocity; however, the latter is only available in a spatially limited way, as is discussed in chapter 4. The predicted spatially distributed depth and velocity data are saved in DEM format, which can be combined with any other spatially distributed GIS information necessary for hazard assessment such as *location characteristics* and *population characteristics*.

## 2.11 Conclusion

In Chapter 2 the main hydraulic modelling techniques have been discussed with respect to their application in flood risk assessment studies and their suitability for simulation of different types of flooding was explained. It was concluded that no currently existing model is available for rapid prediction of inundation extent in highly complex urban area for the flood risk purposes apart from Rapid flood spreading technique currently developed by HR Wallingford.

Numerical methods, model inputs and data used are all subject to uncertainty. The sources of uncertainty were discussed as well as calibration and validation techniques,

which are used to quantify and decrease the level of uncertainty. The remotely sensed digital terrain data provides higher quality terrain description and is widely used in current flood modelling practice. The methods of creation and processing were discussed in detail in this chapter as well as their application.

Finally, the risk based method of flood management was discussed, definitions of flood risk and flood hazard and main methods of their assessment were explained.

# 3 Description and development of a Rapid Flood Inundation Model

A Rapid Flood Inundation Model (RFIM) was developed in order to test the usage of a simple storage cell algorithm for the purpose of flood risk management (Krupka et al., 2007a,b). Storage cell models have been successfully used in practice since the 1960s (Zanobetti, 1970). Gouldby et al. (2008) present an overview of employing systems analysis to a flood system. The Rapid Flood Spreading Method (RFSM) contained in that approach is that described in HR Wallingford (2006) and Lhomme et al. (2008). Work presented here represents an alternative to this approach.

The main requirements that the RFIM should meet are:

- Short and simple set-up
- Short run-time
- Numerical robustness
- Sufficient accuracy with respect to intended use

This chapter contains a description of i) a data pre-processing algorithm and ii) three different variants of a rapid inundation algorithm, followed by a demonstration of the RFIM performance on a simple example. An algorithm that determines the flood velocity predictions is also explained and the chapter concludes with a brief discussion of the program code structure.

The RFIM is based on a number of simplifying assumptions that were made to the two-dimensional governing equations (Eq. 2.6 – 2.8):

- **The Cartesian two-dimensional domain is substituted by a system of flood cells**, which represent the main features of the terrain. The model is applicable only on floodplains where terrain consists of a system of local depressions that act as water storage cells. If there are no natural terrain depressions in the DEM the RFIM does not predict the flooding correctly. However, the topography of most floodplains possesses sufficient relief to make the identification of discrete storage cells a practical proposition. The assumption has been widely applied by others in the context of the RASP analysis framework (HR Wallingford, 2006) and the Thames Estuary 2100 project. In this thesis the validity of the assumption is examined on two Thames embayments at Greenwich and Thamesmead in chapter 4.

- **Omission of time stepping from the solution of the continuity equation**. A single value of volume of inundation is used to calculate flooding on the floodplain. Only the final state and the maximum state of floodplain inundation are being modelled. This crude simplification is justified by the fact that no time-dependant data are required for the purpose of flood risk assessment systems.

- **The slope of the terrain is considered to be the main driver of water transfer**. The flow on the floodplain is expected to build up slowly and hence the inertial terms in the flow equations are omitted. The model assumes that flooding on the floodplain can be predicted by using an extremely simplified representation of the flow process complemented by a extensive description of terrain in the form of a high-resolution DEM. This assumption was also applied by Romanowicz et al. (1996), Horritt and Bates (2001) and Romanowicz and Beven (2003) in their model developments.

- **Volume losses** (such as losses due to infiltration or evapotranspiration) are neglected. The possible error introduced by this assumption is expected to be relatively small compared to the input uncertainty in most cases. However, volume losses to the local sewer system may be significant in real flooding events and, generally, could be included in the model in the form of another

layer of ‘communication links’ between cells. This model option has not been analysed in this project.

- **The calculation domain is restricted only to the floodplain**. The flow entering the floodplain enters a calculation as a boundary condition and is specified simply as a volume inflow. No dynamic interaction between the river and the floodplain is considered. The volume of the inflow needs to be specified for every flooding scenario. The volume of inflow boundary condition can be calculated using possible breach inflow hydrographs based on the analysis of breach formation during a flood event. The boundary condition is a significant source of model uncertainty.

As a result of these assumptions the RFIM predicts inundation by distribution of a water volume over the system of flood cells.

Although the high speed of the calculation is one aim of this project, the model predictions should also be sufficiently accurate; however, no strict accuracy limits were set.

The RFIM is relatively easy to set up. The set-up consists of defining the computational domain within a DEM, which can be easily achieved by any GIS software package. Further DEM processing is undertaken by the RFIM automatically. Natural terrain depressions are detected and the system of flood cells is built taking into account flood cell parameters defined by the modeller. This approach was selected in order to eliminate the modeller’s subjective judgement on the flood cell distribution, which can have a considerable effect on the model results. In the RFIM, the uncertainty introduced by the subjective modeller’s input is minimised, although not totally eliminated. The only way in which the modeller can apply his opinion and experience is through the selection of the flood cell parameters – the *minimum plan area of a flood cell* and the *minimum depth of a flood cell*. It can be argued that by allowing the modeller to set up flood cell parameters some subjectivity still remains, which is true to some extent, but the main improvement over the storage cell models is that the modeller’s judgement on how the flooding would develop is not applied. The modeller is only requested to assess the terrain complexity.

The choice of flood cell parameters affects the number of flood cells covering the floodplain. The sensitivity of the model predictions to the flood cell parameters at Greenwich and Thamesmead test sites was analysed and the results are presented in chapter 4.

In order to minimise the run-time the model code is divided into two parts - **precalculation**, in which extensive DEM analysis is performed and a system of flood cells is constructed. The result of the precalculation is then used as an input to the **inundation routine** that spreads the water over the flood cells from the origin of flooding. To meet the requirements the precalculation needs to be accurate while the inundation routine is optimised to achieve computational efficiency.

Sections 3.1 and 3.2 give a detailed explanation of the precalculation routine and inundation routine respectively. Section 3.3 focuses on the flow velocity estimation methodology and section 3.4 presents the structure of the code.

## 3.1 Precalculation routine

The precalculation routine, which is a key part of the RFIM, processes the terrain data to a form that is directly usable by the inundation routine. It is run only once for the whole floodplain irrespective of the number of flooding scenarios considered.

The precalculation routine breaks down the floodplain into flood cells and recognizes and saves the location and elevation of the communication links between them. The precalculation routine requires the following input information:

- Floodplain DEM
- Raster file specifying the computational domain
- User defined flood cell parameters – minimum cell plan area and minimum cell depth

Figure 3-1 describes the cell building procedure. Initially, the DEM is analysed and low points, defined as those which are surrounded by 8 higher pixels, are found. Then every pixel in the domain is connected to one of these low points following the steepest slope flowpath. At the end of this process computed flood cells form very small watersheds and cover the whole floodplain.

The flood cells recognized at this stage are very small and sometimes cover an area of only a few pixels. The next step of the algorithm tries to decrease the high number of these small cells by merging them to form larger blocks. The flood cell merging process is the most time consuming part of the precalculation because the cells are eliminated in cycles. Every cycle starts with an analysis of the size of all cells currently identified. Then the smallest cells are attached to one of their larger neighbours. The fact that a larger neighbour always absorbs a smaller cell supports the dominance of large terrain depressions during the elimination process. After every elimination cycle the communication links, locations where the spilling between the cells starts, are recalculated in order to establish the changed relationships that will be used in the next cycle. This procedure continues until all small flood cells in the domain are eliminated and all flood cells satisfy the minimum plan area $A_{min}$ condition.

At this stage the number of flood cells has decreased but some cells remain that are large, but relatively shallow. A very similar repetitive calculation to that used for the small cells is now used to attach shallow flood cells to their deeper neighbours until no cell is shallower than the minimum flood cell depth parameter set by the modeller, $d_{min}$.

No advice on appropriate parameter values ($A_{min}$, $d_{min}$) was found in the literature and hence the analysis of a wide range of parameter values carried out in chapter 4 is expected to improve the understanding of these issues and allow some clear recommendations to be drawn regarding the model parameters with respect to different types of floodplains tested.

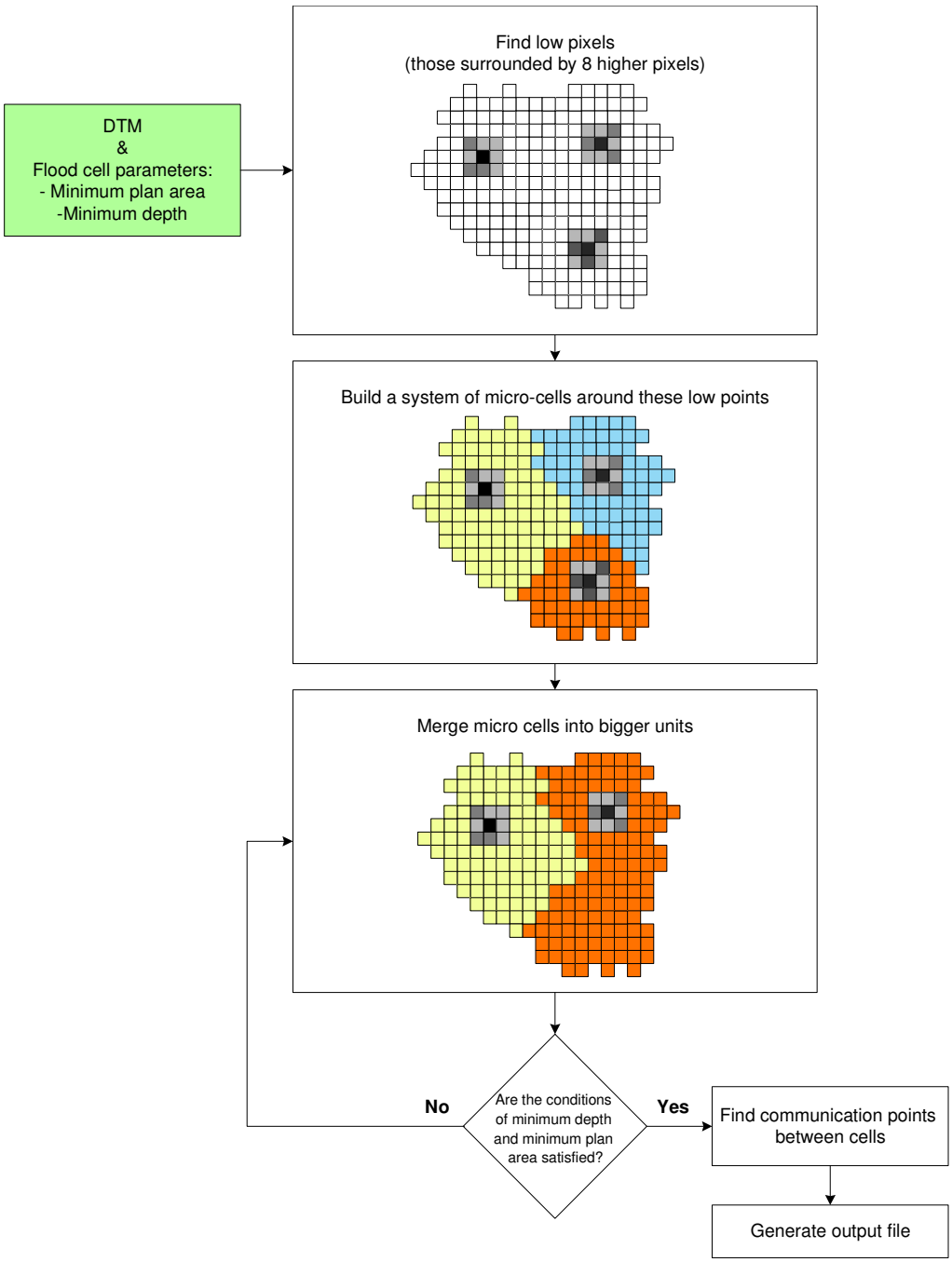


**Figure 3-1: Precalculation workflow diagram**

The best advice to the modeller regarding optimum $A_{min}$ and $d_{min}$ parameters is to select values that describe the area and depth of the typical floodplain depressions. If the terrain forms many small and deep depressions then the parameter values should account for this, while, similarly, if the floodplain consists of large and shallow depressions a different parameter set would be more representative of the conditions. A

wide range of the $A_{min}$ and $d_{min}$ parameter values is analysed and recommendation given in section 4.4.

If too high a value of $A_{min}$ or too high a value of $d_{min}$ is selected then the number of cells recognized by the precalculation would be too low to represent the structure of the terrain, while an excessive number of flood cells would lead to an undesirable increase in run-time of the inundation algorithm.

When all flood cells satisfy the viability conditions the borders between the cells are analysed and the communication links are found. The link is the lowest point of the border, where spilling from one cell to another occurs first.

At the end of the precalculation routine the volume vs. elevation curves of all flood cells are calculated. This data is saved in a text file to be used by the inundation routine. An example of a flood cell distribution for the Greenwich embayment identified by the inundation routine is shown in Figure 3-2. The white areas located inside some flood cells represent either pixels in the DEM for which no elevation data were present or the small sub-catchments for which the cell building process failed to find reasonable links to their neighbours.

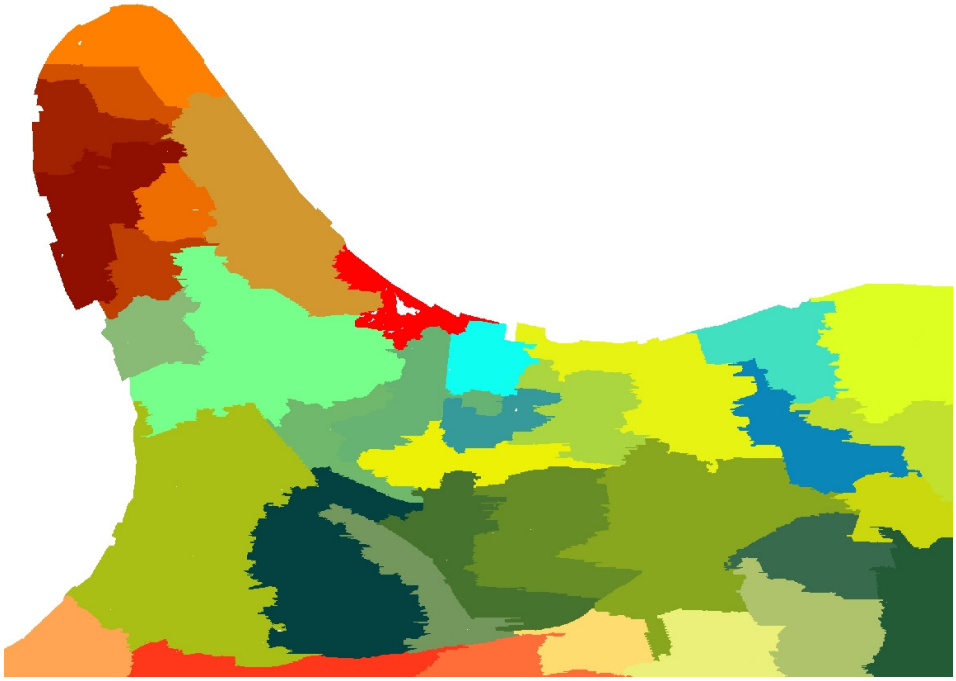

**Figure 3-2: An example of a flood cell distribution at Greenwich embayment**

## 3.2 Inundation routine

The inundation routine distributes the total flood volume over the system of flood cells and requires the following input data:

- The system of flood cells and the links between them built in the precalculation
- The coordinates of the location of the flooding incident
- The total volume of inundation, $V_{total}$
- The peak of the inflow hydrograph, $Q_{breach}$

Both $V_{total}$ and $Q_{breach}$ values can be calculated from the inflow hydrograph of the flood defence breach or overtopping.

The calculation, illustrated by Figure 3-3, is a loop of cell-by-cell flooding. Each flood cell can have one of three states:

- Dry – flood cells that are not flooded
- Active – flood cells in which the water level is rising.
- Inactive – flood cells in which water is present, but the level is not rising.

At the start of the calculation all cells are initially dry. State of each cell may change to active and then potentially to inactive as the water spreads from the origin of the flooding as is shown in the example in Figure 3-4.

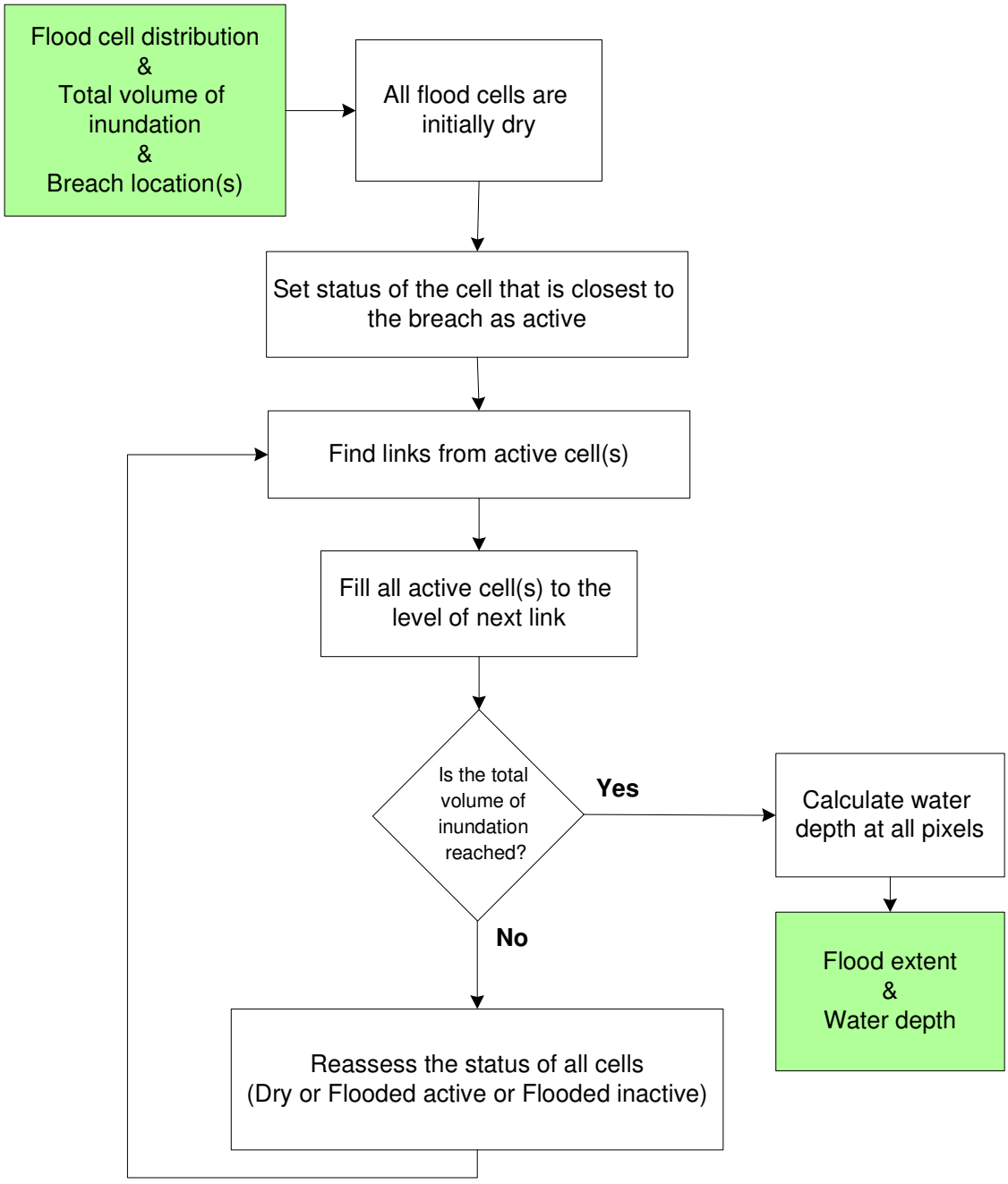


**Figure 3-3: Inundation routine flow chart**

Each inundation calculation starts by filling the flood cell located at the origin of flooding. This cell becomes active. Next, the lowest available link from this active cell to its neighbours is found. The water level in the active cell is set to the elevation of the lowest link and the active cell becomes inactive. At the same moment the neighbouring cell linked through the lowest link becomes active and the water level in this cell is

raised to the level of its lowest available link. Flood spreading continues following the lowest link rule until the total volume of inundation $V_{Total}$ is spread, at which point:

$$\sum_{i=1}^{n} V_i = V_{Total} \qquad \text{(Eq. 3.1)}$$

where n is the number of flooded cells, $V_i$ [$m^3$] denotes the volume stored in the *i-th cell* and $V_{Total}$ [$m^3$] accounts for the total volume of water entering the floodplain (model boundary condition).

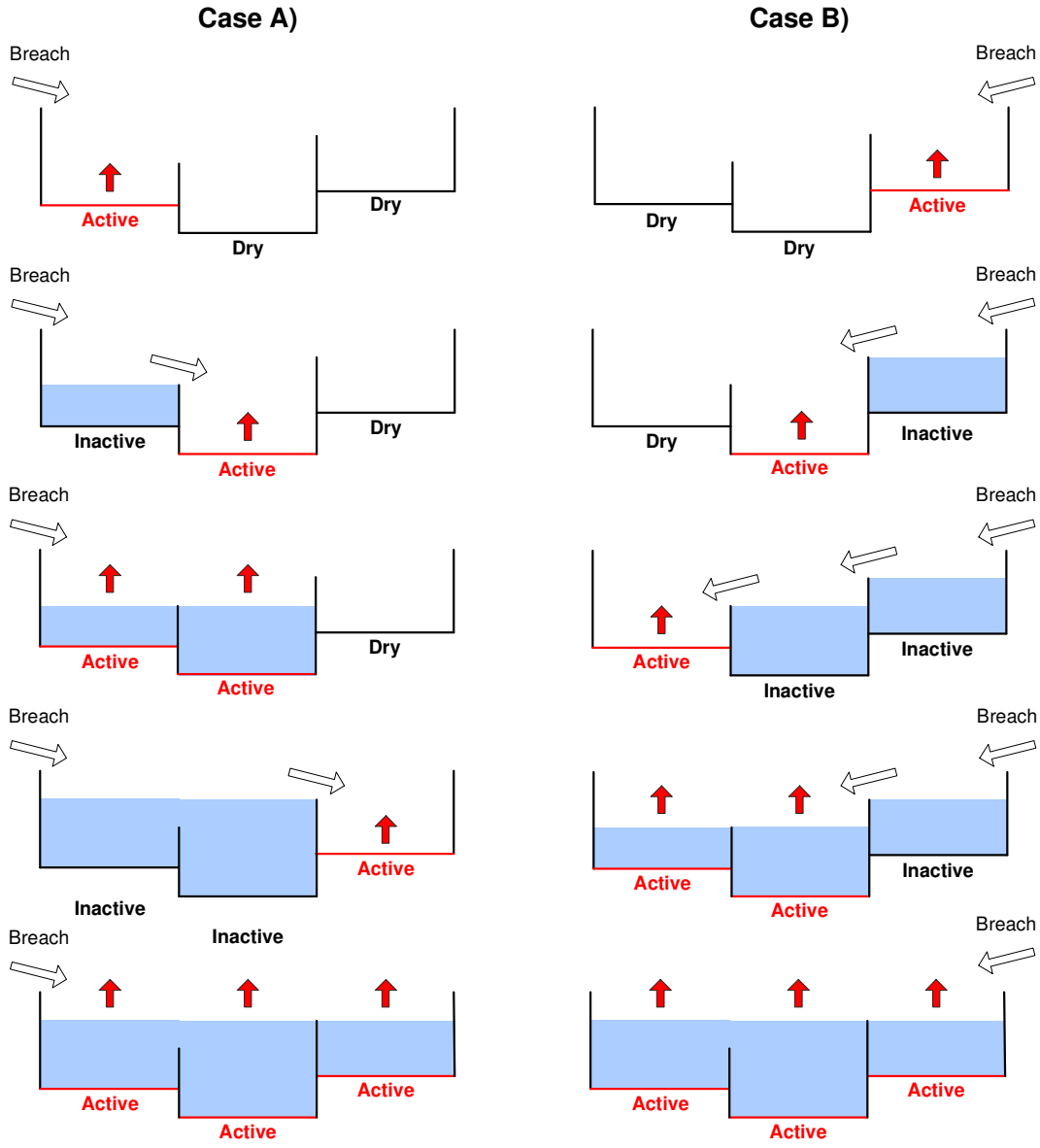


**Figure 3-4: Two examples of inundation routine (flooding scenarios) showing the changing status of flood cells**

Figure 3-4 shows two examples of the inundation routine algorithm as well as the changes in flood cell states during the calculation. In cases A and B the same terrain that consists of three cells is used. In case A the flooding begins from the left cell, while in the case B the flooding begins from the right cell. In both cases the water is spread to the lower located cells.

The order in which cells are flooded is strictly determined by the location of the origin of flooding and the elevation of the links between the cells. The inundation for each flooding scenario is carried out independently of other scenarios.

### *3.2.1 Extra head - momentum equation equivalent*

The inundation routine only takes account of volume transfers, by allowing water to spill to lower situated flood cells. In reality the transfer of water between flood cells requires an extra driving head, $\Delta z$, to overcome friction and other head losses (Figure 3-5). Hence, in order to capture peak water level in each cell, an additional head should be added above the level of the lowest link. The value of $\Delta z$ can either be set constant for all links in the domain or it can be calculated for each link individually to account for the local flow conditions. Both of these approaches are analysed below. In storage cell methods such as those discussed in section 2.4 an updated value of water level in the cells is estimated at each time step from the inflow and outflow budget and stage-volume relationships. In the RFIM, however, no time-stepping is present, so the $\Delta z$ values are estimated only once for the whole simulation.

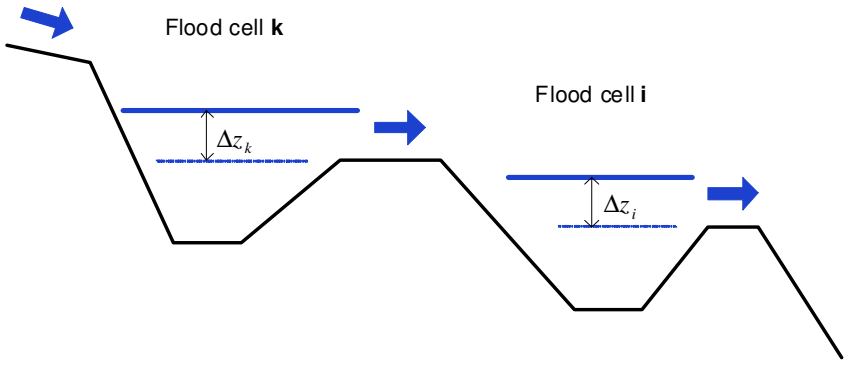

**Figure 3-5: The concept of extra head driving the flow from cell to cell**

Based on this, RFIM can capture:

- **Final flood extent** – final flooded surface area at the end of the inundation when the water has stopped spreading. Final flood extent is determined when zero extra head algorithm is used.

- **Peak flood extent** – flooded surface area corresponding to the maximum depth of water occurring in each cell individually. Peak flood extent is calculated when non-zero extra head (either constant or variable) is applied.

### *3.2.2 Zero extra head*

In the *final flood extent* calculation (Figure 3-6) no extra head is applied to any link ($\Delta z_1 = \Delta z_2 = \Delta z_3 = 0$)..

The RFIM does not allow water to leave the domain and therefore the sum of all volumes stored in the depressions equals the total volume of inundation. In other words, the flood spreading routine is carried out until the sum of volumes equals total volume defined by user.

The zero extra head inundation algorithm can also be interpreted as a representation of flooding with zero friction, i.e. one in in which no head is required to transfer water over the spills to the lower located cells.

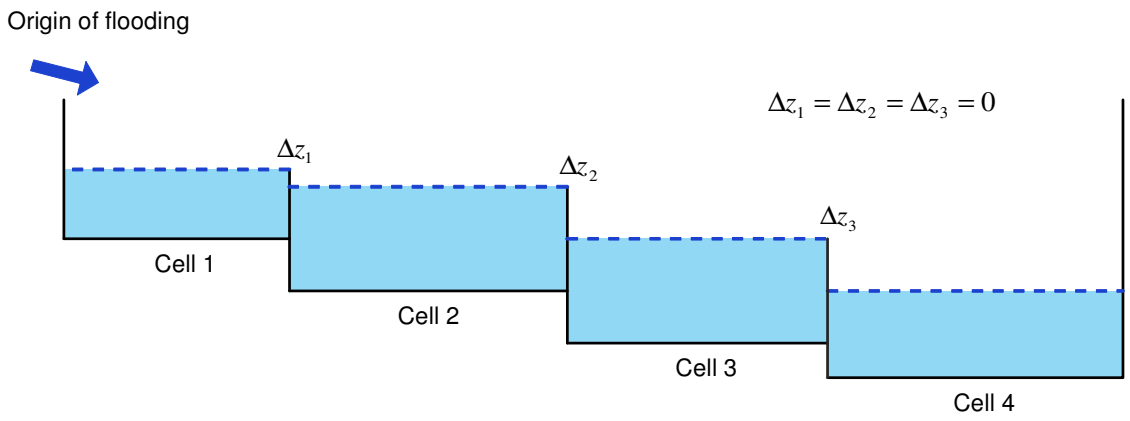

**Figure 3-6: Example of result of final flood extent inundation routine. Zero extra head case.**

.

The way in which cells are flooded is best explained using a simple test terrain. The domain in Figure 3-7 consists of six depressions that have been identified by the precalculation routine. All compartments have plan areas of 20000 $m^2$, flat bottoms at a level of 10.0 meters and are separated from their neighbours by walls. The elevation of the inter-cell walls, which act as the links between cells are depicted in Figure 3-7. A wall also surrounds the whole domain having a crest at a level of 15.0 m, which ensures no water is allowed to leave the domain. A flood incident resulting in the flooding of cell 3 is simulated. The total volume of inundation, which in a real scenario would be calculated from an inflow hydrograph, is set at 55000 $m^3$.

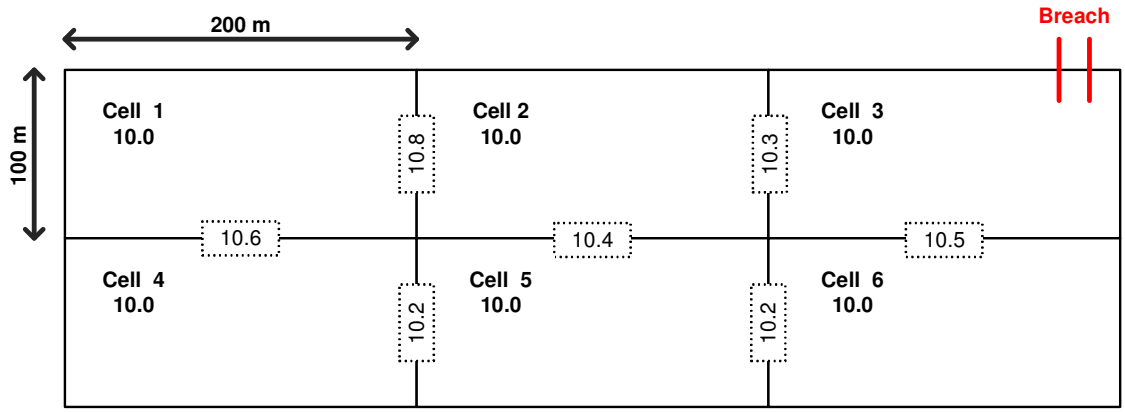


**Figure 3-7: Inundation example - artificial terrain (elevations are in m)**

The inundation routine starts by flooding cell 3 up to the level of the lowest link, which is the link to cell 2 at a level of 10.3 m (see Figure 3-8). At this level a volume of 6000 $m^3$ is stored in Cell 3.

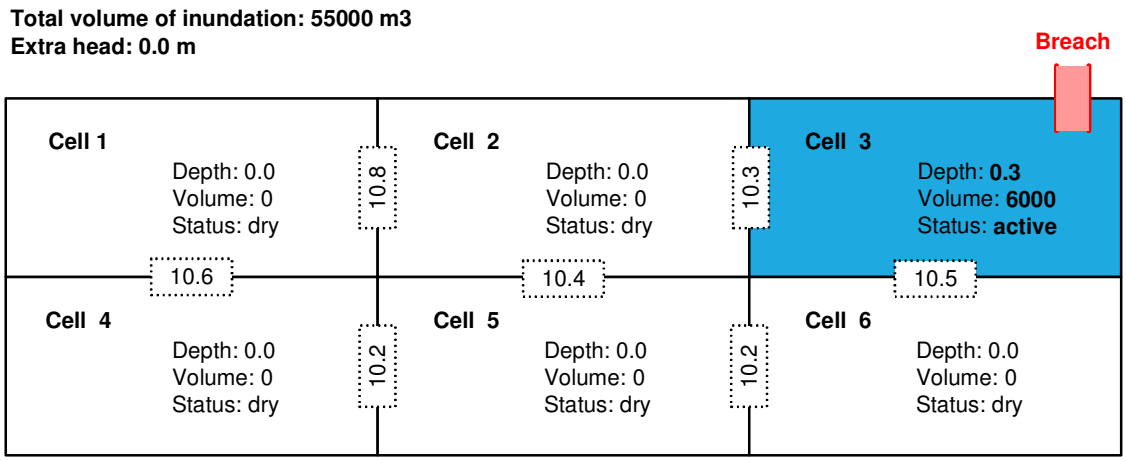


**Figure 3-8: Inundation routine – zero head – step 1 (depths in m, volumes in $m^3$)**

Cell 2 is activated next, while cell 3 becomes inactive (Figure 3-9). The water level rises only in cell 2 again up to the level of the next link. There are three links from cell 2 available – the link to cell 1 at a level of 10.8 m, the link to cell 3 at a level of 10.3 m and the link to cell 5 at a level of 10.4 m. The link back to cell 3 is the lowest of these and is activated.

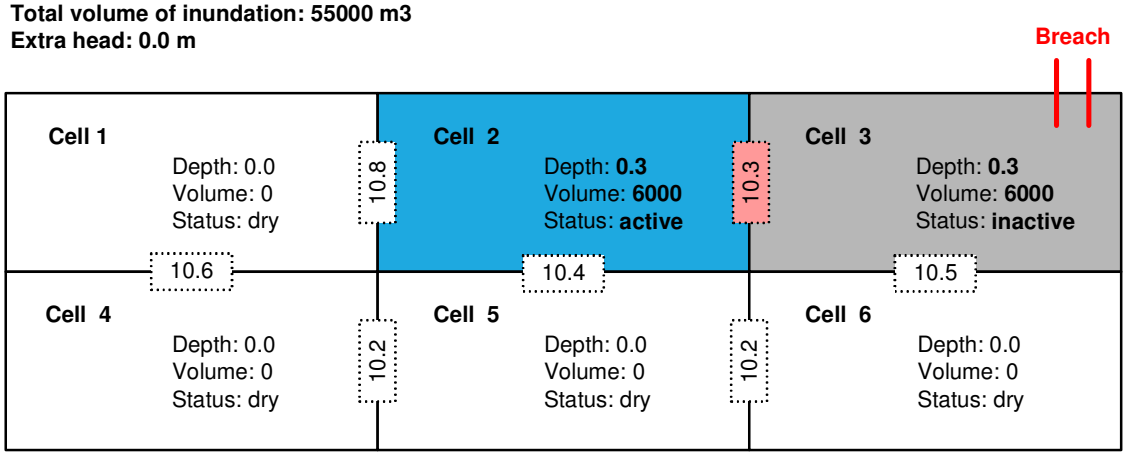


**Figure 3-9: Inundation routine – zero head – step 2 (depths in m, volumes in $m^3$)**

By activating the link between cells 2 and 3 both flood cells become active and the water level increases in both up to the level of the next available lowest link, which is the link from cell 2 to cell 5 at a level of 10.4 m. The volume in both of these cells at the water level of 10.4 m is 8000 $m^3$ (Figure 3-10).

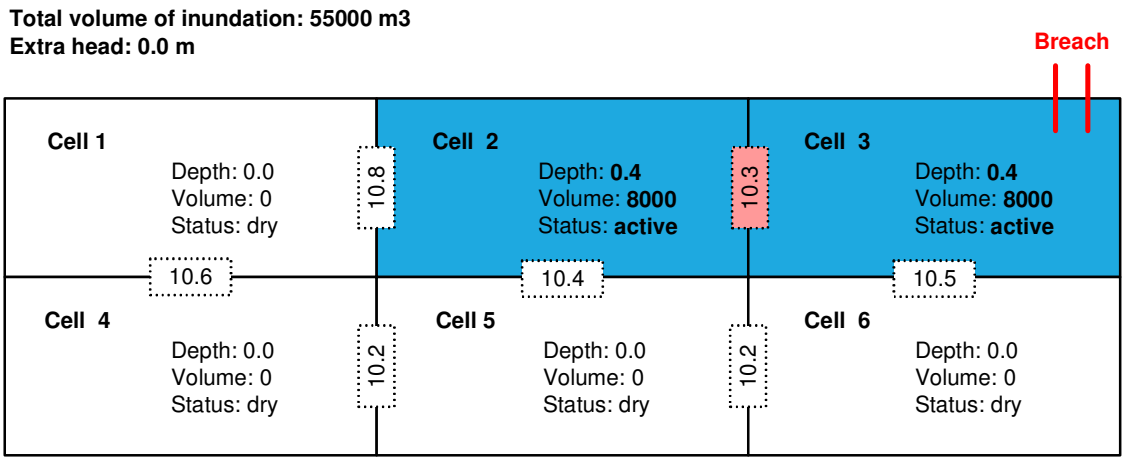


**Figure 3-10: Inundation routine – zero head – step 3 (depths in m, volumes in $m^3$)**

Figure 3-11 shows the next step in which cell 5 is activated through the link at the level of 10.4 m. Cell 2 and cell 3 become inactive. Now the water level rises in cell 5 only. There are two lowest links from cell 5 at a level of 10.2 m, to cell 4 and to cell 6.

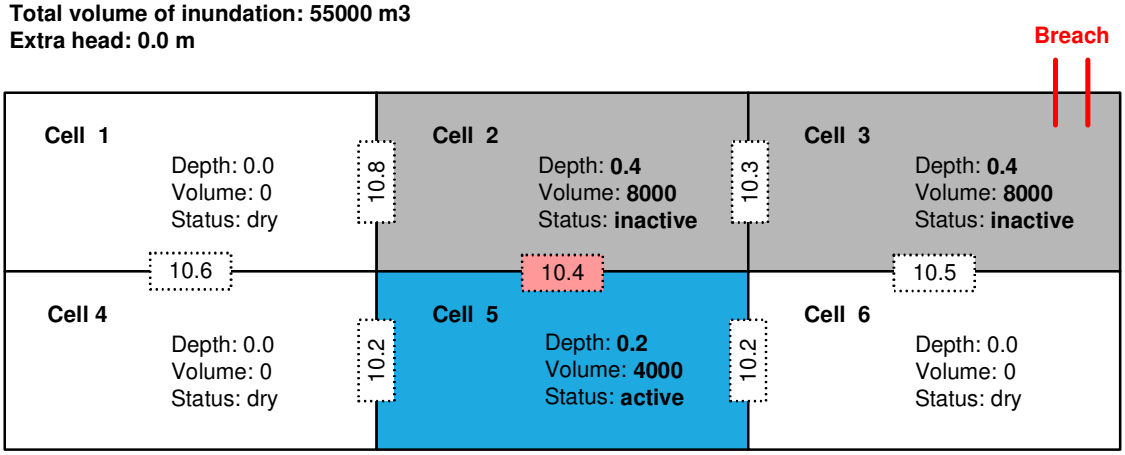


**Figure 3-11: Inundation routine – zero head – step 4 (depths in m, volumes in $m^3$)**

Hence, both cells 4 and 6 are activated next and are filled up to the level of 10.2 m (Figure 3-12), which is the level of the lowest links back to cell 5.

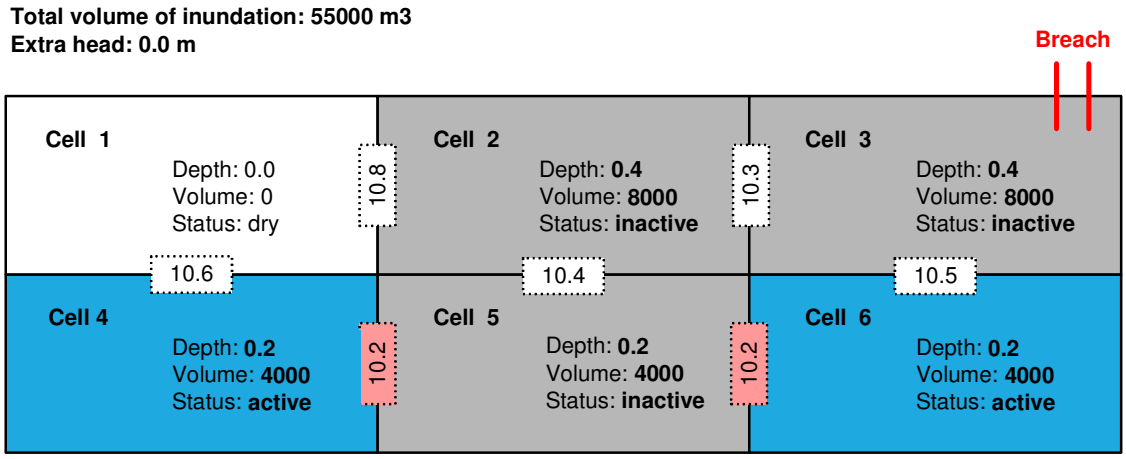


**Figure 3-12: Inundation routine – zero head – step 5 (depths in m, volumes in $m^3$)**

All three cells 4, 5 and 6 are now active and the water in them is rising. The lowest link from these to any neighbour is at a level of 10.4 m, back to cell 2 (Figure 3-13).

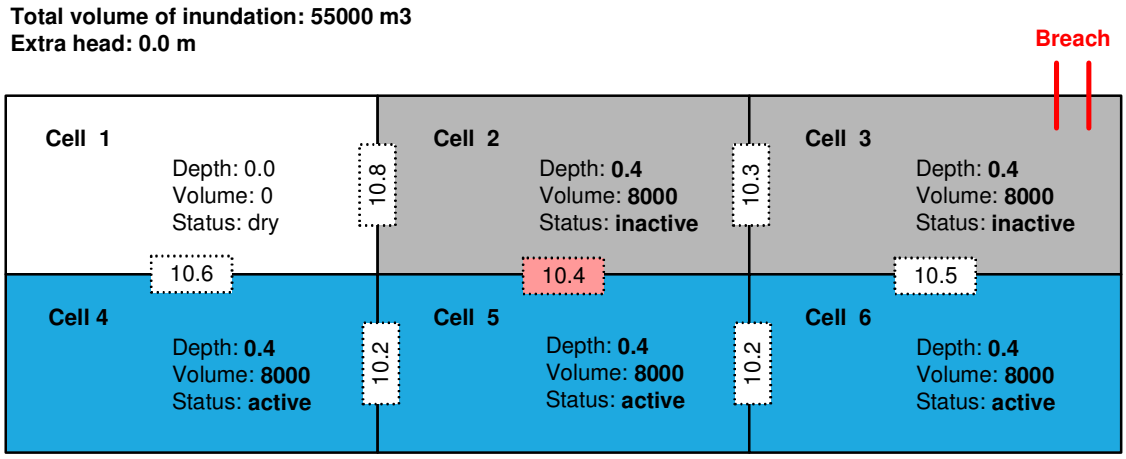


**Figure 3-13: Inundation routine – zero head – step 6 (depths in m, volumes in $m^3$)**

Cells 2 and 3 that were previously filled up to a level of 10.4 m and stayed inactive for a few computational steps become active again. The water level is now raised in all five cells (2, 3, 4, 5, 6) up to the level of the next link, the one between cells 3 and 6 (Figure 3-14). This link can be considered as an internal one because it connects two already active cells. Therefore no switching of any cell's status occurs and the flooding routine continues to search for another lowest link, which in this case is the link from cell 4 to cell 1 at a level of 10.6 m.

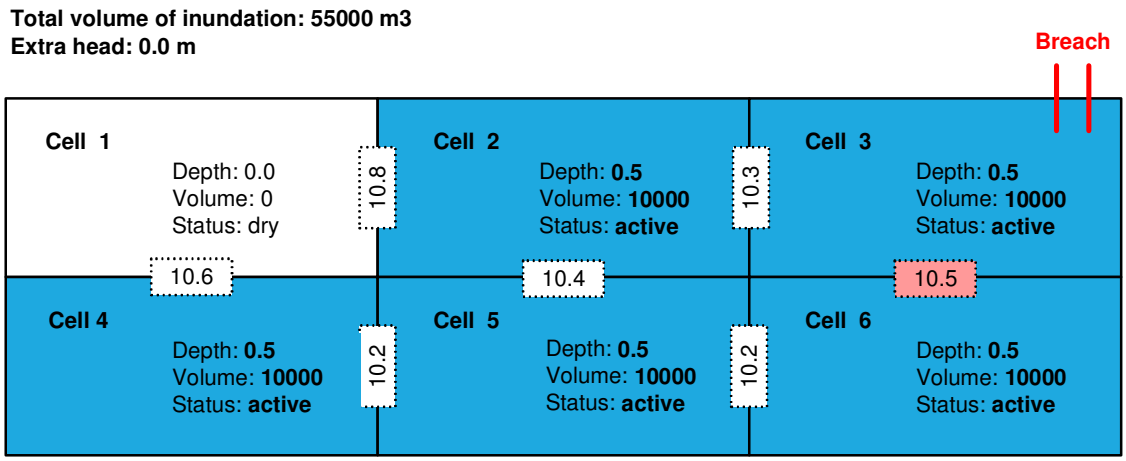


**Figure 3-14: Inundation routine – zero head – step 7 (depths in m, volumes in $m^3$)**

In each water spreading step, the algorithm checks the condition whether the volume present in all cells does not exceed the total volume of inundation, which in this case is 55000 $m^3$. In our example, the total volume of inundation would be exceeded if the water level reached the link from cell 4 to 1. Hence the inundation routine has to stop before the link between cells 4 and 1 is reached. The water level in all five active cells is iterated so the sum of the volume present in all of them equals 55000 $m^3$. Figure 3-15 shows that the iterated water level in all active cells is 10.55 m (with a depth of 0.55 m).

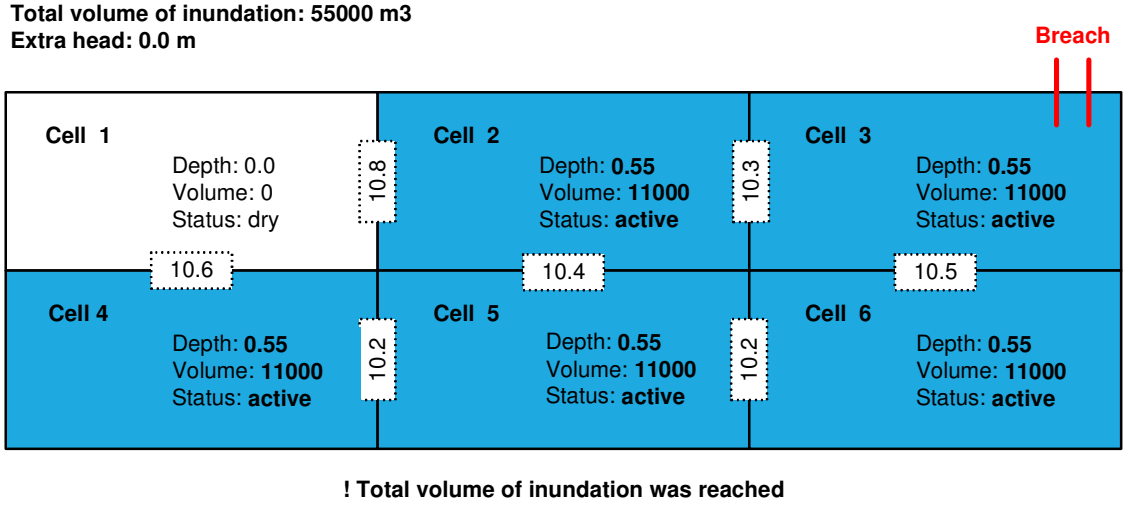


**Figure 3-15: Inundation routine – zero head – step 8 – end of calculation (depths in m, volumes in $m^3$)**

### *3.2.3 Constant extra head*

The constant extra head predicts peak (or maximum) flood extent. Maximum flood extent can be defined as a map that combines peak water levels encountered in each cell. The same flood spreading rules as in zero extra head algorithm are used and hence the same cells are flooded.

In order to predict a peak water level in the cell extra head is added to the elevation of the lowest link in that cell.Hence, the flood extent predicted by constant extra head inundation algorithm is larger compared to that predicted by the extra head case.

The value of the extra head $\Delta z$ can be set either to a uniform value over all flood cells (constant extra head) or can be calculated individually for each link (variable extra head) taking into account local properties such as slope or cross-sectional area of the flowpath.

Figure 3-16 shows an example of the constant extra head case ($\Delta z_1 = \Delta z_2 = \Delta z_3 = const$). The same flood cells are flooded as in *final flood extent (see* Figure 3-6*)*, but the predicted water level in the cells is located above the lowest link level by exact the value of $\Delta z_i$. An example application of the constant extra head inundation routine is presented in Figure 3-17 to Figure 3-24 below.

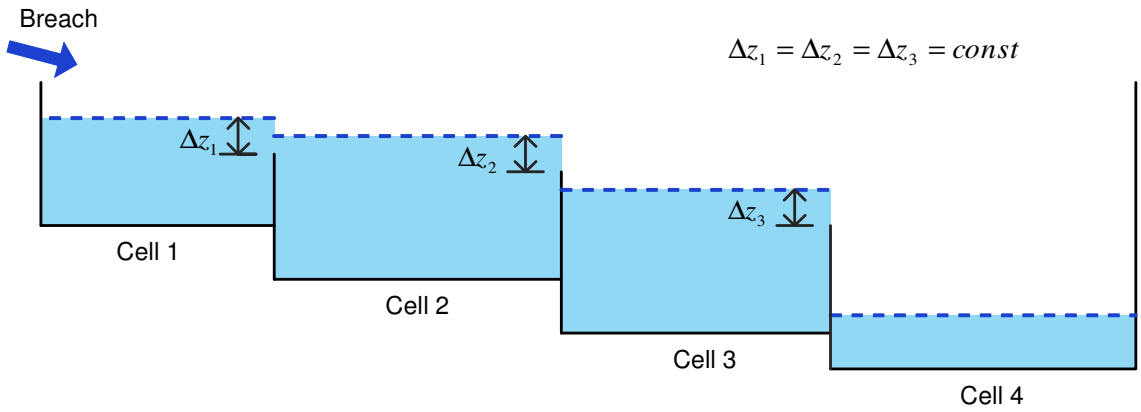


**Figure 3-16: Example of result of maximum flood extent inundation routine. Constant extra head value was used.**

Using a constant value of extra head allows the inundation routine run-time to be minimised. The algorithm simply adds Δz to all flood cells that pass excess water onto their neighbour(s).

As the water level rises and more cells become flooded the links between already flooded cells may be activated. It is assumed that already flooded cells act together like one big cell. Hence, no extra head is added if an already flooded cell is activated again. In other words, the extra head is added to the link only if the linked cell is dry.

It should be emphasized that the water volume stored in the cells below the level of lowest link to neighbouring cells equals the total volume of inundation (defined by user) and no account is taken of volume stored within Δz space. Such volume is stored there only temporarily and will eventually end up in lower located cells.The example below shows the application of flood spreading rules. The topography used in the example below is the same as in the zero head case (Figure 3-7); also the total volume of inundation is again set at 55000 $m^3$. An extra head value Δz of 0.3 m considered.

The calculation starts at cell 3 (Figure 3-17), which is filled up to the level of the lowest link (10.3 m) plus the extra head value (+0.3 m), because cell 2, which will be linked in the next step, is dry.

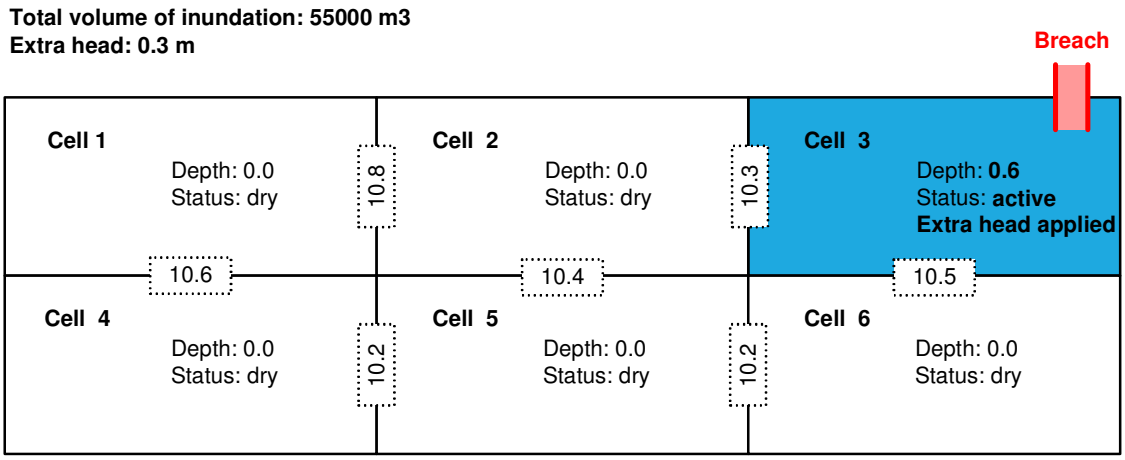


**Figure 3-17: Inundation routine – constant head – step 1 (depths in m)**

Next, cell 2 is activated (Figure 3-18). The water level rises to the level of the lowest link, which is the link back to the cell 3. The extra head value is not added to cell 2, because cell 3 has already been flooded.

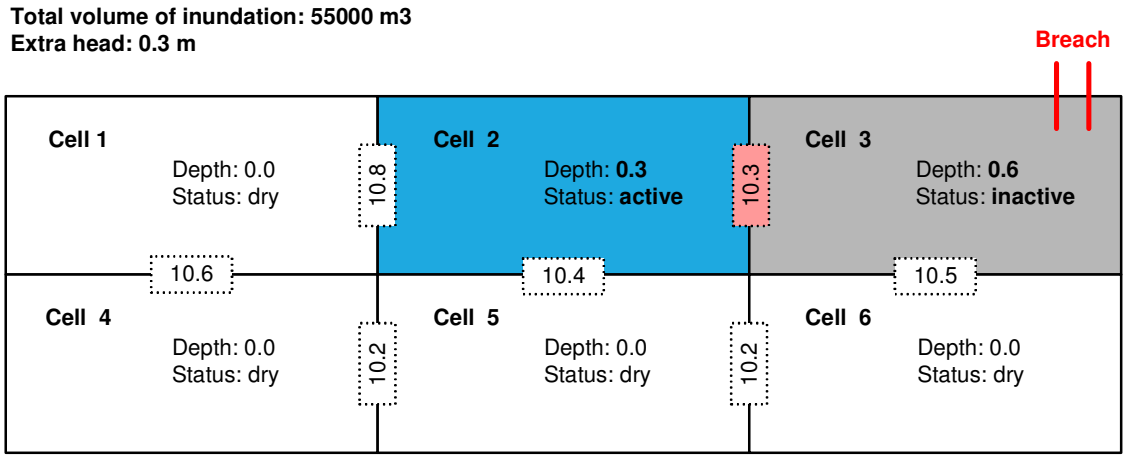


**Figure 3-18: Inundation routine – constant head – step 2 (depths in m)**

Figure 3-19 shows the next step in which both cell 2 and cell 3 are active. The next lowest link is at the level of 10.4 m to cell 5. The extra head is applied to both active cells, because cell 5 is dry. Depths in cell 2 and cell 3 then rise to 0.7 m.

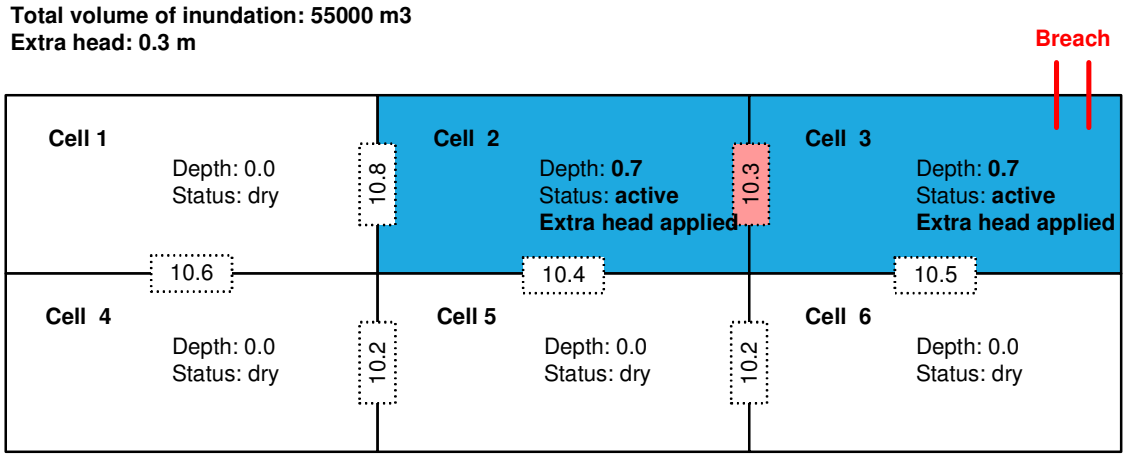


**Figure 3-19: Inundation routine – constant head – step 3 (depths in m)**

Next, cell 5 is active while cell 2 and cell 3 are inactive (Figure 3-20). There are two lowest links from cell 5 to cell 4 and to cell 6, which are both dry, hence, the extra head is applied to cell 5 and the depth in this cell increases to 0.5 m.

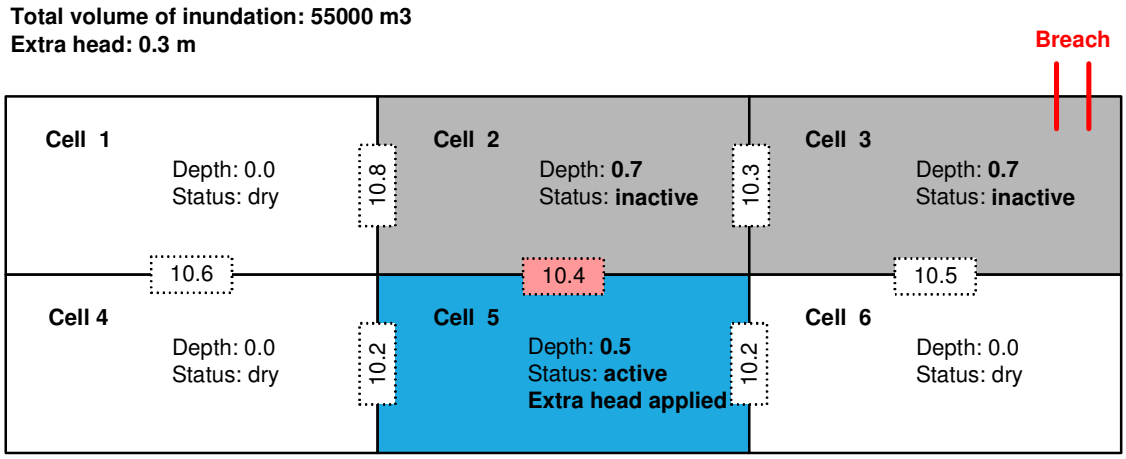


**Figure 3-20: Inundation routine – constant head – step 4 (depths in m)**

In Figure 3-21, cell 4 and cell 6 become active. The lowest links from these cells lead back to cell 5, which is already flooded. Hence no extra head is applied to cell 4 and cell 6.

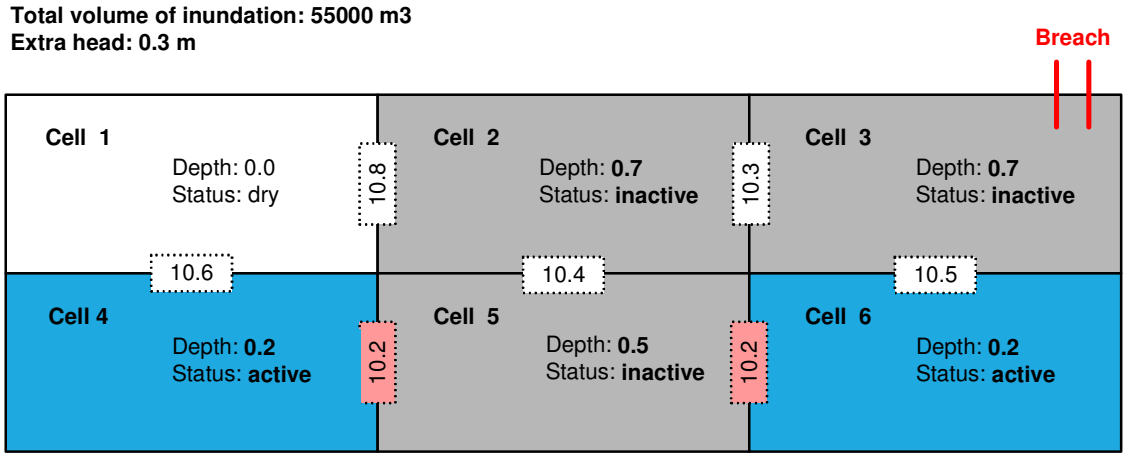


**Figure 3-21: Inundation routine – constant head – step 5 (depths in m)**

All three cells 4, 5 and 6 are now active. The lowest link from these three cells leads back to cell 2, which has been flooded before – no extra head is applied to cells 4, 5 and 6 (Figure 3-22). However, the depths in cell 4 and cell 6 increase to 0.4 m corresponding to the level of the current lowest link.

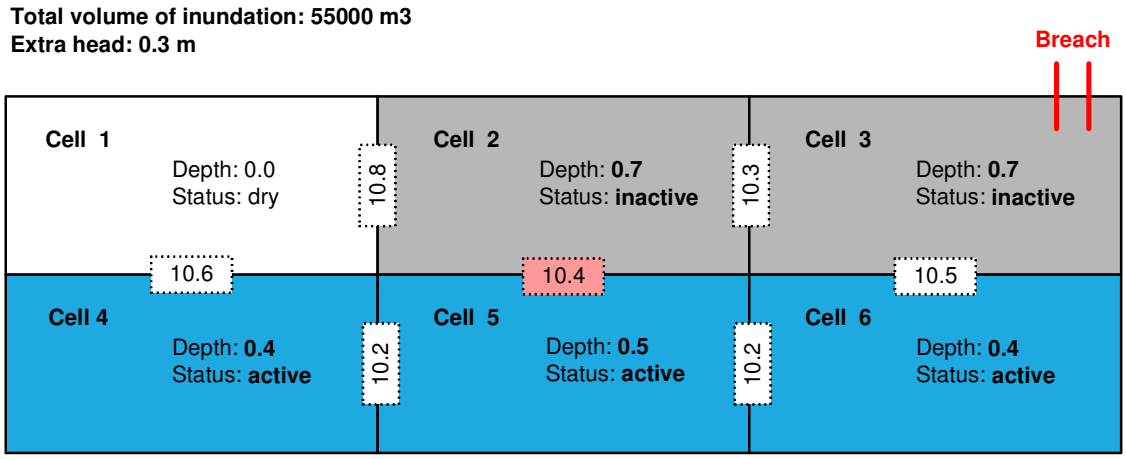


**Figure 3-22: Inundation routine – constant head – step 6 (depths in m)**

In the next step, cells 2 and 3 also become active (Figure 3-23). Now the lowest link from all active cells is the internal link between cells 3 and 6, which both have already been flooded hence no extra head is applied. The water level is increased only in cells 4 and 6 to the depth 0.5 m so they reach the level of the current lowest link (10.5 m between cells 3 and 6).

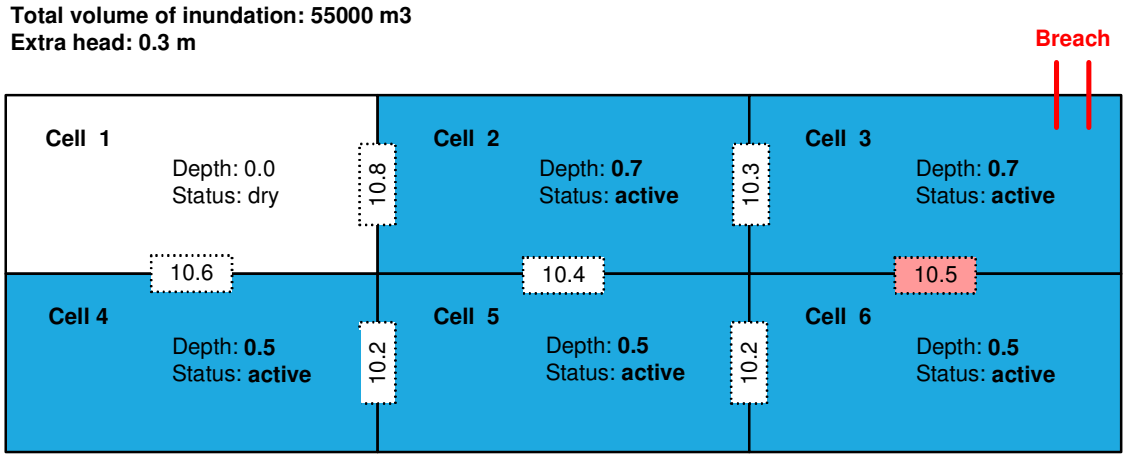


**Figure 3-23: Inundation routine – constant head – step 7 (depths in m)**

As was mentioned above, the flooding pattern is the same as in the zero extra head case. Also exactly the same total volume check to that used in the zero extra head inundation routine is applied to stop the calculation when all the available volume has been spread. Figure 3-24 shows that the water level has been iterated, and rose to give a depth of 0.55 m in cells 4, 5 and 6. See Figure 3-15 for comparison with zero head case.

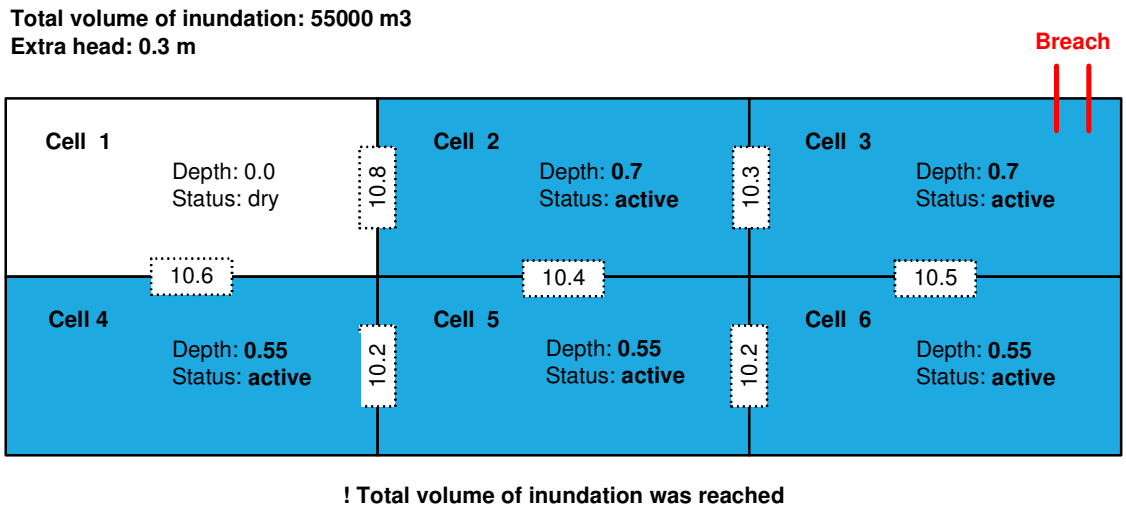


**Figure 3-24: Inundation routine – constant head – step 8 – end of calculation (depths in m)**

It should be stressed that Figure 3-24 depicts the maximum depths experienced by every cell during the inundation, not the final depths.

A realistic $\Delta z$ parameter value needs to be selected in order to represent well any real event. No guidance on this parameter value is available in the literature; hence the model needs to be calibrated to find optimum value(s). An analysis of a wide range of $\Delta z$ values is presented in chapter 4.

### *3.2.4 Variable extra head*

The variable extra head inundation routine calculates the *maximum flood extent* (similarly to the constant head case). Also its structure is very similar to the constant head case – the extra head is added to the same links, but the water level in flood cell $k$ is raised above the link elevation by the value of $\Delta z_k$, which is allowed to differ from the extra head added to other cells. The variable extra head algorithm aims to predict the extra head values as a result of local flow properties. The $\Delta z_k$ represents the depth of flow on the border (crest) between cell $k$ and the receiving neighbouring cell (Figure 3-25). If more than one lowest link at the same level are present then more than one value of $\Delta z_k$ is calculated, but only the highest of them is used.

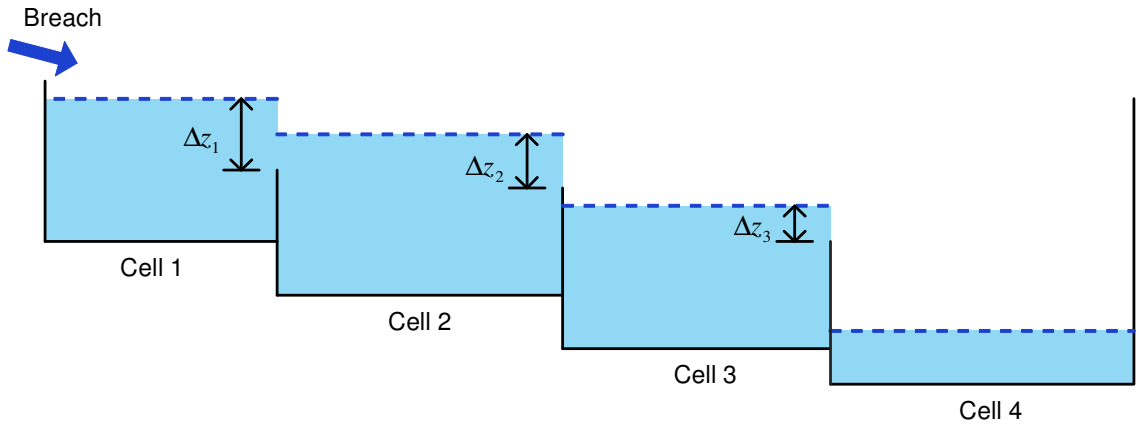


**Figure 3-25: Example of result of maximum flood extent inundation routine. Variable extra head value was used.**

The variable extra head value is calculated by the relationship that takes local terrain properties (such as slope or flowpath cross section) into account. Two types of flow exchange relationship between the cells can be considered:

- ***Weir type link***, where roads and dikes form a boundary between flood cells, which can be represented by a local head loss. A broad crested weir equation is usually applied.

- ***River type link***, where there are no local obstacles to the flow (no singular head losses) and a mean resistance coefficient can be used.

In the RFIM only the *river type link* is considered. It is assumed that there are no major obstacles to the flow on the floodplain. Inclusion of the weir type link option may in some cases improve the extra head calculation and is a subject of further RFIM development.

The total flow through a link, $Q_{link}$, is calculated as the sum of flows through the pixels that lie on the link (Eq. 3.2).

$$Q_{link_{k,l}} = \sum_{pix=1}^{M_{k,l}} Q_{pix} \qquad \text{(Eq. 3.2)}$$

where $Q_{link_{k,l}}$ [m$^3$/s] denotes the flow rate through the link between cells $k$ and $l$, $Q_{pix}$ [m$^3$/s] is the flow through every border element between cells (Figure 3-26), $M_{k,l}$ is the number of border elements present between flood cells $k$ and $l$.

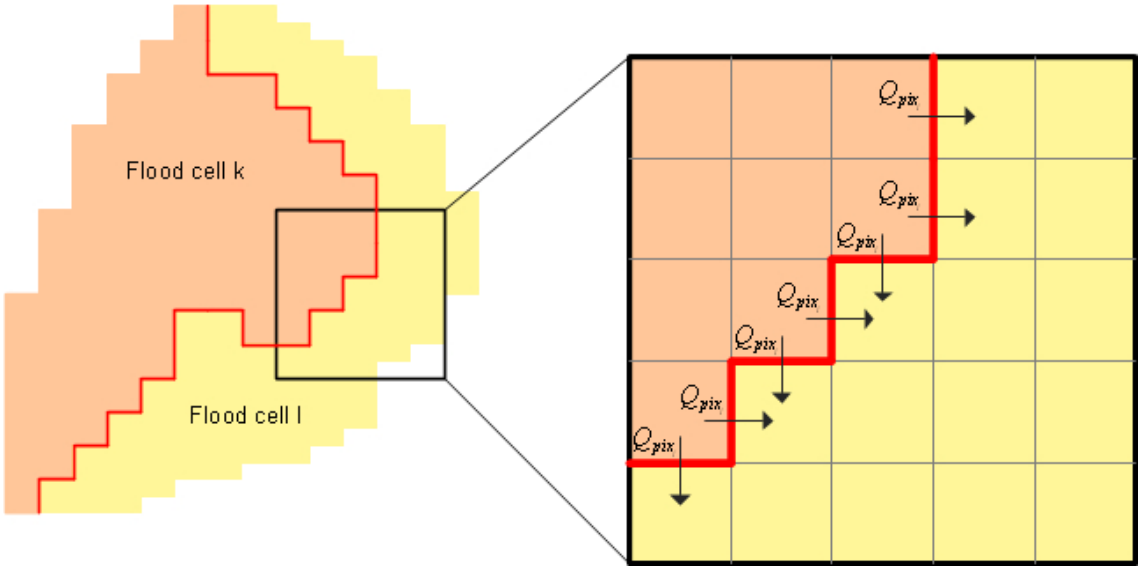


**Figure 3-26: Flood cell border elements**

Flow $Q_{pix_i}$ [m$^3$/s] is defined by the equation:

$$Q_{pix_i} = \frac{1}{n} A_{pix_i} R_{pix_i}^{2/3} S_0^{1/2} = \frac{1}{n} \Delta x \cdot h_{flow_i}^{5/3} \cdot S_0^{1/2} \qquad \text{(Eq. 3.3)}$$

where $n$ denotes the Manning friction coefficient and $S_0$ represents the slope of the terrain at the link and is defined by Eq. 3.6 (see Figure 3-28). Each border element is represented as a rectangular cross-section of width $\Delta x$ [m] and depth of flow $h_{flow_i}$ [m] (Figure 3-27).

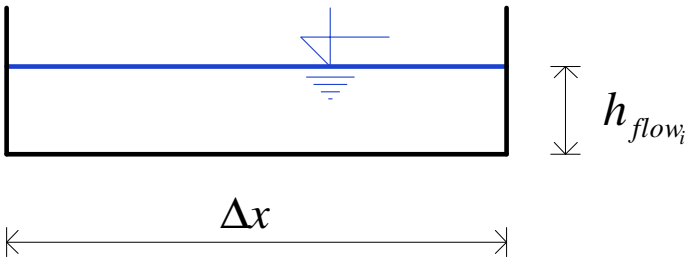

**Figure 3-27: Border element cross section**

$A_{pix_i}$ [m$^2$] is the area of flow through the border element *i*:

$$A_{pix_i} = h_{flow_i} \Delta x \qquad \text{(Eq. 3.4)}$$

and $R_{pix_i}$ [m] is the hydraulic radius of the same element:

$$R_{pix_i} = \frac{A_{pix_i}}{P_{pix_i}} = \frac{\Delta x \cdot h_{flow_i}}{\Delta x} = h_{flow_i} \qquad \text{(Eq. 3.5)}$$

The wetted perimeter $P_{pix_i}$ accounts only for the bottom of the pixel cross section, $\Delta x$, as no friction losses on the left and right side of the pixel cross-section are considered.

The fact that each cell border element in the Cartesian grid is treated separately implies an overestimation of the border length. In the case where the border lies on two sides of a pixel the length of the border would be better represented by a diagonal, of length $\sqrt{2}\Delta x$, instead of $2\Delta x$. In order to keep the algorithm speed high this border length correction was not included in the code. Due to this the border length will be overestimated resulting in lower water depth predictions at the link.

It is assumed that once the water spills from one flood cell to another the water fills the receiving cell from the cell's bottom. Hence, the considered flow path leads from the lowest point of the link (point A) to the lowest point of the receiving flood cell (point B) (see Figure 3-28). The terrain slope between these two points is then calculated, using:

$$S_0 = \frac{z_A - z_B}{|AB|} \qquad \text{(Eq. 3.6)}$$

where $z_A$ [m] and $z_B$ [m] are the terrain elevations at point A and point B respectively, while $|AB|$ [m] denotes the direct distance between them. In most cases the water would not flow in a straight line from A to B, but instead, would follow the direction of the highest slope at each point on the flow path. This feature was not considered in the code.

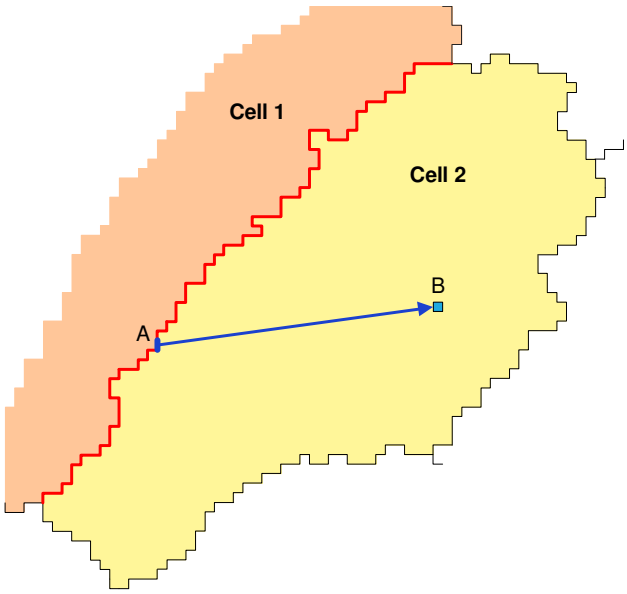


**Figure 3-28: Calculation of slope at the link between the flood cells**

Traditionally, Equations 3.2 – 3.6 can be applied to calculate the flow through the link, $Q_{link_k}$ , using known water levels in the cells. But here the inverse problem needs to be solved and $\Delta z_k$ has to be determined using $Q_{est_k}$ , an estimated value of flow through the link, because the accurate value of the flow through the link is not known at this stage. The calculation of $Q_{est_k}$ is based on the water volume that was transferred from cell *k* to *l*, which is defined as a fraction of the peak flow rate at the breach $Q_{breach}$ [$m^3$/s] and is considered proportional to the volume that has still to be spread by the model $V_{tospread_i}$ [$m^3$]:

$$Q_{est\,k} = Q_{breach} \cdot \frac{V_{tospread_i}}{V_{total}} \qquad \text{(Eq. 3.7)}$$

where $V_{total}$ denotes the total volume of inundation. Equation 3.7 allows the estimated flow rate through the individual links to decrease as the simulation proceeds. In most cases the $Q_{est}$ values reduce with distance from the breach as larger volumes are transferred between cells that lie close to the breach. For example, suppose that the peak of the inflow hydrograph at the breach is 30 $m^3$/s. The estimate flow rates $Q_{est}$ between flood cells would then be:

- Lower than 30$m^3$/s

- High close to the breach and low far from the breach

Figure 3-29 depicts the flow chart of calculation of water level at the link. The calculation is done by iteration and therefore it is the most time consuming part of the variable extra head inundation routine.

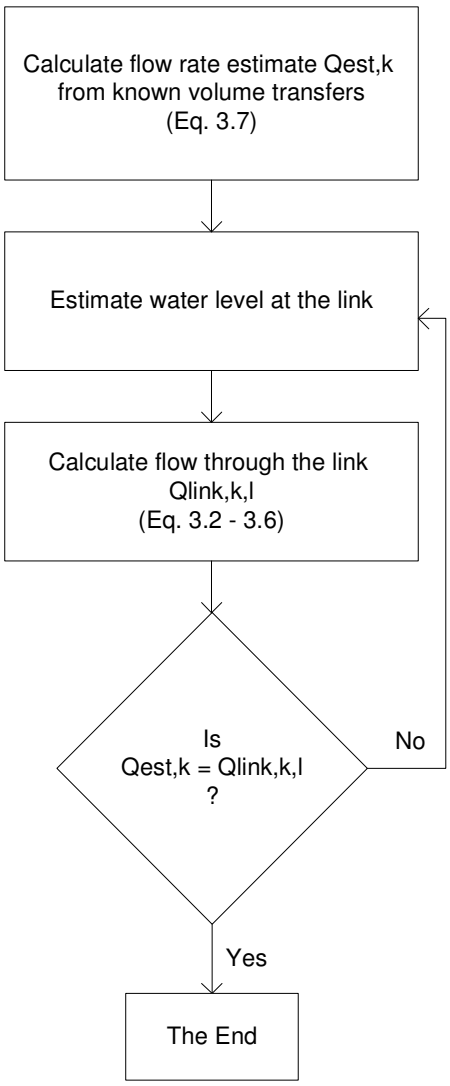


**Figure 3-29: Link depth calculation flow chart**

Although the *n* parameter in Eq. 3.3 has the physical meaning of the Manning friction coefficient it should be referred to as a resistance parameter for two reasons. Firstly, it does not strictly represent the friction of the surface of an urban floodplain and, secondly, as was recognized in the previous model presentations, the term Manning friction coefficient is rather confusing because it implies that the inundation calculation is performed in time steps, which is not the case. The resistance parameter in fact

controls the resistance with which the water is allowed to spill to neighbouring cell. In the examples considered in chapter 4 a single *n* value is applied to the whole floodplain although this may vary in reality.

In Figure 3-30, a flowchart that shows the differences between the constant extra head and the variable extra head routines is presented. Both are very similar up to the point, where in the variable extra head case the individual $\Delta z_k$ values are calculated. The variable extra head algorithm initially applies a constant $\Delta z$ value to all flood cells in order to obtain rough estimates of the volume transfers between cells. These estimates are then used to calculate the individual $\Delta z_k$ values.

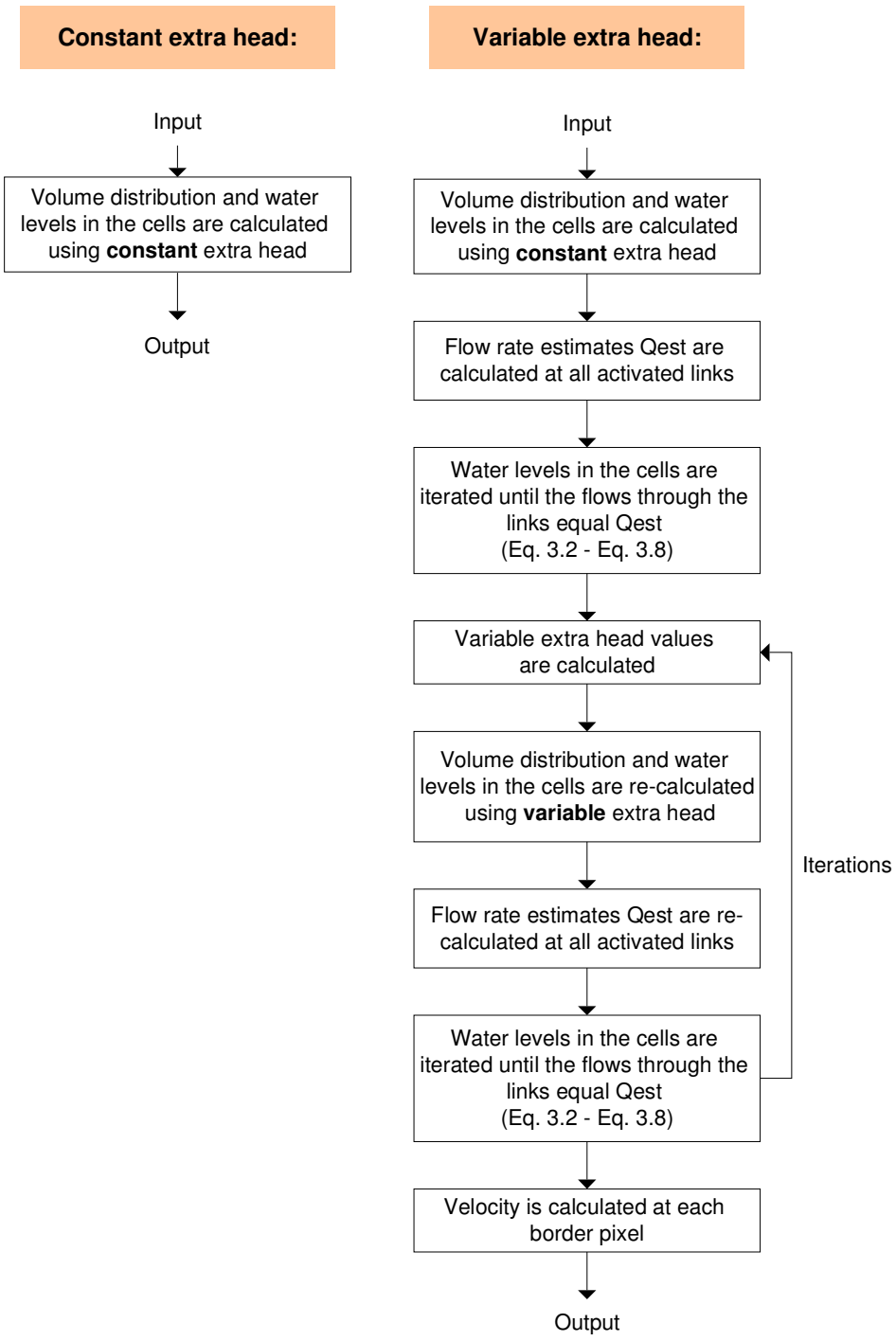


**Figure 3-30: Constant extra head and variable extra head flow charts**

Figure 3-31 to Figure 3-38 depict an example of the application of the variable extra head inundation routine. The topography used and the volume of inundation are the same as in both previous examples, $V_{total}$ of 55000 $m^3$ is applied to cell 3. The resistance coefficient is considered as n = 0.04 and the peak of the inflow through the breach is $Q_{breach}$ = 25 $m^3/s$. The initial value of extra head used in the first iteration step is 0.3 m.

The application of the variable extra head follows the same cell-switching rules as in the constant extra head case – see Figure 3-17 to Figure 3-24 for reference.

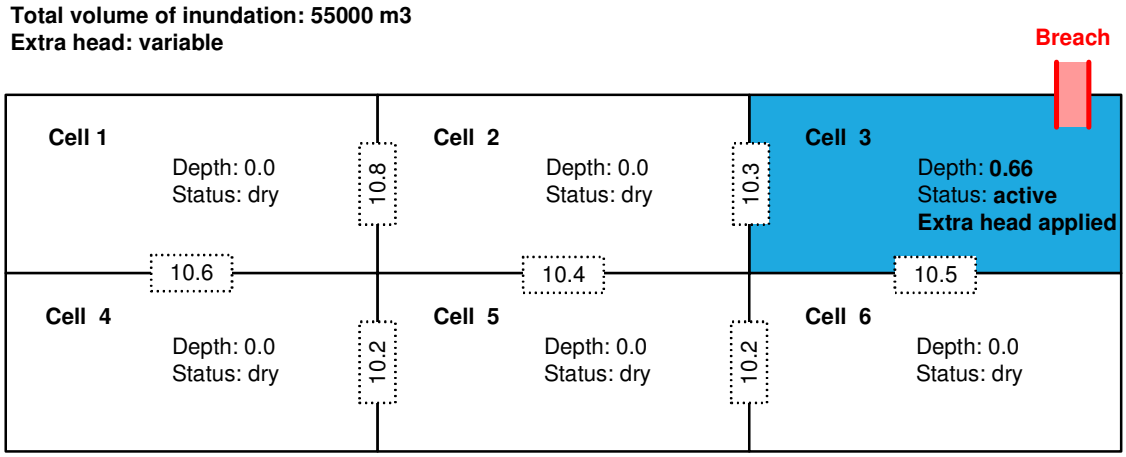


**Figure 3-31: Inundation routine – variable head – step 1 (depths in m)**

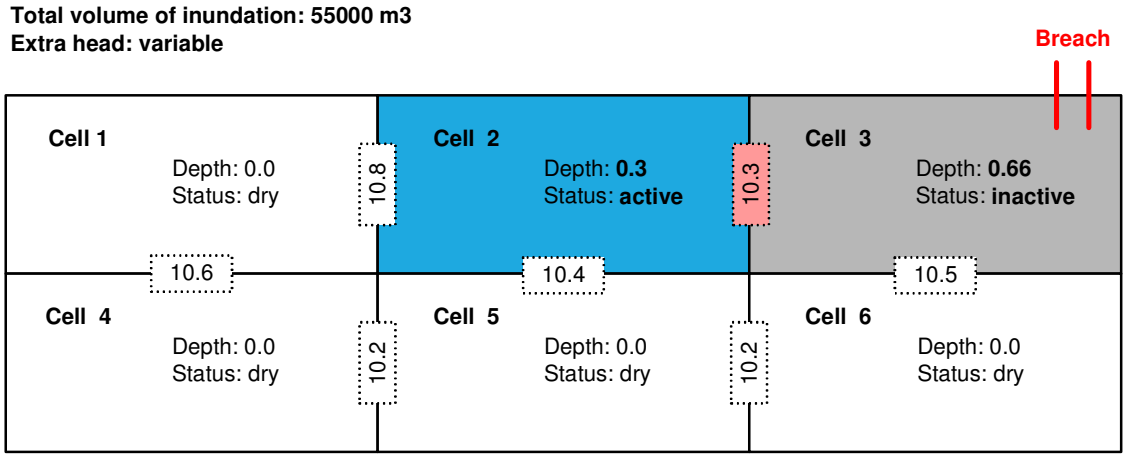


**Figure 3-32: Inundation routine – variable head – step 2 (depths in m)**

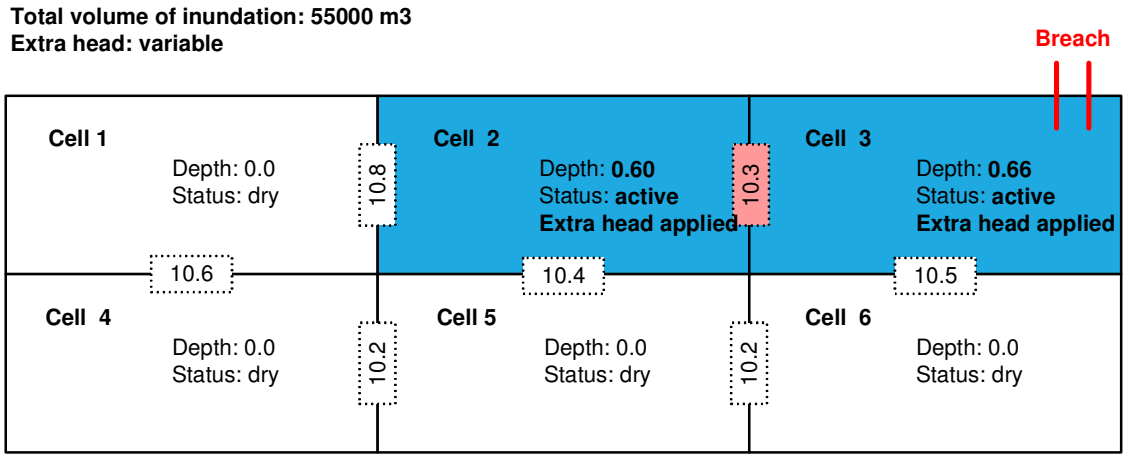


**Figure 3-33: Inundation routine – variable head – step 3 (depths in m)**

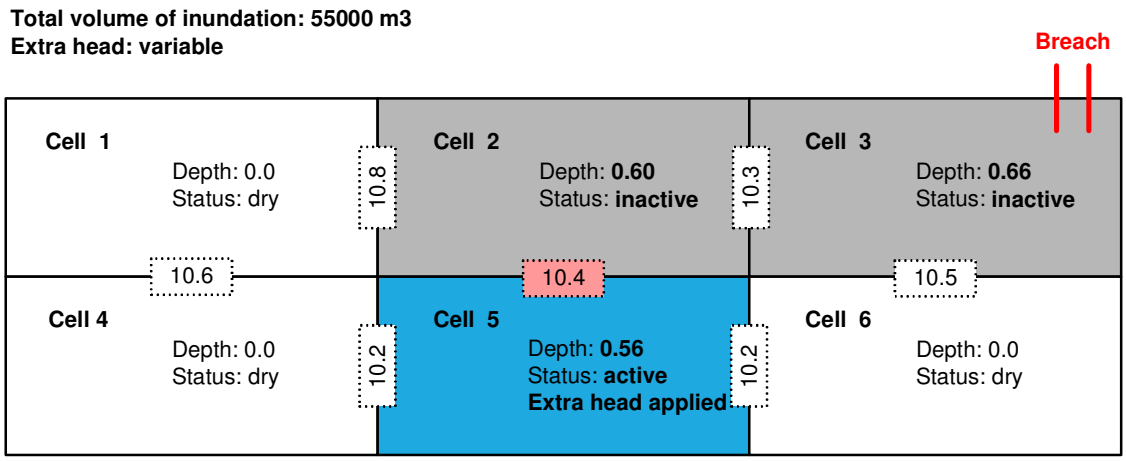


**Figure 3-34: Inundation routine – variable head – step 4 (depths in m)**

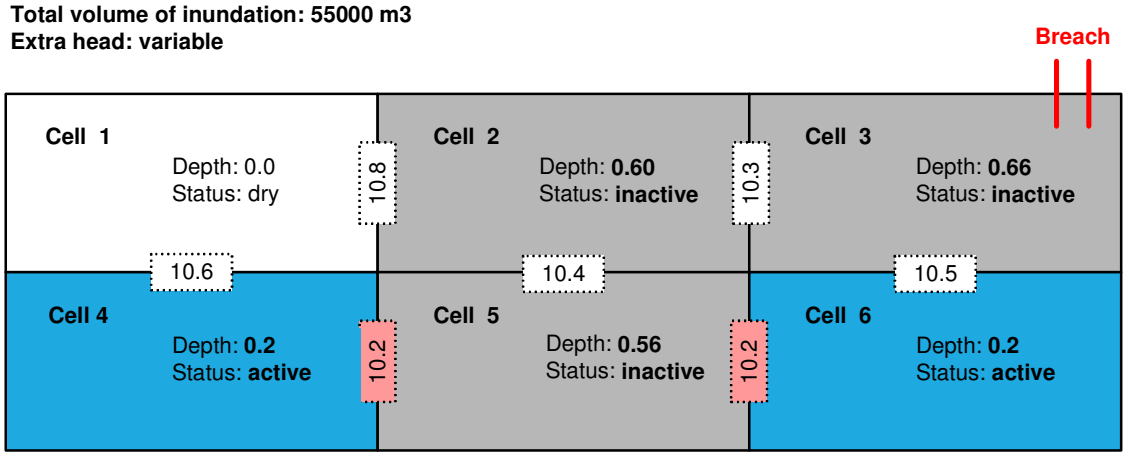


**Figure 3-35: Inundation routine – variable head – step 5 (depths in m)**

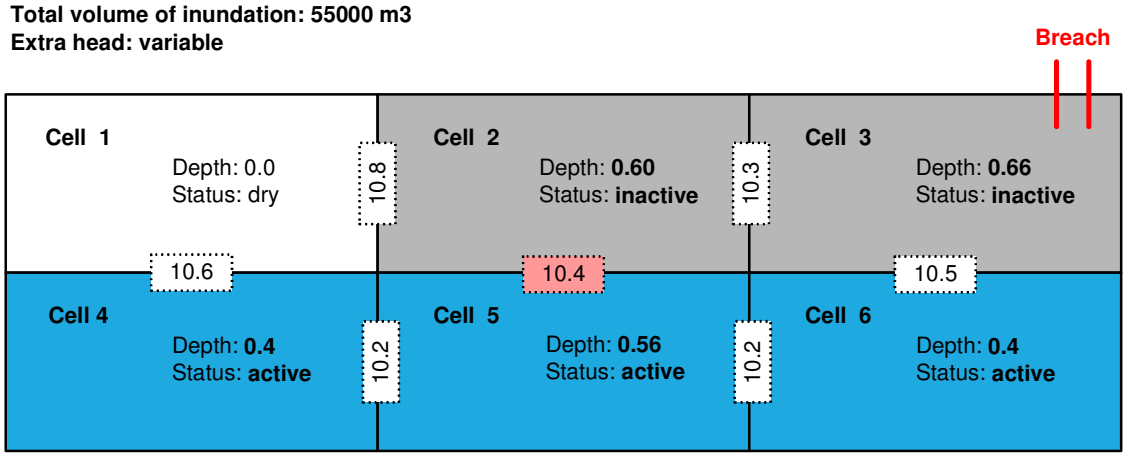


**Figure 3-36: Inundation routine – variable head – step 6 (depths in m)**

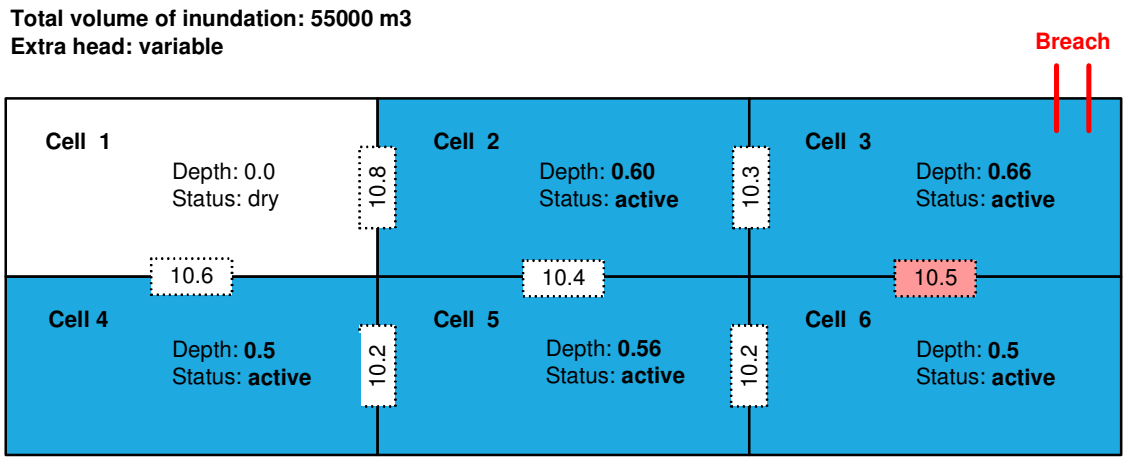


**Figure 3-37: Inundation routine – variable head – step 7 (depths in m)**

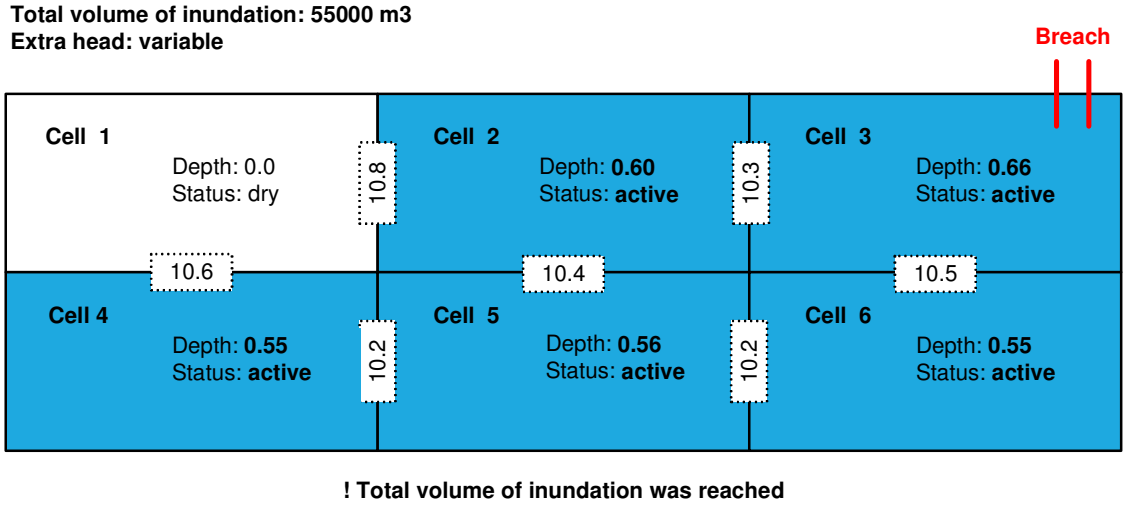


**Figure 3-38: Inundation routine – variable head – step 8 – end of calculation (depths in m)**

The figures show that an extra head of 0.36 m (0.66 - 0.30) was applied to the link from cell 3 to 2; an extra head of 0.20 m (0.60 minus 0.40) was used for the link from cell 2 to 5. A quite high extra head of 0.36 m (0.56 minus 0.20) has been applied to the link from cell 5 to cell 4 and to the link from cell 5 to cell 6. It is clear that although the estimates of the flow, $Q_{est\,k}$ decrease with the distance from the origin of flooding, the extra head values do not necessarily decrease as they depend also on the local slope and shape of the border cross section.

It should be mentioned that the variable extra head routine does not give reliable results in this example because the borders between the floods cells are formed by walls, which

does not comply with the river type link assumption. However, the example was used only to illustrate the sequence of the inundation routine calculation steps.

To summarise section 3.2, the three methods of floodplain inundation were explained and an example of application to an artificial terrain was illustrated. As expected each of these three approaches predicted different water depths, which are presented in Table 3-1.

| Flood cell | Depth in the cell [m] | | |
|---|---|---|---|
| | Zero extra head case (final flood extent calculation) | Constant extra head case (maximum flood extent calculation) | Variable extra head case (maximum flood extent calculation) |
| 1 | 0 | 0 | 0 |
| 2 | 0.55 | 0.70 | 0.60 |
| 3 | 0.55 | 0.70 | 0.66 |
| 4 | 0.55 | 0.55 | 0.55 |
| 5 | 0.55 | 0.55 | 0.56 |
| 6 | 0.55 | 0.55 | 0.55 |

**Table 3-1: Comparison of depth predictions [m]**

Detailed tests of all three algorithms on more complicated real DEMs are given in chapter 4.

## 3.3 Local velocity calculation

In order to predict flood hazard the local depth and local velocity data can be combined (see section 2.10.10).

The RFIM calculates the local velocity $v_{pix}$ by Eq. 3.8, but only on the border between the flood cells using the already calculated water level at the communication link:

$$v_{pix_i} = \frac{1}{n} R_{pix_i}^{2/3} S_0^{1/2} = \frac{1}{n} \cdot h_{flow_i}^{2/3} \cdot S_0^{1/2} \qquad \text{(Eq. 3.8)}$$

Although the local velocity predictions are spatially limited, it can be hypothesised, that in reality, the high flood risk zones would be located on the borders between the natural terrain depressions, which are areas of high volume transfer and where high velocity can be expected.

The value of $v_{pix}$ accounts for the hydraulic conditions of the whole flow path between cells, as the flow depth is calculated using flow path slope $S_0$ (Eq. 3.3). The velocity predictions produced by the RFIM are analysed and compared to TUFLOW model predictions in chapter 4.

## 3.4 Program structure

The RFIM was programmed in Fortran 90. The development was carried out in stages starting with the development of the precalculation routine and continued through the variants of the inundation routine. As a result the RFIM consists of four separate codes that are described in more detail below:

- Precalculation routine – ***poolfinder.f90*** file
- Inundation routine with zero extra head – ***inundation1.f90*** file
- Inundation routine with constant extra head – ***inundation2.f90*** file
- Inundation routine with variable extra head – ***inundation3.f90*** file

The zero extra head code served as a development stage for the inundation2 and inundation3 algorithms. The zero extra head case can also be simulated by inundation2 code, with the head value set to $\Delta z = 0$.

The precalculation routine (poolfinder.f90 file) is programmed separately from the inundation routine as it focuses not on calculation speed, but rather on the quality of the

output. The precalculation routine takes longer to run, because it contains many loops in which time-demanding pixel-to-pixel calculations are performed.

The precalculation requires the following input files:

- DEM raster file

- Raster file that defines the calculation domain. The file is produced by the modeller in order to avoid areas of the DEM that are not of interest. Pixels included in the domain are assigned domain = 1 and those that are excluded from the domain have domain = 0. This approach speeds up the calculation by focusing on the parts of the DEM where flooding is expected. It should be emphasized that the domain should represent a hydraulically independent area. For example, Figure 3-2 depicts the calculation domain at Greenwich embayment, which was restricted only to the right bank, because the breaches of the right bank flood defences were simulated. The left bank area and the river channel were eliminated from the calculation domain and the speed of the calculation significantly increased. It is clear that the hydraulic conditions of the floodplain should be carefully analysed before the domain is defined, to prevent the erroneous exclusion of relevant areas.

The precalculation routine produces several output files – some of which are used by the inundation routine and some report the flood cell-building process:

- **Pool.txt** – raster file; describes the spatial distribution of the flood cells. It is used by the inundation routine.

- **Pond.txt** – text file; describes the stage-volume relationships and the description of the links between flood cells. It is used by the inundation routine as the main input file.

- **Low_points.txt** – raster file; describes the location of the local depression (lowest pixels). It is saved for the case when the modeller needs to check the cell building process.

- **Pool_initial.txt** – raster file; describes the initial distribution of many flood cells (pools) before the pools are merged into fewer cells. It is saved for the case when the modeller needs to check the cell building process.

- **Pool_decrease_curves.txt** – text file; reports the decreasing number of flood cells throughout the pool attaching iteration. It is saved for the case when the modeller needs to check the cell building process.

Inundation routine (inundation2.f90 and inundation3.f90 algorithms) use the following input files:

- **Pond.txt** – describes the system of flood cells over which the water volume is spread. It is a product of the precalculation.

- **Pool.txt** – produced by the precalculation. See the description above.

The inundation calculations are limited only to a small number of necessary *cell-to-cell* operations. It should be borne in mind that the typical number of flood cells is of the order of tens or hundreds, which makes the calculation fast and efficient compared to pixel-to-pixel operations performed in two-dimensional models. However, high speed cannot be achieved in the local velocity and final water depth calculations, which are hence the most time demanding parts of the inundation routine. Further development of these two parts would make the inundation simulated more efficient and are certainly a subject of further development of the model.

The following files are created by the inundation routine output:

- **Pond_result.txt** – text file; contains the inundation calculation data – status of the flood cells, water levels and volumes during the inundation.

- **Final_depths.asc** – raster file; describes the spatial distribution of water depth over the floodplain

- **Flooding_order.asc** – raster file; describes the order in which the flood cells were flooded.

- **Velocities.asc** – raster file; describes spatial distribution of local velocity. This map can be combined with a final depths map to locate the high flood risk areas.

# 4 Case study applications

## 4.1 Verification

To assess the model code, first a couple of numerical experiments that are simple enough to confirm the effect of the conceptual algorithm are presented. Two simple artificial terrain datasets were constructed in order to test whether the precalculation recognizes the terrain depressions correctly and whether the inundation routine spreads the water in an order that is expected based on common hydraulic principles.

The performance of the RFIM was then tested at two Thames river test sites – Greenwich and Thamesmead embayments. Both locations are densely populated areas that are subject to severe consequences should any flooding occur.

### *4.1.1 Case 1*

The first example is a flooding event on a cascade consisting of ten flood cells. All cells have the same shape, stage-volume relationship and all links are described by the same cross-section and local terrain slope. This verification case aims to test the variable extra head algorithm. According to the previous explanation the calculated flow through the links should decrease with the distance from the breach. Consequently, the extra head values should also decrease with the distance from the breach. Figure 4-1 shows the details of the artificial terrain.

Flood of total volume of 60000 $m^3$ flows through a breach into cell 1 with a maximum flow rate of 10 $m^3/s$.

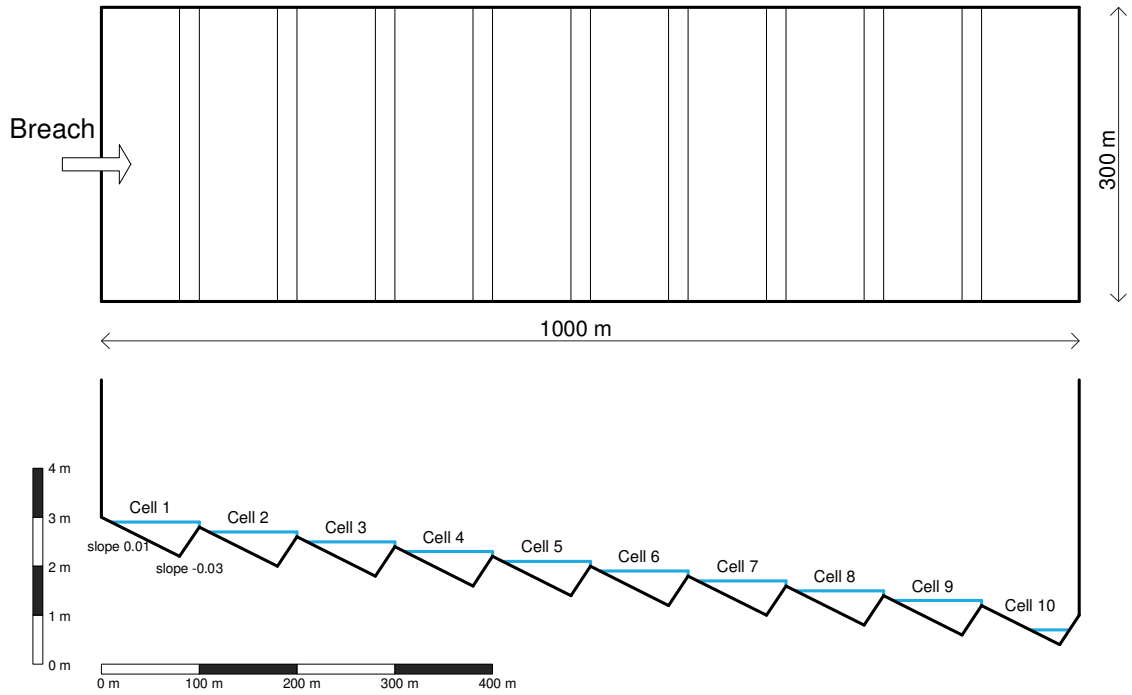


**Figure 4-1: Verification test – cascade**

Table 4-1 below presents the calculated flow estimates at all links and the Δz values. $Q_{est}$ decreases linearly as the volume is being spread.

| Flooding | $Q_{est}$ [$m^3/s$] | Extra head Δz [m] |
|---|---|---|
| From cell 1 to cell 2 | 8.910 | 0.071 |
| From cell 2 to cell 3 | 7.824 | 0.066 |
| From cell 3 to cell 4 | 6.735 | 0.059 |
| From cell 4 to cell 5 | 5.644 | 0.054 |
| From cell 5 to cell 6 | 4.557 | 0.048 |
| From cell 6 to cell 7 | 3.470 | 0.040 |
| From cell 7 to cell 8 | 2.380 | 0.032 |
| From cell 8 to cell 9 | 1.290 | 0.023 |
| From cell 9 to cell 10 | 0.207 | 0.009 |

**Table 4-1: Predicted flow rate and extra head values at the links between flood cells**

### *4.1.2 Case 2*

The second verification case tests the ability of the RFIM to correctly account for the two-dimensional nature of the inundation. Similarly to any quasi two-dimensional model, the RFIM calculation is not performed on a two-dimensional grid. Instead the grid is substituted by the set of relationships between the cells designed in a way that they are able to mimic the flood spreading. This test verifies that such relationships in the RFIM are correctly designed.

The test terrain consists of 11 x 11 flood cells that are identical in shape. Cell dimensions are 100 x 100 m. All cells are divided from their neighbours by a wall, which reaches 1 m above the cell bottoms (see Figure 4-2). The connection between cells was adjusted as shown on Figure 4-3 in order to prevent the precalculation routine from recognizing diagonal links between cells. If there was no adjustment the diagonal flow between cells would be directed through very narrow link cross-section resulting in unreasonably high extra head values. A similar situation may occur in real flooding RFIM applications, but are expected to be rare.

The precalculation routine correctly recognized all flood cells (parameters set to minimum plan area of 8000 $m^2$ and minimum depth of 0.8 m). The source of flooding is located in the central flood cell. The volume of flooding $V_{Total}$ is set to 1100000 $m^3$ and the peak flow rate through the breach $Q_{breach}$ is 20 $m^3/s$.

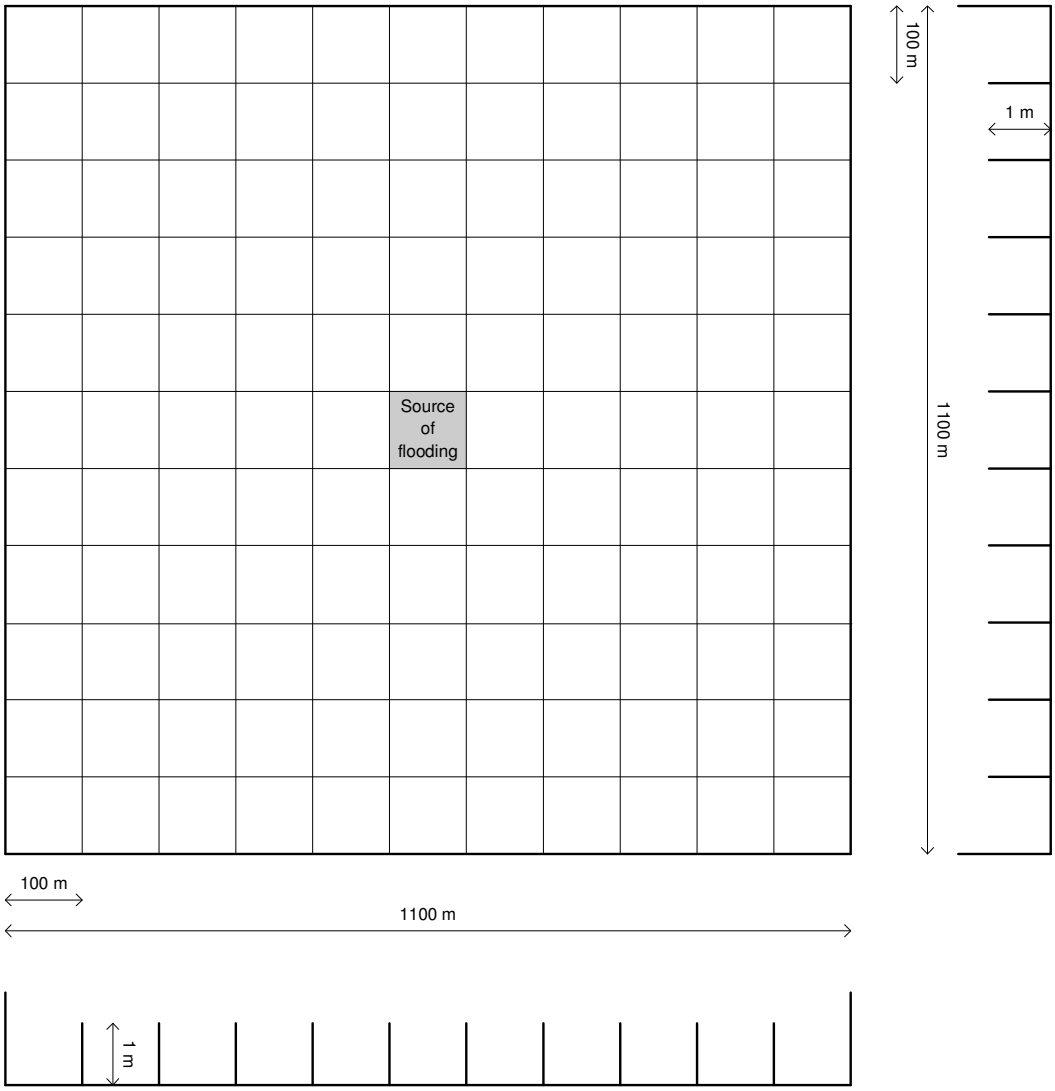


**Figure 4-2: Terrain – case 2**

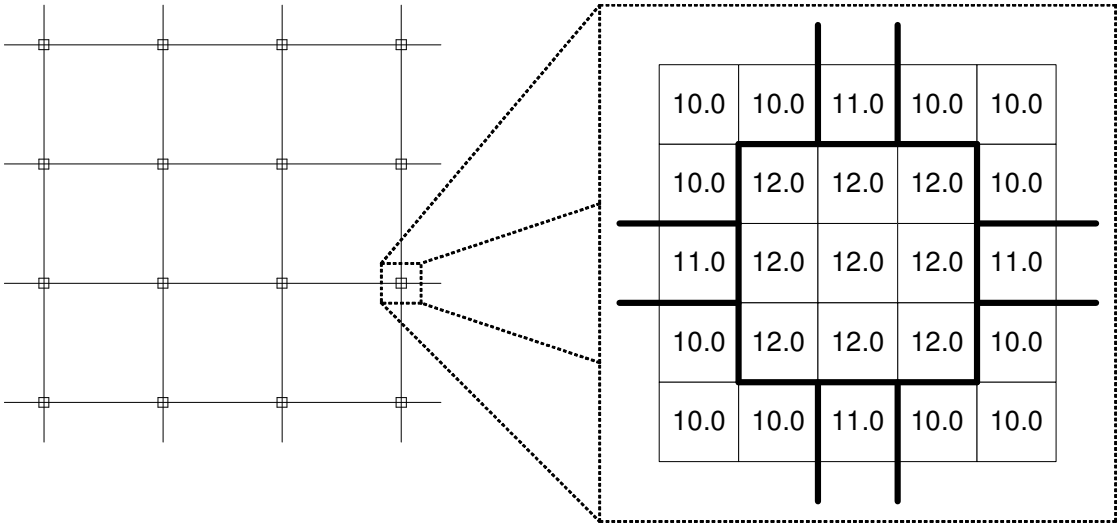


**Figure 4-3: Detail of wall connection (elevation in meters).**

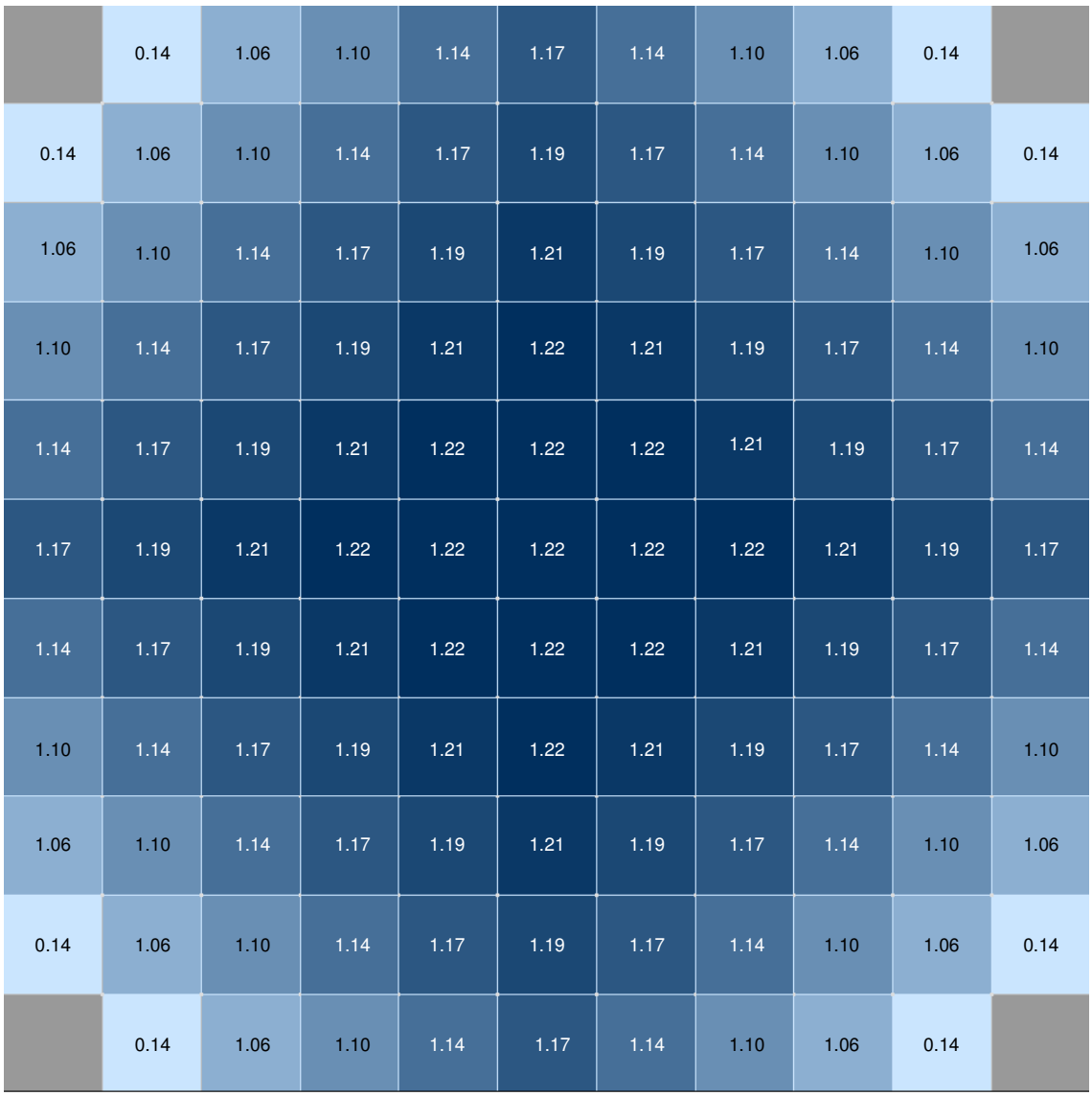


**Figure 4-4: Depths predicted by the RFIM [m] – Case 2**

Figure 4-4 depicts the maximum water depth predicted by the variable extra head inundation routine. The result is symmetrical about the x- and y-axes, which suggest that the symmetry of the terrain was correctly recognized.

Test case 2 also tested, similarly to test case 1, the variable extra head calculation. The extra head values range from 0.22 m (depth 1.22 m) in the centre of the domain that is close to the origin of flooding to 0.06 m (depth 1.06 m) in the corners that are far from the flood origin. Two cells in each corner of the domain are flooded only partially to the level of 0.14 m.

## 4.2 Test sites description

The Rapid flood inundation model was tested on Greenwich and Thamesmead, two embayments on the River Thames in London. Over the course of history, development in and around London has encroached significantly into the River Thames floodplain. As a result, the reach between Teddington Weir and Dartford Creek is now at risk of tidal flooding during a 1:1000 year event. The probability of such an event is predicted to increase in the future due to a combination of sea level rise and geological settlement of southeast England. The Environmental Agency has realised that it needs to improve its ability to plan for a tidal flood event in this location.

If flooded to a depth of 1 m, the direct damages to commercial and property assets within the Thames floodplain would exceed £30 billion (Sayers et al., 2007), which explains the motivation for the effort to improve knowledge of flood risk in this area.

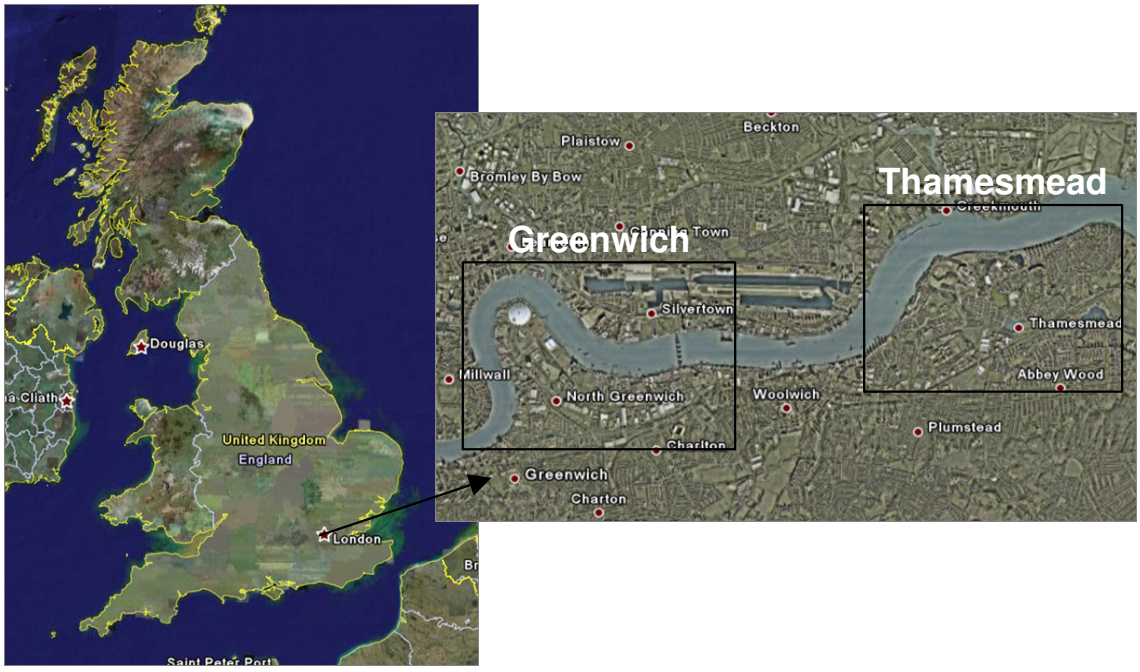


**Figure 4-5: Location of Greenwich and Thamesmead test sites**

The tidal Thames floodplain can be divided into 23 embayments, including Greenwich and Thamesmead, each considered hydraulically discrete. Greenwich embayment (Figure 4-5) was selected by Halcrow and HR Wallingford for testing various hydraulic

floodplain modelling approaches in order to identify the most appropriate ones (Wicks et al., 2004). As a result of extensive research in this area, high-resolution DEMs are available for both test sites.

Both Greenwich and Thamesmead embayments are densely populated built-up areas, very flat with the size of DEM 3390 m x 2412 m for Greenwich and 3596 m x 2570 m for Thamesmead. No flooding has been observed in either of these locations in recent history and, therefore, no real event measured data, which would be used for calibration or assessment of the models, is available. In such a case, simulations obtained by other models become the only possible option for assessing the performance of the RFIM. Fortunately, the previous tests at Greenwich (Wicks et al., 2004, Evans et al., 2007) created insight into typical flood patterns. Based on this earlier work the flood extent maps calculated by the two-dimensional hydrodynamic TUFLOW model were chosen as a benchmark for both Greenwich and Thamesmead case studies presented in this thesis.

## 4.3 Model assessment methodology

In order to analyse the model performance, a Monte Carlo simulation approach was used by generating 5000 random parameter sets. All parameter sets were used with all three inundation algorithms (zero extra head, constant extra head and variable extra head) on both test sites. Three flooding scenarios were considered for Greenwich and one flooding scenario was considered for Thamesmead. The structure of the tests is given in Figure 4-6.

The DEM used in both RFIM and TUFLOW models is an unfiltered (i.e. buildings are included) grid of 2 m resolution. A Manning friction coefficient of n = 0.025 and a time step $\Delta t = 1$ second were used on both test sites in TUFLOW.

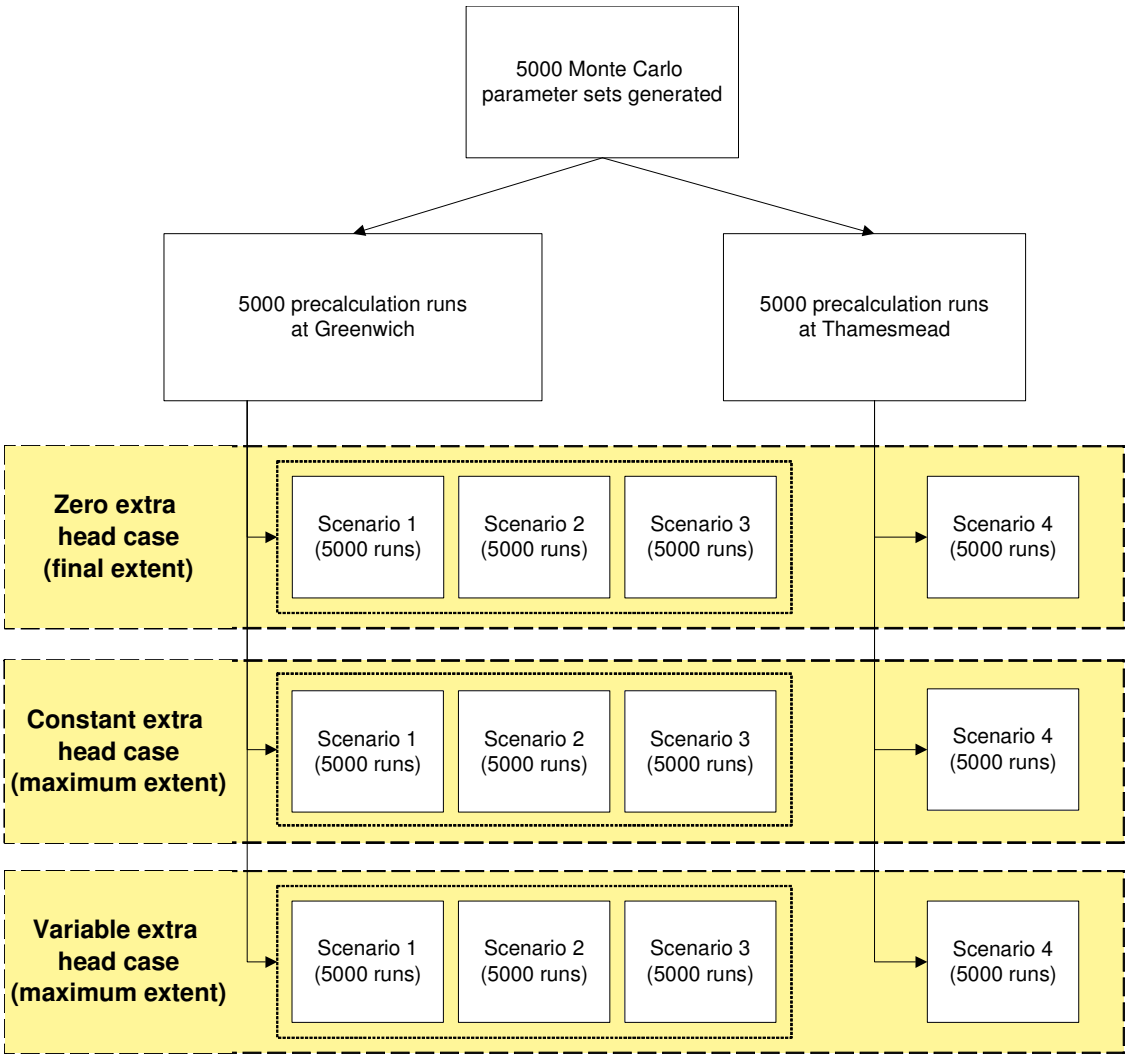


**Figure 4-6: Structure of the RFIM tests.**

Each of the 5000 parameter sets consists of $A_{min}$, $d_{min}$, $\Delta z$ and n values. These values were randomly generated from a uniform distribution in the ranges given in Table 4-2. The randomness ensures that each parameter set is independent of the others.

- The minimum cell plan area parameter, $A_{min}$, is applied in the precalculation routine and controls the size of the cells. It ensures that no cell is smaller than this value.

- The minimum cell depth parameter, $d_{min}$, is also applied in the precalculation routine and controls the depth of the cells. It ensures that no cell is shallower than this value.

- The extra head parameter, $\Delta z$, is applied in the inundation routine and directly sets the value of extra head in the flood cells. This parameter is used only in the constant extra head case calculation.

- The resistance coefficient parameter, $n$, is also applied in the inundation routine and controls the individual values of extra head in the cells. This parameter is used only in the variable extra head calculation.

In agreement with the RFIM assumption that the floodplain consists of natural depressions, the range of parameters $A_{min}$ and $d_{min}$ (Table 4-2) was selected to represent all possible sizes of natural terrain depressions present at Greenwich and Thamesmead.

| Parameter | Interval |
|---|---|
| Minimum cell plan area $A_{min}$ | < 500 , 50000 > $m^2$ |
| Minimum cell depth $d_{min}$ | < 0.10 , 2.00 > m |
| Extra head $\Delta z^{(1)}$ | < 0.00 , 2.00 > m |
| Resistance coefficient $n^{(2)}$ | < 0.01 , 0.20 > |

**Table 4-2: Parameter intervals. (1) Extra head value $\Delta z$ is applied only in the constant extra head calculation (2) Resistance coefficient $n$ is applied only in the variable extra head calculation**

For each parameter set both precalculation and inundation routines were run on the Greenwich and Thamesmead DEMs of 2 m grid resolution. Each flood extent map produced by the inundation routine was compared to the TUFLOW model predictions. Two objective functions were used to assess the agreement between the two. The first criterion used was the spatial measure of fit F:

$$F = \frac{Num(S_{RFIM} \cap S_{TUFLOW})}{Num(S_{RFIM} \cup S_{TUFLOW})} \qquad \text{(Eq. 4. 1)}$$

Where $S_{RFIM}$ and $S_{TUFLOW}$ represent the sets of pixels classified as wet by the rapid flood inundation model and by TUFLOW, respectively. The *Num* function gives the number of members of the set. The numerator represents the intersection of the two flood extent maps while the denominator represents their unification. In the case of total agreement

of flood extents, *F* would become equal to 1, while in case of zero agreement *F* would be 0. The higher the F value, the closer to TUFLOW the prediction is.

The spatial measure of fit gives a good measure of the percentage of pixels that are correctly predicted as flooded, but it does not assess the quality of the depth prediction at these pixels. Therefore a second measure is used - a root mean square error (RMSE) of the flood depth predictions compared to the TUFLOW results:

$$RMSE = \sqrt{\frac{1}{n}\sum_{i=1}^{n}\left(h_{RFIM_i} - h_{TUFLOW_i}\right)^2} \qquad \text{(Eq. 4. 2)}$$

Where *i* is the *i*-th pixel of the domain consisting of *n* pixels; $h_{RFIM_i}$ and $h_{TUFLOW_i}$ are predicted water depths at the *i*-th pixel in the rapid flood inundation model and TUFLOW, respectively. The RMSE calculation accounts only for pixels in which both models predicted flooding, in order to eliminate the effect of areas that remained dry or that were predicted as flooded only by one model. The lower the RMSE value, the better the agreement between the TUFLOW and RFIM predictions.

The values of objective functions *F* and *RMSE* are then plotted against each parameter. It should be noted that, in the compliance with the GLUE methodology (Beven and Binley, 1992), each parameter set is assessed as a whole and sensitivity to a single parameter without the effect of other parameters of the set is not analysed. Hence, the plot of the objective function against a single parameter needs to be interpreted with care, because the influence of the other parameters in the set is 'masked'.

The plots of objective function reveal information about the behaviour of the model over the whole parameter space. If any pattern is recognized and areas of either good or bad performance are identified then the flood extent map is analysed closer, allowing possible imperfections in the volume spreading method to be explained.

The analysis also aims to draw conclusions on the existence of general optimum parameter values or range(s) that are scenario-independent or test site-independent.

#### *4.3.1.1 Greenwich test site*

Three inundation scenarios were tested at Greenwich embayment, covering two event magnitudes and two breach locations. The scenarios were selected in a way that the sensitivity of the parameters to event magnitude and to flood incident location could be tested. Breach locations were chosen such that the expected flooding pattern is not obvious and instead a rather more complex flooding behaviour is anticipated. The input values of the total volume of inundation $V_{total}$ and the inflow peak $Q_{max}$ are representative of the expected typical storm surge event in this location and were selected with respect to the previous Greenwich and Thamesmead numerical modelling tests by Wicks et al. (2004) and Alevyzaki (2007).

##### *4.3.1.1.1 Scenario 1*

The breach is located in the north-west part of the Greenwich embayment (Figure 4-7).

Breach location: A (coordinates x = 538812, y = 180136)

Total volume of inundation $V_{total} = 77000\ m^3$

Peak flow at the breach $Q_{max} = 47.0\ m^3/s$

Scenario 1 was modelled by TUFLOW and the final flood extent map (Figure 4-7) and the maximum flood extent map (Figure 4-8) were produced to be used as a benchmark for the RFIM predictions. The maximum flood extent map consists of maximum depths encountered at each pixel. The final flood extent captures the end of the simulation when the water is still and all the flood volume is stored in depressions.

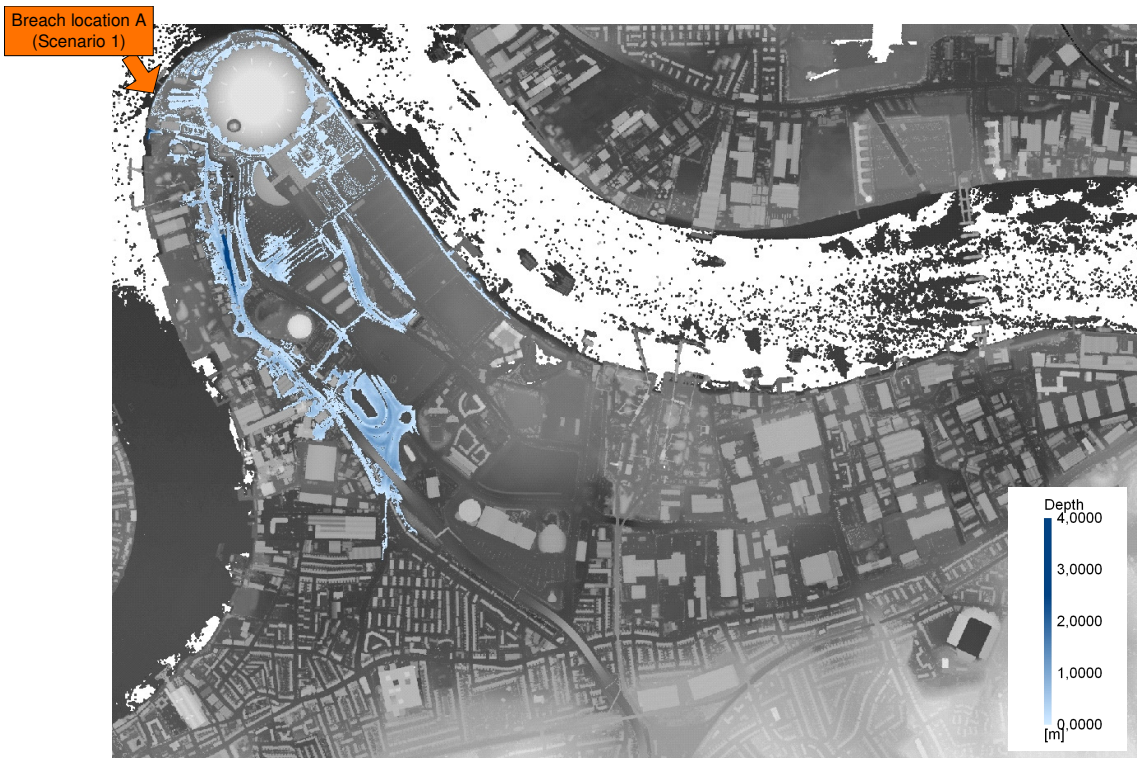


**Figure 4-7: TUFLOW prediction of final flood extent - Scenario 1**

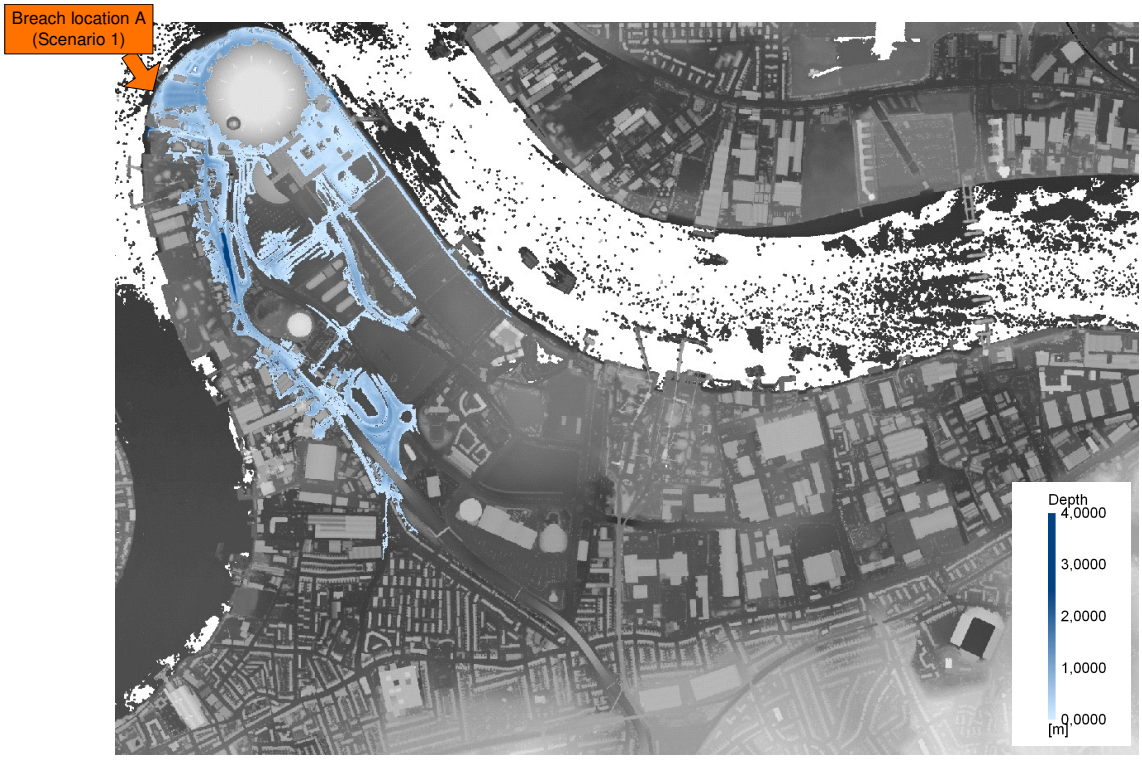


**Figure 4-8: TUFLOW prediction of maximum flood extent - Scenario 1**

*4.3.1.1.2 Scenario 2*

The breach is located in the north-eastern part of Greenwich embayment (Figure 4-9). The inflow boundary data are similar to those in Scenario 1:

Breach location: B (coordinates x = 540033, y = 179355)

Total volume of inundation $V_{total}$ = 75000 $m^3$

Peak flow at the breach $Q_{max}$ = 44.8 $m^3/s$

Maps of final flood extent and maximum flood extent for Scenario 2 produced by TUFLOW are depicted in Figure 4-9 and Figure 4-10 respectively.

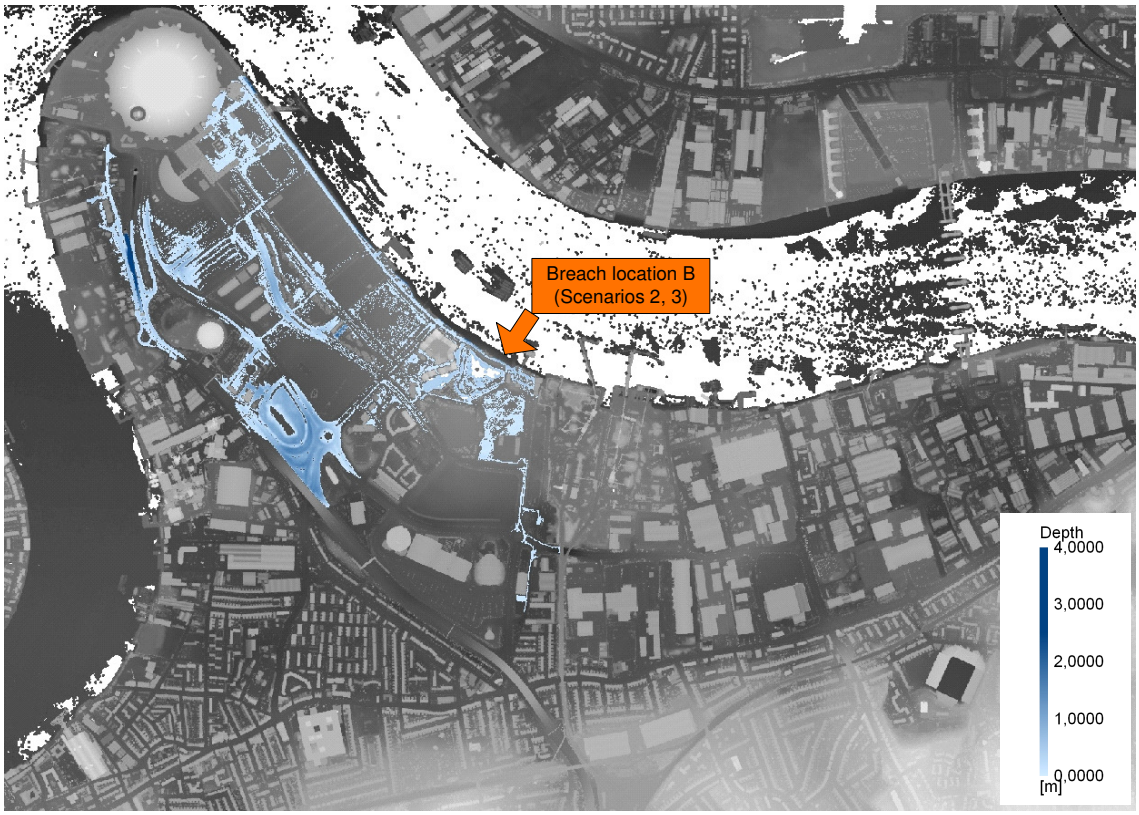


**Figure 4-9: TUFLOW prediction of final flood extent - Scenario 2**

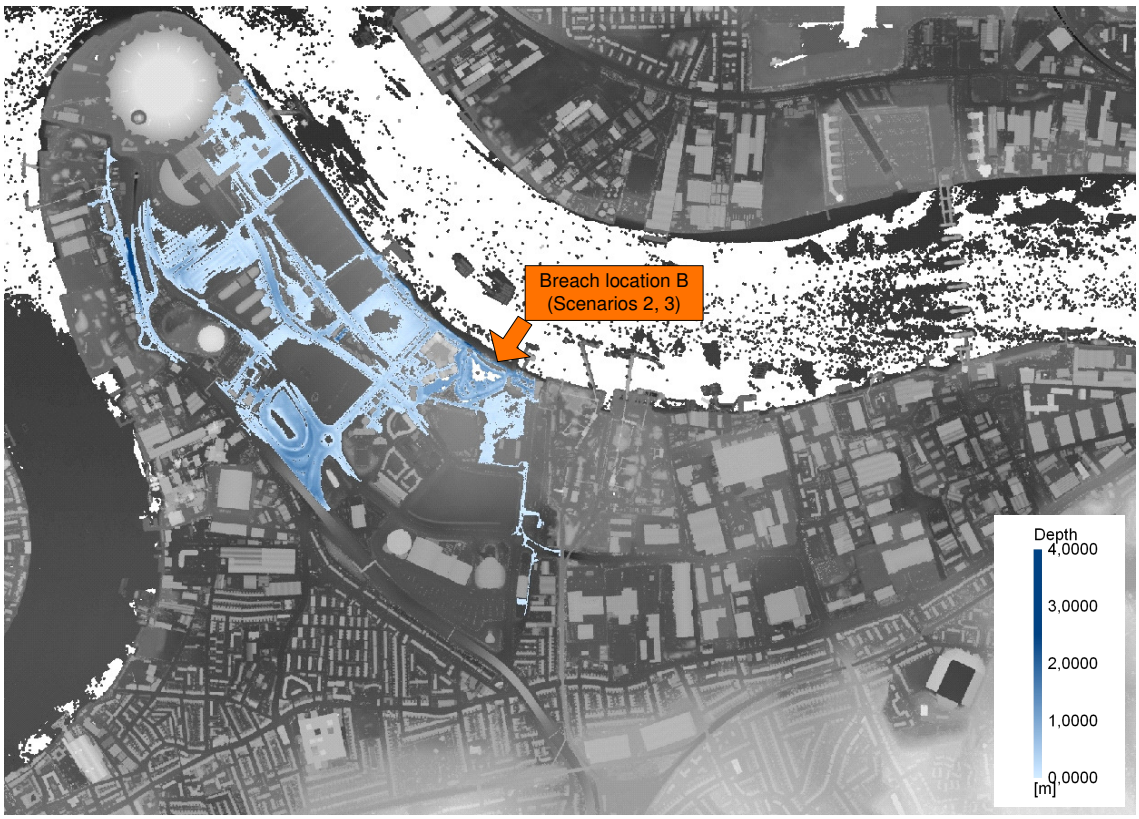


**Figure 4-10: TUFLOW prediction of maximum flood extent - Scenario 2**

*4.3.1.1.3 Scenario 3*

In Scenario 3 the breach location remains the same as in the Scenario 2, but the total volume of inundation and the peak flow through the breach are much higher.

Breach location: B (coordinates x = 540033, y = 179355)

Total volume of inundation $V_{total}$ = 230200 $m^3$

Peak flow at the breach $Q_{max}$ = 142 $m^3/s$

Maps of final flood extent and maximum flood extent for Scenario 3 produced by TUFLOW are presented in Figure 4-11 and Figure 4-12 respectively.

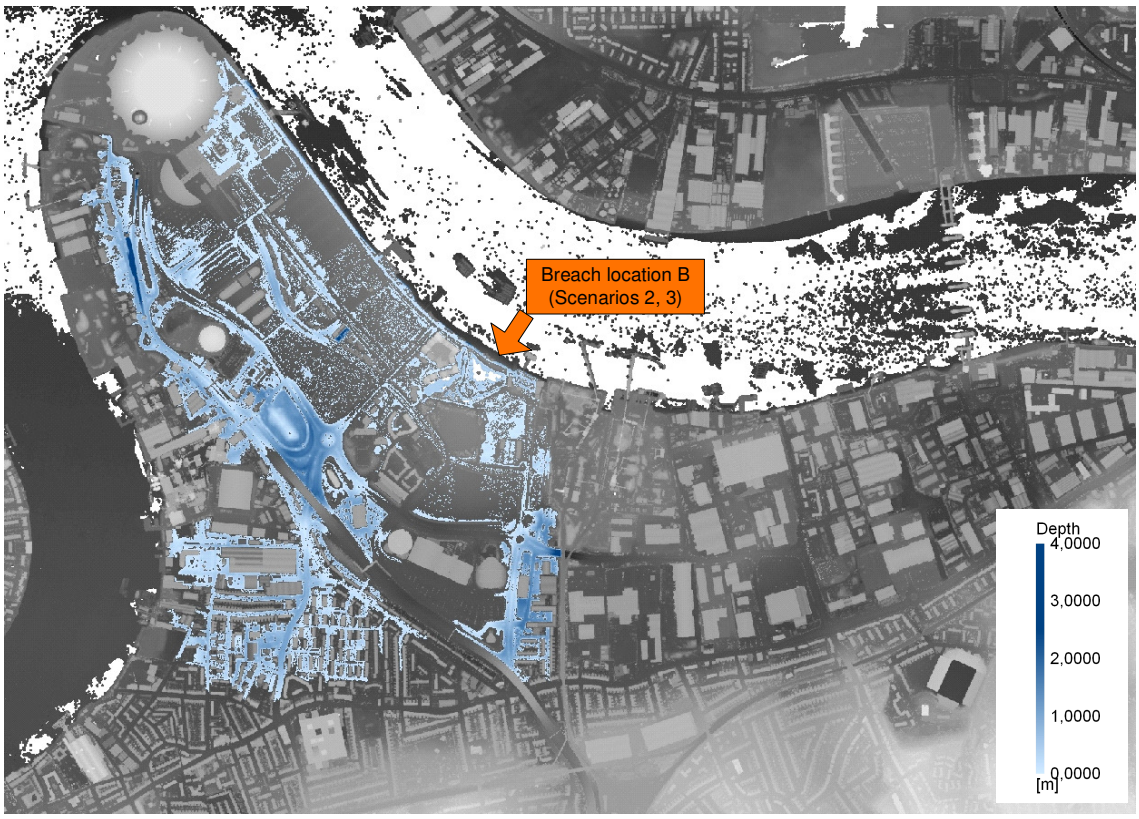


**Figure 4-11: TUFLOW prediction of final flood extent - Scenario 3**

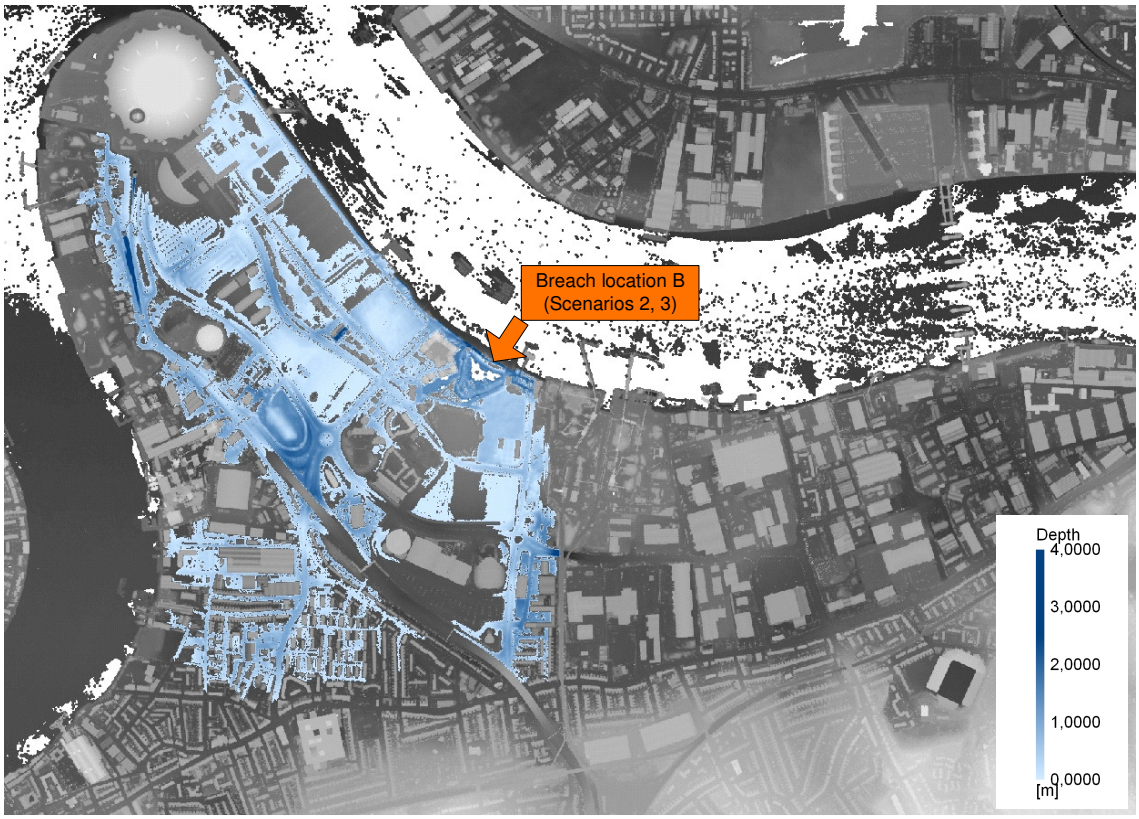


**Figure 4-12: TUFLOW prediction of maximum flood extent - Scenario 3**

TUFLOW uses the inflow hydrograph at the breach as a boundary condition. The RFIM uses only $V_{total}$ and $Q_{max}$ values instead. Hence, a timescale had to be added to the RFIM volume data to make them applicable in TUFLOW. The hydrographs were built in a way that ensures that both models use the same $V_{total}$ and $Q_{max}$ values. The duration of the TUFLOW inflow hydrograph was set to 1 hour and the following three point (i.e. triangular) hydrographs were used (Table 4-3).

| Scenario | Time (s) | | |
|---|---|---|---|
| | 0 | 1800 | 3600 |
| Scenario 1 | 0 $m^3/s$ | $Q_{max}$ = 47.0 $m^3/s$ | 0 $m^3/s$ |
| Scenario 2 | 0 $m^3/s$ | $Q_{max}$ = 44.8 $m^3/s$ | 0 $m^3/s$ |
| Scenario 3 | 0 $m^3/s$ | $Q_{max}$ = 142.0 $m^3/s$ | 0 $m^3/s$ |

**Table 4-3: Inflow hydrographs for Greenwich embayment flooding scenarios used in TUFLOW**

It should be mentioned at this point that an interesting observation was made regarding the way in which TUFLOW interprets an inflow hydrograph. It was found that TUFLOW interpolates the Q values between three defined hydrograph values non-linearly.

#### *4.3.1.2 Thamesmead test site*

Similarly to Greenwich the sensitivity of model parameters was tested also at the Thamesmead embayment. In this case only one flooding scenario of magnitude similar to Scenario 1 and Scenario 2 was tested.

Thamesmead is covered by natural depressions similar to Greenwich, which are interconnected, however, by a network of man-made channels that predetermine the flowpaths.

##### *4.3.1.2.1 Scenario 4*

In Scenario 4 the breach is located at the north-east part of Thamesmead embayment.

Breach location: C (Figure 4-13) (coordinates x = 547996, y = 181304)

Total volume of inundation $V_{total}$ = 79750 $m^3$

Peak flow through the breach $Q_{max}$ = 45.0 $m^3/s$

Similarly to the Greenwich flooding scenarios, the Thamesmead RFIM predictions were also compared to final flood extent map and maximum flood extent map calculated by TUFLOW model (Figure 4-13 and Figure 4-14). Both flood extents look similar with the channels present on the floodplain filled by water.

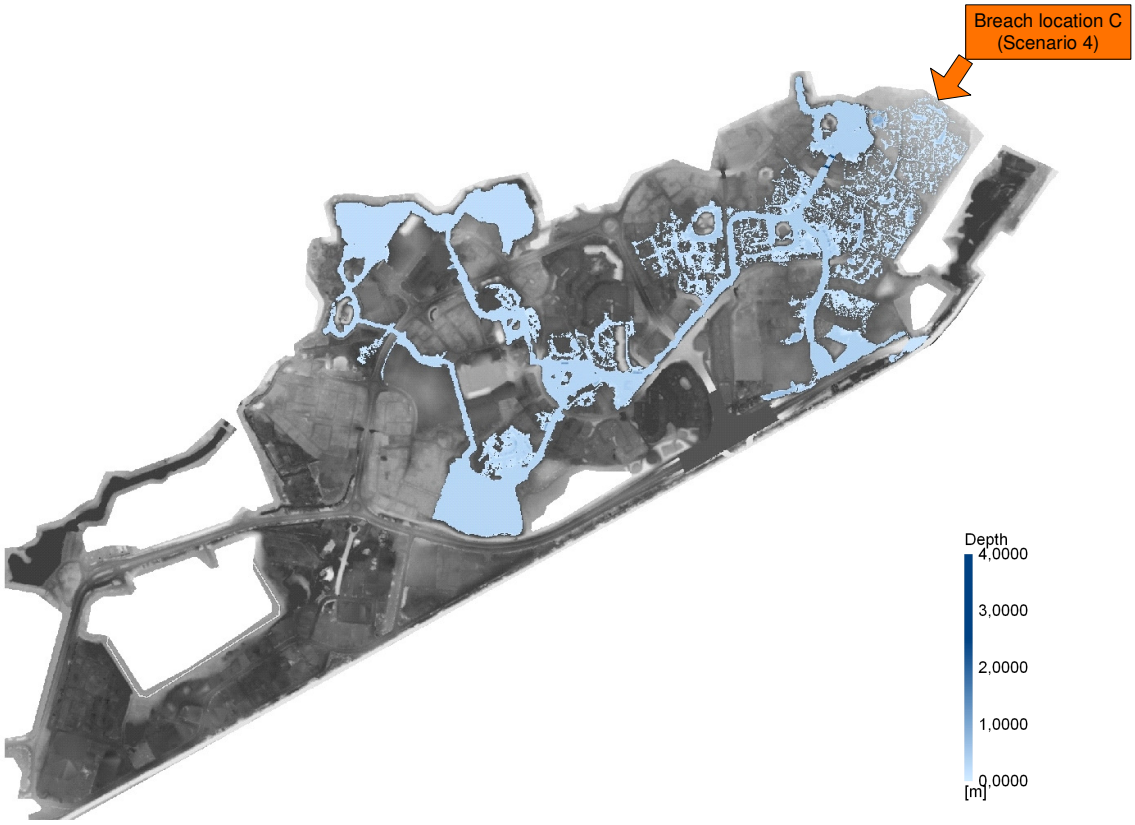


**Figure 4-13: TUFLOW prediction of final flood extent - Scenario 4**

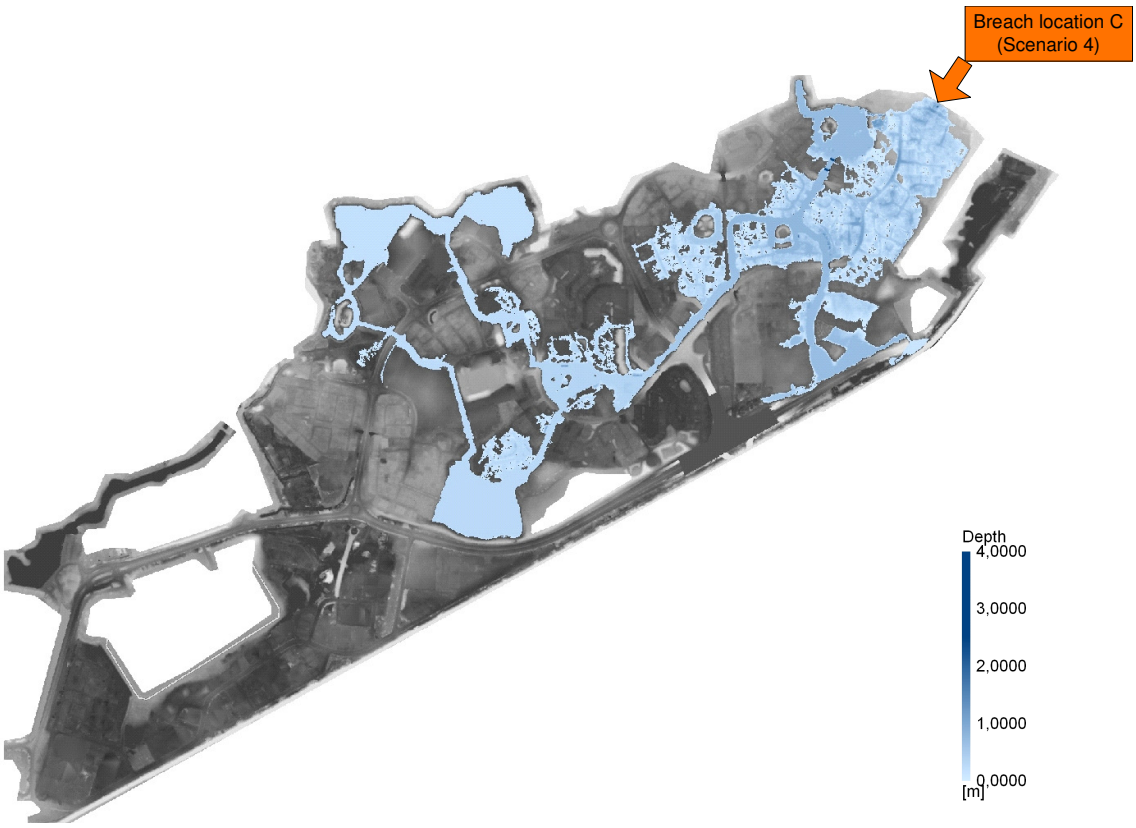


**Figure 4-14: TUFLOW prediction of maximum flood extent - Scenario 4**

Inflow hydrograph details are given in Table 4-4.

| Scenario | Time (s) | | |
|---|---|---|---|
| | 0 | 1800 | 3600 |
| Scenario 4 | 0 $m^3/s$ | $Q_{max}$ = 45.0 $m^3/s$ | 0 $m^3/s$ |

**Table 4-4: Inflow hydrographs for Thamesmead embayment flooding scenarios used in TUFLOW**

The $V_{total}$ and $Q_{max}$ values applied in both RFIM and TUFLOW simulations are of the same value.

The scenarios were designed in a way that the effect of test site, breach location and flood severity can be analysed:

- Scenario 1, Scenario 2 and Scenario 3 are run on Greenwich, Scenario 4 is run on Thamesmead

- Scenario 1, Scenario 2 and Scenario 4 are of a similar flood severity

- Scenario 2 and Scenario 3 represent the same flood defence breach location, but a different flood severity

## 4.4 Results

### *4.4.1 Precalculation routine*

Precalculation was carried out for Greenwich and Thamesmead for each parameter set ( $A_{min}$ and $d_{min}$ values) resulting in 5000 different flood cell distributions.

#### *4.4.1.1 Greenwich test site*

The number of flood cells recognized at Greenwich varied between 11 and 1894. In Figure 4-15 two graphs depict the number of flood cells plotted against each of the two parameters, and Figure 4-16 shows the number of flood cells as a result of the combination of the parameters. Each parameter set is represented by a dot and is present in all three plots. It is seen that most of the parameter combinations resulted in the order of tens of flood cells. Only a small fraction of parameter sets, those with low $A_{min}$ and low $d_{min}$ values, resulted in more than 200 flood cells. The higher the $A_{min}$ value and higher the $d_{min}$ value, the fewer flood cells were recognized.

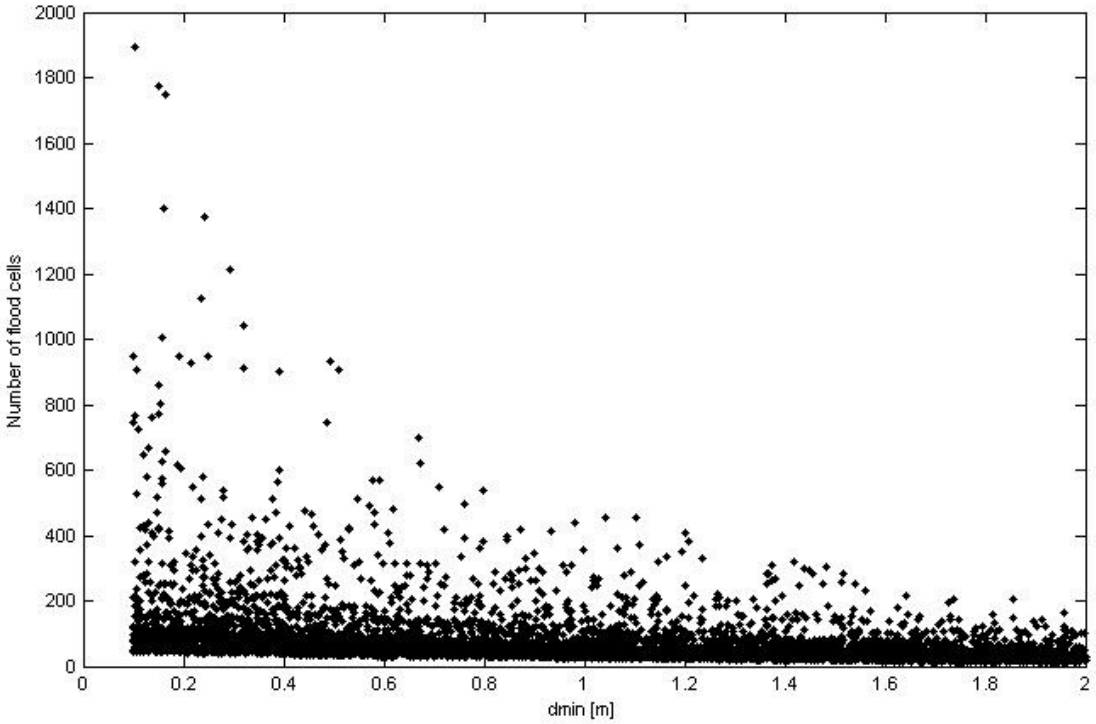


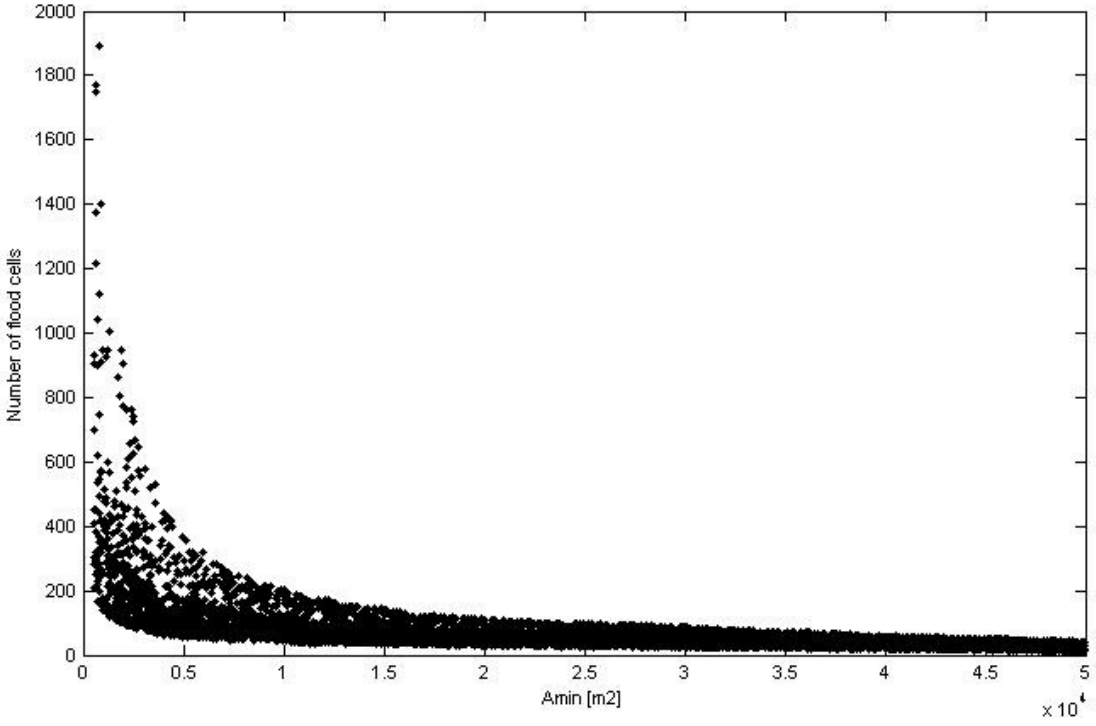


**Figure 4-15: Number of flood cells built by precalculation as a function of $A_{min}$ and $d_{min}$ parameters – Greenwich.**

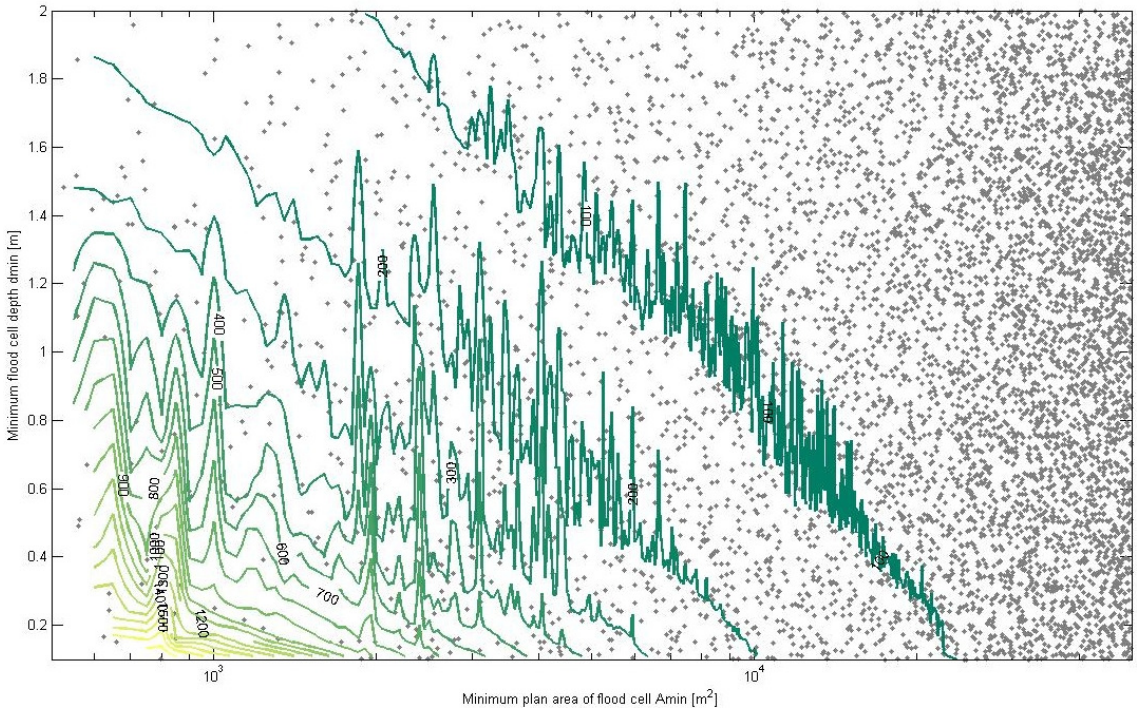


**Figure 4-16: Number of flood cells at Greenwich embayment calculated by the precalculation as a function of parameters $A_{min}$ and $d_{min}$. Each dot represents one parameter set.**

Interestingly, the contour lines (depicting the number of flood cells) in Figure 4-16 are not smooth. This can be explained by the way in which the precalculation is undertaken. At some point the floodplain is covered by a high number of very small flood cells. The algorithm initially attaches the cells that are smaller than the $A_{min}$ parameter. This is done in steps, firstly, the smallest cells are attached and then the larger ones. The rate of this attaching algorithm is controlled by the $A_{min}$ value. As a result a small change in the $A_{min}$ parameter leads to a different way in which the flood cells are attached, resulting in different flood cell numbers for very similar parameter sets, which explains the 'wiggly' line in Figure 4-16.

The precalculation routine is a time-consuming part of the RFIM, which would be carried out only once in a real flood risk study. In this research each parameter set required its own precalculation run making the task rather time consuming. The 5000 precalculation runs performed on a fast desktop PC took more than 14 days.

#### *4.4.1.2 Thamesmead test site*

The number of flood cells recognized at Greenwich varied between 1 and 937, which is approximately half of the number of Greenwich flood cells. Thamesmead embayment is crossed by a network of channels that form a strong communication links between flood cells. Importantly, the links lie in the bottom of the cells. Therefore the application of the minimum flood cell depth parameter condition (no cell is shallower than $d_{min}$) should theoretically produce one large single flood cell regardless of the combination of parameter values used. Surprisingly, it was found that this does not happen when the Thamesmead DEM is used. The DEM always contains some pixels of unreasonably high or unreasonably low elevation value due to random measurement error of the LIDAR. The unreasonably low located pixels are picked up by the precalculation algorithm as flood cell bottoms, and therefore the cell, which they are member of, passes the $d_{min}$ test and is recognized as a separate flood cell. Only use of a perfectly correct DEM would lead to the expected behaviour.

Similarly to Greenwich, a plot presenting the number of flood cells recognized by the precalculation as a function of the $A_{min}$ and $d_{min}$ parameters is depicted in Figure 4-17. When compared to Greenwich (Figure 4-15), the plots are of similar shape but the number of cells recognized at Thamesmead is considerably lower.

Most of the $A_{min}$ and $d_{min}$ combinations resulted in the number of flood cells being below 100 as can be seen in Figure 4-18.

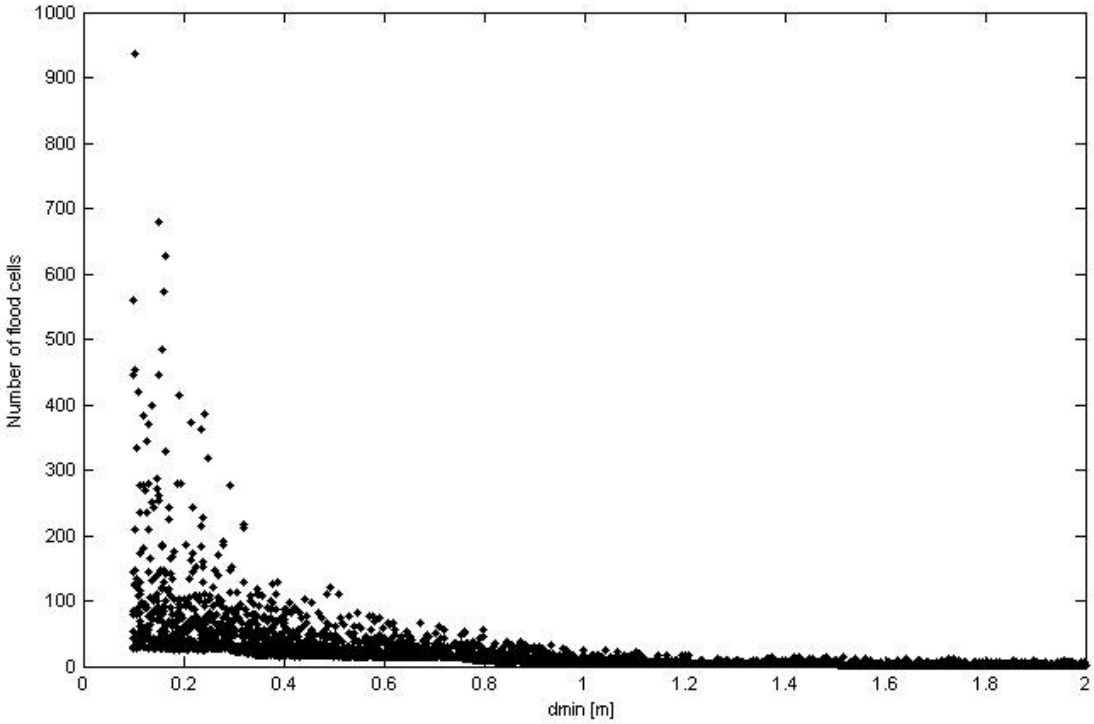


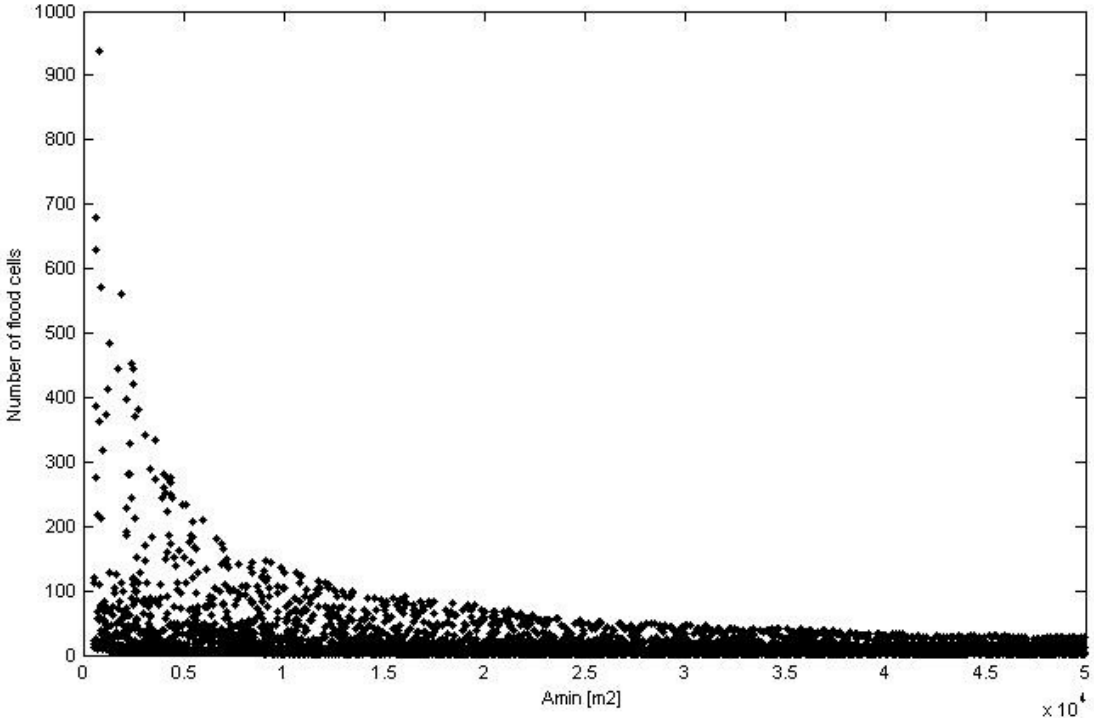


**Figure 4-17: Number of flood cells built by precalculation as a function of $A_{min}$ and $d_{min}$ parameters – Thamesmead.**

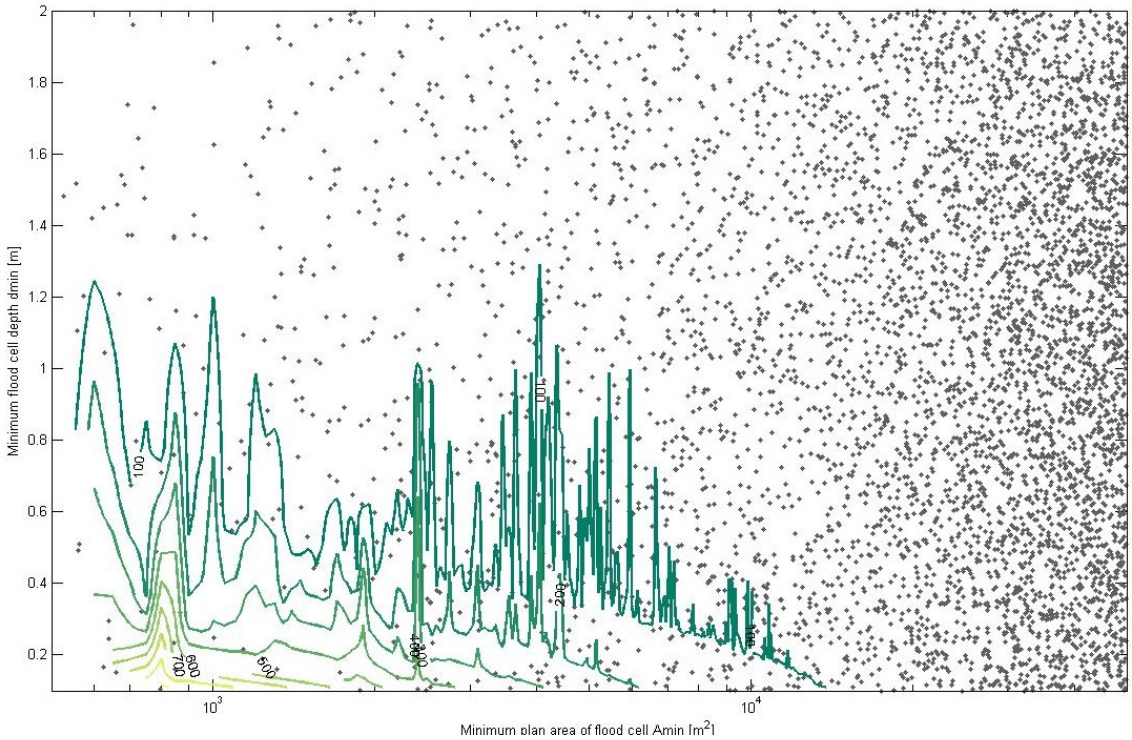


**Figure 4-18: Number of flood cells at Thamesmead embayment calculated by the precalculation as a function of parameters $A_{min}$ and $d_{min}$. Each dot represents one parameter set.**

The features of contour lines in Figure 4-18 depicting the number of flood cells correspond with the result for Greenwich (Figure 4-16). The contour lines are also not smooth for the reasons explained above.

### *4.4.2 Inundation routine*

Three versions of the inundation routine (zero extra head, constant extra head and variable extra head) showed numerical robustness throughout the testing. No problems regarding numerical stability were encountered when applied to a range of different flood cell distributions.

The RFIM flood extent predictions can be generally considered as relatively good especially with respect to a run-time of less than 0.3 seconds (see Table 4-7). To obtain the same result from the two-dimensional hydrodynamic model TUFLOW would take a run-time of order of hours or tens of hours (Table 4-5). For example the Thamesmead benchmark simulation of final flood extent lasted for more than 47 hours, while the RFIM predictions that showed very similar flood extents lasted for 0.24 seconds. It should be mentioned that all TUFLOW simulations were set up so the prediction of final flood extent at the end of the flooding event could be obtained.

| Scenario | TUFLOW run-time [hours : minutes] |
|---|---|
| 1 (Greenwich) | 6:11 |
| 2 (Greenwich) | 6:09 |
| 3 (Greenwich) | 10:12 |
| 4 (Thamesmead) | 47:09 |

**Table 4-5: TUFLOW run-times**

A wide range of model input parameter sets was analysed and the best predictions obtained from these tests were compared to those produced by TUFLOW for all four scenarios. The RFIM flood extent predictions are comparable to the TUFLOW results. From a visual inspection the simulations are also realistic compared with various models used by Wicks et al. (2004) for Greenwich and by Alevyzaki (2007) for Thamesmead. The best predictions in terms of spatial measure of fit F (Eq. 4.1) obtained by the RFIM are presented in Figure 4-19 to Figure 4-22. As can be seen, the RFIM over- or underpredicts flooding locally, but the overall flooding pattern is similar

to that produced by TUFLOW (represented by red line). Especially Scenario 4 showed very good agreement in terms of spatial flood extent (Figure 4-22).

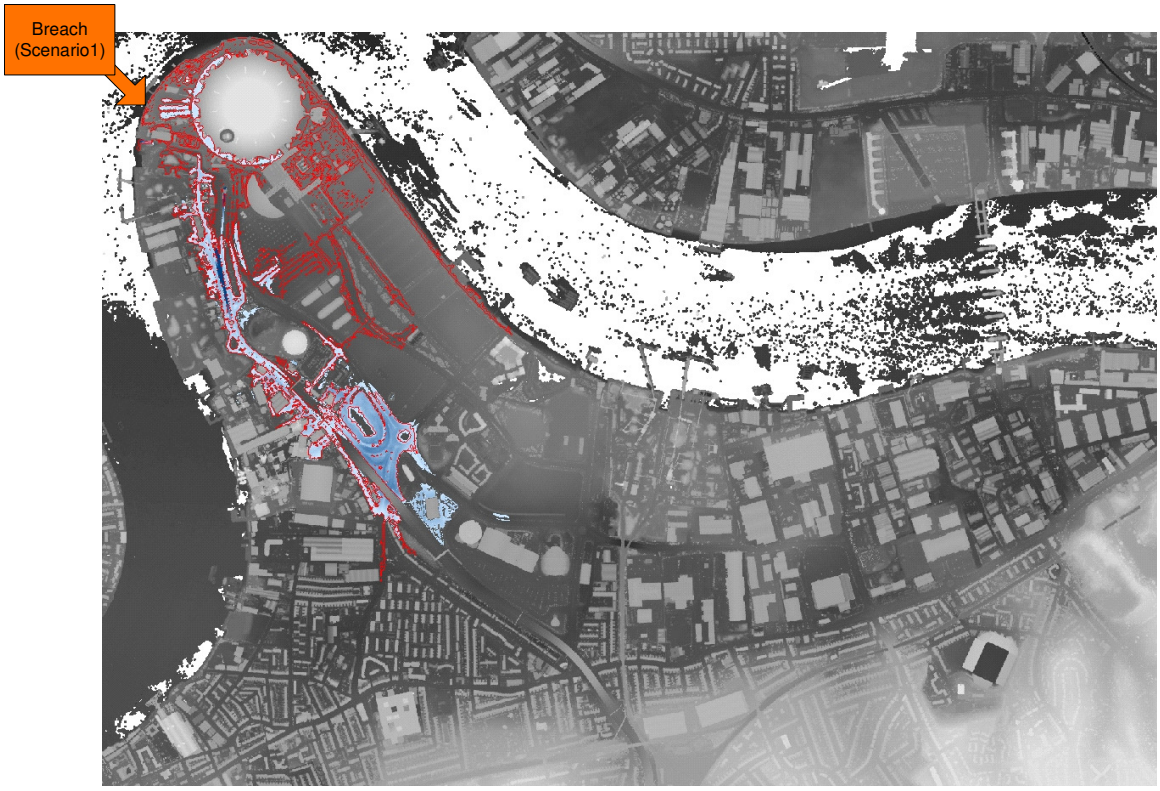


**Figure 4-19: The best RFIM prediction of final flood extent (in terms of F) – zero extra head - Scenario 1. The red contour represents the TUFLOW final flood extent prediction.**

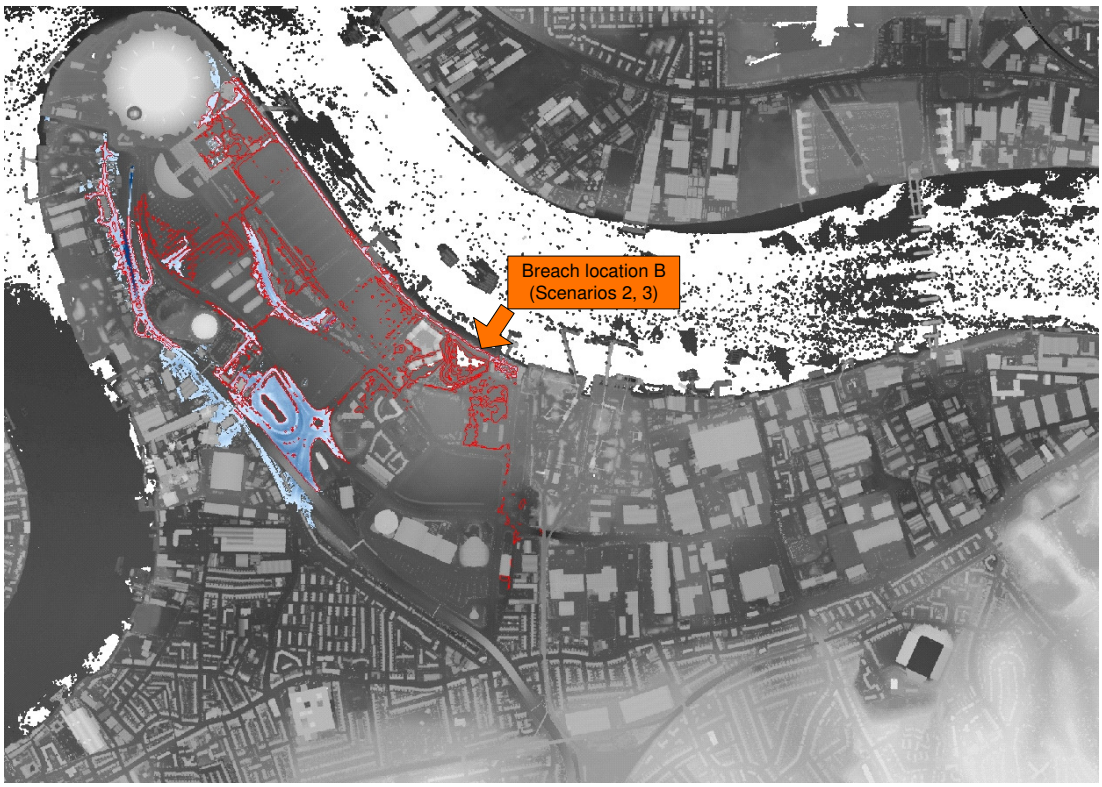


**Figure 4-20: The best RFIM prediction of final flood extent (in terms of F) - zero extra head - Scenario 2. The red contour represents the TUFLOW final flood extent prediction.**

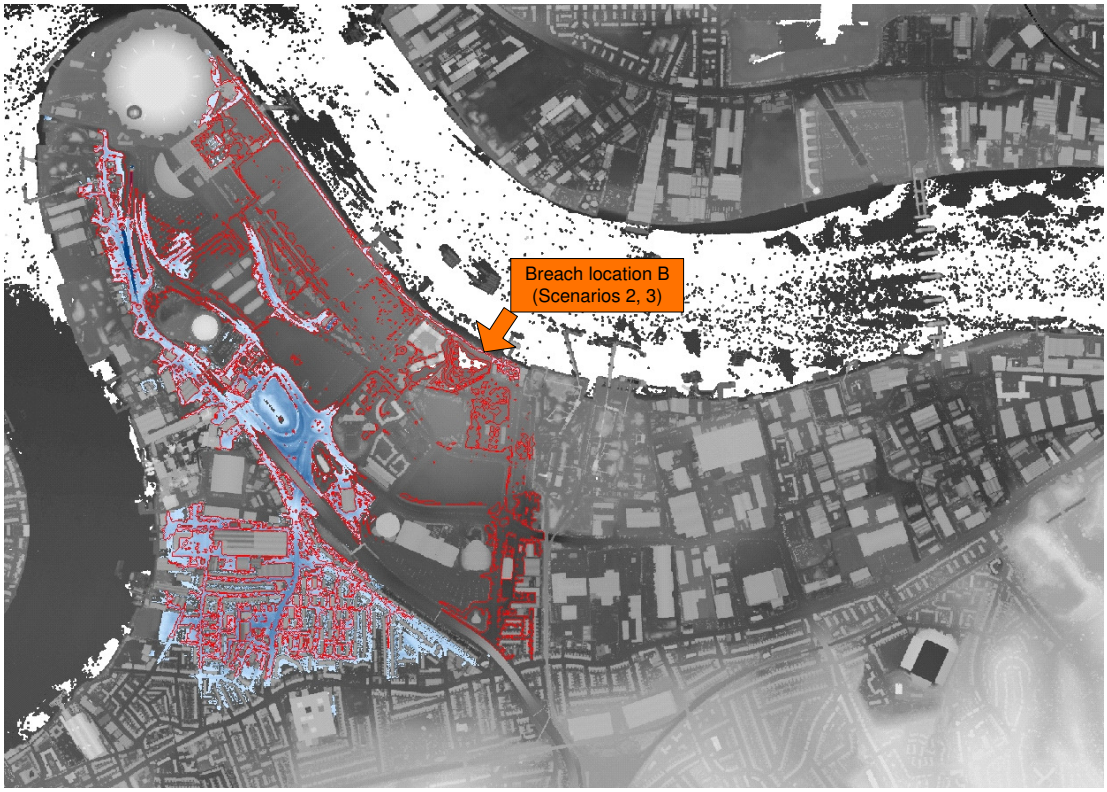


**Figure 4-21: The best RFIM prediction of final flood extent (in terms of F) - zero extra head - Scenario 3. The red contour represents the TUFLOW final flood extent prediction.**

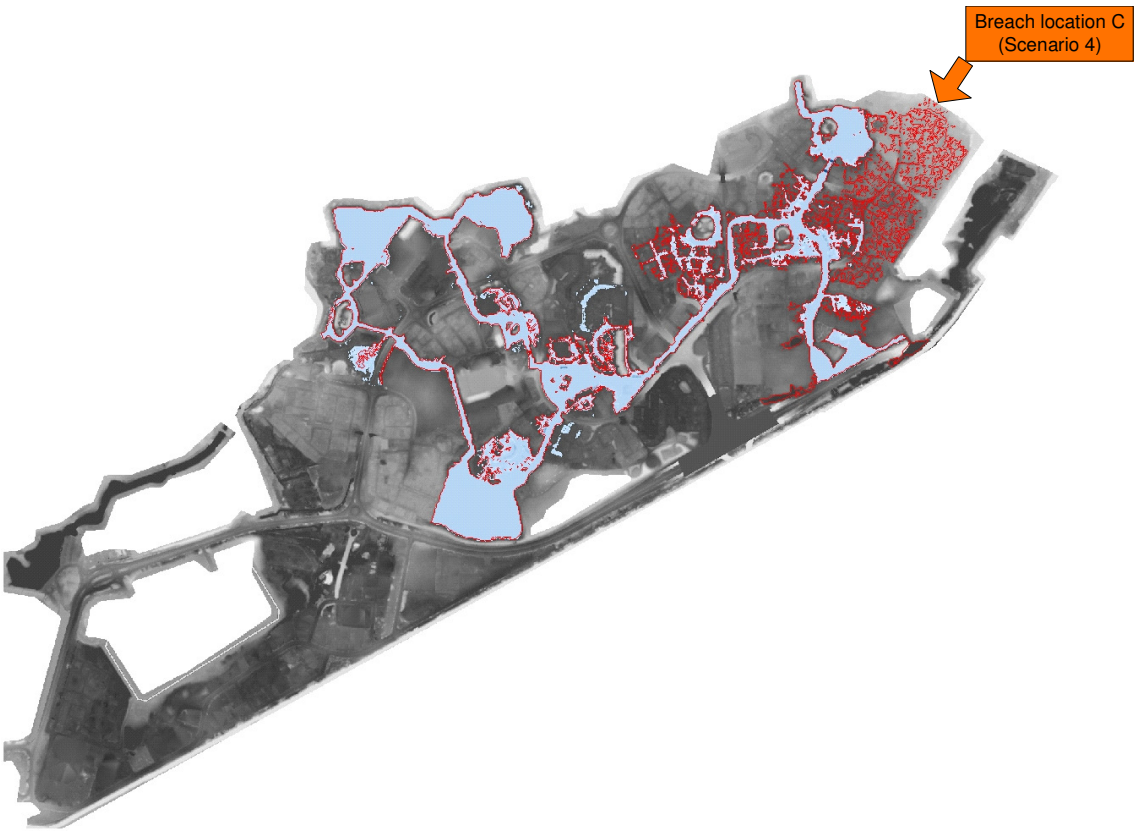


**Figure 4-22: The best RFIM prediction of final flood extent (in terms of F) - zero extra head - Scenario 4. The red contour represents the TUFLOW final flood extent prediction.**

A detailed analysis of the RFIM predictions for all flooding scenarios is presented in the sections 4.4.2.1 to 4.4.2.3.

### *4.4.2.1 Zero extra head inundation routine – final flood extent calculation*

In this section the basic volume spreading algorithm, which was explained in section 3.2.2, is applied. The flood volume is spread over the floodplain and no extra head is added to any flood cell. The predictions represent the final flood extent.

#### *4.4.2.1.1 Scenario 1*

Figure 4-23 shows the performance of the RFIM over the parameter space measured in terms of spatial measure of fit F (Eq. 4.1) and plotted over parameters $d_{min}$ and $A_{min}$. Each parameter set is represented by a single dot present in both graphs.

The plots depict the dependence of the predictions on $d_{min}$ over the analysed range. Four main areas can be recognized in the top graph in Figure 4-23. Maximum performance was observed for $d_{min}$ in the interval between 0.85 m and 1.45 m, which suggests that flood cells of such depth best represent flooding from this breach in the RFIM. Very low performance was observed for $d_{min}$ between 1.43 m and 1.70 m.

In the second graph in Figure 4-23, the dots form almost horizontal lines showing insensitivity to this parameter in a wide range of $A_{min}$ between 500 $m^2$ and 5000 $m^2$.

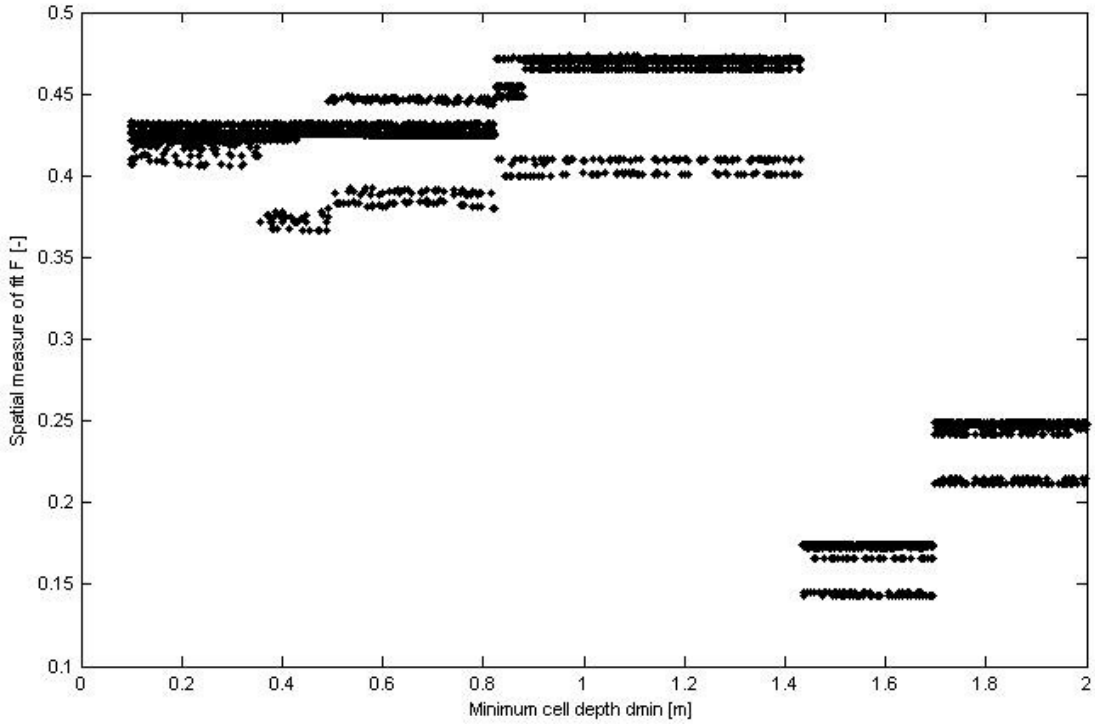


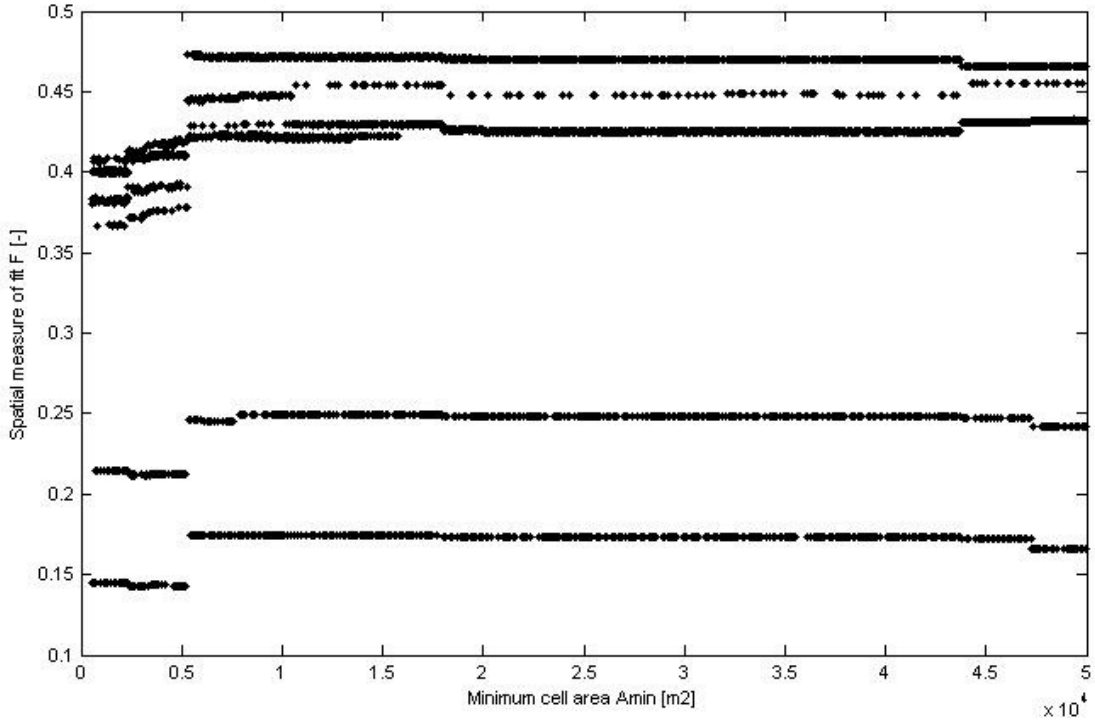


**Figure 4-23: Spatial measure of fit F - zero extra head case in Scenario 1 plotted against $d_{min}$ parameter and $A_{min}$ parameter**

The F values range between 0.143 and 0.473 depending on the parameter set. A closer look at the flood extent is needed in order to explain the relatively low F values and identify reasons for such behaviour.

The best RFIM flood extent prediction (that with the highest F) is presented and compared to the TUFLOW final flood extent prediction (red contour) in Figure 4-19. The comparison reveals that the RFIM has failed to predict the flooding in the eastern direction from the breach, while flooding in other areas is slightly overpredicted both in terms of spatial extent and depth of water due to the fact that the net volume of inundation in both models is the same.

A closer look at the flood spreading routine applied to this parameter set is needed to identify the reason why large parts of the DEM were incorrectly predicted as dry. The RFIM spreads the volume by filling flood cells following the direction of the lowest link between cells. In other words, if there are several neighbouring cells, only the one with the lowest link is flooded. If there are two lowest links at the same elevation then both are activated as was the case in the test reported in section 4.1.2. If the links have different elevations water cannot spread in multiple directions. Figure 4-24 depicts the flood cell distribution close to the breach as determined by the precalculation routine. The flood spreading starts in Cell 3, which is closest to the breach. The spreading continues in the following order: Cell 3, Cell 1, back to Cell 3, Cell 4, Cell 7, Cell 8, etc. The sequence shows that Cell 10 has not been activated in the crucial first few steps as a result of the lowest link rule and the regions south-easterly of the breach were not flooded. It is possible that a similar situation occurred again later in the simulation, but with less obvious consequences. The imperfections in the RFIM flood extent predictions caused by the lowest link rule can be observed throughout most of the tests performed at Greenwich.

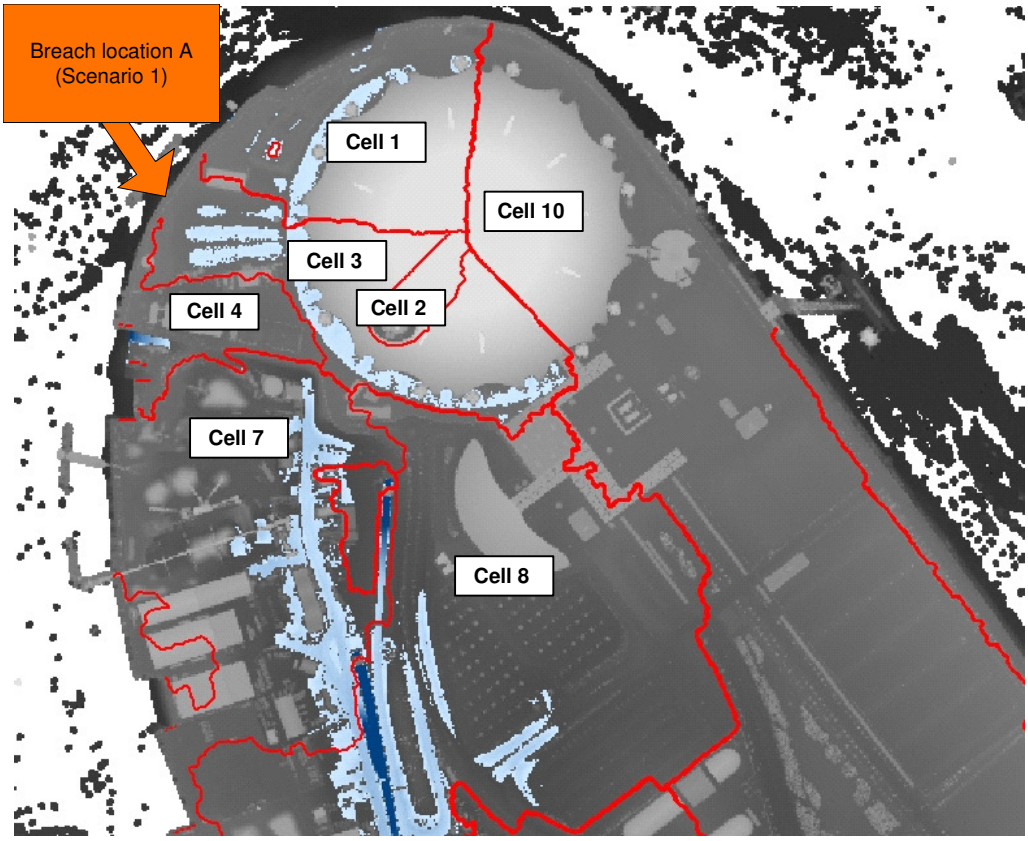


**Figure 4-24: Detail of flood cell distribution and flooding pattern close to the breach - Scenario 1. Red line represents the border between flood cells.**

Development of the multiple directions flood spreading was recognized as the main area of possible RFIM improvement and is believed to be of the best benefit. The original version of the Rapid Flood Spreading Methodology (RFSM) developed by HR Wallingford presented in HR Wallingford (2006) also did not account for spilling in multiple directions. This feature was incorporated recently and resulted in an improved ability to capture the flooding patterns on the floodplain. Lhomme et al. (2008) explain the method and gives comparison of the original and upgraded version of the RFSM.

In order to assess the effect that an introduction of multiple directions spreading would have, the order in which the cells are flooded in TUFLOW can be superimposed on the RFIM flood spreading algorithm. Such a test is recommended for future research.

Lhomme et al. (2008) also show that the performance of the method depends crucially on the suitability of the floodplain for simple volume-based model with respect to the assumptions.

The analysis that was carried out on the worst parameter set revealed an imperfection that can be generalized. The imperfection is associated with the precalculation routine. Figure 4-25 depicts the predicted flood extent for the worst (in terms of F) parameter combination. Apart from the underprediction of flooding in the south eastern direction due to the lowest link rule, the flooding reaches much farther south than on the TUFLOW map (Figure 4-7), while the extent of flooding in other areas is underestimated.

In this case the reason for such behaviour can be found in the precalculation part of the RFIM. The overpredicted flooded area is located in a single large flood cell, which is treated as a single unit, as is shown in Figure 4-25. The presence of the large flood cell was caused by the part of the precalculation algorithm that is responsible for decreasing the number of very small cells. In some cases the algorithm produces a few very large cells, while in other cases a higher number of smaller cells are created. The presence of one large cell can be avoided by the introduction of a maximum flood cell, $A_{max}$, that would complement the $A_{min}$ parameter.

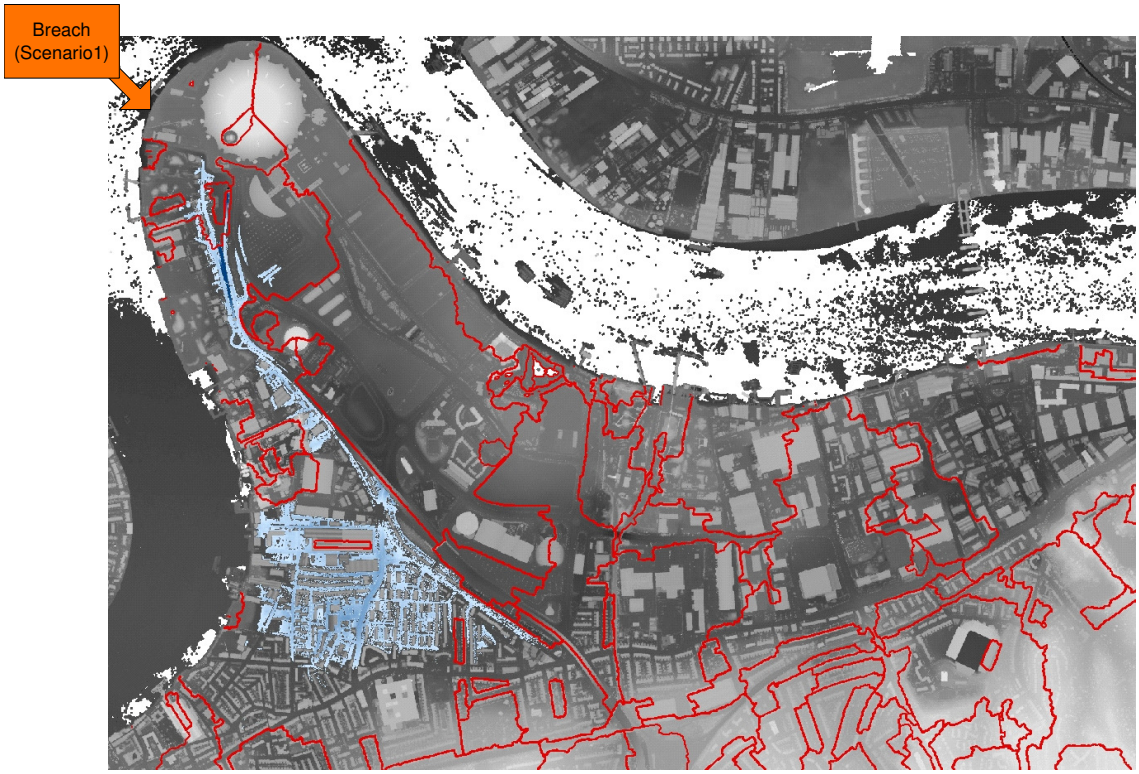


**Figure 4-25: The flood cell distribution used for the worst RFIM prediction.**

#### *4.4.2.1.2 Scenario 2*

Scenario 2 represents a flood of similar magnitude to Scenario 1, but the breach is located differently – in the location B (Figure 4-9). Scenario 2 was designed to test possible dependency of the optimal parameter values on the breach location.

The comparison of the F plot for Scenario 1 and Scenario 2 (Figure 4-23 and Figure 4-26), reveals that the optimum parameter values lie in very different parts of the parameter space. The optimal parameter $d_{min}$ in Scenario 2 can be found in the interval between 0.1 m and 0.5 m, which is close to the lower boundary of the tested interval. In other words, the shallower flood cells represent this breach scenario better unlike in Scenario 1 where the optimum $d_{min}$ interval lay between 0.85 m and 1.45 m. The plots show no similarity between Scenario 1 and Scenario 2. The sensitivity to $d_{min}$ and relative insensitivity to $A_{min}$, however, are common to both Scenarios. The range of F values is similar in both Scenarios.

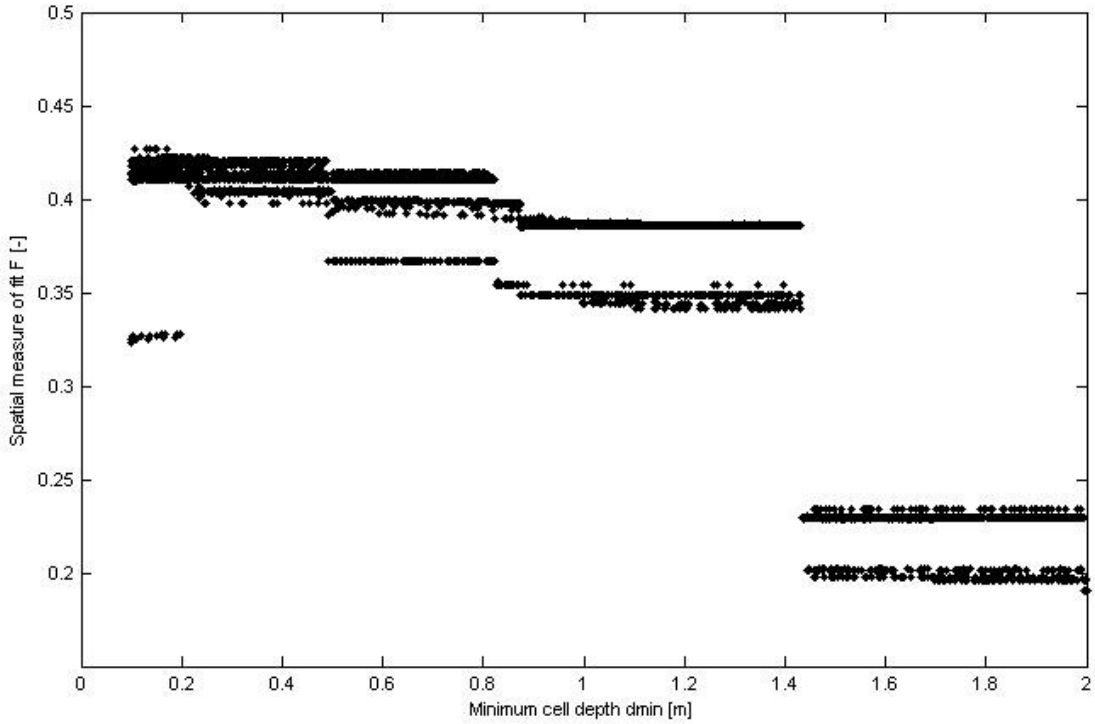


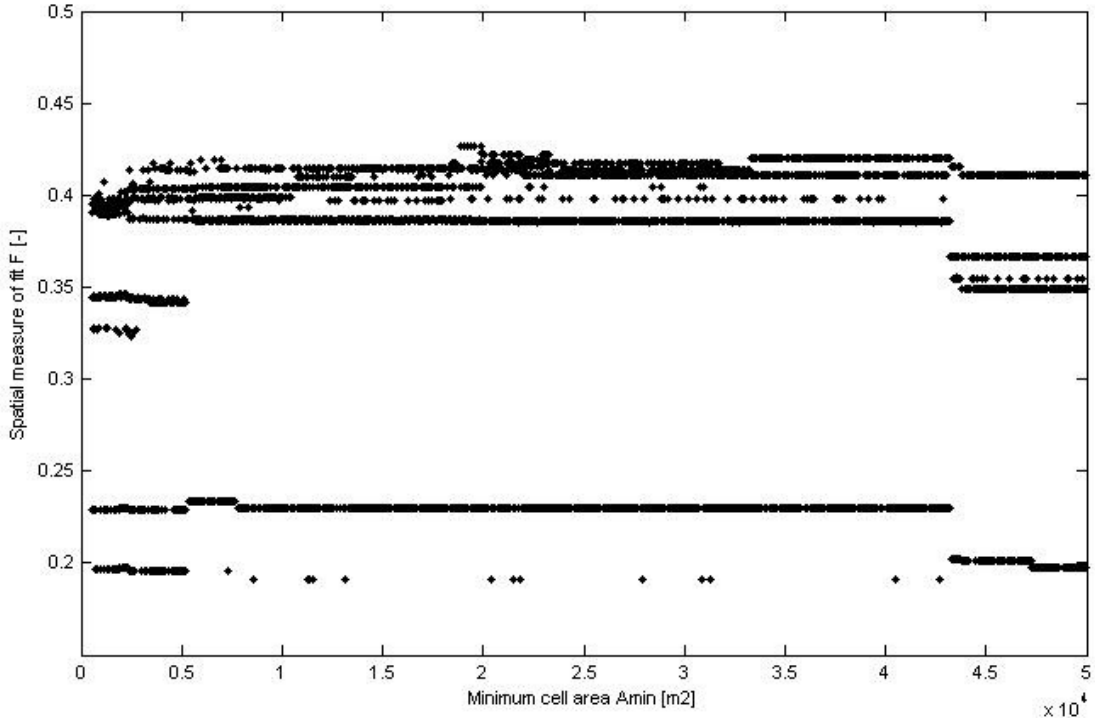


**Figure 4-26: Spatial measure of fit F - zero extra head case in Scenario 2 plotted against $d_{min}$ parameter (a) and $A_{min}$ parameter (b), respectively**

The best prediction in terms of F is shown in Figure 4-20. The comparison to the TUFLOW prediction (red line in Figure 4-20) reveals that although the maximum F is of a relatively low value (0.427), the flood extent map shows a similar inundation pattern. Certain locations were incorrectly predicted by RFIM as dry, due to the lowest link rule.

Additionally, a closer look at the TUFLOW result reveals that TUFLOW correctly fills all depressions on the flowpaths between the cells that were flooded at some point during the simulation, while the RFIM does not capture that feature. The RFIM algorithm fills all cells from the bottom and does not necessarily reach the pathway as it might lie too high to be flooded. The pixels on the flowpaths predicted by TUFLOW as flooded represent a relatively large area and hence are responsible for the relatively poor agreement with the RFIM in terms of F.

The generally low F values are also a result of the fact that the flood underprediction in some areas leads to overprediction somewhere else, because the net volume of inundation is the same for both TUFLOW and RFIM.

To conclude, although a slightly higher maximum F number was observed in Scenario 1, the flooding pattern for most parameter sets was recognized better in Scenario 2. Also optimum parameter values change with the location of the breach.

*4.4.2.1.3 Scenario 3*

The breach in Scenario 3 is located at the same place as in Scenario 2, but the flood is more severe.

The sensitivity of the model outputs to model parameters is shown in Figure 4-27. The plots are more complicated compared to Scenario 1 and Scenario 2 - the dots that represent individual parameter sets are more scattered, which can be simply explained by the fact that more cells were flooded.

The F values in the top plot in Figure 4-27 are skewed to the left, similarly to Scenario 2 (Figure 4-26), and optimum values of $d_{min}$ can be found on the left side of the analysed

interval. The best (and also the worst) performance can be obtained for $d_{min}$ between 0.10 m and 0.25 m.

The agreement with TUFLOW observed in Scenario 3 is generally better than in the previous two scenarios. The worst performing parameter set in Scenario 3 resulted in F = 0.475, while the best reached the value of F = 0.523, which shows that the algorithm was less sensitive to both parameters. This can be explained by the larger volume applied, which flooded areas (such as south-west parts in Figure 4-21), that were predicted as dry in Scenario 2. In Scenario 3 these were predicted as flooded by both models regardless of the parameter set used in the calculation.

Comparison of Scenario 2 and 3 revealed that in this case the optimum parameter values did not change with the magnitude of the event provided that the breach location remained unchanged. It is worth mentioning that the RFIM inundation routine is programmed in a way that two flooding events with the same breach location but different flood severity are simulated in exactly the same way, but the volume spreading in a higher magnitude event lasts longer until its larger volume of water is spread. In this case the imperfections in predictions caused by the lowest link rule had the same effect in both scenarios.

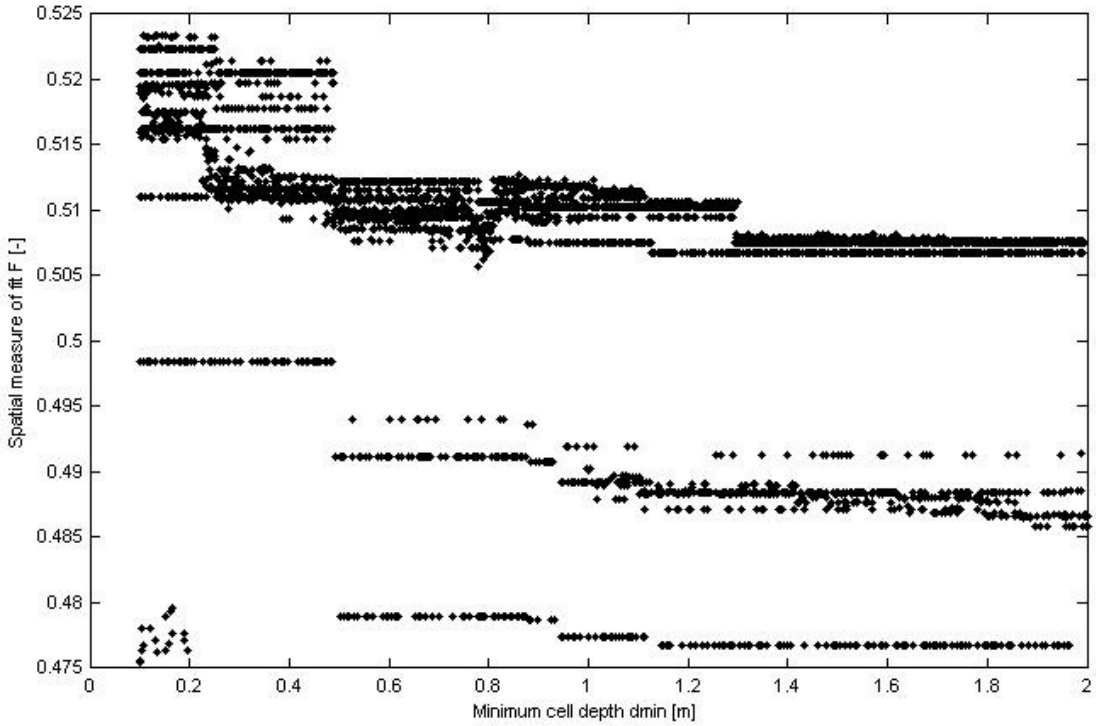


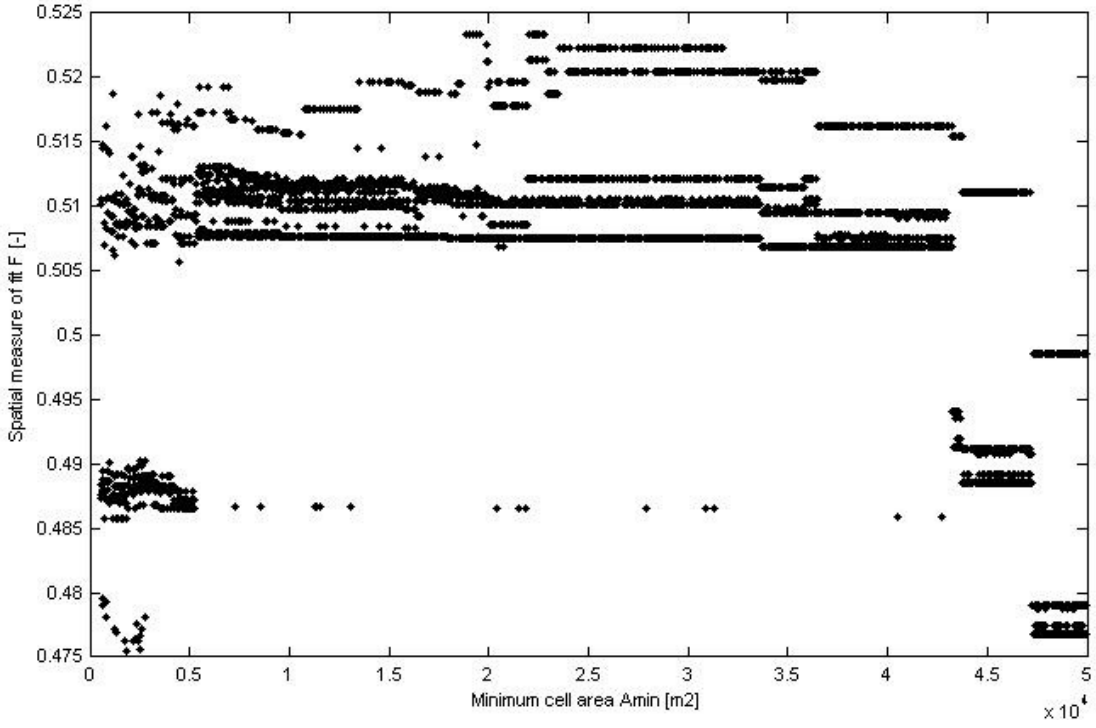


**Figure 4-27: Spatial measure of fit F - zero extra head case in Scenario 3 plotted against $d_{min}$ parameter (a) and $A_{min}$ parameter (b) respectively**

#### *4.4.2.1.4 Scenario 4*

The sensitivity plot of Scenario 4 (Figure 4-28) shows similar behaviour to the previous scenarios. The measure of fit F is sensitive to the minimum cell depth parameter $d_{min}$ and almost insensitive to the minimum cell area parameter $A_{min}$ with the best performance obtained for $d_{min}$ in the rather short interval 0.3 m – 0.4 m and reasonably good performance at $d_{min}$ = 0.3 m – 1.1 m. The pattern of the dots in Figure 4-28 is different to those observed at Greenwich, which confirmed the conclusion already made that the optimum parameter values depend on the test site features (e.g. topography) and hence are dependent on breach location and test site since different topographic features of a floodplain are exposed to inundation. Hence, no general recommendation on the optimum parameter values can be given.

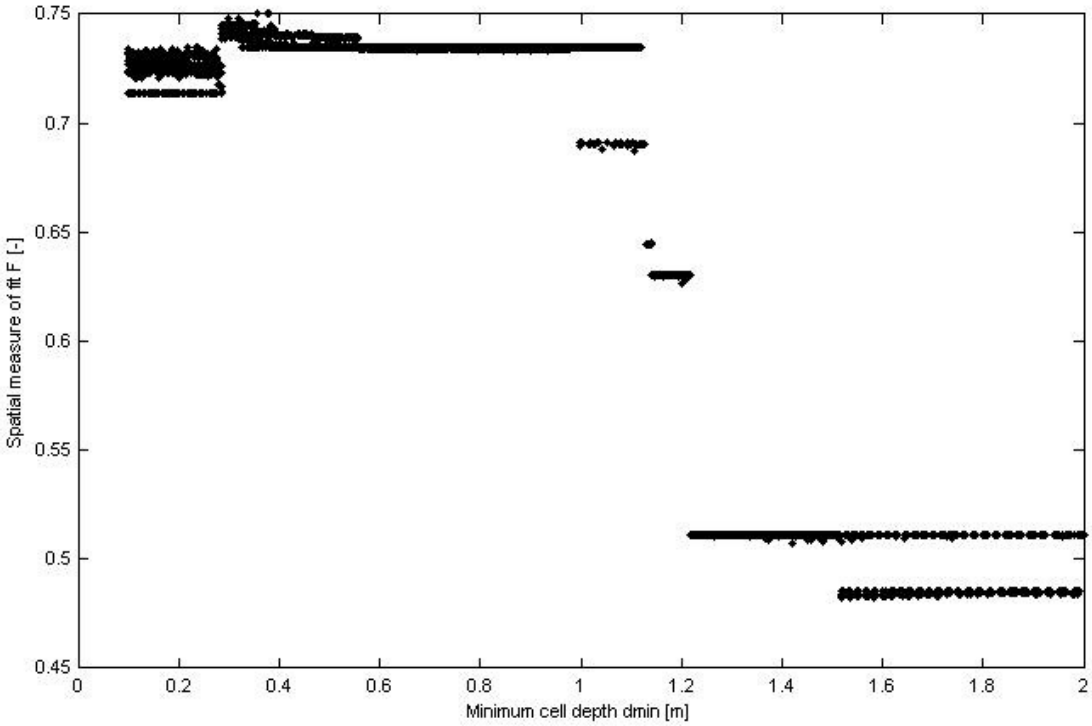


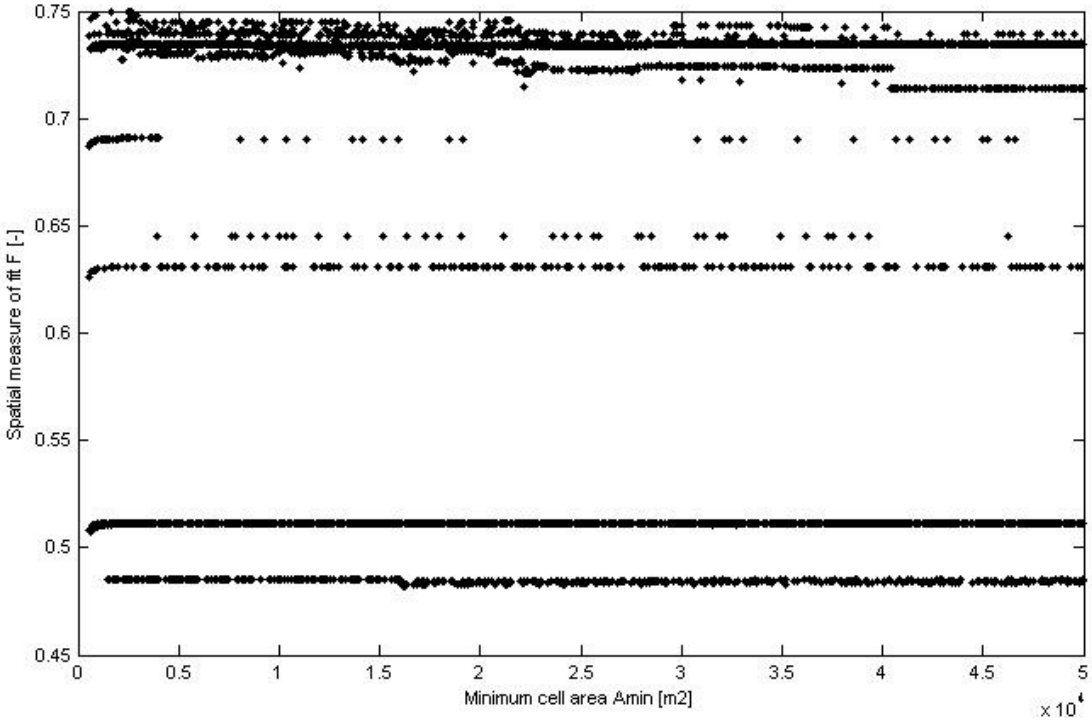


**Figure 4-28: Spatial measure of fit F - zero extra head case in Scenario 4 plotted against $d_{min}$ parameter (a) and $A_{min}$ parameter (b) respectively**

Figure 4-28 also shows that the values of spatial measure of fit F for Thamesmead are considerably higher than those observed on Greenwich. Flooding on Thamesmead embayment is primarily determined by a system of interconnected channels rather than independent depressions (Figure 4-22). Most of the flooding volume ends up in those channels, which was correctly recognized by both TUFLOW and the RFIM. However, the RFIM was not able to capture flooding on the complex pathway close to the flood defence breach (Figure 4-22). The general inability to capture flooding on pathways was explained in section 4.4.2.1.2.

#### *4.4.2.1.5 Discussion*

The tests of four different flooding scenarios revealed some common aspects of model behaviour and also uncovered the properties that are scenario-dependent. All scenarios had in common the sensitivity of the predictions to the $d_{min}$ parameter, although the optimum values lay in different areas of the parameter space in each case. All scenarios showed the inability of the RFIM to model the flooding on flowpaths and the difficulties to capture the spreading of the flood in more than one direction.

Performance of the model in terms of spatial measure of fit F for all four scenarios plotted against the number of flood cells is shown in Figure 4-29. The first three plots depict Greenwich scenarios, the fourth plot shows Thamesmead tests. The graphs show that the best performance was obtained for a narrow interval of the number of cells, different in each Scenario. If the number of cells was high, the multiple directions spreading problem (the lowest link rule) occurred. On the other hand if there were too few cells, and it was implied that in such case cells were large in area, their number was insufficient to capture the flooding, which lead to the behaviour shown in Figure 4-25.

Figure 4-29 also shows that $d_{min}$, $A_{min}$ were well selected as the RFIM precalculation parameters. If the number of cells was chosen as the only model parameter, no deeper insight into the behaviour of the model would be uncovered. The optimum number of flood cells itself does not ensure that the prediction would be correct as the quality of predictions depends primarily on the combination of the $A_{min}$ and $d_{min}$ parameters. As a result no clear recommendation on the optimum number of cells can be given.

To conclude, on the two test sites the optimum parameter values of $A_{min}$ and $d_{min}$ were dependent on the test site and the breach location, but were independent of the event magnitude. Due to this behaviour the general recommendation on the optimum parameter values valid for any breach location cannot be provided.

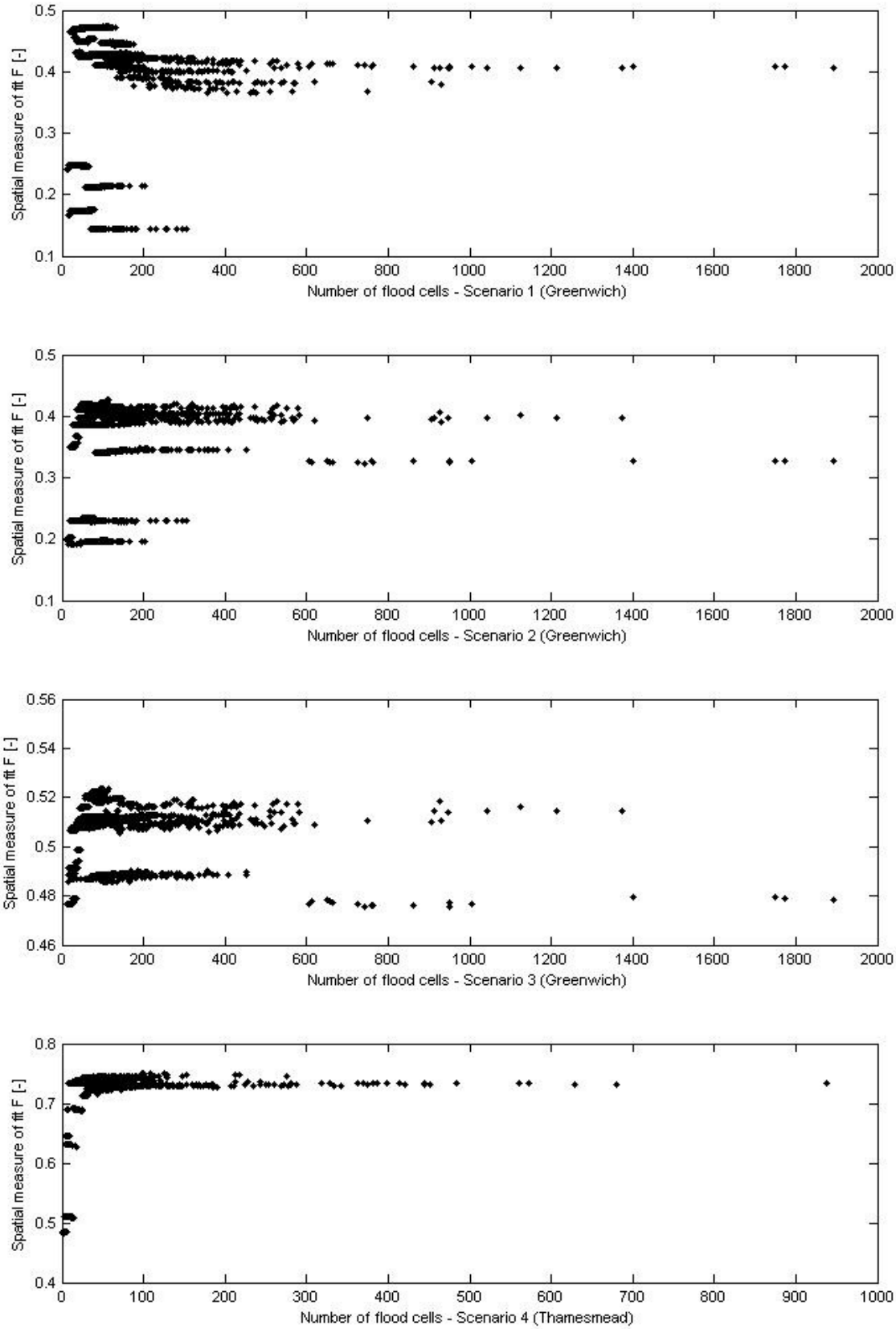


**Figure 4-29: Spatial measure of fit F of final flood extent predictions for all four scenarios plotted against the number of flood cells.**

#### *4.4.2.2 Constant extra head inundation routine – maximum flood extent calculation*

The constant extra head inundation routine predicts the maximum flood extent encountered during the flood. The flood cell switching algorithm is the same as the one used in the zero head case and the same cells are predicted as flooded in both cases. The constant extra head $\Delta z$ is added to the lowest link level.

The RFIM predictions for all four scenarios were compared to maximum flood extent maps produced by TUFLOW at Greenwich or Thamesmead, respectively (Figure 4-8, Figure 4-10 and Figure 4-12).

##### *4.4.2.2.1 Scenario 1*

The model performance was compared to TUFLOW in terms of the spatial measure of fit F (Figure 4-30) and RMSE (Figure 4-31). In the first two graphs in Figure 4-30, the sensitivity of the predictions to $d_{min}$ and $A_{min}$ parameters is depicted. The plot shows a similar pattern to that of the zero head case (Figure 4-23), although the dots are more scattered, owing to the sensitivity to the $\Delta z$ parameter, which is detailed in the third graph in Figure 4-30. The optimum range of the $d_{min}$ parameter is roughly the same as in the zero extra head case, which confirms that the flood spreading algorithm used is the same and that the same cells are flooded in both cases. The highest F values were observed for $\Delta z$ in the range between 0.5 m and 1.1 m.

Figure 4-31 shows a comparison of predictions in terms of water depth. Water depths at pixels that were predicted as flooded by both TUFLOW and RFIM are compared and the difference is quantified as a root mean square error – RMSE (Eq. 4.2). The plots show that the RMSE values of each parameter set depend on the $d_{min}$ and $A_{min}$ parameters (flood cell distribution), but are also significantly sensitive to the value of extra head $\Delta z$ (third graph in Figure 4-31). The best agreements with TUFLOW (lowest RMSE values) were observed for $\Delta z$ equal to 0.50 m with relatively good predictions for $0.10 \text{ m} \leq \Delta z \leq 1.05 \text{ m}$ depending on the flood cells set-up.

To conclude, the range of the optimum Δz parameter, in terms of the highest flood extent agreement (F), is similar to the optimum Δz value range giving the best agreement of water depths (RMSE).

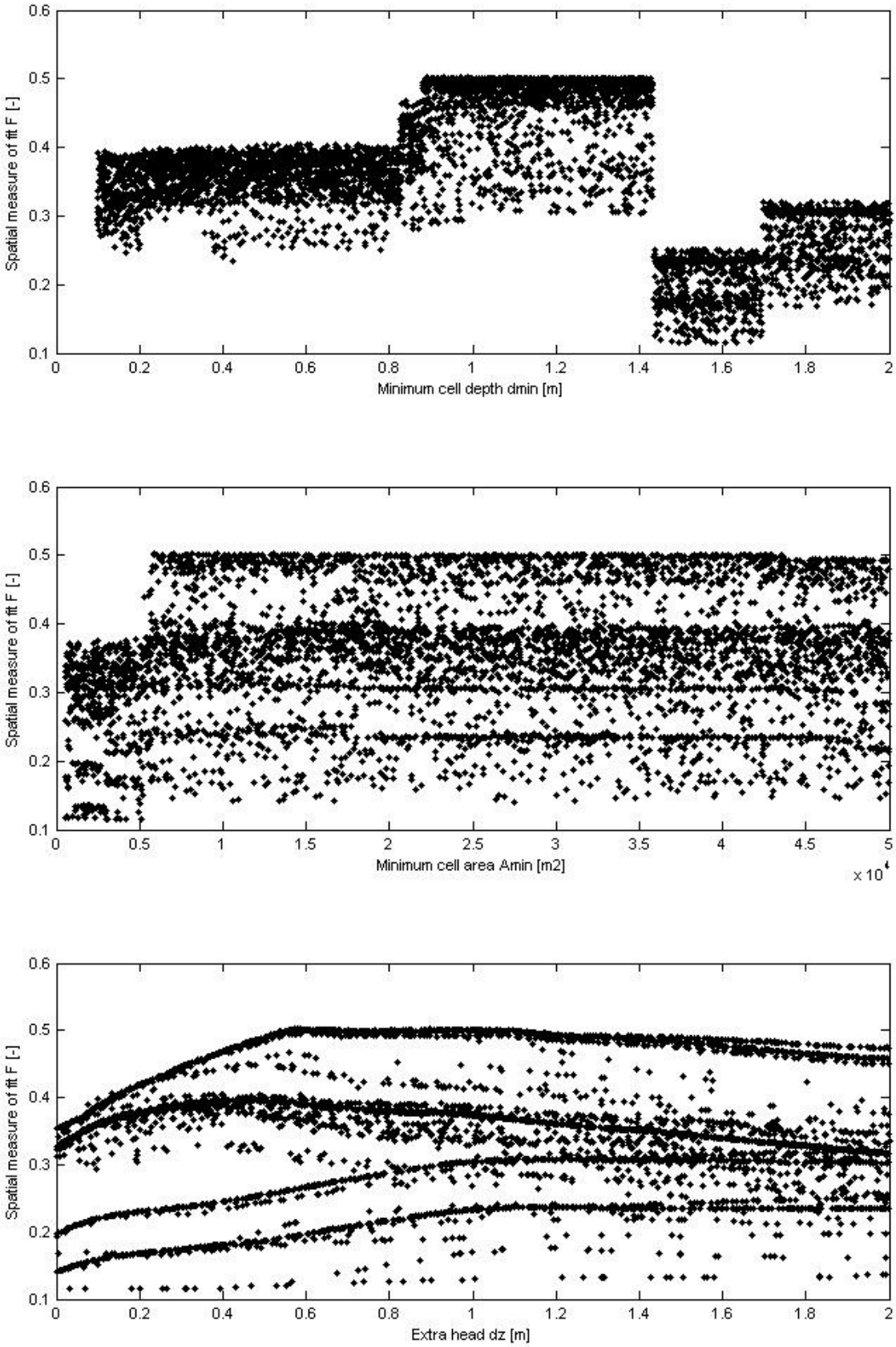


**Figure 4-30: Spatial measure of fit F – constant extra head case in Scenario 1 plotted against $d_{min}$, $A_{min}$ and $\Delta z$**

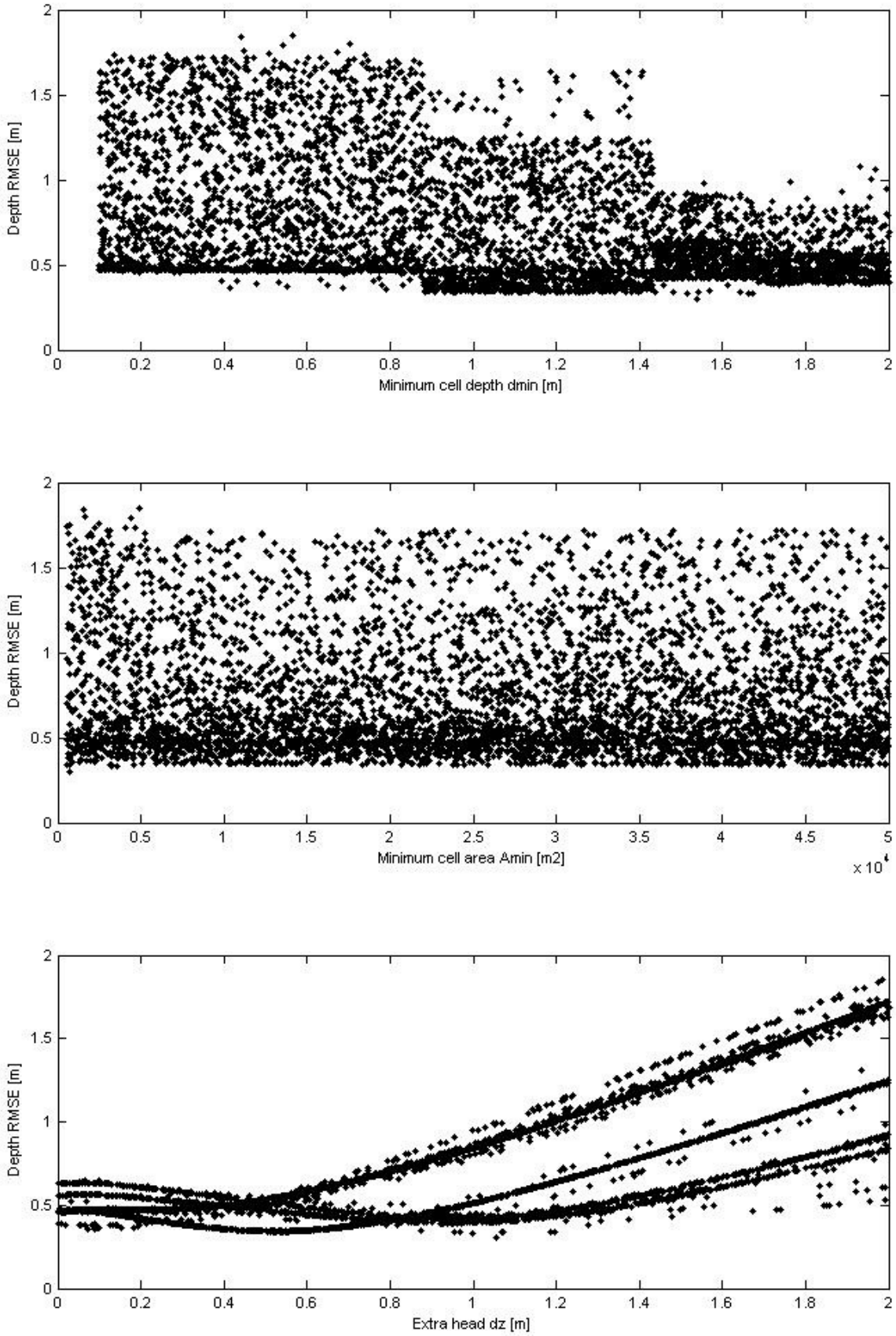


**Figure 4-31: RMSE - constant extra head case in Scenario 1 plotted against $d_{min}$, $A_{min}$ and $\Delta z$**

Although the introduction of the constant value of extra head attempts to predict the maximum flood extent, the values of extra head observed at cells during a real flood would not be constant everywhere on the floodplain, and would depend on local flow conditions. The RFIM therefore overpredicts water depth in some areas, while other areas suffer from underprediction. Figure 4-32 presents the difference in depths between the RFIM and TUFLOW models for the parameter set that showed the highest F value. The red colour represents areas where the RFIM underpredicted the depth; the green colour highlights areas where overprediction was achieved. It can be seen that underprediction was observed close to the breach suggesting that the constant $\Delta z$ value used by the model was too low, while areas remote from the breach were overpredicted by the model because of too high value of $\Delta z$ was used.


**Figure 4-32: Depth difference of the best RFIM prediction (constant extra head, Scenario 1) compared to TUFLOW. Green represents RFIM overprediction, red represents RFIM underprediction.**

#### *4.4.2.2.2 Scenario 2*

Tests performed on Scenario 2 show behaviour consistent with Scenario 1 (Figure 4-33 and Figure 4-34). As in Scenario 1, the optimum $d_{min}$ and $A_{min}$ values lie in the same part of the parameter space as in the zero extra head case. The optimum $\Delta z$ values can be found around 0.65 m when the fit of flood extent F is analysed and they lie in the interval 0.1 m – 0.65 m when the RMSE measure is applied. It can be seen that the dots in the third plot in Figure 4-34 form curves. Each curve represents flood cell distributions that behave hydraulically in a very similar way. It could be expected that with increasing extra head the curves would increase linearly in the region above the optimum value because the water level in the cells is directly affected by $\Delta z$. The curves are not straight lines, however, because the constant extra head value is not added to all flooded cells, but only to those that convey flooding (cells that pass water volume to their neighbour(s)). This observation is generally valid in all Scenarios; with the almost linear curves in the RMSE graph occurring in Scenario 4 (Figure 4-40).

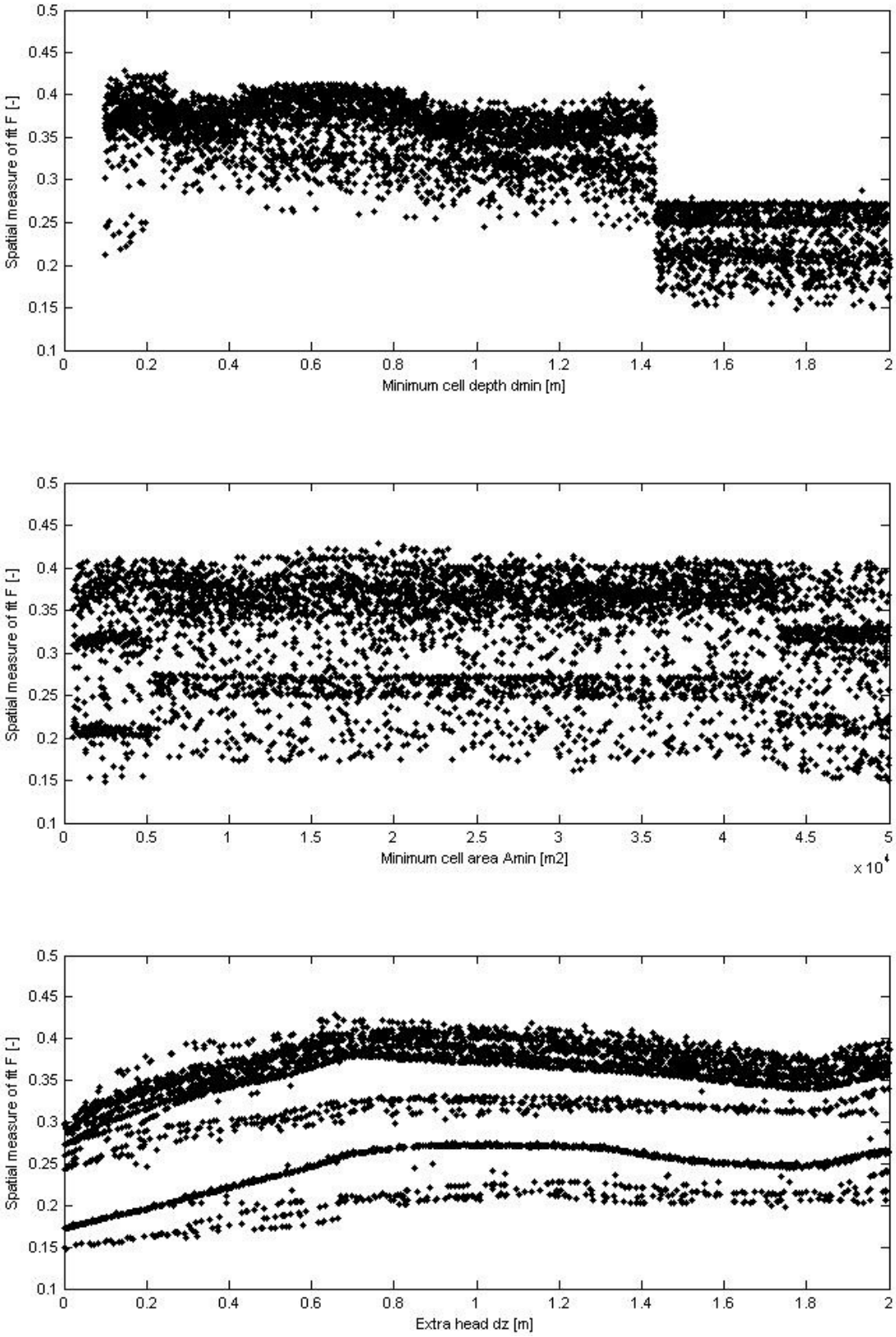


**Figure 4-33: Spatial measure of fit F – constant extra head case in Scenario 2 plotted against $d_{min}$, $A_{min}$ and $\Delta z$**

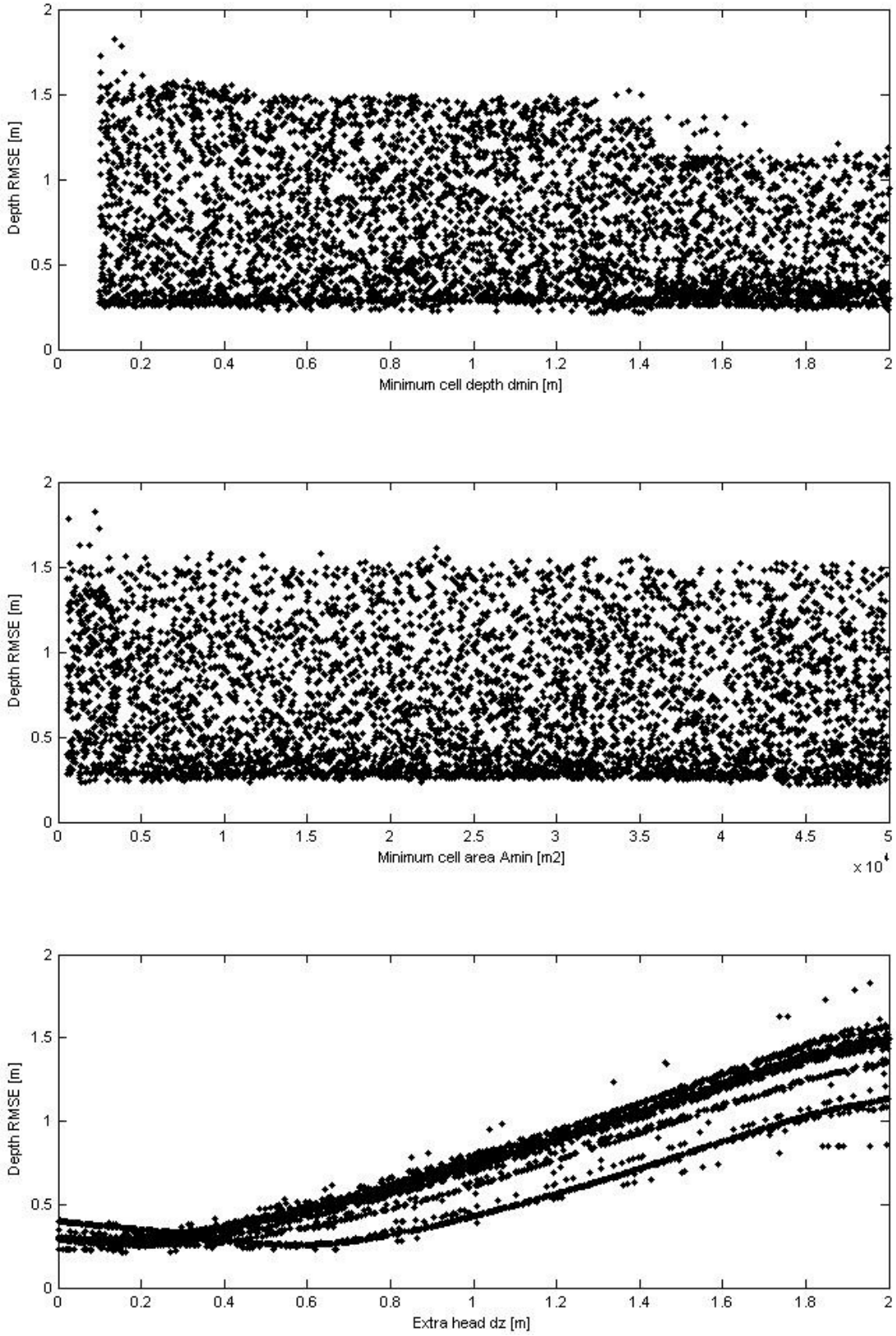


**Figure 4-34: RMSE - constant extra head case in Scenario 2 plotted against $d_{min}$, $A_{min}$ and $\Delta z$**

A detailed look at over/underpredictions shows a similar behaviour to that observed for Scenario 1. It can be seen in Figure 4-35 that the depths in areas far from the breach are overpredicted. In this case, however, the level of underprediction close to the breach is relatively low and the calculated depths are similar to those from TUFLOW.


**Figure 4-35: Depth difference of the best RFIM prediction (constant extra head, Scenario 2) compared to TUFLOW. Green represents RFIM overprediction, red represents RFIM underprediction.**

#### *4.4.2.2.3 Scenario 3*

The sensitivity of the RFIM predictions to the model parameters is shown in Figure 4-36 and Figure 4-37. Surprisingly, the optimum values of parameter $\Delta z$ in terms of the spatial measure of fit with TUFLOW (the bottom plot of Figure 4-36) lie at the top boundary of the analysed interval, at $\Delta z = 2.0$ m. Although such a value of extra head leads to the best spatial agreement it is unrealistically high. A realistic water depth on flowpaths that could be expected during a real flood is of the order of 1 m.

The optimum values of Δz in terms of the lowest RMSE lie around 0.6 m (Figure 4-37), which is in a similar part of the parameter space to that in Scenario 2 (Figure 4-34). Two events of different intensity and the same breach location show very similar optimum Δz parameter values suggesting that the parameter optimum is not dependant on the flooding event magnitude.

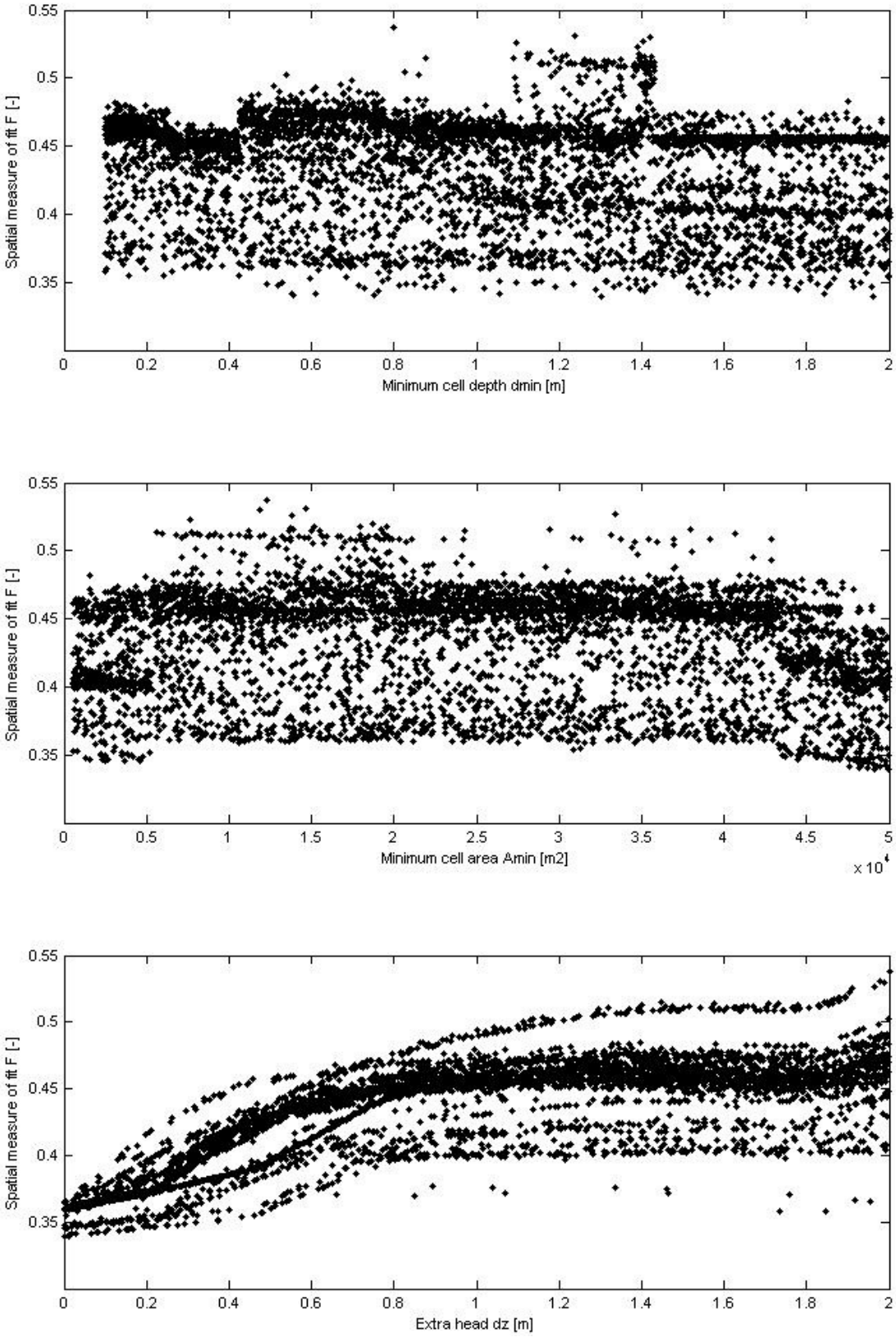


**Figure 4-36: Spatial measure of fit F – constant extra head case in Scenario 3 plotted against $d_{min}$, $A_{min}$ and $\Delta z$**

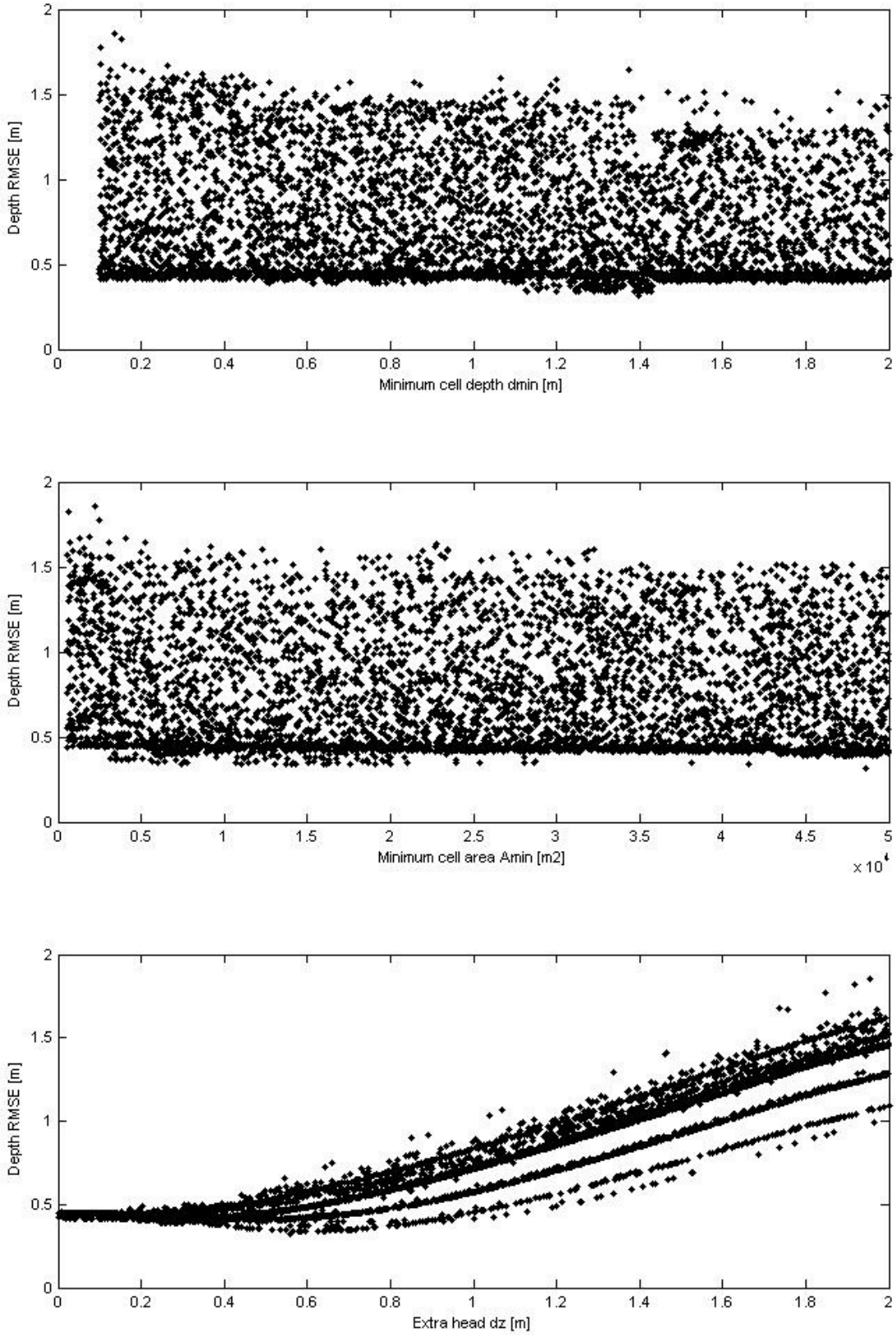


**Figure 4-37: RMSE - constant extra head case in Scenario 3 plotted against $d_{min}$, $A_{min}$ and $\Delta z$**

The under/overprediction map of the parameter set with the best F value (Figure 4-38) shows that the unrealistically high depths predicted by the RFIM are much higher than those predicted by TUFLOW (most of the map is green). The poor RMSE result confirms the observations already made that in Scenario 3 the parameter sets with high F (i.e. good performance) give high depth RMSE (i.e. poor performance). To conclude, for Scenario 3 no optimum parameter sets that would give both correctly predicted flood extent and correctly predicted water depths were found.


**Figure 4-38: Depth difference of the best RFIM prediction (constant extra head, Scenario 3) compared to TUFLOW. Green represents RFIM overprediction, red represents RFIM underprediction.**

#### *4.4.2.2.4 Scenario 4*

As was shown for the zero extra head algorithm and also for the constant extra head algorithm for the Thamesmead test site the best RFIM predictions do not suffer from the single direction of spreading problem encountered with the Greenwich site. Figure 4-39 and Figure 4-40 show that the highest F values and lowest RMSE values were obtained

for the same Δz interval 0.5 – 0.6 m. Hence, the optimum Δz gives good predictions both in terms of spatial flood extent and as well as in terms of water depth.

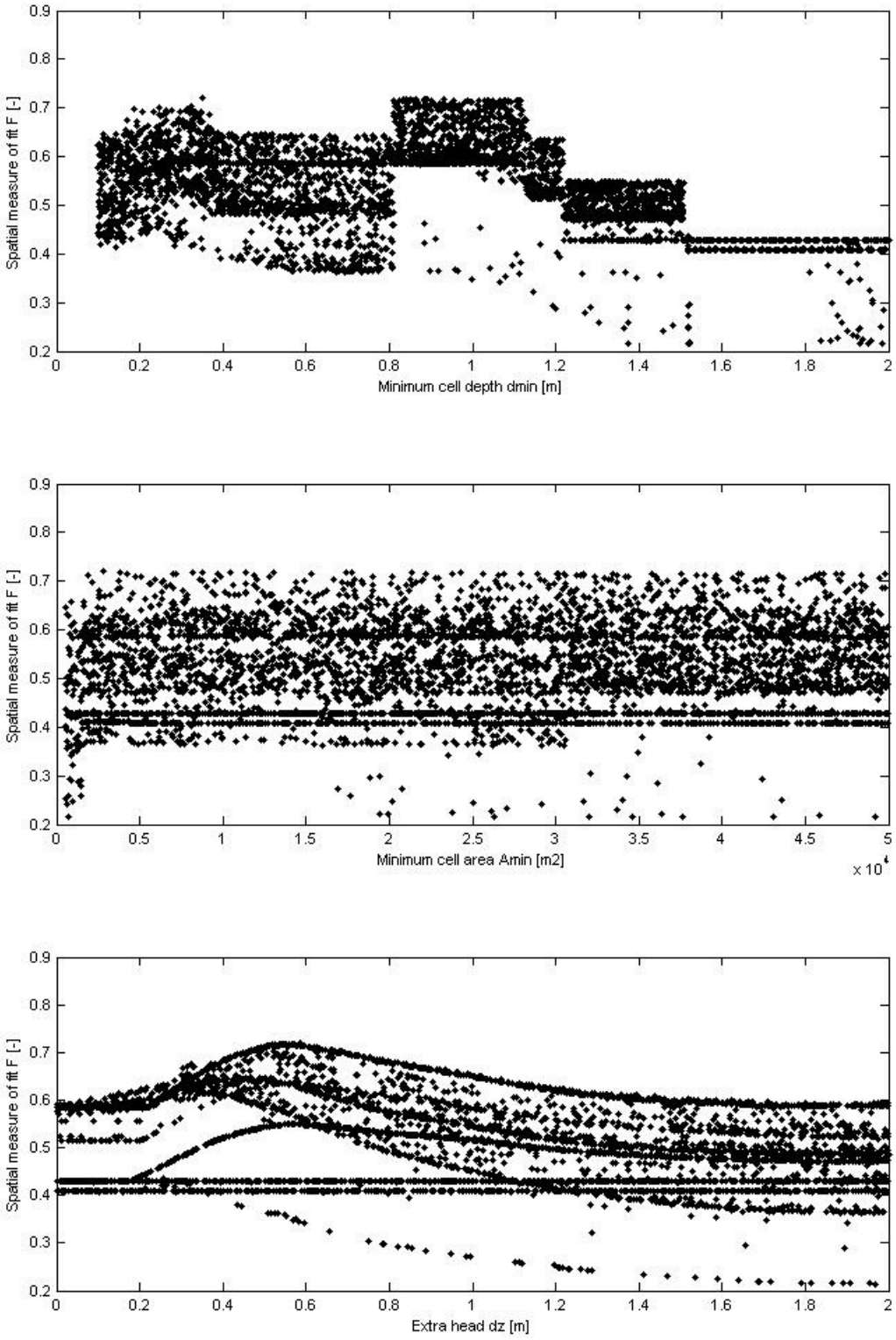


**Figure 4-39: Spatial measure of fit F – constant extra head case in Scenario 4 plotted against $d_{min}$, $A_{min}$ and Δz**

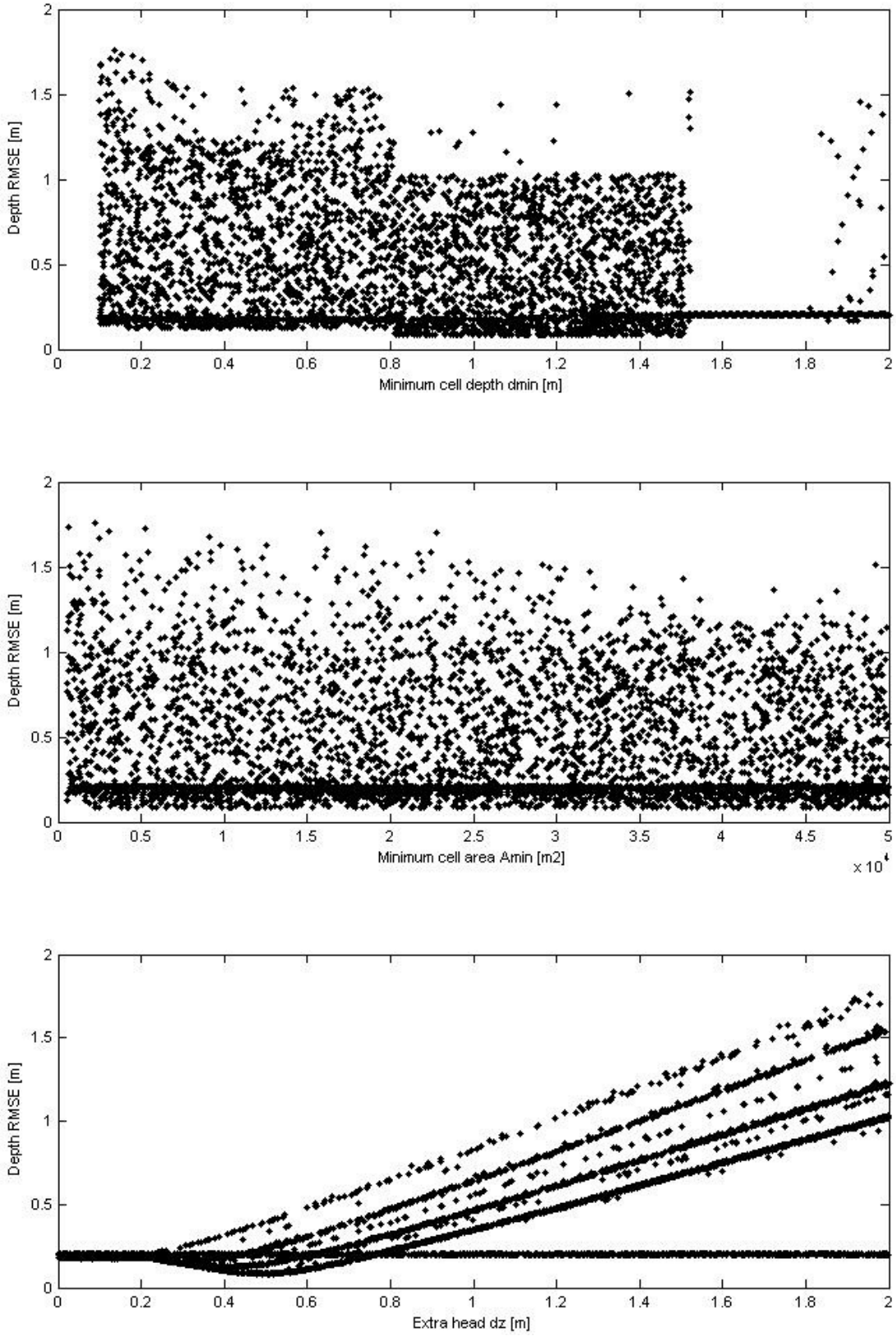


**Figure 4-40: RMSE - constant extra head case in Scenario 4 plotted against $d_{min}$, $A_{min}$ and $\Delta z$**

The depth under/overprediction map (Figure 4-41) is mostly yellow showing no, or very little, difference between the RFIM and TUFLOW results. The flooding closest to the breach (in orange and red) was underpredicted by the RFIM – the value of Δz added to the link elevation was not high enough. Depths in green areas were overpredicted by the RFIM.


**Figure 4-41: Depth difference of the best RFIM prediction (constant extra head, Scenario 4) compared to TUFLOW. Green represents RFIM overprediction, red represents RFIM underprediction.**

#### *4.4.2.3 Variable extra head inundation routine – maximum flood extent calculation*

Placing the water level in a cell above the level of a link by a constant Δz value leads to under- and overpredictions of water depths as was shown in section 4.4.2.2. To improve the model an algorithm that calculated a different value of extra head for each cell, based on local flow conditions, was developed (see section 3.2.4 for details).

The sensitivity of the predictions from the new algorithm to the flow resistance parameter *n* was analysed by comparison to TUFLOW results. Although the *n* parameter used in the RFIM is intended to represent floodplain friction, it can be expected that the optimum *n* value does not represent solely the roughness of the floodplain surface, but also accounts for other factors including the accuracy of the algorithm itself. A Manning friction coefficient of 0.025 was used in the benchmark TUFLOW predictions.

##### *4.4.2.3.1 Scenario 1*

The simulations of Scenario 1 show limited sensitivity to the resistance parameter *n* if the spatial measure of fit F is assessed, as the parameter sets represented by the dots form almost horizontal lines (bottom plot in Figure 4-42). The F values vary over a large interval, from 0.12 to 0.50. F is more sensitive to the $d_{min}$ parameter. This is consistent with the observations made in the zero extra head and constant extra head tests of Scenario 1.

The best agreement with TUFLOW in terms of depth RMSE (lowest RMSE values) was observed for *n* in the interval 0.01 – 0.02. Interestingly, the third plot in Figure 4-43 has a horizontal base, which means that the predictions were insensitive to the *n* parameter in some flood cell set-ups. This can be explained by the fact that variable extra heads $\Delta z_i$ are added not to all flood cells, but only to those which pass water to their neighbours. Additionally, RMSE is calculated only at pixels where both TUFLOW and RFIM predicted flooding. If all those pixels are located in the cells where no $\Delta z_i$ is added then no sensitivity to the *n* parameter would be observed.

Figure 4-43 has to be analysed with care as the scale on the y-axis covers a wide range of RMSE values. Several parameter sets showed very large disagreement with TUFLOW, the maximum RMSE calculated was 4.19 m. Closer inspection revealed that the reason for such behaviour can be found in the way $\Delta z_i$ is calculated. The Manning equation is used to calculate the flow depth through the link (see section 3.2.4). In some cases the cross section of the flow through the link is very narrow, which results in high flow depth prediction and therefore high $\Delta z_i$ value at this location. It is recommended that the variable extra head algorithm is altered so this $\Delta z_i$ overprediction cannot occur.

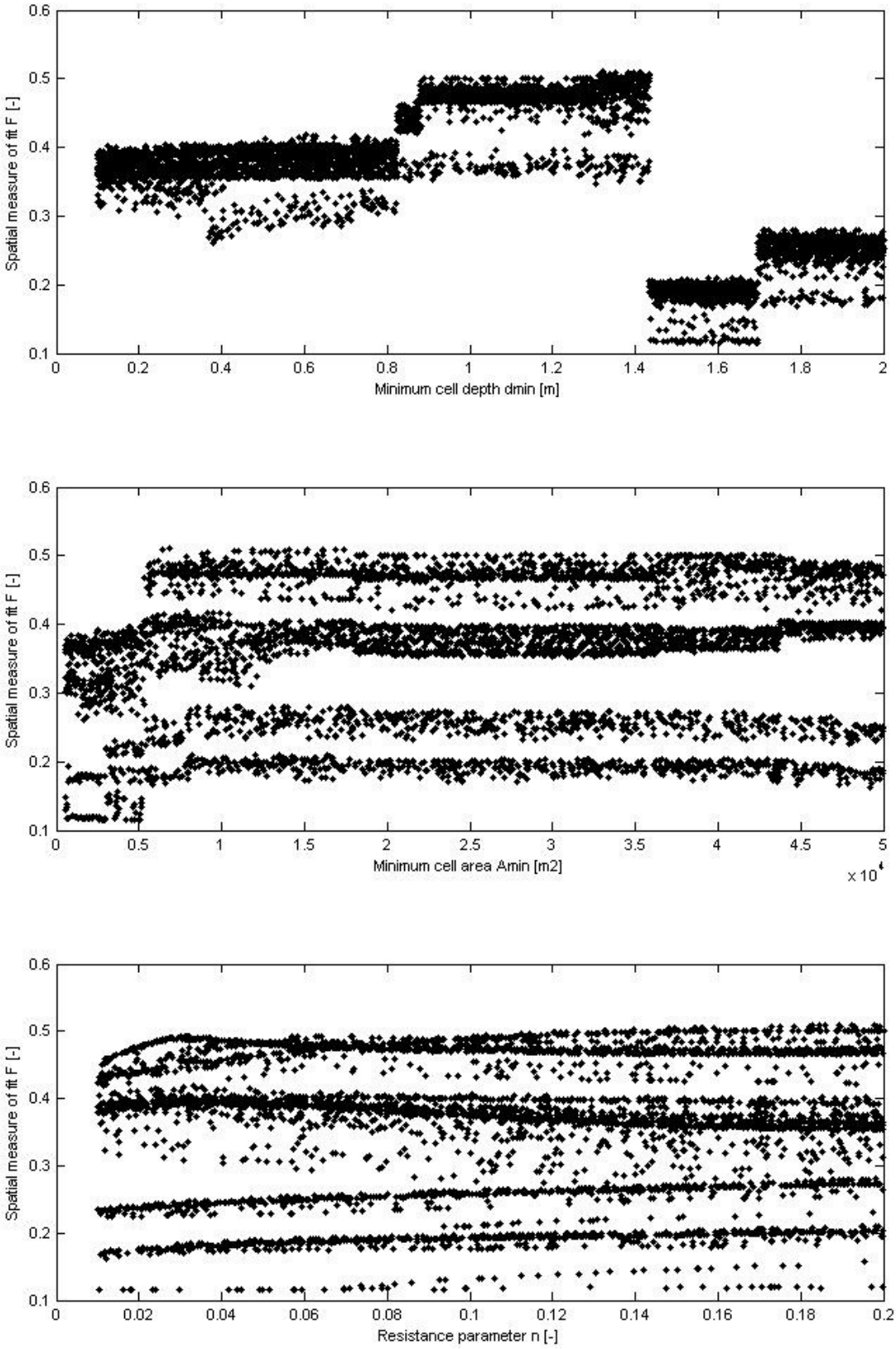


**Figure 4-42: Spatial measure of fit F - variable extra head case in Scenario 1 plotted against $d_{min}$, $A_{min}$ and n parameters**

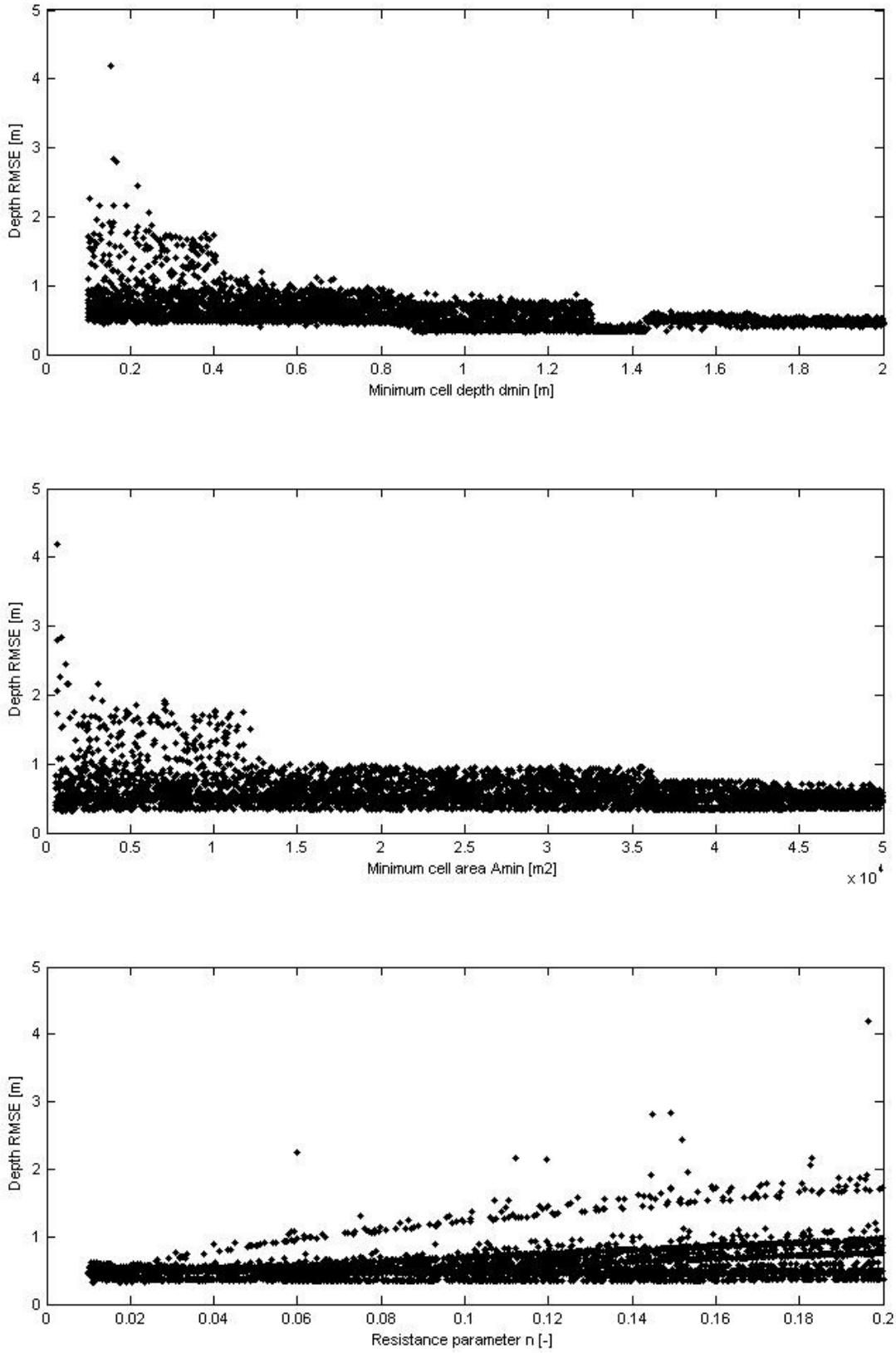


**Figure 4-43: RMSE - variable extra head case in Scenario 1 plotted against $d_{min}$, $A_{min}$ and n parameters**

Comparison of Figure 4-32 and Figure 4-44 shows that incorporation of the variable value extra head eliminated the depth underprediction close to the breach, but worsened the predictions in another part of the floodplain (Figure 4-44). It can be concluded that in Scenario 1 the predictions were improved only locally, while the best RMSE achieved over all 5000 parameter sets is actually worse than in the constant extra head case. Additionally, the run-time of the variable extra head code is longer than the constant extra head code, due to the iteration of the Manning equation that calculates $\Delta z_i$. These issues are discussed further in section 4.4.2.4.

To conclude, the increased run-time of the variable extra head algorithm for Scenario 1 did not lead to significantly improved flood inundation depth predictions.

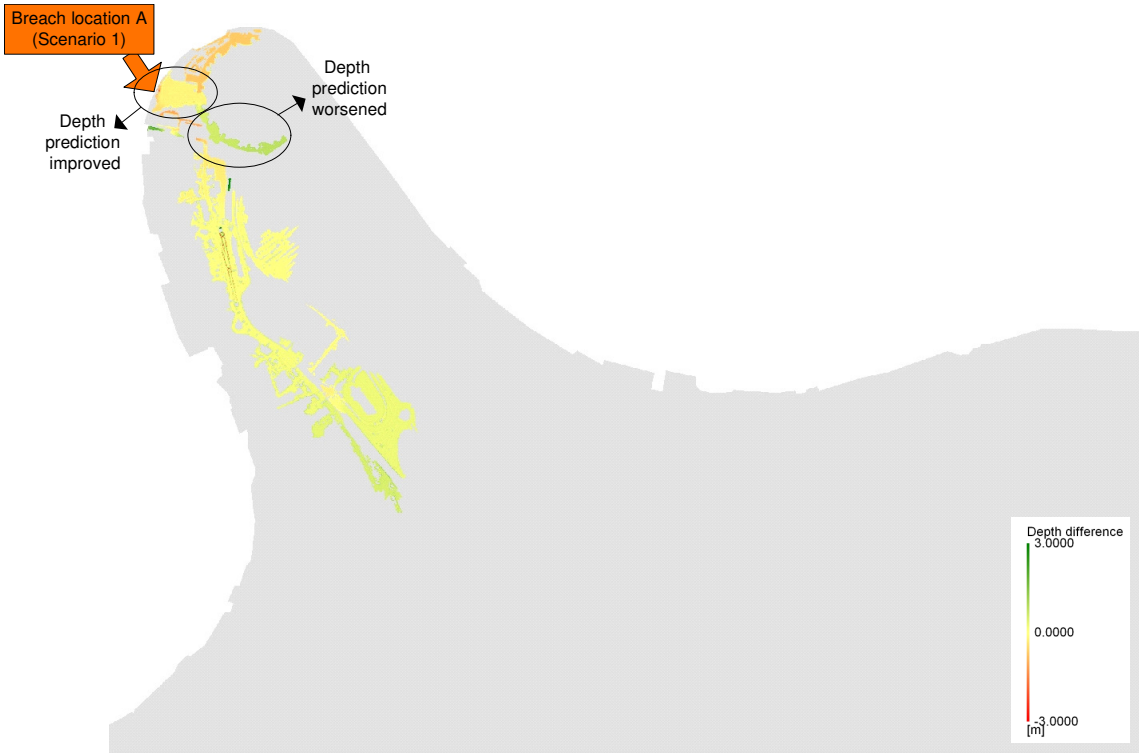


**Figure 4-44: Depth difference of the best RFIM prediction as compared to TUFLOW (variable extra head, Scenario 1), green represents RFIM overprediction, and red represents RFIM underprediction**

The quality of predictions over all 5000 parameter sets can be presented in a form of inundation probability. Figure 4-45 depicts the map of the probability of flooding. The black colour represents pixels where flooding was predicted in all 5000 simulations,

while white pixels were not flooded in any simulation. The TUFLOW prediction is also included on the map for comparison.

The probability of flooding also reflects the uncertainty of the RFIM predictions. If the flood extent was represented only by the black colour this would mean that all parameter sets resulted in the same flood extent and hence the uncertainty of the model would be low.

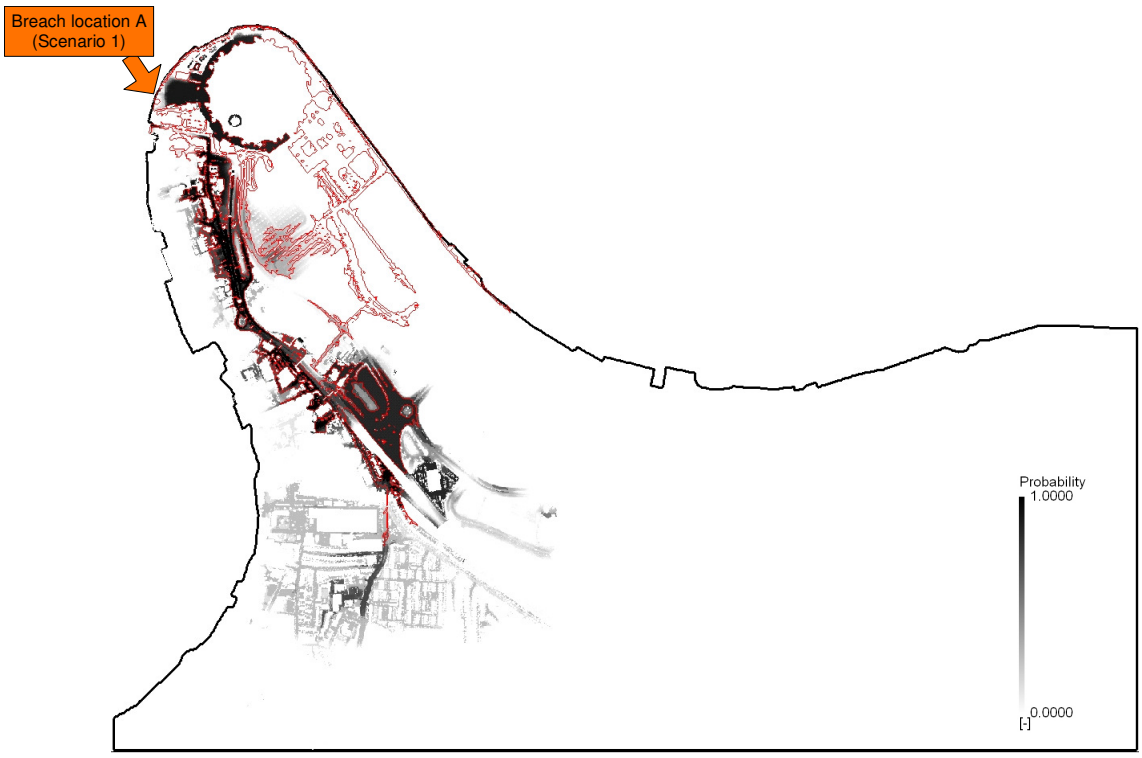


**Figure 4-45: Probability of flooding over all 5000 simulations (variable extra head, Scenario 1). Red boundary represents the TUFLOW maximum flood extent prediction**

*4.4.2.3.1.1 Velocity predictions*

The velocity predictions are presented in Figure 4-46. The parameter set, for which the best spatial agreement (highest F value) was achieved, was used. The velocity prediction by the RFIM can only be made on the borders between flood cells. Three main areas (Area 1-1, Area 1-2 and Area 1-3) were selected for a closer inspection that is depicted in Figure 4-47. In area 1.2 the RFIM predicted higher velocities than TUFLOW while in areas 1.1 and 1.3 the TUFLOW predictions are higher. The velocity calculation in the RFIM is considerably affected by the estimates of the volume

transfers between the cells. If the overall flooding pattern is not correctly predicted, as in this case, the volume transfers and velocity predictions are inaccurate as well. More water was spread in the overpredicted areas (western part of floodplain) resulting in higher velocity predictions in that area.

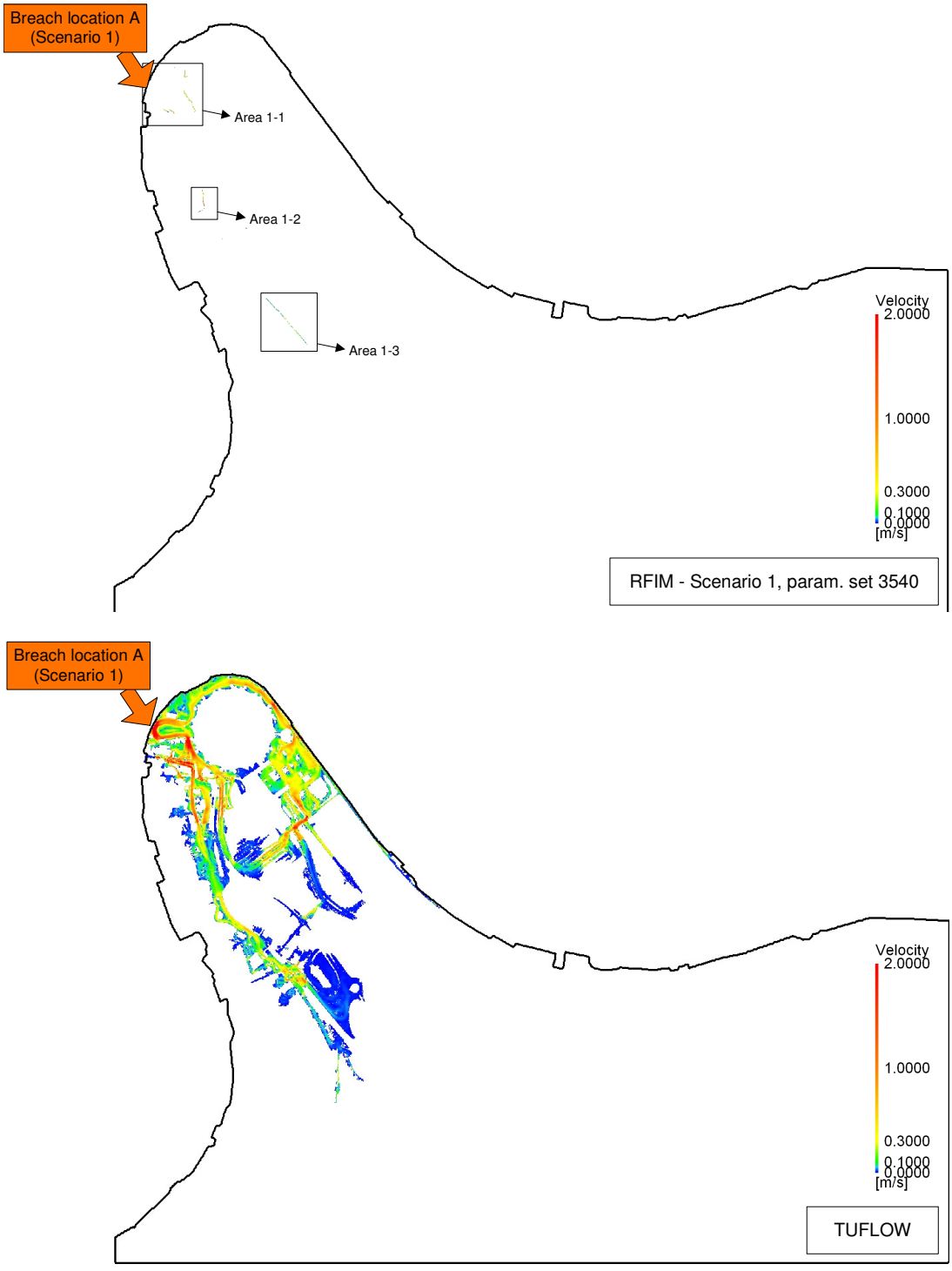


**Figure 4-46: Velocity predictions by: RFIM (top) by TUFLOW (bottom) – Scenario 1**

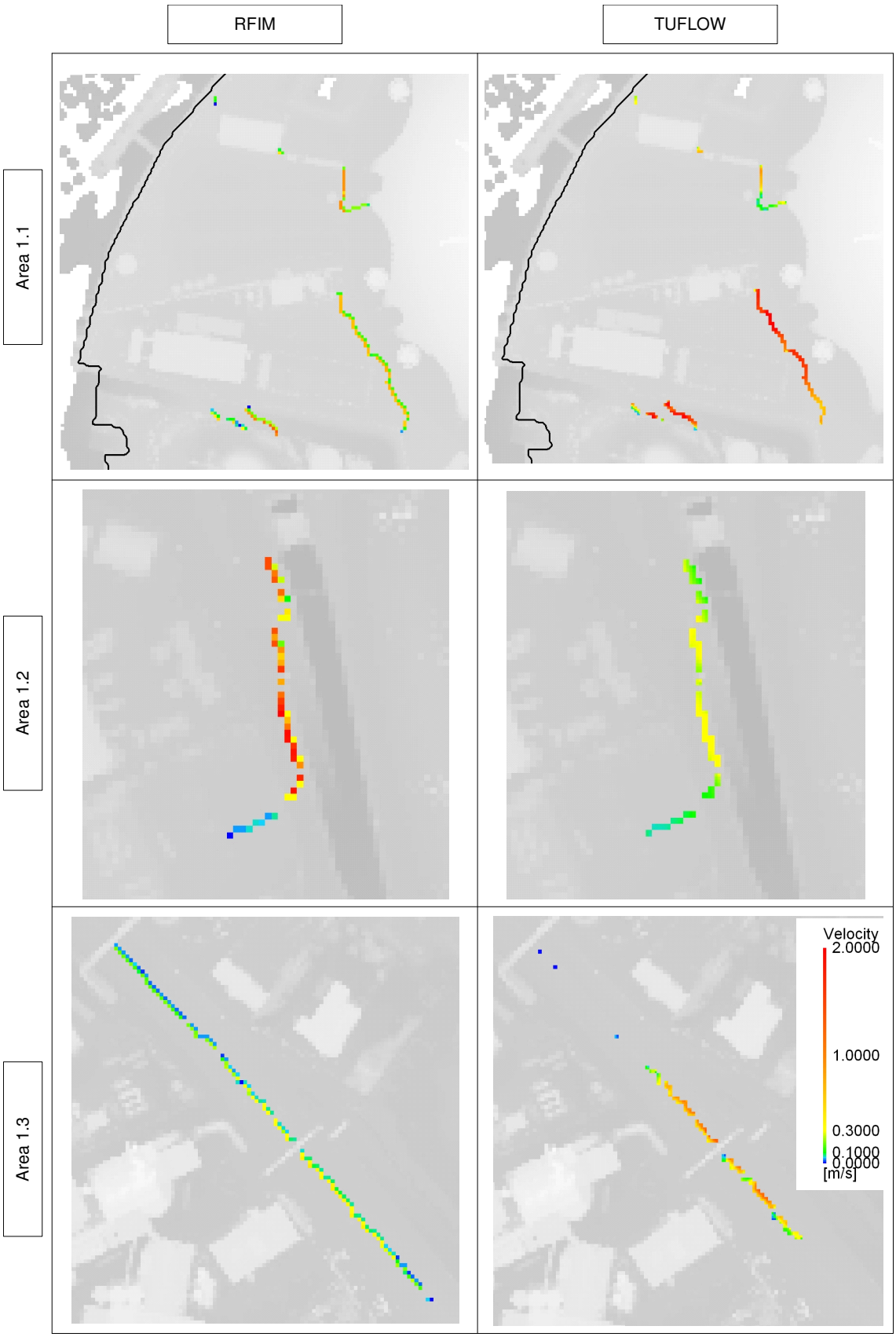


**Figure 4-47: Detailed comparison of the flow velocity predictions – Scenario 1**

#### *4.4.2.3.2 Scenario 2*

In Scenario 2 the expected sensitivity of F to $d_{min}$ parameter can be observed (Figure 4-48) and shows that the flood cell distribution is, again, crucial for the correct prediction of flood extent. Some sensitivity to the *n* parameter can also be observed, similarly to Scenario 1.

The plots of the sensitivity of RMSE to the flood cell parameters in Figure 4-49 also show a very similar behaviour to that described for Scenario 1 with the best agreement with TUFLOW (lowest RMSE value) observed for *n* values around 0.01, close to the lower boundary of the analysed interval.

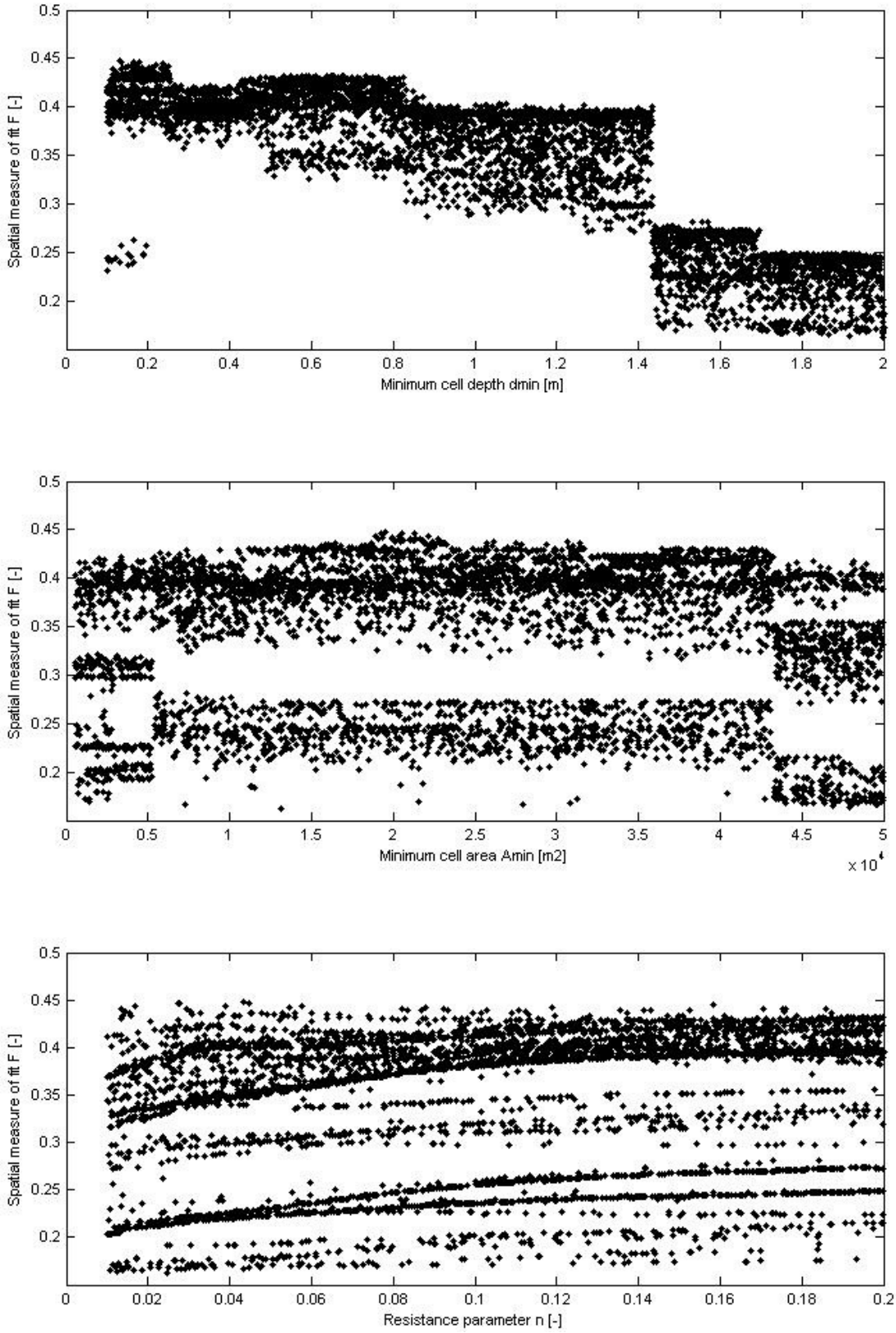


**Figure 4-48: Spatial measure of fit F - variable extra head case in Scenario 2 plotted against $d_{min}$, $A_{min}$ and n parameters**

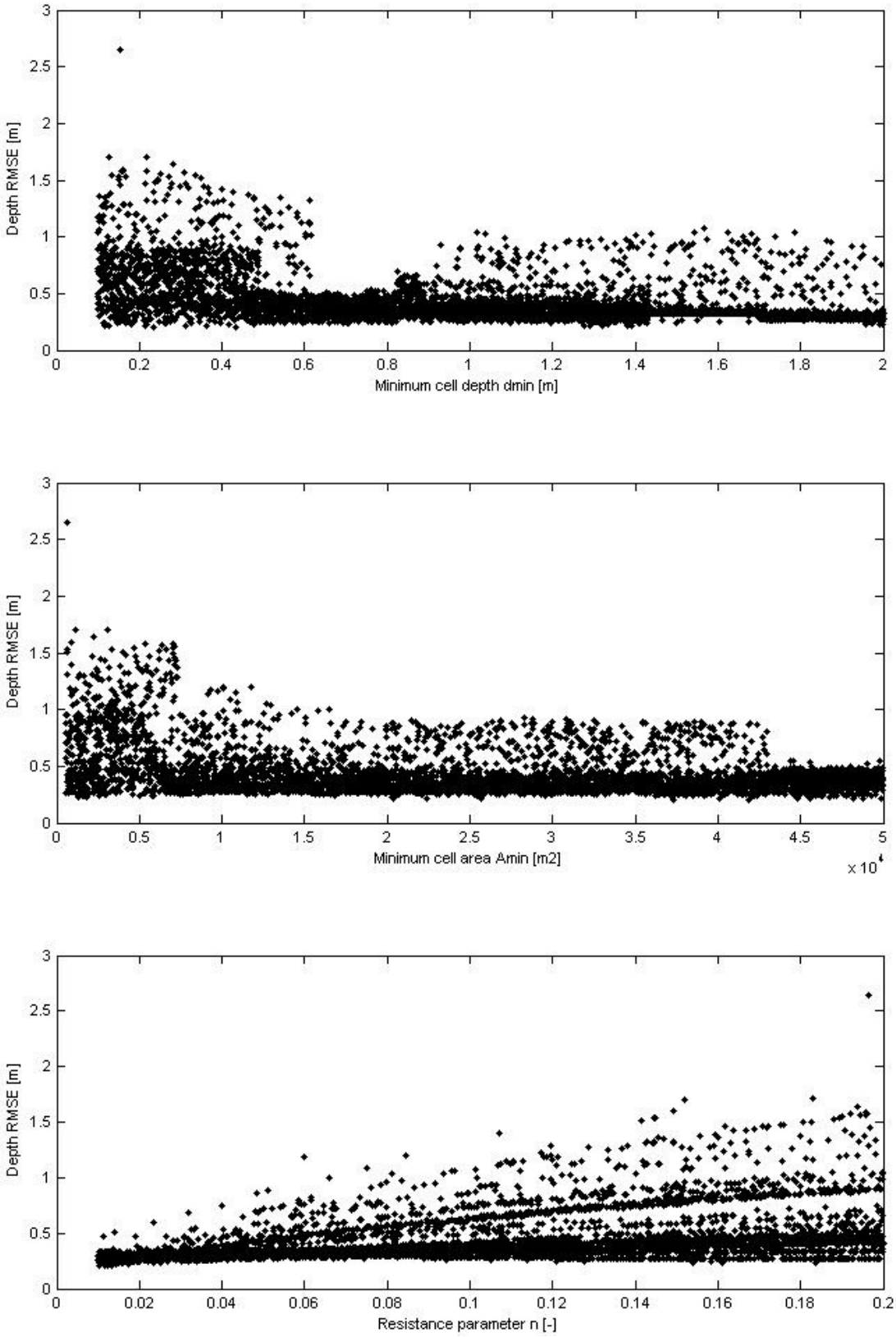


**Figure 4-49: RMSE - variable extra head case in Scenario 2 plotted against $d_{min}$, $A_{min}$ and n parameters**

The under/overprediction map (Figure 4-50) shows that the application of variable extra head resulted in general improvement in depth predictions (see Figure 4-35 for comparison with extra head case), but a detailed analysis reveals that while the depth prediction was improved in some parts of floodplain, in others it was actually worse, similarly to Scenario 1. In Scenario 2, the variable extra head method showed the best improvement over the constant extra head algorithm from all the analysed scenarios.


**Figure 4-50: Depth difference of the best RFIM prediction as compared to TUFLOW (variable extra head, Scenario 2), green represents RFIM overprediction, and red represents RFIM underprediction**

Figure 4-51 depicts the probability of flooding for Scenario 2. The map shows that most of the parameter sets predicted flooding similarly to TUFLOW (black colour). Some parameter sets overpredicted the flooding in the south western part of the domain.


**Figure 4-51: Probability of flooding over all 5000 simulations (variable extra head, Scenario 2). Red boundary represents the TUFLOW maximum flood extent prediction**

*4.4.2.3.2.1 Velocity predictions*

The velocity predictions calculated by RFIM and TUFLOW are shown in Figure 4-52. The RFIM velocity data are, again, limited only to the borders between flood cells. Three areas are depicted in more detail in Figure 4-53. The comparison shows that the RFIM locally overpredicted the velocities.

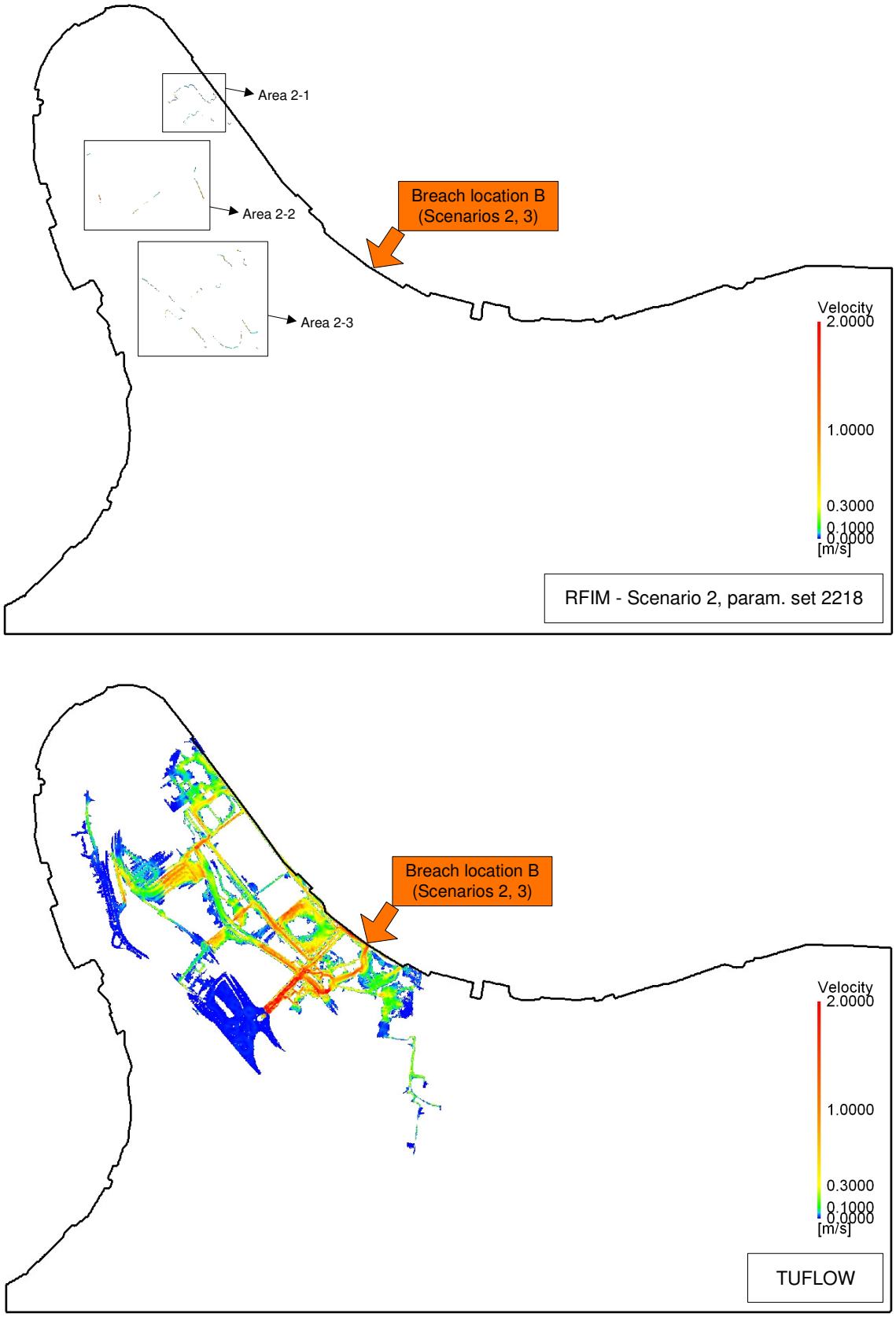


**Figure 4-52: Velocity predictions by: RFIM (top) by TUFLOW (bottom) – Scenario 2**

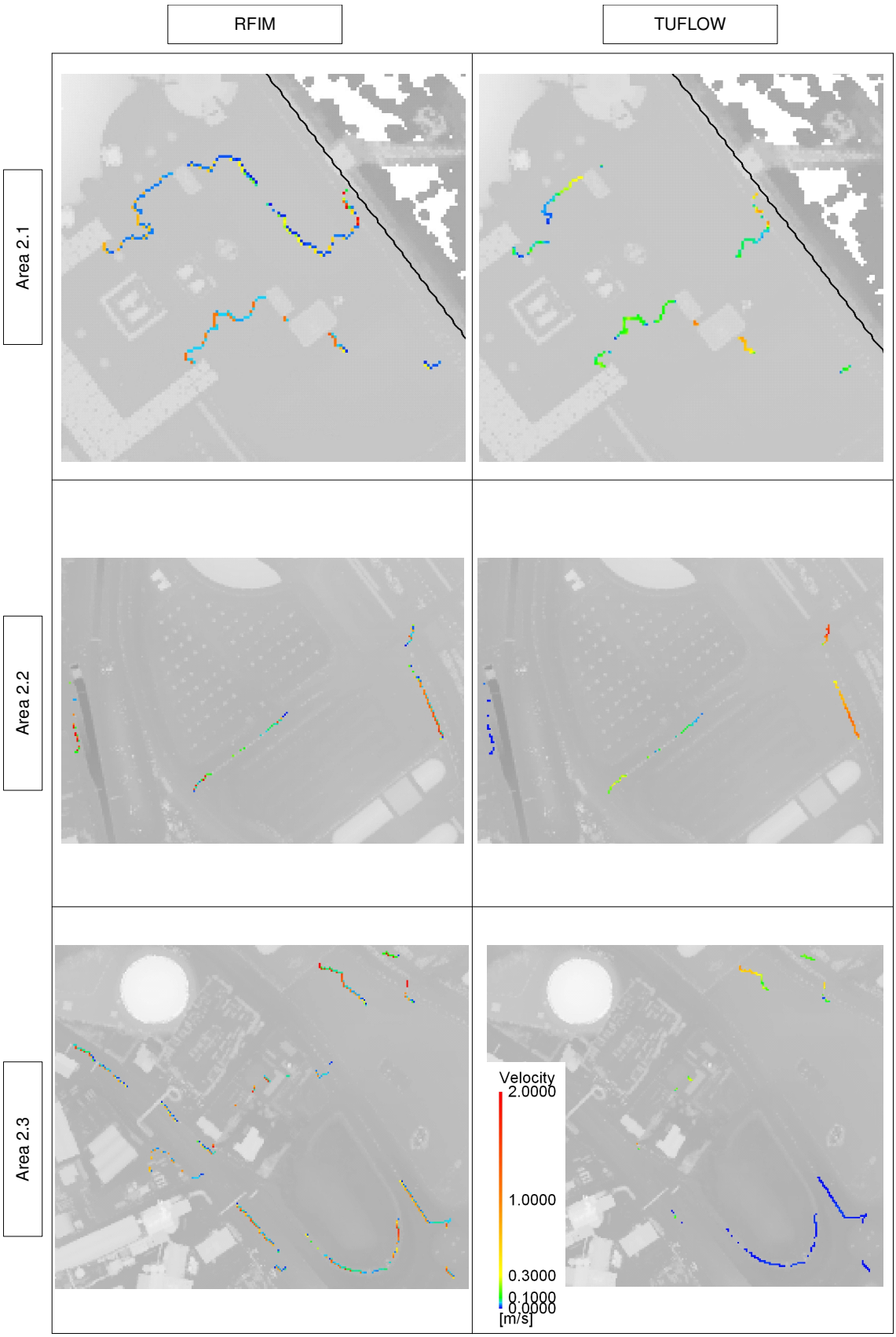


**Figure 4-53: Detailed comparison of the flow velocity predictions – Scenario 2**

#### *4.4.2.3.3 Scenario 3*

Comparison of the RFIM and TUFLOW predictions for Scenario 3 shows behaviour consistent with the previous 2 scenarios as far as sensitivity to resistance parameter *n* is concerned. Low values of *n* (0.01 – 0.05) give relatively poor predictions in terms of F, and the best predictions in terms of depth RMSE. The best RMSE was observed for *n* ~ 0.02, which is close to the Manning friction coefficient used in the TUFLOW comparison prediction (n = 0.025).

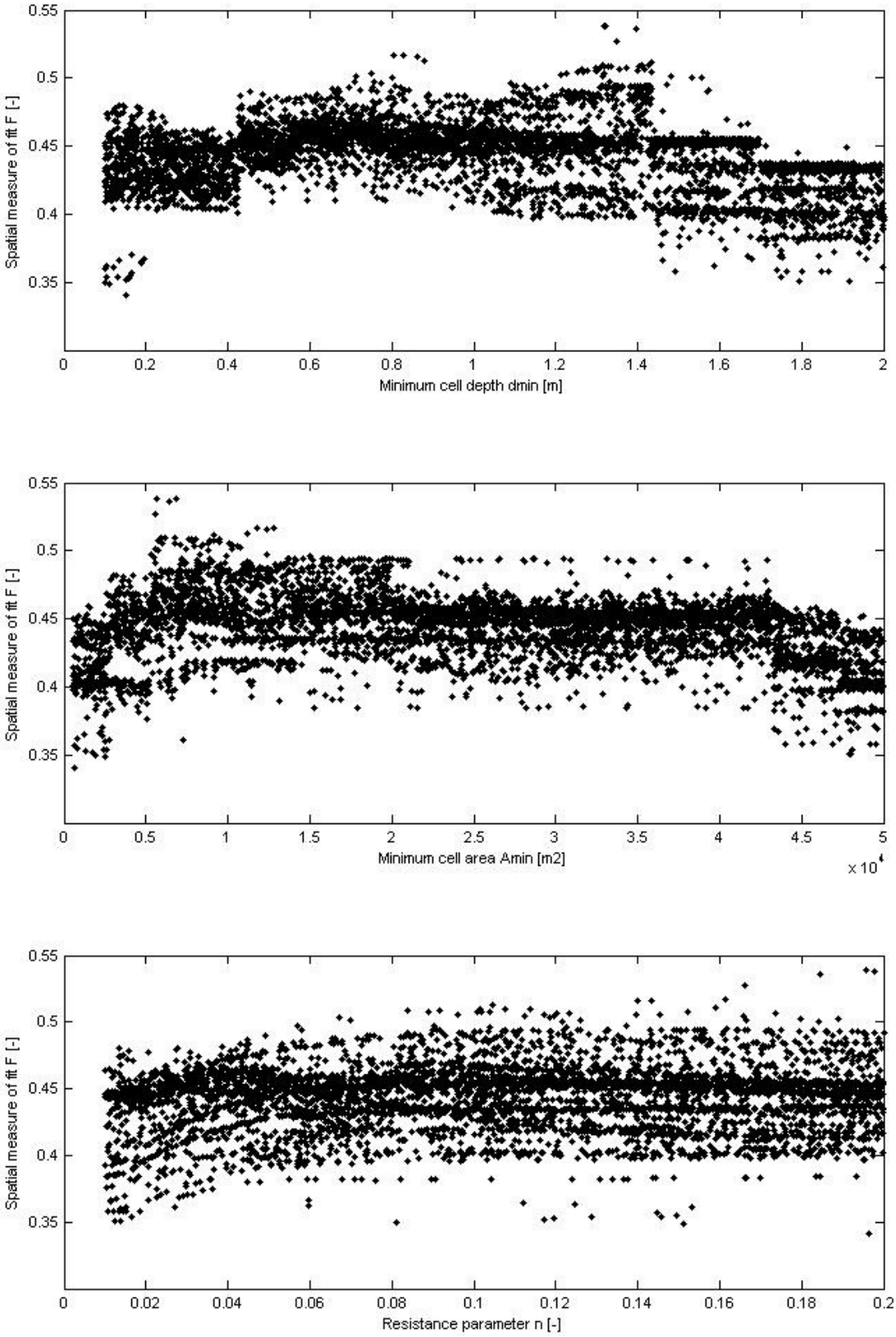


**Figure 4-54: Spatial measure of fit F - variable extra head case in Scenario 3 plotted against $d_{min}$, $A_{min}$ and n parameters**

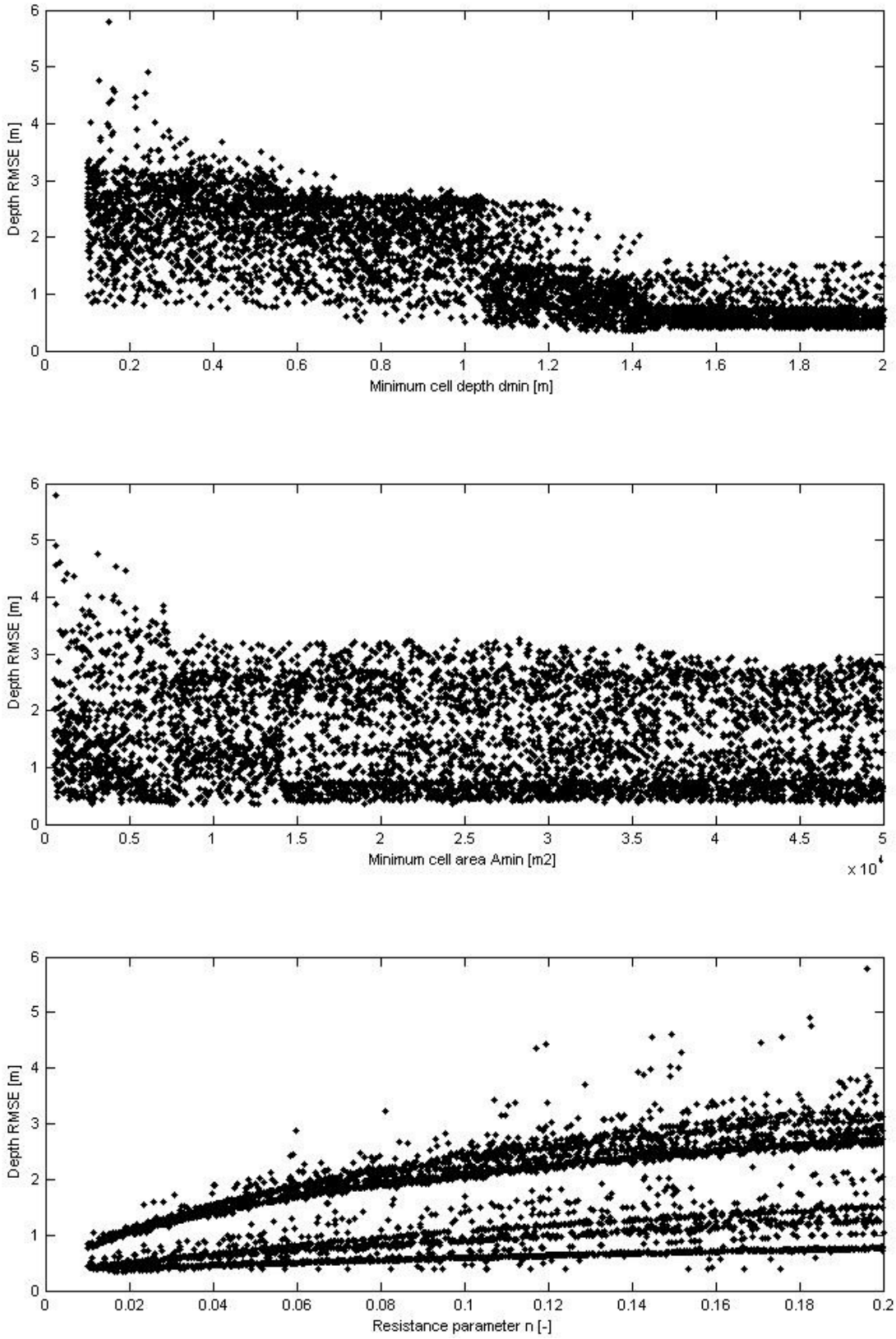


**Figure 4-55: RMSE - variable extra head case in Scenario 3 plotted against $d_{min}$, $A_{min}$ and n parameters**

In Scenario 3, the introduction of variable extra head did not lead to better agreement in water depths with TUFLOW predictions, similarly to Scenario 1 as discussed in 4.4.2.4. The same conclusion can be drawn from Figure 4-56, which depicts the under/overpredictions obtained from the variable extra head inundation routine. The RFIM mostly overpredicted large areas; mainly the same ones as in the constant extra head case (Figure 4-38), and no significant improvement was achieved even on a local flood cell scale. In Scenario 3, the variable extra head method showed the worst performance from all the scenarios.

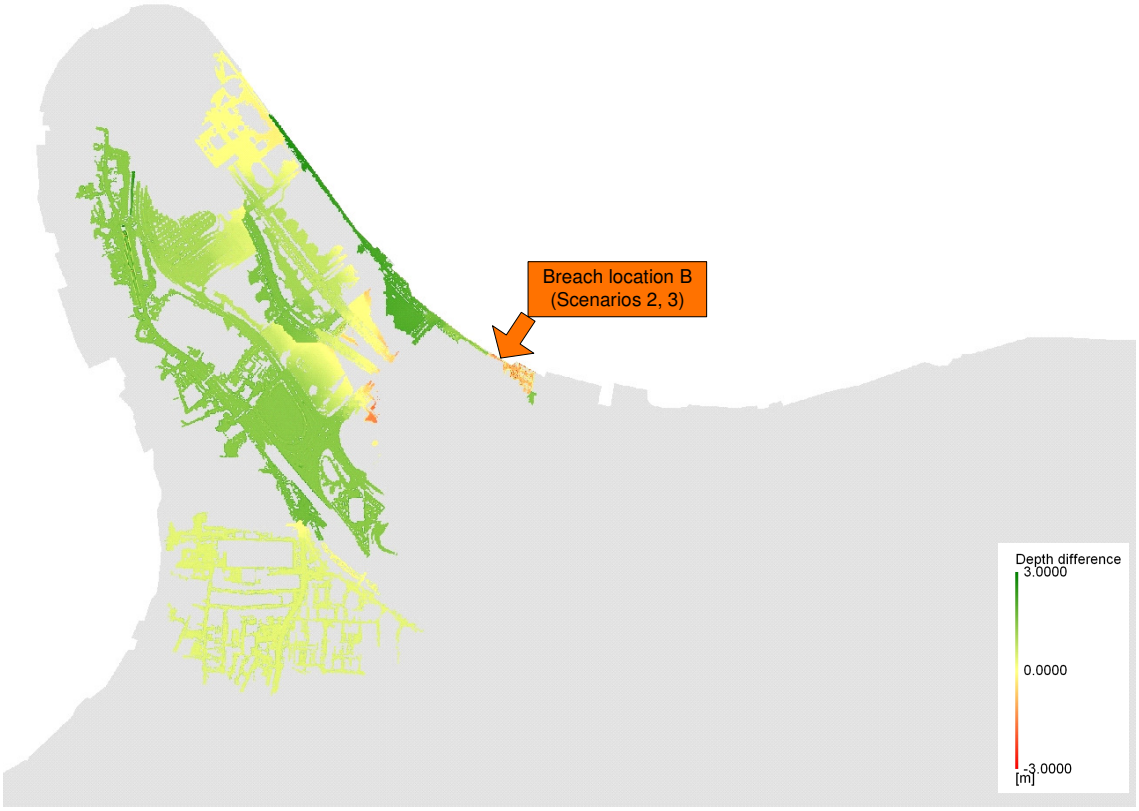


**Figure 4-56: Depth difference of the best RFIM prediction as compared to TUFLOW (variable extra head, Scenario 3), green represents RFIM overprediction, and red represents RFIM underprediction**

Figure 4-57 shows the probability of flooding for Scenario 3. Similarly to Scenario 2, the black areas (flooded for most of the parameter sets) were those also predicted as flooded by the TUFLOW model. Overpredictions in southern and western regions occurred only for some parameter sets as they are represented by the shades of grey.


**Figure 4-57: Probability of flooding over all 5000 simulations (variable extra head, Scenario 3). Red boundary represents the TUFLOW maximum flood extent prediction**

*4.4.2.3.3.1 Velocity predictions*

The map of velocity predictions in Scenario 3 is depicted in Figure 4-58 and in more detail in Figure 4-59. In this scenario, the velocities are underestimated in some areas and overestimated in others. The under/overestimation depends on whether the calculated volume transfer in certain location is similar to that in TUFLOW. It can be seen that the RFIM overpredicted the velocities in the western part of Area 3-1 (Figure 4-59) and underpredicted the velocities in the eastern part.

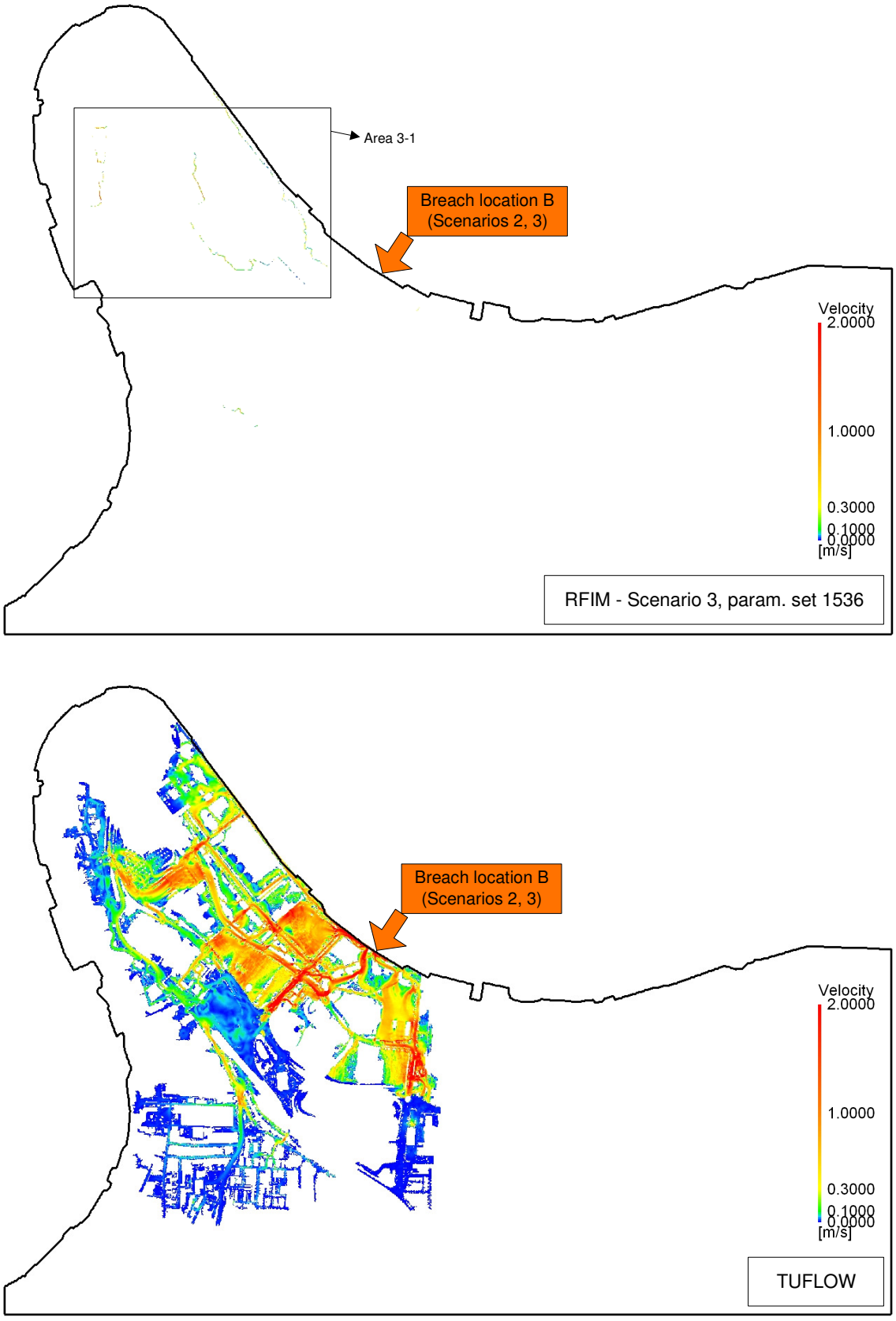


**Figure 4-58: Velocity predictions by: RFIM (top) by TUFLOW (bottom) – Scenario 3**

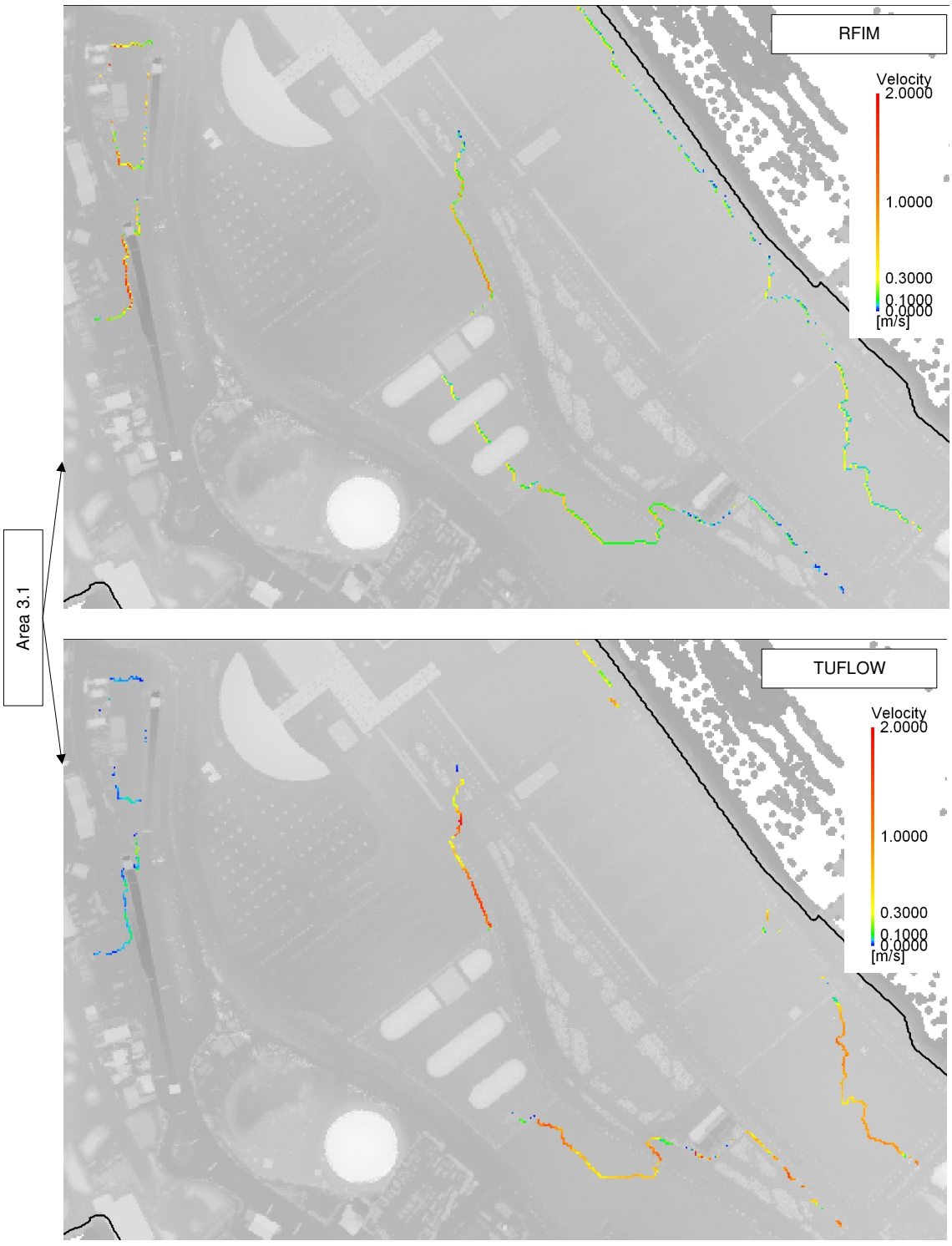


**Figure 4-59: Detailed comparison of the flow velocity predictions – Scenario 3**

#### *4.4.2.3.4 Scenario 4*

Figure 4-60 and Figure 4-61depict the sensitivity of F and depth RMSE to the flood cell model parameters. The first two plots in each figure confirm the greater sensitivity to

$d_{min}$ found before. The third plots show that the highest F was obtained for a resistance parameter of 0.06, while the lowest depth RMSE was observed for the *n* of 0.05. The curves are rather flat around the optimum values and good agreement with TUFLOW in terms of both spatial agreement and depth agreement can be produced for *n* in the interval 0.04 – 0.08.

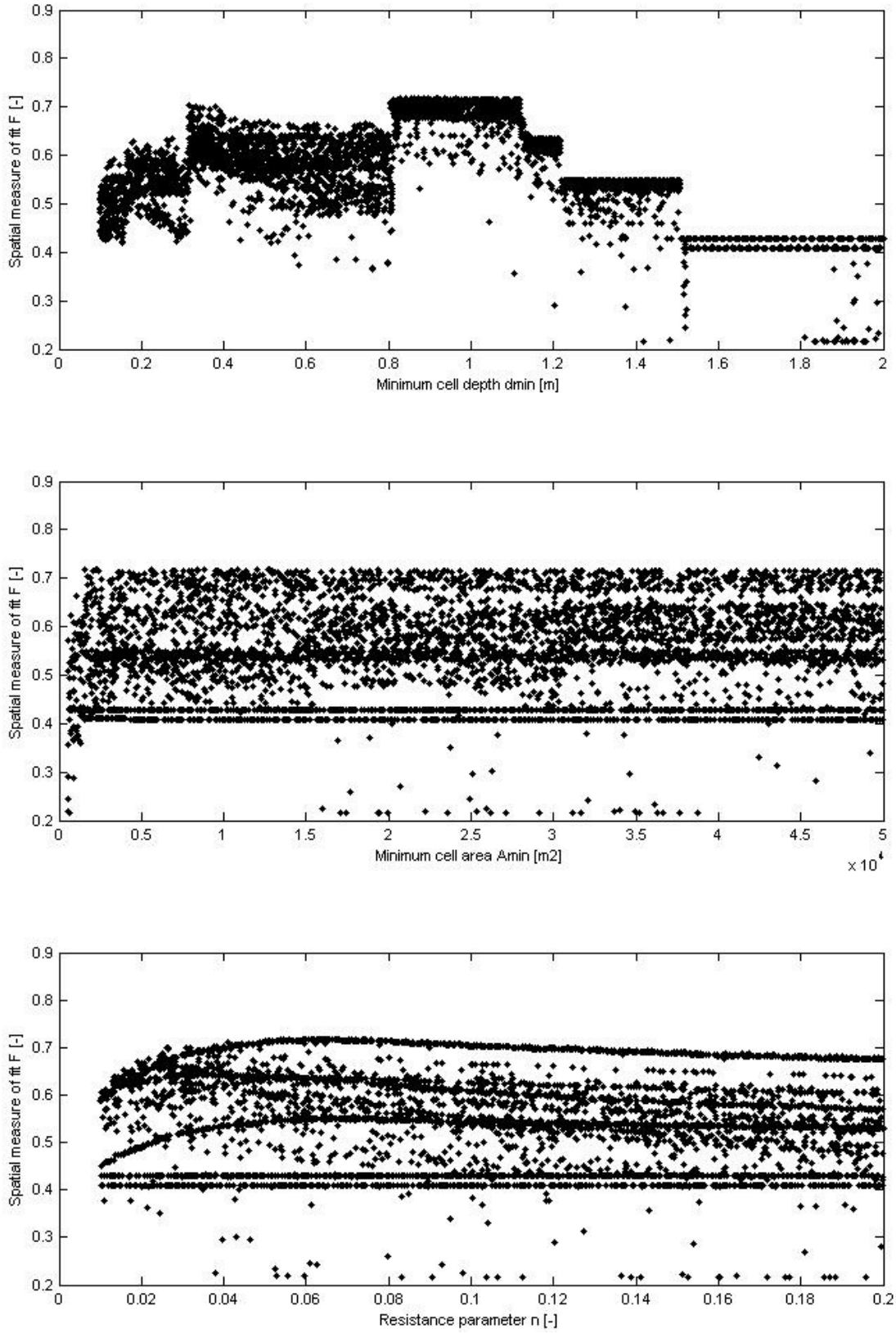


**Figure 4-60: Spatial measure of fit F - variable extra head case in Scenario 4 plotted against $d_{min}$, $A_{min}$ and n parameters**

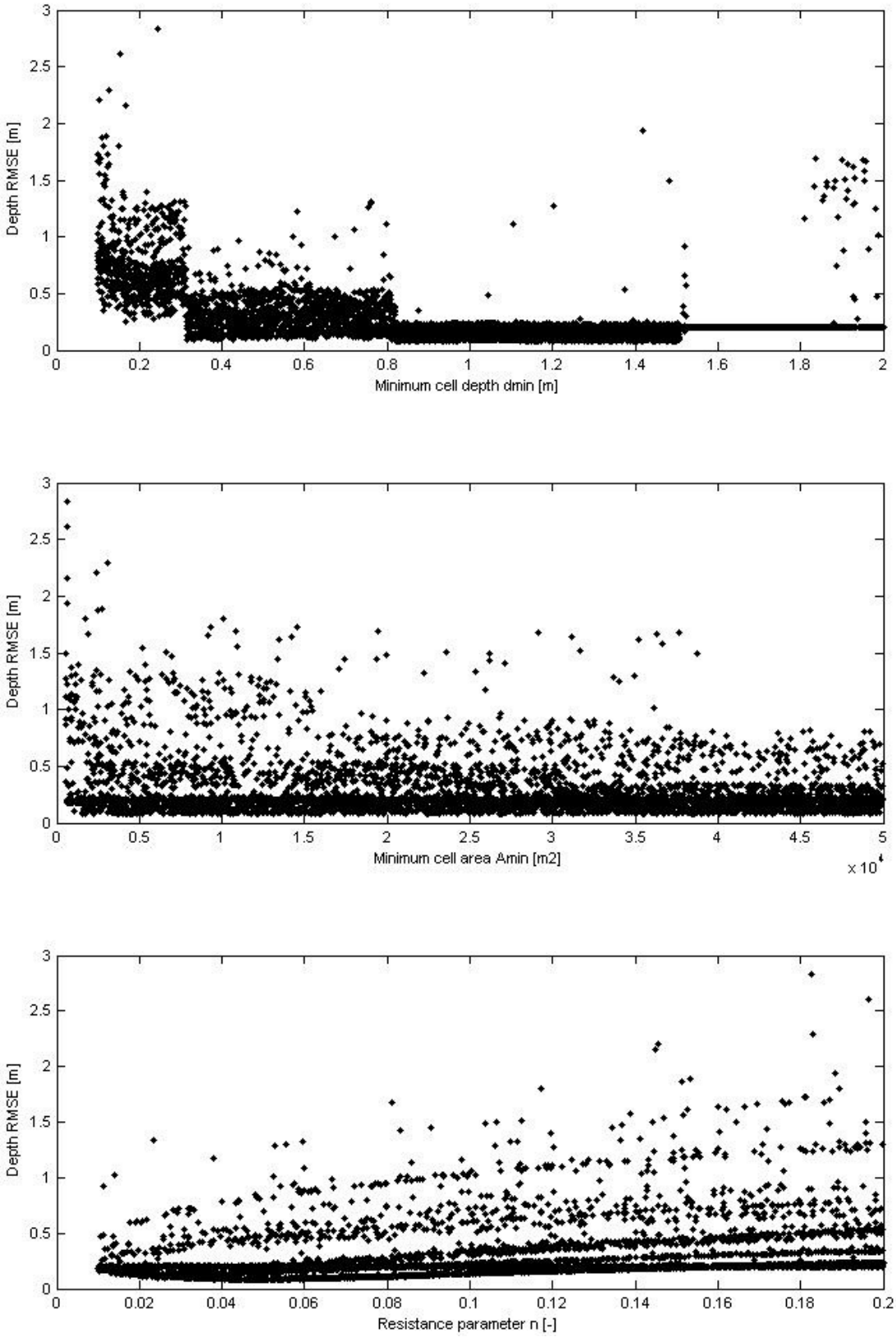


**Figure 4-61: RMSE - variable extra head case in Scenario 3 plotted against $d_{min}$, $A_{min}$ and n parameters**

The map of depth under/overprediction (Figure 4-62) shows that no significant improvement was achieved by the introduction of variable extra head over the constant extra head inundation routine (Figure 4-41). The same areas were under/over predicted in both cases. Although the run-time of the inundation routine more than doubled, the minimum depth RMSE achieved by both algorithms were almost the same. Therefore the extra run-time was not justified. The performance of the different inundation routine versions with respect to the run time is discussed in detail later, see section 4.4.2.4.

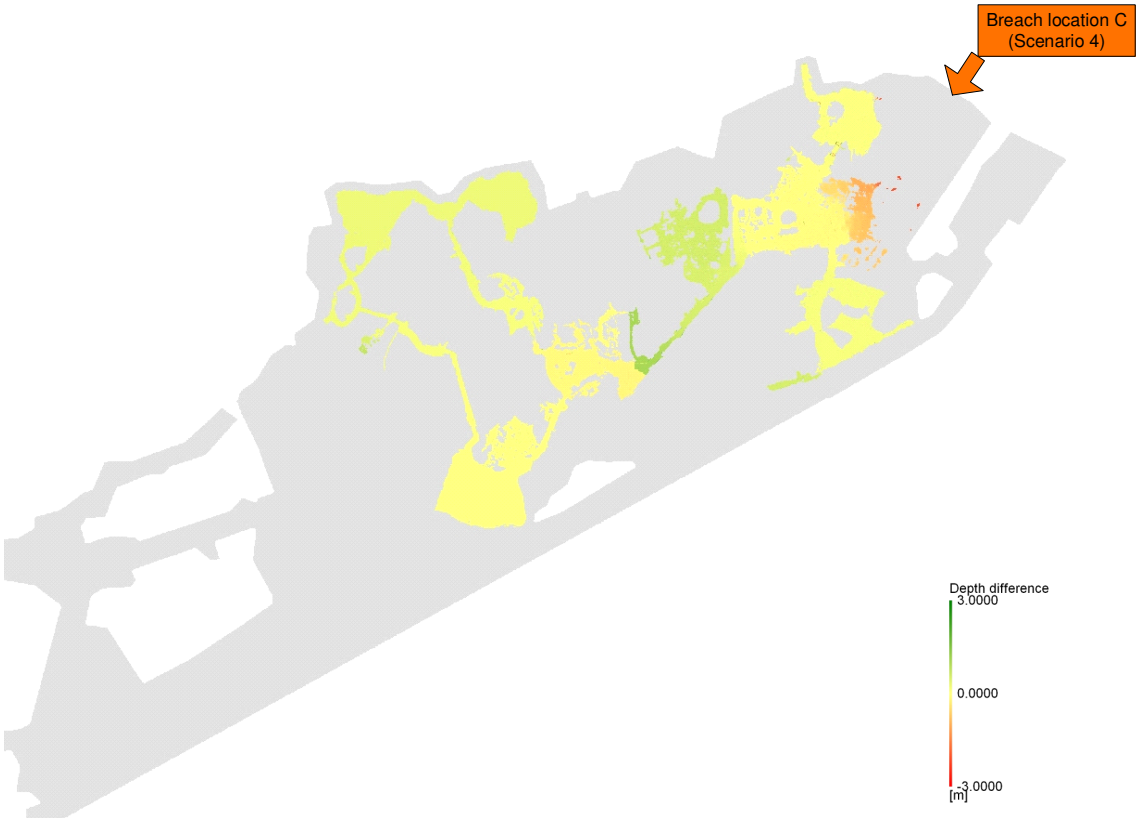


**Figure 4-62: Depth difference of the best RFIM prediction as compared to TUFLOW (variable extra head, Scenario 4), green represents RFIM overprediction, and red represents RFIM underprediction**

Figure 4-63 depicts the probability of flooding for Scenario 4. Parameter sets combining such $A_{min}$ and $d_{min}$ values that only a single large flood cell was constructed are responsible for the non-zero probability of flooding in the south-western part of the Thamesmead embayment. This area is not hydraulically connected to the north-eastern part of the floodplain. Apart from the case when only one flood cell was constructed all other flood cell distributions resulted in very similar RFIM predictions to those produced by TUFLOW.


**Figure 4-63: Probability of flooding over all 5000 simulations (variable extra head, Scenario 4). Red boundary represents the TUFLOW maximum flood extent prediction.**

The tests of Scenario 4 showed consistency that was not observed in all three previous scenarios. The plots allowed optimum value of $n$ to be clearly identified. Additionally, the $n$ value that produced good performance in terms of F did well also in terms of depth RMSE. The best results were obtained for $n$ of 0.06, which was, however, higher than the value used in the TUFLOW predictions ($n$ = 0.025).

#### *4.4.2.3.4.1 Velocity predictions*

Velocity predictions were produced in only few locations (Figure 4-64) owing to the small number of flood cells. Detailed analysis of area 4-1 shows that there the RFIM locally overpredicted the velocity values in most of the pixels (Figure 4-65).

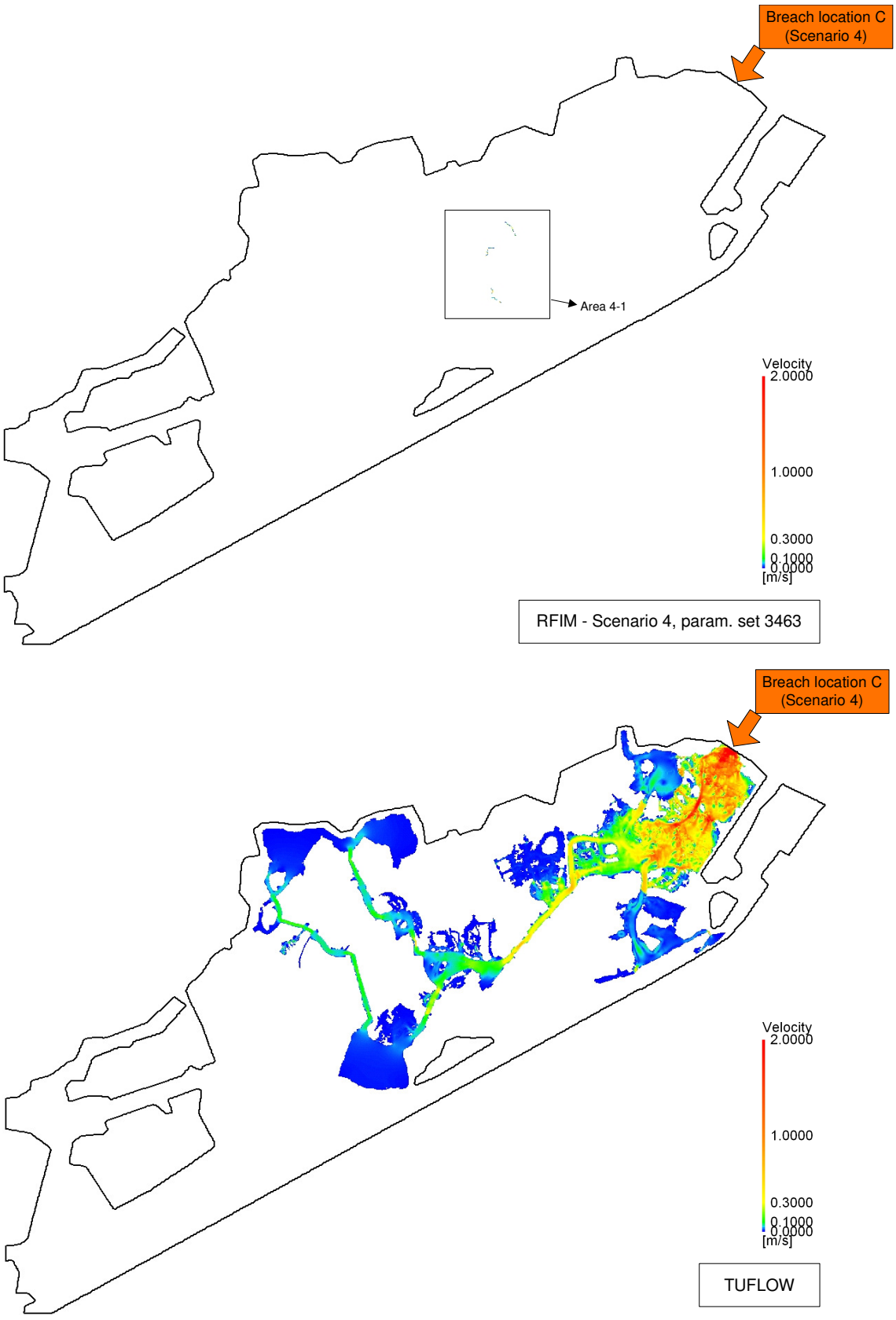


**Figure 4-64: Velocity predictions by: RFIM (top) by TUFLOW (bottom) – Scenario 4**

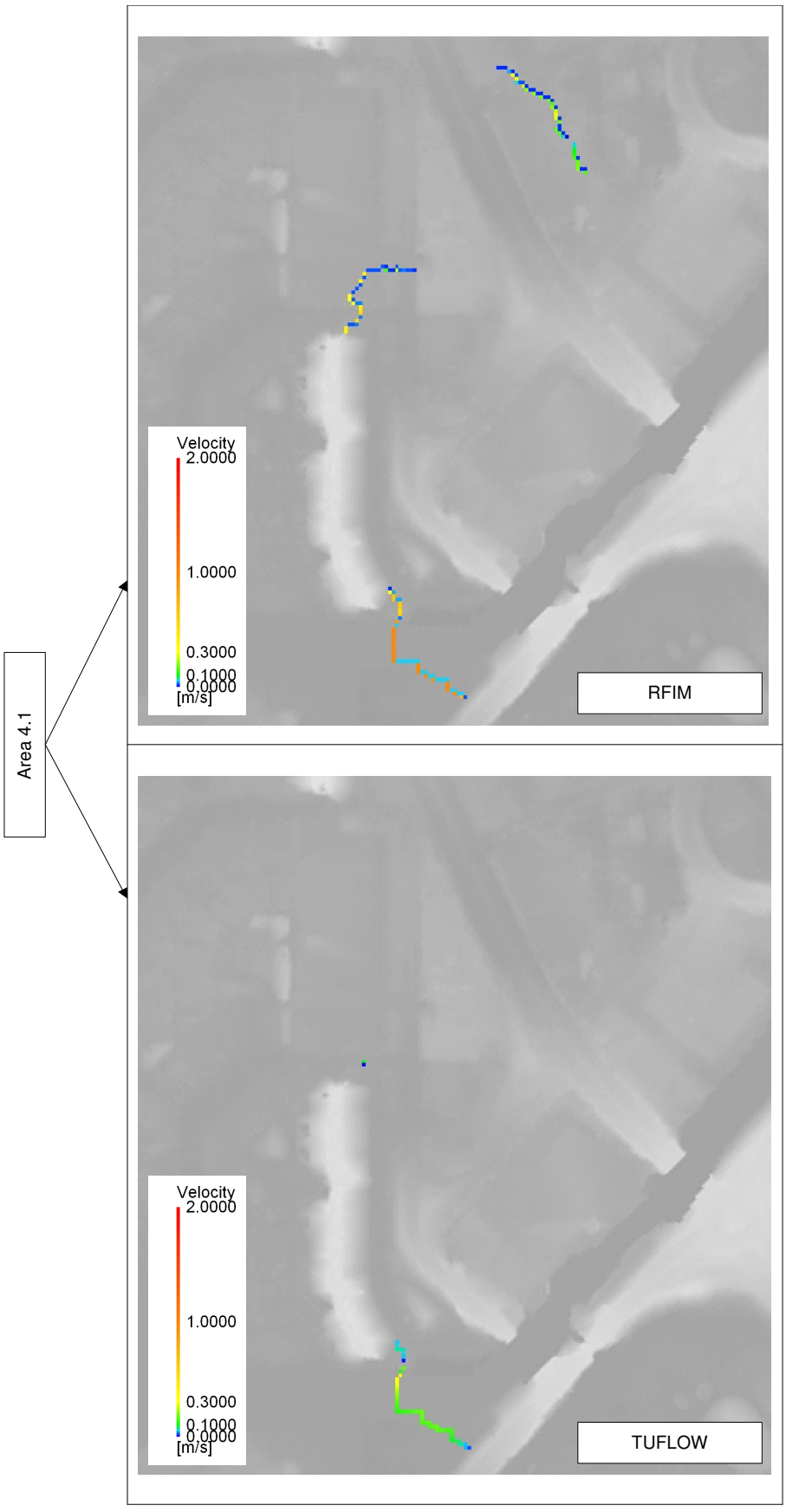


**Figure 4-65: Detailed comparison of the flow velocity predictions – Scenario 4**

#### *4.4.2.4 Multi-direction spreading*

As was discussed in the previous chapters, the ability of the RFIM to predict flood spreading pattern correctly suffers due to inability of the algorithm to spread the water from the cell in more than one direction. In reality, the amount of water spreading in different directions is controlled by the dynamics of the flood; however, RFIM does not take dynamics of the flood into account and any water split estimate is over-simplified.

The water spreading rules were adjusted to allow multi-direction spreading:

- All links with level higher than the first link and lower than the first link + extra head elevation are activated within one calculation step, and

- Extra head value $\Delta z$ is added to all flood cells.

The updated rules were introduced to constant extra head algorithm and applied to all three Greenwich scenarios, but only to one parameter set per scenario. The almost hand calculation was done in Microsoft Excel software. The flood maps were then compared to TUFLOW result and also to original RFIM predictions.

As can be seen in Figure 4-66 to Figure 4-68 the revised algorithm lead to improved predictions in Scenario 1 and 3, while in the case of Scenario 2 the relaxed rules lead to significant overprediction in some areas.

It should be emphasized that although the parameter sets which produced high agreement with TUFLOW in original RFIM algorithm were selected, these may not produce high level of agreement in the multi-direction spreading experiment. Full analysis of 5000 parameter sets would be required and the best then compared to original RFIM method to produce reliable comparison. It can be expected that the best parameter set out of 5000 would produce better predictions than the original single direction RFIM.

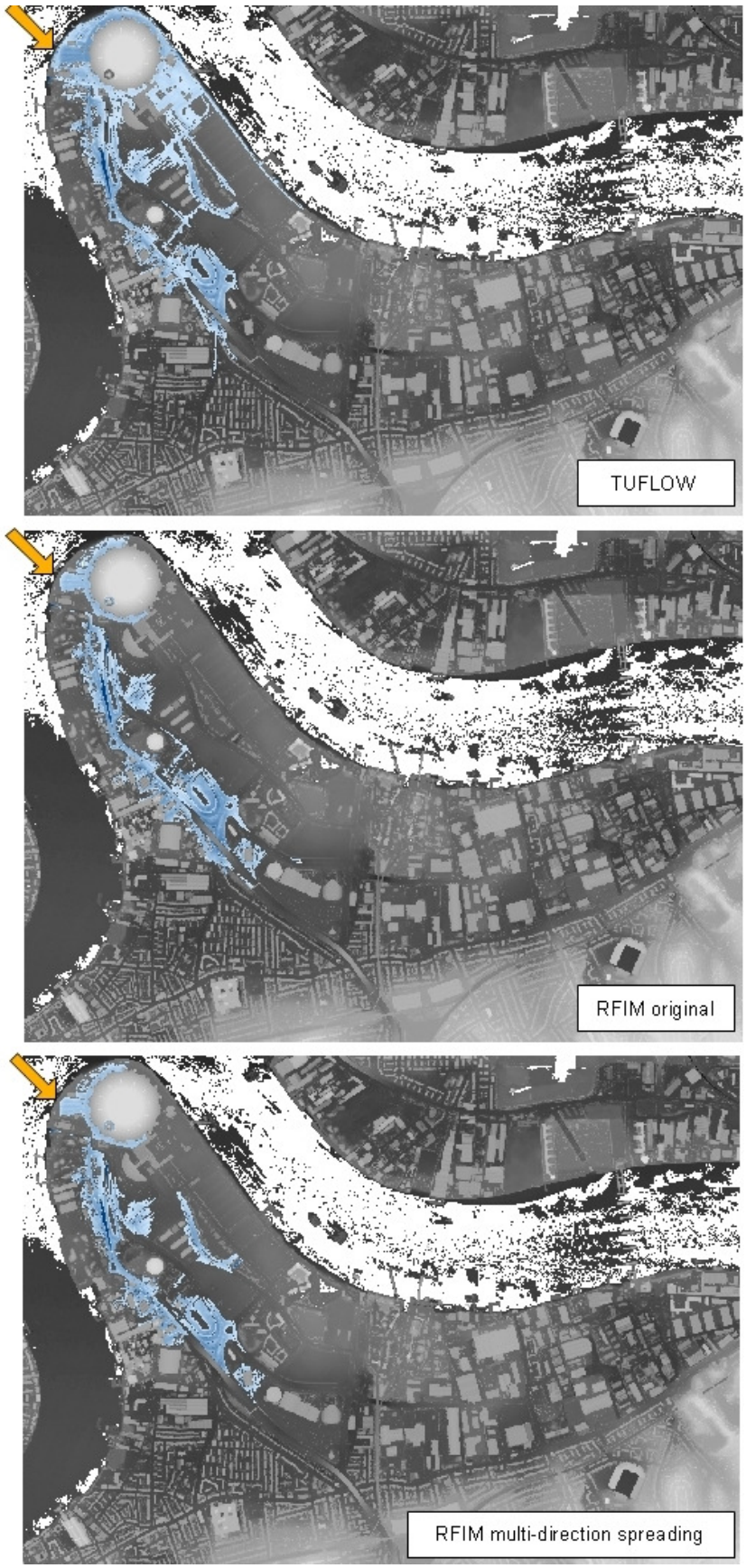


**Figure 4-66: Multi-direction spreading test. Scenario 1. Parameter set 115.**

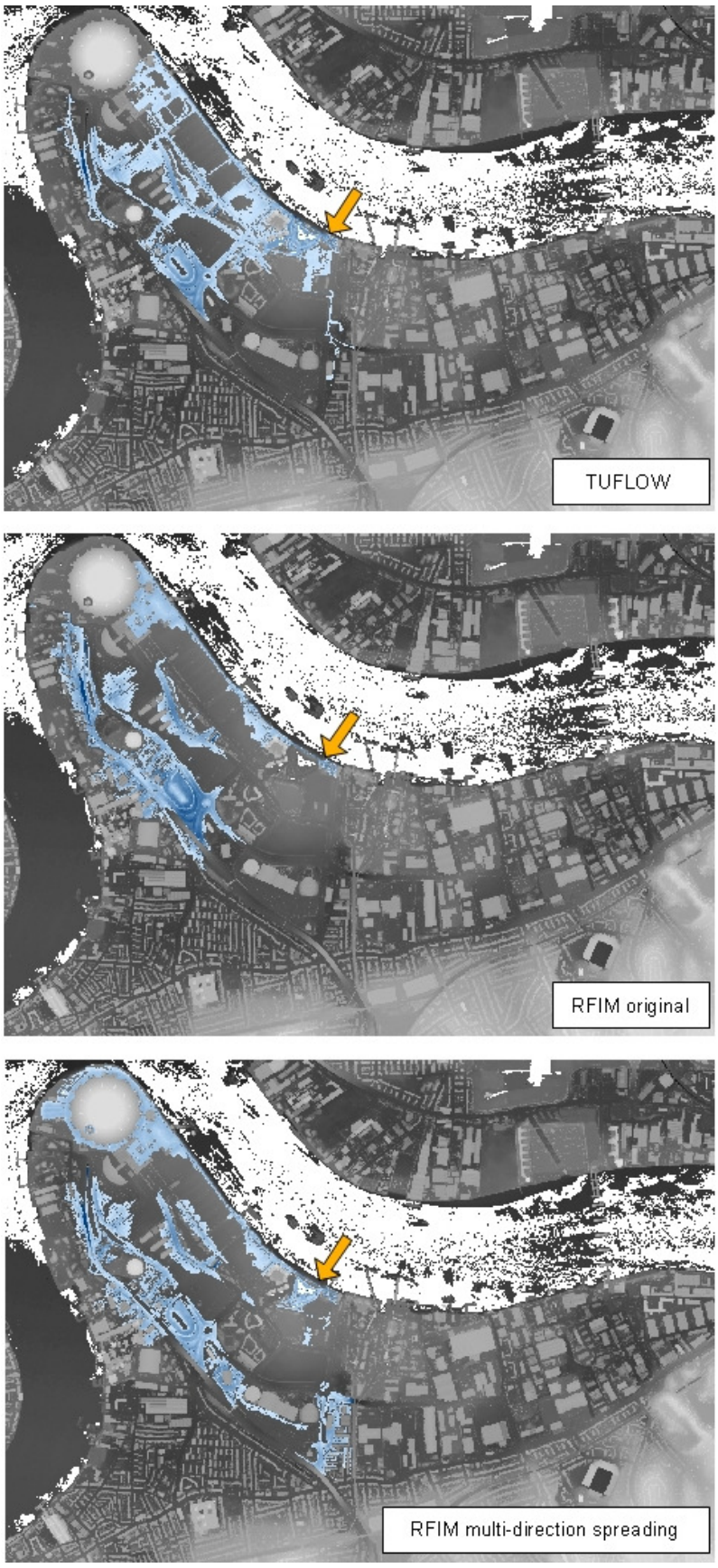


**Figure 4-67: Multi-direction spreading test. Scenario 2. Parameter set 1072.**

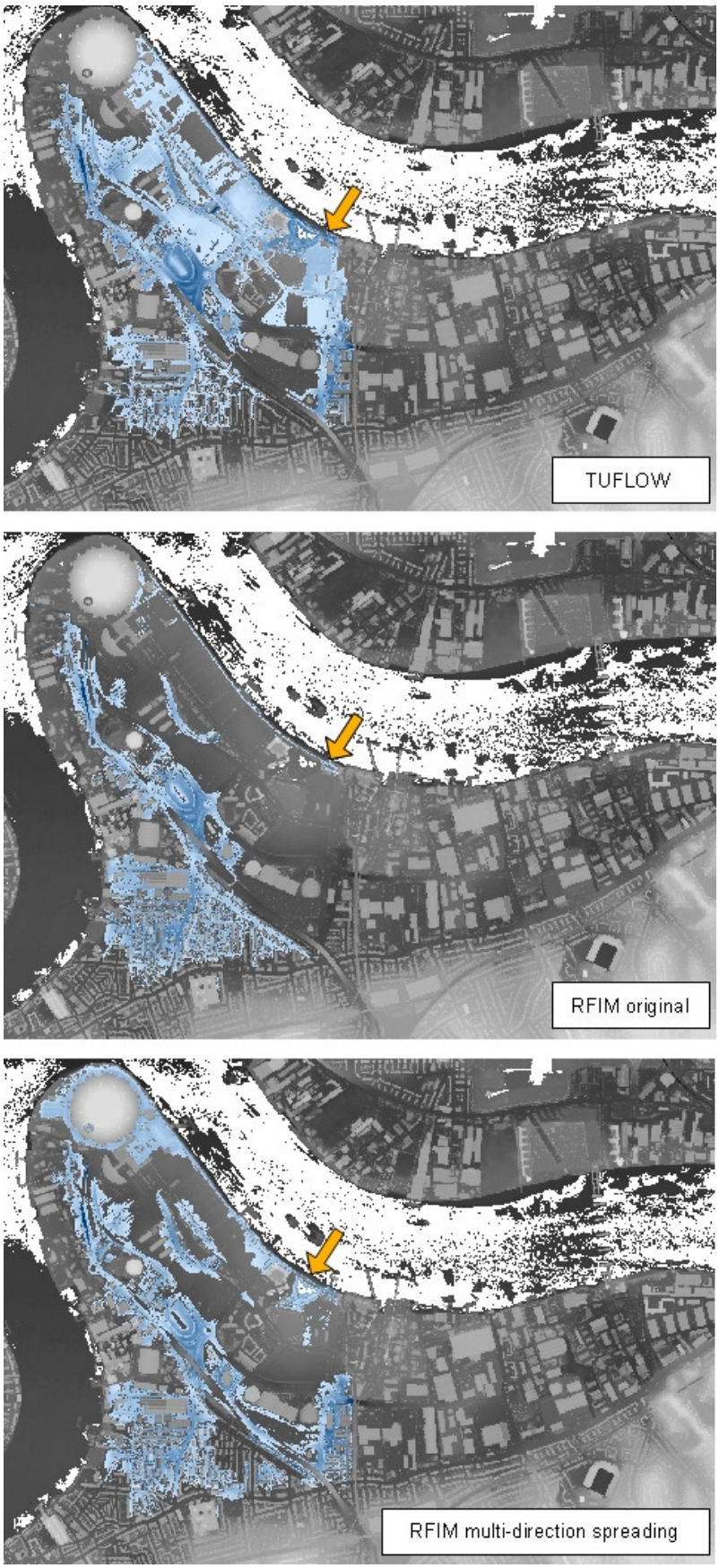


**Figure 4-68: Multi-direction spreading test. Scenario 3. Parameter set 1072.**

#### *4.4.2.5 General discussion*

An overview of the RFIM results is summarised in Table 4-6, in which the best and worst values of F and RMSE over the 5000 parameter sets are presented for each scenario.

The higher the value of F the better is the agreement with TUFLOW in terms of spatial flood extent while the lower the RMSE value, the closer is the RIFM depths prediction to TUFLOW. Highlighted columns in Table 4-6 show the best agreement with TUFLOW achieved for all scenarios.

The table shows that the variable extra head inundation routine lead to slightly better agreement with TUFLOW in terms of the spatial measure of fit F when compared to constant extra head case, but no significant improvement in terms of depth predictions (depth RMSE) was observed.

| | Inundation routine | Scenario | Min F [-] | Max F [-] | Min RMSE [m] | Max RMSE [m] |
|---|---|---|---|---|---|---|
| Final flood extent prediction | Zero extra head | 1 (Greenwich) | 0.1430 | 0.4734 | 0.2385 | 0.3491 |
| | | 2 (Greenwich) | 0.1908 | 0.4267 | 0.1665 | 0.3156 |
| | | 3 (Greenwich) | 0.4754 | 0.5234 | 0.3259 | 0.3555 |
| | | 4 (Thamesmead) | 0.4820 | 0.7500 | 0.0480 | 0.0679 |
| Maximum flood extent prediction | Constant extra head | 1 (Greenwich) | 0.1152 | 0.5020 | 0.3019 | 1.8504 |
| | | 2 (Greenwich) | 0.1480 | 0.4286 | 0.2159 | 1.8243 |
| | | 3 (Greenwich) | 0.3393 | 0.5375 | 0.3181 | 1.8568 |
| | | 4 (Thamesmead) | 0.2145 | 0.7205 | 0.0825 | 1.7577 |
| | Variable extra head | 1 (Greenwich) | 0.1152 | 0.5099 | 0.3158 | 4.1921 |
| | | 2 (Greenwich) | 0.1621 | 0.4480 | 0.2018 | 2.6440 |
| | | 3 (Greenwich) | 0.3409 | 0.5387 | 0.3481 | 5.7824 |
| | | 4 (Thamesmead) | 0.2155 | 0.7183 | 0.0824 | 2.8356 |

**Table 4-6: The RFIM performance – the minimum and maximum values of F and RMSE achieved over 5000 parameter sets.**

*4.4.2.5.1 Inundation routine run-time*

The run-time of each version of the inundation routine is presented in Table 4-7. The data was calculated as an average over the 5000 simulations. In the each run a cell distribution raster file was read, the inundation routine was run, depths at each pixel were calculated and, finally, the depth data was written into a raster file. It was found that, on average, the run-time consumed by file handling operations (opening, reading and writing files) was 1.75 seconds for Greenwich and 1.86 seconds for Thamesmead.

The run-times of the zero extra head and the constant extra head algorithms without the file handling took 0.17 second or less for Greenwich and 0.28 second or less for Thamesmead (Table 4-7) and fell safely within the specified limit of 5 seconds, recommended by HR Wallingford for their Rapid Flood Spreading Methodology (HR

Wallingford, 2006). The slightly longer run-times for Thamesmead were caused by a slightly larger DEM (computational domain).

The variable extra head algorithm showed run-times of 4.12 to 6.17 seconds at Greenwich and 2.99 seconds at Thamesmead. Longer run-times, compared to zero extra head or constant extra head cases, resulted from the iteration of the Manning equation in the $\Delta z_i$ calculation in variable extra head case. At Thamesmead, the number of flood cells was lower compared to Greenwich which explains the shorter run time of the variable extra head inundation algorithm. Interestingly, the tests showed that the variable extra head algorithm was not only longer to run than the constant extra head algorithm, but also did not produce significantly improved predictions as was discussed in section 4.4.2.4. Hence, no justification for the extra run-time was found.

The Monte Carlo tests use a high number of flood cell distributions (parameter sets), which all need to be read before the inundation routine calculation begins. In a practical flood risk analysis only a single flood cell distribution would be used for all inundation scenarios and hence a large proportion of this data transfer would be avoided.

| | Inundation routine | Scenario | Average run-time [s] | |
|---|---|---|---|---|
| | | | Including file handling | Without file handling |
| Final flood extent prediction | Zero extra head | 1 (Greenwich) | 1.91 | 0.16 |
| | | 2 (Greenwich) | 1.86 | 0.11 |
| | | 3 (Greenwich) | 1.90 | 0.15 |
| | | 4 Thamesmead) | 2.10 | 0.24 |
| Maximum flood extent prediction | Constant extra head | 1 (Greenwich) | 1.87 | 0.12 |
| | | 2 (Greenwich) | 1.86 | 0.11 |
| | | 3 (Greenwich) | 1.92 | 0.17 |
| | | 4 (Thamesmead) | 2.14 | 0.28 |
| | Variable extra head | 1 (Greenwich) | 5.87 | 4.12 |
| | | 2 (Greenwich) | 5.98 | 4.23 |
| | | 3 (Greenwich) | 7.92 | 6.17 |
| | | 4 (Thamesmead) | 4.85 | 2.99 |

**Table 4-7: Run-time of inundation routine calculated as an average over 5000 simulations.**

The run-times including file handling presented in Table 4-7 were affected by other processes run on the PC at the same time as the RFIM simulations. For example, the same inundation routine test simulation was run several times and resulted in different run-times. However, the differences observed were marginal.

The simulations were run on an Intel Core2 Quad 2.4 GHz CPU with 4 GB of RAM. The CPU consisted of four processors, but the parallelization of the individual inundation routine run was not tested, because the inundation algorithm consists of sequential steps that does not allow for parallelization. Two simultaneous parallel inundation routine runs were tested; however, the observed speed was limited by the usage of a single hard drive that was not able to cope with intensive data transfer. This bottle neck problem can be avoided by adding multiple hard drives. The data produced

by 5000 simulations occupied 100 GB of disk space for Greenwich and 115 GB for Thamesmead!

The RFIM predictions are generally uncertain. Firstly, the input data (DEM) are not perfectly accurate and errors in terrain description influence the quality of the RFIM predictions and are responsible for a certain level of uncertainty in the model output. Secondly, boundary conditions, such as volume of inundation $V_{Total}$ or peak of inflow $Q_{max,}$ are themselves a product of modelling and may carry considerable uncertainty. As was shown for the Greenwich and Thamesmead tests, the uncertainty associated with the precalculation routine and more importantly with the inundation routine can be considered as high. Further uncertainty of the RFIM output is introduced by the flood against which the RFIM is calibrated. At some sites, such as Greenwich and Thamesmead, no real flood data are available and other model predictions, which are also uncertain, need to be used.

The Rapid Flood Inundation Model was developed to primarily predict flood extent estimates to be used in the flood risk assessment tasks. It was recognized, however, that the simple and fast water volume budget calculation can be applied more widely. For example, the RFIM can be used to predict the extent of flood water remaining on the floodplain after the flood recession, which is often important for shallow floodplains in lower reaches of rivers. The RFIM can also be used prior to the application of more sophisticated inundation models in order to identify the most important flooding scenarios, i.e. to decrease the number of final model runs. In some cases, scenarios with different flood defence breach location or/and different inflow hydrograph can lead to the same or similar flood extents, as was shown for example in Alevyzaki (2007) who applied the RFIM to the Thamesmead embayment. It was shown that some flooding scenarios are representative of hundreds of others and identification of these can considerably save limited computational resources.

# 5 Conclusions and recommendations

In this thesis, a rapid flood spreading method was developed based on the demand for a fast algorithm usable for flood risk management purposes. Using a high resolution DEM a procedure that automatically divides the floodplain into a system of flood cells and three variants of a flood spreading routine were developed. In this method, a flood is considered as a volume of water that fills the depression closest to the flood source and then spreads via links to neighbouring cells throughout the floodplain, gravity is considered to be the main driver of the flow. To determine flood inundation extent the total flood volume is required as an input condition. If estimates of maximum water depth and water velocity are required then the peak inflow value is also required.

The model was validated using simplified DEMs and applied to the Greenwich and Thamesmead embayments on the River Thames. The results were compared to two-dimensional hydrodynamic model predictions from the TUFLOW model. The performance of the model was assessed and the sensitivity of the model parameters was analysed.

## 5.1 Conclusions

The major findings of this research are listed below:

- The Rapid Flood Inundation Model (RFIM) is capable of producing relatively realistic final flood extent and maximum flood extent predictions using CPU times of less than 1 second for large complex urban floodplains. A condition of the RFIM application is that floodplain topography can be represented by interconnected terrain depressions.

- If the floodplain is sloped and no depressions are present, the RFIM routes water across the floodplain to the lowest flood cell of the domain. In such cases the RFIM does not produce reliable flood predictions of inundated extent or maximum water level. Comparison of benchmark simulations at Greenwich and

Thamesmead test sites showed different levels of agreement between the RFIM and predictions made using the two-dimensional hydrodynamic model TUFLOW, confirming the observation made by Lhomme et al. (2008) that the quality of prediction is site-dependant and breach location dependant.

- It was demonstrated that the assumptions that underpin the RFIM were reasonable at Greenwich and Thamesmead test sites.

- It was recognized that no a priori knowledge of probable flow paths or flood cell distribution is required to set up the model. The precalculation stage of the RFIM recognizes the terrain depressions and flowpaths automatically.

- In some cases, the precalculation routine builds a system of one large dominant flood cell surrounded by smaller ones. This leads to poor quality simulations of inundation extent. This problem can be avoided by introducing a limit on the maximum permissible flood cell area in the precalculation routine.

- In some scenarios, the prediction shows inaccuracies when compared to the two-dimensional hydrodynamic model. In such cases the RFIM suffers from the simplified representation of the hydraulic processes. The RFIM calculation allows water to spread from any cell in only one direction (via a lowest link), which was shown in section 4.4.2.1.1 to be deficient for some patterns of inundation. The errors caused by the single direction spreading depend on breach location and are such that large areas that were predicted to be flooded by TUFLOW model were not recognized as flooded by the RFIM. As was shown in section 4.4.2.4, the algorithm can be improved by re-designing the inundation routine in order to allow water to spread in multiple directions. The sensitivity analysis of the RFIM predictions to the model parameters ($A_{min}$, $d_{min}$, $\Delta z$, n) presented in section 4.4 should be interpreted with respect to this problem.

- The RFIM is sensitive to the minimum flood cell depth parameter $d_{min}$, which ensures that no cell is shallower than $d_{min}$. It can be hypothesised that the sensitivity to $d_{min}$ would be decreased if the inundation routine was improved by allowing flood spreading in multiple directions.

- The sensitivity analysis revealed that the optimum $d_{min}$ parameter is scenario-dependent and test site-dependent. Different optima were found for different scenarios and test sites.

- In some flooding scenarios sensitivity to $A_{min}$ was observed, but only in limited areas of the parameter space (Figure 4-23). The $A_{min}$ parameter ensures that no cell on the floodplain has a smaller plan area than $A_{min}$. It can be argued that if a constant value of $A_{min}$ was used in all simulations a very similar level of prediction accuracy would be achieved. In such cases the complexity of the precalculation part of the RFIM would be decreased as well as its run-time. More testing is required to confirm the insensitivity of predictions to the $A_{min}$ parameter.

- Using the optimum number of flood cells itself does not ensure that the prediction would be correct as the quality of predictions depends primarily on the combination of the $A_{min}$ and $d_{min}$ parameters.

- The Greenwich embayment tests showed that the current version of the inundation routine experiences difficulties when dealing with a large number of flood cells due to single direction spreading. With an increasing number of cells the probability of this error occurring increases.

- The model does not account for flooding occurring on the flow pathways, as the water volume is spread by filling the terrain depressions from their lowest point up. In the cases considered here this underprediction of flooding on flowpaths is most significant in the flood cell closest to the breach.

- The velocity predictions are spatially limited only to the borders between flooded cells. It was observed that the under/overprediction of local velocity reflects the under/overprediction of volume transfers between the cells. It is expected that if the flood spreading algorithm was improved by allowing multiple direction spilling the accuracy of velocity predictions would improve.

- The analysis showed that the run time of the zero extra head and the constant extra head inundation routines is of the order of couple of seconds, which falls within the limit of 5 seconds, recommended by HR Wallingford for their RFSM algorithm (HR Wallingford, 2006).

- The RFIM was developed to primarily deliver flood extent estimates to be used in flood risk assessment tasks. During the development and presentation stage of the project it was realized that simple and fast volume budget calculation can be applied to more tasks than was originally intended. For example,

    - The RFIM can be used to predict the location of remaining flood water after the flood event recession, which is often important for shallow floodplains in lower reaches of rivers.

    - The RFIM can also be used prior to the application of more sophisticated inundation models in order to identify the most important flooding scenarios, i.e. to decrease the number of final model runs. At some test sites, as was shown for example in Alevyzaki (2007) for the Thamesmead embayment, scenarios with different flood defence breach locations or/and different inflow hydrographs can lead to the same or similar flood extents. Identifying the scenarios that are representative of hundreds of others can considerably save computational resources.

- The inundation routine code consists of a set of sequential steps and hence does not allow for effective parallelization. The inundation routine runs are, however, independent and can be parallelized within the flood risk assessment task that is run on a floodplain basis. This presents an opportunity for running the sets of inundation routines on multiple processors and reducing the whole flood risk analysis run-time.

## 5.2 Recommendations for future research

- It was found that the algorithm gives lower quality predictions in cases in which the real flooding spreads in two directions. The revision of the inundation

routine algorithm that will allow water spreading in multiple directions would considerably improve the quality of the predictions and is recommended as the improvement that will most benefit the model.

- In order to assess the effect that the introduction of multiple directions spreading would have, the order in which the cells are flooded in TUFLOW model can be superimposed on the RFIM flood spreading algorithm.

- The RFIM does not permit any water volume to be gained or lost during the calculation. In other words, no interaction of the floodplain with the surrounding areas, subsurface (infiltration or interaction with sewer network) or atmosphere (evaporation or precipitation) is taken into account. The water loss due to infiltration or evaporation or gain due to rainfall is considered as negligible compared to the uncertainty of inputs, boundary conditions and parameter values. The water loss due to interaction with urban drainage systems, however, may affect the final flood extent significantly as it introduces new links between the flood cells that are not currently recognized by the model. It is recommended to include the subsurface links in the precalculation algorithm.

- It was shown that the presence of large flood cells leads to incorrect predictions, in which hydraulically unrelated areas are predicted as flooded. It is recommended that a condition on the maximum area of a flood cell should be introduced to the precalculation routine in order to avoid the construction of large cells.

- The accuracy of predictions and speed of the variable extra head inundation routine can be improved by revision of the velocity calculation.

- With respect to the application of the RFIM for flood risk assessment purposes, it is necessary to implement automatic input of boundary conditions, such as breach location and $V_{Total}$ and $Q_{max}$ values.

# 6 References


Abt S.R. et al., 1989, Human stability in a high flood hazard zone. Water Resources Bulletin, 25, 4

Ahokas E., Kaartinen H., Hyyppä J., 2003, A quality assessment of airborne laser scanner data, International Archives of Photogrammetry and Remote Sensing, Vol. XXXIV, 3/W13

Alevyzaki S., 2007, Investigation of the Flooding at a Coastal Site, Using a Flood Inundation Model. MSc thesis – Department of civil Engineering, University of Glasgow

Aronica G., Hanking B., Beven K., 1998, Uncertainty and equifinality in calibrating distributed roughness coefficients in a flood propagation model with limited data. Advances in Water Resources, Vol. 22, No. 4, 349-365

Ball D.J., Green C.H., 2007, Human behaviour, in Future flooding and coastal erosion risks, edited by Thorne C.R., Evans E.P., and Penning-Rowsell E.C., Thomas Telford Publishing, London

Bates P.D, De Roo A.P.J., 2000, A simple raster-based model for flood inundation simulation, Journal of Hydrology, 236, 54-77

Bates P.D., Horritt M.S., Aronica G., Beven K.J., 2004, Bayesian updating of flood inundation likelihoods conditioned on flood extent data, Hydrological processes 18 (17), 3347-3370

Bettess R., 2007, Reliability of flood defences, Presented in FLOODsite Special Session, 32nd IAHR Congress, Venice, 1-6 July

Beven K., Binley A., 1992, The future of distributed models: Model calibration and uncertainty prediction, Hydrological Processes, 6, 279-298

Beven K., 1993, Prophecy, reality and uncertainty in distributed hydrological modelling. Adv. Water Resources, 16, 41-51

Beven K., 2001, How far can we go in distributed hydrological modelling?, The Dalton Lecture, Hydrology and Earth System Sciences, 5(1), 1-12

Beven K., 2007, Personal communication.

Bradbrook K.F., Lane S.N., Waller S.G., Bates P.D., 2004, Two dimensional diffusion wave modelling of flood inundation using a simplified channel representation, Intl. J. River Basin Management Vol. 2, No. 3, 211-223

Cunge J.A., Holly F.M., Verwey A., 1980, Practical aspects of computational river hydraulics. Pitman Publishing. London

Cunge J.A., 1975, Chapter 17 - Two-dimensional modelling of flood plains. Unsteady flow in open channels. Water Resources Publications. Fort Collins, USA

DEFRA – UK Department for Environment, Food and Rural Affairs, 2003, Flood Risks to People Phase 1, R&D Technical Report FD2317

DEFRA – UK department for Environment, Flood and Rural Affairs, 2006, Flood Risks to People Phase 2, FD2321/TR1 The Flood Risks to People Methodology

DEFRA – UK Department for Environment, Food and Rural Affairs, 2004-2006, "Making Space for Water" http://www.defra.gov.uk/environ/fcd/policy/strategy.htm

De Roo A.P.J., Van Der Knijff J., Schmuck G., 2000, A simple floodplain inundation model to assist in floodplain management, New trends in Water and Environmental Engineering for Safety and Life

European Commission, 2000, First Report on the Harmonisation of Risk Assessment Procedures, DG Health & Consumer Protection

Evans E.P., Wicks J.M., Whitlow C.D. and Ramsbottom D.M., 2007, The evolution of a river modelling system. Proceedings of the Institution of Civil Engineers

Falconer R.A., 1986, A water quality simulation study of a natural harbour. American Society of Civil Engineers, Journal of Waterway, Port, Coastal and Ocean Engineering, 112, No. 1, 15-34

Fewtrell T., Bates P., Horritt M., Trigg M., 2007, The effect of temporal and spatial coarsening on storage cell predictions of urban flood inundation, Proc.32nd IAHR Congress, Venice, 1-6 July, paper SS05-13-O

FloodRiskNet, 2007, www.floodrisknet.org.uk, Catalogue of methods developed in Research Priority Area 9 of the FRMRC

Foresight, 2004, Future Flooding Executive Summary, Office of Science and Technology, www.foresight.gov.uk

Frank E., Ostan A., Coccato M., Stelling G.S., 2001, Use of an integrated one-dimensional/two-dimensional hydraulic modelling approach for flood hazard and risk mapping, River Basin Management, eds R.A. Falconer & W.R. Blain, WIT Press, Southampton UK, 99-108

Gouldby B., Sayers P., Mulet-Marti J., Hassan M.A.A.M., Benwell D., 2008, A methodology for regional-scale flood risk assessment, Proceedings of the Institution of Civil Engineers, Water Management 161, Issue WM3, 169-182

Graham W.J., 1999, A Procedure for Estimating Loss of Life Caused by Dam Failure, DSO-99-06, Denver CO: Bureau of Reclamation, Dam Safety Office

Green C.H., Penning-Rowsell E.C.., 2007, Socio-economic drivers, cities and science., published in Future flooding and coastal erosion risks, edited by Thorne C.R., Evans E.P., Penning-Rowsell E.C., Thomas Telford Publishing

Halcrow, Wallingford Software, 1997, ISIS Flow - User manual

Hall J.W., Dawson R.J., Sayers P.B., Rosu C., Chatterton J.B., Deakin R., 2003, A methodology for national-scale flood risk assessment, Water & Maritime Engineering 156, Issue WM3, 235-247

Hall J.W., Simm J.D., Evans E.P., 2007, Introduction to the Foresight 'Future Flooding' methodology, published in Future flooding and coastal erosion risks, edited by Thorne C.R., Evans E.P., Penning-Rowsell E.C., Thomas Telford Publishing

Hervouet J.M., Petitjean A., 1999, Malpasset Dam-break revisited with 2-dimensional computations, Journal of Hydraulic Research, 37, Issue 6, 777-788

Horritt M.S., 1999, A statistical active contour model for SAR image segmentation, Image and Vision Computing, 17, No.3, 213-224

Horritt M.S., Bates P.D., 2001a, Predicting floodplain inundation: raster-based modelling versus the finite-element approach, Hydrological Process, 15, 825-842

Horritt M.S., Bates P.D., 2001b, Effects of spatial resolution on a raster based model of flood flow, Journal of Hydrology, 253, 239-249

Horritt M.S., Mason D.C. and Luckman A.J., 2001, Flood boundary delineation from Synthetic Aperture Radar imagery using a statistical active contour model, International Journal of Remote Sensing, 22, No. 13, 2489-2507

Horritt M.S., Bates P.D., 2002, Evaluation of 1-D and 2-D numerical models for predicting river flood inundation. Journal of Hydrology, 268, 87-99

HR Wallingford, 2006, Thames Estuary 2100 – Rapid flood spreading methodology (RFSM), Final report

Hunter N.M., Horritt M.S., Bates P.D., Wilson M.D., Werner M.G.F., 2005, An adaptive time step solution for raster-based storage cell modelling of floodplain inundation, Advances in Water Resources, 28, No. 9, 975-991

Hunter N.M., Bates P.D., Horritt M.S., Wilson M.D., 2005, Improved simulation of flood flows using storage cell models, Proceedings of the Institution of Civil Engineers, Water Management 159, 9-18

Hunter N.M., Bates P.D., Horritt M.S., De Roo P.J., Werner M.G.F., 2005, Utility of different data types for calibrating flood inundation models within a GLUE framework, Hydrology and Earth System Sciences, 9(4), 412-430

Hunter N.M., Bates P.D., Horritt M.S. Wilson M.D., 2007, Simple spatially-distributed models for predicting flood inundation: A review. Geomorphology

Hunter N.M., Bates P.D., Neélz S., Pender G., Villanueva I., Wright N.G., Liang D, Falconer R.A., Lin B., Waller S., Crossley A.J., Mason D.C., 2008, Benchmarking 2D hydraulic models for urban flooding, Proceedings of the Institution of Civil Engineers, Water Management, Feb, WM1, 13 – 30

ICE - Institution of Civil Engineers, 2001, Learning to Live with Rivers. Final Report of the ICE Presidential Commission to Review the Technical Aspects of Flood Risk Management in England and Wales, Institution of Civil Engineers, London

Intergovernmental Panel on Climate Change, 2007, The AR4 Synthesis Report, http://www.ipcc.ch/pdf/assessment-report/ar4/syr/ar4_syr.pdf

Krupka M., Pender G., Wallis S., Sayers P.B. and Mulet-Marti J., 2007a, A rapid flood inundation model, Proc. 32th IAHR Congress, Venice, 1-6 July, paper SS05-04-O

Krupka M., Wallis S., Pender S., Neélz S., 2007b, Some practical aspects of flood inundation modelling, Transport phenomena in hydraulics, Publications of the Institute of Geophysics, Polish Academy of Sciences, E-7 (401)

Lhomme J., Bouvier C., Perrin J.-L., 2004, Applying a GIS-based geomorphological routing model in urban catchments, Journal of Hydrology 299, 203-216

Lhomme J., Sayers P., Gouldby B., Samuels P., Wills M., Mulet-Marti J., 2008, Recent development and application of a rapid flood spreading method, River Flow 2008, September

Liang D., Falconer R.A., Lin B., 2007, Linking one- and two-dimensional models for free surface flows, Proceedings of the Institution of Civil Engineers, Water Management 160, 145-151

Liggett J.A., Cunge J.A., 1975a, Chapter 4 – Numerical methods of solution of the unsteady flow equations. Edited by Mahmood K. and Yevjevich V., Water Resources Publications. Fort Collins, USA

Liggett J.A., 1975b, Chapter 2 – Basic equations of unsteady flow. Edited by Mahmood K. and Yevjevich V., Water Resources Publications. Fort Collins, USA

Lin B., Wicks J.M., Falconer R.A., Adams K., 2006, Integrating 1D and 2D hydrodynamic models for flood simulation, Proceedings of the Institution of Civil Engineers, Water Management 159, 19-25

Marks K., Bates P.D., 2000, Integration of high-resolution topographic data with floodplain flow models, Hydrological Processes, 14, 2109-2122

Neélz S., Pender G., Villanueva I., Wilson M.D., Wrigh N.G., Bates P., Mason D and Whitlow C., 2006, Using remotely sensed data to support flood-modelling, Proceedings of the Institution of Civil Engineers, Water Management 159, Issue WM1, 35-43

Neélz S.P. and Pender G., 2006, The influence of errors in Digital Terrain Models on flood flow routes, River Flow 2006, September, ISBN 0 415 408148, 1955 – 1962

Neil J., 2008, presented at Flood Risk Management Research Consortium Annual Assembly, July, Heriot-Watt University

Ponce V.M., Simons D.B., 1977, Shallow wave propagation in open channel flow, Journal of the Hydraulic Division, ASCE 103, 1461-1476, Paper 13392

Ponce V.M., Li R.M., Simons D.B., 1978, Applicability of kinematic and diffusion models, Journal of the Hydraulic Division – ASCE 104(3), 353-360

Refsgaard J.C., 2001, Towards a formal approach to calibration and validation of models using spatial data, In Grayson R.B., Blöschl G., Spatial Patterns in Catchment Hydrology: Observations and Modelling, Cambridge University Press, Cambridge, 329-354

RESCDAM, 2000, The Use of Physical Models in Dam-Break Flood Analysis, Final Report of Helsinki University of Technology data (as Appendix 2 to Final Report of RESCDAM dated June 2001)

Reynard N.S., 2007, Climate change, published in Future flooding and coastal erosion risks, edited by Thorne C.R., Evans E.P., Penning-Rowsell E.C., Thomas Telford Publishing

Romanowicz R., Beven K., Tawn J.A., 1994, Evaluation of predictive uncertainty in nonlinear hydrological models using a Bayesian approach, Statistics for the Environment2: Water Related Issues. Edited by Barnett V. and Turkman K.F., John Wiley & Sons Ltd.

Romanowicz R., Beven K.J., Tawn J., 1996, Bayesian calibration of flood inundation models, Floodplain Processes. Edited by Anderson M.G., Walling E. and Bates P.D., John Wiley & Sons Ltd.

Romanowicz R., Beven K., 2003, Estimation of flood inundation probabilities as conditioned on event inundation maps, Water Resources Research, Vol. 39 (3), 1073-1085

Samuels P.G., 1990, Cross-section location in 1-D models. In: White W.R., Watts J. (Eds.), 2nd International Conference on River Flood Hydraulics, Wiley, Chichester, 339-350

Samuels P.G., 2006, Risk and uncertainty in flood management, in River basin modelling for flood risk mitigation, edited by D.W. Knight and A.Y. Shamseldin, 481-517, Taylor & Francis Group plc, London

Sayers P.B., Hall J.W., Meadowcroft I.C., 2002a, Towards risk-based flood hazard management in the UK, Proceedings of ICE, 150, 36-42, Paper 12803

Sayers P.B., Hall J.W., Rosu C., Chatterton J. B.J. & Deakin R., 2002b, Risk assessment of flood and coastal defences for strategic planning (RASP) - A high level methodology – Evaluation Report. SR 603 Draft. HR Wallingford.

Sayers, P.B., Gouldby, B.P., Simm, J.D., Meadowcroft, I. and Hall, J., 2002c. Risk, Performance and Uncertainty in Flood and Coastal Defence - A Review, DEFRA/Environment Agency - Flood and Coastal Defence R&D Programme, Wallingford.

Sayers P.B., Gouldby B., Tarrent O., 2007, Thames estuary – the application of a regional scale systems analysis model to flood risk management options assessment, HR Wallingford, Paper 06-2

Shiono K., Knight D.W., 1991, Turbulent open-channel flows with variable depth across the channel, Journal of Fluid Mechanics, Vol. 222, 617-646

Smith M.J., Edwards E.P., Priestnall G., Bates P., 2005, Creation of Digital Elevation Models for Flood Inundation Modelling, FRMRC UFMO Report

Syme W.J., 1991, Dynamically linked two-dimensional/one-dimensional hydrodynamic modelling program for rivers, estuaries & coastal waters, MengSc thesis, University of Queensland, Australia

Syme W.J., 2001, TUFLOW – Two & one-dimensional Unsteady FLOW Software for Rivers, Estuaries and Coastal Waters, IEAust 2D Seminar, Sydney

Tapsell S.M., Ball D.J., 2007, Flood event management, in Future flooding and coastal erosion risks, edited by Thorne C.R., Evans E.P., and Penning-Rowsell E.C., Thomas Telford Publishing, London

The European Parliament and the Council of the European Union, 2007, Directive 2007/60/EC of the European Parliament and of the Council

Thorne C.R., Evans E.P., Penning-Rowsell E.C., 2007, Future flooding and coastal erosion risks, Thomas Telford Publishing, London

Timbe L., Willems P., 2004, Uncertainties in hydrodynamic flood simulation, ACTIF 2nd Workshop, Quantification, reduction and dissemination of uncertainty in flood forecasting, http://www.actif-ec.net/Workshop2/papers/ACTIF_S1_08.pdf

United Nations University, 2004, Two billion people vulnerable to floods by 2050; Number expected to double or more in two generations due to climate change, deforestation, rising seas, population growth, News release, http://www.unu.edu/news/ehs/floods.doc

Vrouwenvelder A.C.W.M. and Steenhuis C.M., 1997, Tweede waterkeringen Hoeksche Waard, berekening van het aantal slachtoffers bij verschillende inundatiescenario's (Secondary flood defences in the Hoeksche Waard, calculation of the number of fatalities for various flood scenarios, in Dutch), TNO 97-CON-R0332

Wallis S.G., Knight D.W., 1984, Calibration studies concerning a one-dimensional numerical tidal model with particular reference to resistance coefficients, Estuarine, Coastal and Shelf Science, Vol. 19, 541-562

Wicks J., Syme J., Hassan M.A.A.M., Lin B., Tarrant O., 2004, 2D modelling of floodplains – is it worth the effort?, Proceedings of the River and Coastal Flooding Conference, Defra, UK, 1-10

Wikipedia, 2008, http://www.wikipedia.org/

Willems P., 2000, Probabilistic immission modelling of receiving surface waters, PhD Thesis, KU Leuven University

Wilson M.D., Atkinson P.M., 2003, Sensitivity of a flood inundation model to spatially-distributed friction, International Geoscience and Remote Sensing Sympsium, Vol 3, 1579-1581

Wilson M.D., Atkinson P.M., 2005a, Prediction uncertainty in elevation and its effect on flood inundation modelling, in GeoDynamics, Atkinson P.M., Foody G.M., Darby S., Wu F. (eds), John Wiley & Sons Ltd

Wilson M.D., Atkinson P.M., 2005b, The use of elevation data in flood inundation models: a comparison of ERS InSAR and combined contour and Differential GPS, International Journal of River Basin Management, 3 (1), 3-20

World Health Organization, 2002, Floods: Climate change and adaptation strategies for human health. Report on a WHO meeting, London, 30 June – 2 July 2002

Zanobetti D., Lorgeré H., Preissmann A., Cunge J.A., 1970, Mekong Delta mathematical model program construction, J. Waterways and Harbors Division, ASCE, 96, No.WW2, May